

**GROUND MOVEMENT RESPONSE DUE TO EARTH PRESSURE BALANCE
SHIELD TUNNELING IN HANGKOK SUBSOIL**

Mr. Sektay Lim

**A Dissertation Submitted in Partial Fulfillment of the Requirements
for the Degree of Doctor of Philosophy Program in Civil Engineering**

Department of Civil Engineering

Faculty of Engineering

Chulalongkorn University

Academic Year 2006

Copyright of Chulalongkorn University

GROUND MOVEMENT RESPONSE DUE TO EARTH PRESSURE BALANCE SHIELD TUNNELING IN
BANGKOK SUBSOILS

Mr. Soktay Lim

A Dissertation Submitted in Partial Fulfillment of the Requirements
for the Degree of Doctor of Philosophy Program in Civil Engineering

Department of Civil Engineering

Graduate School Chulalongkorn University

Academic Year 2006

Copyright of Chulalongkorn University

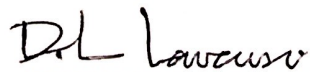
พฤติกรรม การเคลื่อนตัวของพื้นดินเนื่องมาจากการใช้ EARTH PRESSURE BALANCE SHIELD ขุดเจาะอุโมงค์
ที่ดินชั้นล่างลงไปของกรุงเทพ

นาย Soktay Lim


วิทยานิพนธ์นี้เป็นส่วนหนึ่งของการศึกษาตามหลักสูตรปริญญาวิศวกรรมศาสตรบัณฑิต
สาขาวิชาวิศวกรรมโยธา
บัณฑิตวิทยาลัย จุฬาลงกรณ์มหาวิทยาลัย
ปีการศึกษา 2549
ลิขสิทธิ์ของจุฬาลงกรณ์มหาวิทยาลัย

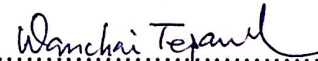
Thesis Title	GROUND MOVEMENT RESPONSE DUE TO EARTH PRESSURE BALANCE SHIELD TUNNELING IN BANGKOK SUBSOIL
By	Soktay Lim
Field of Study	Civil Engineering
Thesis Advisor	Associate Professor Wanchai Teparaksa, D. Eng.
Thesis Co-advisor	Professor Satoru Shibuya, Ph.D.


Accepted by the Faculty of Engineering, Chulalongkorn University in
Partial Fulfillment of the Requirements for the Doctoral Degree

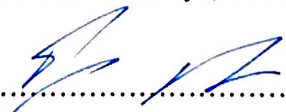
 Dean of the Faculty of Engineering
(Professor Direk Lavansiri, Ph.D.)


THESIS COMMITTEE


 Chairman
(Associate Professor Boonsom Lerdirunwong, D. Ing.)

 Thesis Advisor
(Associate Professor Wanchai Teparaksa, D. Eng.)

 Thesis Co-advisor
(Professor Satoru Shibuya, Ph.D.)

 Member
(Assistant Professor Tirawat Boonyatee, D. Eng.)

 Member
(Tanate Srisirojanakorn, Ph.D.)

 Member
(Attasit Sawatparnich, Ph.D.)

นายชกไธ ลิม: การเคลื่อนตัวของดินเนื่องจากการจากขุดเจาะอุโมงค์ด้วยหัวเจาะแรงดันดินสมดุล
ในดินกรุงเทพฯ (GROUND MOVEMENT RESPONSE DUE TO EARTH
PRESSURE BALANCE SHIELD TUNNELING IN BANGKOK SUBSOIL) อ.
ที่ปรึกษา: รศ. ดร. วันชัย เทพรักษ์, อ.ที่ปรึกษาร่วม: PROF. SATORU SHIBUYA,
Ph.D. 176 หน้า.

พฤติกรรมทรุดตัวของดินยังคงเป็นคำถามโดยเฉพาะอย่างยิ่งสำหรับการขุดเจาะอุโมงค์ใน
พื้นที่เขตเมืองที่มีประชากรอาศัยหนาแน่นและมีอุปสรรคสิ่งกีดขวางมากมายตลอดแนวการขุดเจาะ
อุโมงค์ งานวิจัยนี้ทำการศึกษาพฤติกรรมทรุดตัวของดินเนื่องจากการขุดเจาะอุโมงค์และทำการ
วิเคราะห์กลับด้วยวิธีไฟไนต์อีลิเมนต์ สองมิติเพื่อการประมาณค่าการทรุดตัวอย่างเหมาะสมในการขุด
เจาะอุโมงค์ในกรุงเทพฯ

อุโมงค์ระบายน้ำขนาดเส้นผ่านศูนย์กลางภายนอก 5.55 ม. ในโครงการคลองระบายน้ำแสน
สบ-คลองลาดพร้าว-สถานีสูบน้ำพระโขนง ได้ทำการขุดเจาะด้วยหัวเจาะแรงดันดินสมดุลทั้งการขุดเจาะ
อุโมงค์ในชั้นทรายแน่นและดินเหนียวแข็งดินดานที่ความลึกศูนย์กลางอุโมงค์ประมาณ 27.50 ม. ต่ำจาก
ผิวดิน ผลการตรวจวัดการเคลื่อนตัวของดินจากการขุดเจาะอุโมงค์สามารถแบ่งได้เป็น 3 ส่วนคือ การทรุด
ตัวก่อนถึงหัวเจาะ การทรุดตัวในหัวเจาะ และการทรุดตัวของช่องว่างระหว่างอุโมงค์กับดินภายหลังการ
เจาะผ่านของหัวเจาะ (Tail Void) การทรุดตัวที่ผิวดินหลักๆ เกิดขึ้นจากช่องว่างระหว่างอุโมงค์กับดิน
ภายหลังการเจาะผ่านของหัวเจาะประมาณ 63-67 % ของการทรุดตัวทั้งหมด สำหรับการขุดเจาะอุโมงค์
ระบายน้ำทั้งในชั้นทรายแน่นและชั้นดินเหนียวแข็งดินดาน

การวิเคราะห์การทรุดตัวของดินได้ทำการวิเคราะห์ด้วยวิธีไฟไนต์อีลิเมนต์โดยอ้างอิงพฤติกรรม
การพังทลายของดินชนิด Mohr-Coulomb เพื่อยืนยันผลการตรวจวัดการทรุดตัวที่ผิวดินทั้งกรณีการขุด
เจาะอุโมงค์ปกติ การขุดเจาะอุโมงค์ผ่านได้ฐานรากเสาเข็มสะพานคลองตัน และขุดเจาะอุโมงค์ผ่าน
ด้านข้างฐานรากเสาเข็มมอเตอร์ไฟฟ้า BTS อัตราส่วนระหว่าง Young Modulus กับกำลังรับแรง
เฉือนของดิน (E_u/S_u) จากการวิเคราะห์กลับด้วยวิธีไฟไนต์อีลิเมนต์ พบว่ามีค่าประมาณ 240, 360 และ
480 สำหรับดินเหนียวอ่อน ดินเหนียวแข็งปานกลาง และดินเหนียวแข็งมากตามลำดับ ในขณะที่ ค่า
Drain Modulus (E' , kN/m²) ในชั้นทรายแน่นมีค่าประมาณ $2000N_{60}$ ผลการประเมินการทรุดตัวที่
ผิวดินด้วยวิธี Empirical พบว่าค่าขอบเขตความกว้างของการทรุดตัว (i) มีค่าประมาณ $0.24z_0 -$
 $0.35z_0$ สำหรับการขุดเจาะอุโมงค์ในชั้นทรายแน่น และเพิ่มกว้างขึ้นเป็นประมาณ $0.46z_0$ สำหรับการขุด
เจาะอุโมงค์ในชั้นดินเหนียวแข็งดินดาน

ภาควิชา.....วิศวกรรมโยธา.....
สาขาวิชา.....วิศวกรรมโยธา.....
ปีการศึกษา2549.....

ลายมือชื่อนิติ.....
ลายมือชื่ออาจารย์ที่ปรึกษา.....
ลายมือชื่ออาจารย์ที่ปรึกษาร่วม.....

4671844721: MAJOR CIVIL ENGINEERING

KEY WORD: EPB SHIELD TUNNELING/ GROUND LOSS/ GROUND MOVEMENTS/ OBSTRUCTIONS/ FE BACK SIMULATION

SOKTAY LIM: GROUND MOVEMENT RESPONSE DUE TO EARTH PRESSURE BALANCE SHIELD TUNNELING IN BANGKOK SUBSOIL.

THESIS ADVISOR: ASSOC. PROF. WANCHAI TEPARAKSA, D. Eng.,

THESIS CO-ADVISOR: PROF. SATORU SHIBUYA, Ph.D., 176 pp.

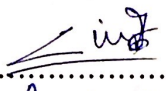
Ground surface and subsurface movement behaviors remained the questions, especially for the tunnels bored in the densely populated urban area where the several obstructions are usually found along the tunneling route. This research aims to study the behavior of ground surface and subsurface deformations due to tunneling and to do the back analysis based on the 2D FE analysis for an appropriate settlement prediction of tunnel in Bangkok.

An OD 5.55 m flood diversion tunnel of Saensaep-Latphroa Phrakhanong project was bored by means of EPB shield machine in both dense silty sand and hard silty clay layers with centerline at about 27.50 m below ground surface. Half route of the tunnel was bored underneath two bridges and busy roads. The recorded ground surface and subsurface response can be classified into 3 phases as deformation in front of the shield face, deformation within the shield body and deformation due to tail void behind the shield. The major ground surface settlement induced by tail void is about 63-67% of total ground surface settlement for tunneling in both dense silty sand and hard silty clay layers. The 2D FE analysis was carried out based on Elasto-Plastic (Mohr-Coulomb) failure criteria to confirm with ground settlements monitored at different cases of tunneling: tunnel bored without obstructions, under the Klongtan bridge pile foundation and adjacent to the BTS sky train pile foundation. The ratio E_u/S_u for FE analysis has been confirmed as 240, 360 and 480 for soft clay, medium stiff clay and stiff silty clay layers, respectively. In addition, $E'(\text{kN/m}^2) = 2000.N_{60}$ can be used for dense silty sand layers. The surface settlement trough width, i , based on empirical method is found between $0.24z_0$ and $0.35z_0$ for tunnel excavated in dense silty layer and it is increased to $0.46z_0$, which is wider, for tunnel in hard silty clay.


Department.....Civil Engineering.....

Field of study.....Civil Engineering.....

Academic year.....2006.....

Student's signature..........

Advisor's signature..........

Co-advisor's signature..........

ACKNOWLEDGEMENT

Many people have supported me in different ways during my doctoral program at both Chulalongkorn University and Kobe University. Without their helps and supports, this work is not possible.

I would like to thank JICA and AUN/Seed-Net for their financial support without their funding the starting point cannot happen.

I deeply appreciate the enormous academic support from three professors: Associate Professor Dr. Wanchai TEPARAKSA, major advisor, for his advice on this work and for provision on necessary documents; Professor Dr. Satoru SHIBUYA, co-advisor, for his encouragement and invaluable advice not only during my research in geotechnical laboratory at Kobe University, but also during my works at Chulalongkorn University; Assistant professor Dr. Tirawat BOONYATEE, committee member, for his encouragement and revision of some parts related to the review of Finite Element Method.

This field data collection won't be possible without cooperation and involvement of the following personnel of a joint venture of Italian-Thai Development PCL and Nishimatsu Construction Co., Ltd. in Bangkok: Mr. Kobchai PORNPRASIT and Mr. Sumate SANGMANEE, site engineers.

I am grateful to Assistant Professor Dr. Sangrawee CHAOPRICHA, Technical writing professor for being my editor.

In addition, the author likes to express his cordial thanks to all the thesis committee members for their invaluable comments during the thesis proposal defense.

A further word of thanks is devoted to all the former master students of Geotechnical Engineering Division, Chulalongkorn University, and the PhD students under supervision of Associate Professor Dr. Wanchai TEPARAKSA for their support on FEM analysis and the research activities.

Finally, very special gratitude goes to my family in Cambodia, my parents, brother and sisters, and especially my wife, Sodany TANN and my daughter Seavmey LIM for their mental support, continuous encouragement, and patience.

CONTENTS

	Page
Abstract in Thai.....	iv
Abstract in English.....	v
Acknowledgement	vi
Contents	vii
List of Tables	xi
List of Figures	xii
List of Symbols	xviii
Chapter I.....	1
Introduction.....	1
1.1 Motivation and Background	1
1.2 Statement of the Problem.....	3
1.3 Research Objectives.....	3
1.4 Research Scope	4
1.5 Strength of the Study	4
1.6 Layout of the Thesis.....	5
Chapter II	6
TBM and Tunneling Method	6
2.1 History of Shield Tunneling Methods.....	6
2.2 Different Kinds of TBMs.....	8
2.2.1 Rock TBMs.....	8
2.2.2 Soft Ground TBMs	10
2.2.3 Slurry Shield Machine	11
2.2.4. EPB Shield Machine	12
2.3 Criteria for Selection of Soft Ground TBMs	13
2.4 EPB Tunneling Method	17
2.4.1 History of EPB Shield Machine: its development and implementation	17
2.4.2 Tunnel Excavation	20
2.4.3 Erection of Segmental Lining.....	22

2.4.4 Grouting of Tail Void	24
Chapter III	26
Geology and Subsoil Conditions	26
3.1 Geology of Bangkok Soil.....	26
3.2 Underground Water of Bangkok.....	28
3.3 Subsoil Conditions along the Tunneling Route of the Project.....	29
Chapter IV	32
Tunnel Induced Ground Movements	32
4.1 Causes of Soil Displacements around Tunnels in Soft Soil.....	32
4.1.1 Displacement Vectors in Soft Soils	32
4.1.2 Causes of Soil Displacements	33
4.2 Predicting Methods of Ground Displacements	38
4.2.1 Empirical Methods.....	40
4.2.2 Analytical Methods	48
4.2.3 Laboratory Testing.....	53
4.2.4 Numerical Analysis Methods.....	55
4.3 Appropriate Methods for Analyses of the Research Project.....	58
Chapter V	59
Project Description and Monitoring System.....	59
5.1 General Description	59
5.2 Soil Profiles of Selected Analysis Sections	63
5.3 TBM Used in the Project	65
5.4 Tunnel Properties	67
5.5 Monitoring System.....	68
5.5.1 Inclimeters.....	69
5.5.2 Extensometers	71
5.5.3 Total Earth Pressure Cells.....	74
5.5.4 Convergence Bolts	75
5.6 Layouts of Instrumentation at the Sites of the Study	76
Chapter VI.....	78
Numerical Method and Analyses.....	78
6.1 Sign Conventions and Units.....	79
6.1.1 Sign Conventions	79
6.1.2 Units.....	79

6.2 Geometric Input	80
6.3 Mesh Generation	80
6.4 Elements and Accuracy of Calculation	81
6.5 Structural Elements	82
6.6 Interfaces	83
6.7 Soil Models	83
6.8 Automatic Load Stepping	85
6.9 Staged Construction	85
6.10 Upgraded Lagrangian Analysis	86
6.11 Mohr Coulomb Model and Analysis Options	86
6.11.1 Mohr Coulomb Model	86
6.11.2 Undrained Analysis with Effective Parameters	89
6.11.3 Undrained Analysis with Undrained Parameters	91
6.11.4 Relationship between Undrained Shear Strength and Soil Stiffness	91
6.11.5 Determination of Coefficient of Lateral Earth Pressure	96
6.12 PLAXIS Used in Previous Research Studies	98
6.13 Analysis Method of this Study	99
6.13.1 Selection of Field Monitored Data	100
6.13.2 Classification of Ground and Structural Movements	100
6.13.3 Empirical Method of Analysis	100
6.13.4 FE Analysis	101
6.13.4.1 Model Configuration	101
6.13.4.1 Simulation of Tunnel Excavation	102
Chapter VII	103
Observed and Computed Ground and Structural Movements	103
7.1. Ground Movements	103
7.1.1. Behaviors of Ground Surface and Subsurface Deformation	107
7.1.2. Ground Surface Settlements	108
7.1.3. Subsurface Settlements	111
7.1.4. Lateral Displacements	112
7.2. Structural Responses	114
7.3 Internal Forces of Segmental Lining	119
7.4. Discussion	128
7.4.1. Surface and Subsurface Deformation	128

7.4.2. Effects of Existing Structures on FE Analysis.....	129
Chapter VIII.....	130
Conclusions and Recommendations	130
8.1 Conclusions.....	130
8.2 Recommendations.....	131
References.....	133
Appendices.....	142
Appendix A.....	143
Summary of Soil Testing Results	143
Appendix B	150
Monitored Data	150
Appendix C	163
EPB Shield Machine	163
Appendix D.....	167
Model Geometries for FE Analyses and Output Graphics	167
Vita.....	176

LIST OF TABLES

	Page
Table 2.1 Conventional Machines (Monsees, 1996)	15
Table 2.2 Special Machines (Monsees, 1996)	16
Table 2.3 Tunnels constructed with EPB tunneling method.....	19
Table 5.1 Types of Instrumentation and Measurements	69
Table 6.1 Structural properties for FEM analyses at Klongtan Bridge and BTS-Sukhumvit areas.....	95
Table 6.2 Soil parameters for FEM analyses at Klongtan Bridge area.....	95
Table 6.3 Soil parameters for FEM analyses at BTS-Sukhumvit area	96
Table 7.1 Magnitude of structural settlements at Klongtan Bridge area	119
Table A.1 Summary of test results from borehole No.8	144
Table A.2 Summary of test results from borehole No.9	146
Table A.3 Summary of test results from borehole No.18	148
Table B.1 Data of ground surface settlement, array number GS16	151
Table B.2 Data of ground surface settlement, array number GS17	152
Table B.3 Data of ground surface settlement, array number GS18	153
Table B.4 Data of ground surface settlement, array number GS-BTS	154
Table B.5 Data of ground surface settlement, array number G35	154
Table B.6 Data of extensometer number ME-1 (Klongtan Bridge area).....	155
Table B.7 Data of extensometer number ME-2 (BTS-Sukumvit area)	155
Table B.8 Lateral movements obtained from IC (BTS-Sukumvit area).....	156
Table B.9 Lateral movements obtained from IC (cont.).....	157
Table B.10 Lateral movements obtained from IC (cont.).....	158
Table B.11 Lateral movements obtained from IC (cont.).....	159
Table B.12 Data of Klongtan bridge's settlement	160
Table B.13 Data of 3-storey chophouses' settlement	161
Table B.14 Data of 4-storey chophouses' settlement	162

LIST OF FIGURES

	Page
Figure 2.1 Marc Isambard Brunel's rectangular tunneling shield (Gardner, 1996).....	7
Figure 2.2 Open TBM or gripper TBM (Wirth Company).....	9
Figure 2.3 Shielded TMB (LOVAT Company).....	10
Figure 2.4 Principle of slurry shield machine (EFNARC, 2005)	12
Figure 2.5 Principle of EPB shield machine (Herrenknecht Company).....	13
Figure 2.6 Applicability of soft ground machines versus grain size (Monsees, 1996)	14
Figure 2.7 Typical EPB shield introduced by Sato Kogyo Company, 1963 (cited by Suwansawat, 2002)	17
Figure 2.8 Reversing belt conveyor transporting excavated soil (BMA flood diversion project, Saensaep-Latphrao Phrakhanong).....	21
Figure 2.9 Train cars transporting excavated soil (BMA flood diversion project, Saensaep-Latphrao Phrakhanong).....	21
Figure 2.10 Hydraulic jacks pushing on the segmental lining behind the shield (BMA flood diversion project, Saensaep-Latphrao Phrakhanong).....	22
Figure 2.11 Reinforced segmental linings of BMA flood diversion project (Saensaep-Latphrao Phrakhanong)	23
Figure 2.12 Erector arm installing a segmental lining at the crown of the tunnel (BMA flood diversion project, Saensaep-Latphrao Phrakhanong).....	23
Figure 2.13 Tunnel lining after erection (BMA flood diversion project, Saensaep-Latphrao Phrakhanong)	24
Figure 2.14 Grouting pipe attaching to grout hole (BMA flood diversion project, Saensaep-Latphrao Phrakhanong).....	25
Figure 3.1 Map of Thailand (Shibuya and Tamrakar, 2003)	27
Figure 3.2 General subsoil profile (Teparaksa, 1999)	27
Figure 3.3 Piezometric level of Bangkok subsoils (Teparaksa, 1999)	29
Figure 3.4 Boreholes and soil profile along the route of the BMA flood diversion tunnel (Saensaep-Ladphrao Phrakhanong)	30

Figure 4.1 Vectors of soil displacements around model tunnel (a) in clay (Mair, 1979) and (b) in sand (Potts, 1976) (cited by O'Reilly and New, 1982).....	33
Figure 4.2 Causes of ground loss during shield tunneling.....	35
Figure 4.3 Ground movements due to shield advancement (JSCE, 1996)	37
Figure 4.4: Behaviors of ground displacements caused by EPB tunneling (Teparaksa, 2005a).....	38
Figure 4.5 Settlement trough above an advancing tunnel (Attewell et al., 1986).....	40
Figure 4.6 Transverse settlement trough (Peck, 1969)	41
Figure 4.7 Relation between settlement trough width parameter and depth of tunnel for different soil conditions (Peck, 1969)	42
Figure 4.8 Variation of trough width parameter, i , with tunnel depth (O'Reilly and New, 1982).....	43
Figure 4.9 Shape of surface and subsurface settlement profiles (Mair et al., 1993)....	45
Figure 4.10 Variation of subsurface settlement trough width parameter, i , with depth for tunnel in clays (Mair et al., 1993)	45
Figure 4.11 Variation of K for subsurface settlement profile with depth above tunnel in clays (Mair et al., 1993)	46
Figure 4.12 Subsurface settlements above the tunnel axis in London Clay (Mair et al., 1993)	47
Figure 4.13 Correlation of maximum subsurface settlement (Luangpitakchumpol et al., 2005)	48
Figure 4.14 Point sink (ground loss) and virtual image technique (Sagaseta, 1987)...	49
Figure 4.15 Ground loss and ovalization of a tunnel (Verruijt and Booker, 1996)	51
Figure 4.16 Definition G_{AP} (Lee et al., 1992)	53
Figure 5.1 Location of BMA flood diversion tunnel (Saensaep-Latphrao Phrakhanong project)	60
Figure 5.2 Klongtan bridge area (BMA flood diversion tunnel project)	61
Figure 5.3 Klongtan bridge and old shophouses.....	62
Figure 5.4 BTS-Sukumvit area (BMA flood diversion tunnel project)	62
Figure 5.5 BTS sky train and shophouses above the curvature alignment	63
Figure 5.6 Subsoil profile at Klongtan Bridge area and cross section (section AA) ...	64
Figure 5.7 Subsoil profile at BTS-Sukumvit area and cross section (section BB)	64
Figure 5.8 General feature of articulated shield (Sramoon et al., 2006).....	65

Figure 5.9 Schematic of articulated EPB shield for MBA flood diversion tunnel (Saensaep-Latphrao Phrakhanong project)	66
Figure 5.10 Sectional view of tunnel lining	67
Figure 5.11 Water sealing material (Hydrotite, RS type)	68
Figure 5.12 Inclinator system (Slope Indicator Company, 2004)	70
Figure 5.13 Incremental and cumulative deviation (Slope Indicator Company, 1994)	71
Figure 5.14 Extensometers above and at the side of the tunnel (BMA flood diversion tunnel project)	72
Figure 5.15 Components of magnetic extensometer and their positions after installation (Slope Indicator Company, 2004)	73
Figure 5.16 Total earth pressure cell and its position after embedding in the tunnel segmental lining (BMA flood diversion tunnel project)	74
Figure 5.17 Typical installation of convergence bolts and monitoring patterns	75
Figure 5.18 Tape extensometer (BMA flood diversion tunnel project)	76
Figure 6.1 Coordinate system and sign conventions for stress components (Brinkgreve, 2002)	79
Figure 6.2 Nodes and stress points in soil elements (Brinkgreve, 2002)	82
Figure 6.3 Position of nodes and stress points in a 3-node and a 5-node beam element (Brinkgreve, 2002)	82
Figure 6.4 Results from standard drained triaxial tests (a) and Mohr Coulomb model (b) (Brinkgreve, 2002)	87
Figure 6.5 Mohr Coulomb yield surface in principal stress space for cohesionless soil (Brinkgreve, 2002)	88
Figure 6.6 Typical shear modulus and shear strains for different geotechnical works (Mair, 1993)	92
Figure 6.7 Variations of $G_{\text{sec(in-situ)}}/S_u$ with shear strains; (a) S_u from MTX, (b) S_u from field vane shear tests (Shibuya et al., 2001)	92
Figure 6.8 Shear modulus of Bangkok clays (a) soft clay and (b) stiff clay (Teparaksa, 2005a and b)	93
Figure 7.1 Input geometries of different analysis sections at Klongtan Bridge area; (a) GS16, (b) GS17 and (c) GS18	104
Figure 7.2 Input geometries of different analysis sections at BTS-Sukhumvit area; (a) GS-BTS and (b) GS35	105

Figure 7. 3 Finite element mesh generated at section AA (Klongtan Bridge area) ...	106
Figure 7.4 Finite element mesh generated at section BB (BTS-Sukhumvit area)	106
Figure 7.5 Behaviors of surface and subsurface deformation at extensometer ME-1 (Klongtan Bridge area)	107
Figure 7.6 Behaviors of surface and subsurface deformation at extensometer ME-2 (BTS-Sukhumvit area).....	108
Figure 7.7 Surface settlements monitored and computed at Klongtan Bridge area; (a) GS16, (b) GS17 and (c) GS18	109
Figure 7.8 Surface settlements monitored and computed at BTS-Sukhumvit area (a) GS-BTS and (b) GS35	110
Figure 7.9 Subsurface settlements along Extensometer ME-1 at Klongtan Bridge area	111
Figure 7.10 Subsurface settlements along Extensometer ME-2 at BTS-Sukhumvit area.....	112
Figure 7.11 Lateral displacements caused by tunnel in hard silty clay at BTS-Sukhumvit area (Inclinometer, IC).....	113
Figure 7.12 Location of structural settlement points monitored on Klongtan bridge	115
Figure 7.13 Location of point H monitored on Klongtan bridge	116
Figure 7.14 Behaviors of bridge foundation settlements caused by EPB tunneling in dense silty layer	116
Figure 7.15 Location of point C ₁ and C ₂ monitored on 3-storey shophouse	117
Figure 7.16 Behaviors of 3-storey old shophouse settlements in response to EPB tunneling in dense silty layer	118
Figure 7.17 Behaviors of 4-storey old shophouse settlements in response to EPB tunneling in dense silty layer	118
Figure 7.18 Bending moments in the tunnel lining at the final phase of simulation for section GS16, the extreme bending moment is 151.78 kNm/m.....	120
Figure 7.19 Axial forces in the tunnel lining at the final phase of simulation for section GS16, the extreme axial force is -510.18 kNm/m	120
Figure 7.20 Shear forces in the tunnel lining at the final phase of simulation for section GS16, the extreme shear force is 115.31 kNm/m	121
Figure 7.21 Axial forces in the tunnel lining at the final phase of simulation for section GS17, the extreme axial force is -505.34 kNm/m	122

Figure 7.22 Shear forces in the tunnel lining at the final phase of simulation for section GS17, the extreme shear force is 113.49 kNm/m	122
Figure 7.23 Bending moments in the tunnel lining at the final phase of simulation for section GS17, the extreme bending moment is 155.27 kNm/m.....	123
Figure 7.24 Axial forces in the tunnel lining at the final phase of simulation for section GS18, the extreme axial force is -485.61 kNm/m	123
Figure 7.25 Shear forces in the tunnel lining at the final phase of simulation for section GS18, the extreme shear force is 109.52 kNm/m	124
Figure 7.26 Bending moments in the tunnel lining at the final phase of simulation for section GS18, the extreme bending moment is 150.42 kNm/m.....	124
Figure 7.27 Axial forces in the tunnel lining at the final phase of simulation for section GS-BTS, the extreme axial force is -439.08 kNm/m.....	125
Figure 7.28 Shear forces in the tunnel lining at the final phase of simulation for section GS-BTS, the extreme shear force is 129.82 kNm/m	126
Figure 7.29 Bending moments in the tunnel lining at the final phase of simulation for the section GS-BTS, the extreme bending moment is -132.43 kNm/m.....	126
Figure 7.30 Axial forces in the tunnel lining at the final phase of simulation for section GS35, the extreme axial force is -370.15 kNm/m	127
Figure 7.31 Shear forces in the tunnel lining at the final phase of simulation for section GS35, the extreme shear force is -142.78 kNm/m.....	127
Figure 7.32 Bending moments in the tunnel lining at the final phase of simulation for section GS35, the extreme bending moment is -147.08 kNm/m	128
Figure A.1 Typical soil profile of borehole No.8	145
Figure A.2 Engineering properties of borehole No.8 for FE analysis	145
Figure A.3 Typical soil profile of borehole No.9	147
Figure A.4 Engineering properties of borehole No.9 for FE analysis	147
Figure A.5 Typical soil profile of borehole No.18	149
Figure A.6 Engineering properties of borehole No.18 for FE analysis	149
Figure C.1 Articulated EPB shield for MBA flood diversion tunnel (Saensaep-Latphrao Phrakhanong project)	164
Figure C.2 Front view of EPB	165
Figure C.3 Back view of EPB.....	165
Figure C.4 Backup unit of EPB	166
Figure D.1 Input geometry of section GS16.....	168

Figure D.2 Deformation mesh generated at section GS16	168
Figure D.3 Total displacement arrows at section GS16	168
Figure D.4 Total displacement shadings at section GS16	169
Figure D.5 Input geometry of section GS17	169
Figure D.6 Deformation mesh generated at section GS17	169
Figure D.7 Total displacement arrows at section GS17	170
Figure D.8 Total displacement shadings at section GS17	170
Figure D.9 Input geometry of section GS18	170
Figure D.10 Deformation mesh generated at section GS18	171
Figure D.11 Total displacement arrows at section GS18	171
Figure D.12 Total displacement shadings at section GS18	171
Figure D.13 Input geometry of section GS-BTS	172
Figure D.14 Deformation mesh generated at section GS-BTS.....	172
Figure D.15 Total displacement arrows at section GS-BTS.....	172
Figure D.16 Total displacement shadings at section GS-BTS.....	173
Figure D.17 Input geometry of section GS35	173
Figure D. 18 Deformation mesh generated at section GS35	173
Figure D.19 Total displacement arrows at section GS35	174
Figure D.20 Total displacement shadings at section GS35	174
Figure D.21 Input geometry of section ME-2.....	174
Figure D.22 Deformation mesh generated at section ME-2	175
Figure D.23 Total displacement arrows at section ME-2	175
Figure D.24 Total displacement shadings at section ME-2	175

LIST OF SYMBOLS

2D	two dimensions or two dimensional
3D	three dimensions or three dimensional
A	sectional area, total area of settlement trough
BKK	Bangkok
BMA	Bangkok Metropolitan Administration
BTS	Bangkok Mass Transit System
c	cohesion
c_u	undrained cohesion
CH	inorganic clays of high plasticity
CL	inorganic clays of low to medium plasticity
Co	company
D	tunnel diameter
DEM	distinct element method
d_{eq}	equivalent thickness of a beam or plate
E	elastic stiffness or Young's modulus
E'	drained Young's modulus
E_{50}	average secant modulus
E_c	elastic stiffness of concrete
E_{oed}	oedometer modulus
E_{sec}	secant Young's modulus
E_u	undrained Young's modulus
E_{ur}	unloading Young's modulus
FDM	finite difference method
FE	finite element
FEM	finite element method
FVS	Field vane shear test
EPB	earth pressure balance
g	acceleration of earth gravity
G	shear modulus

G_{AP}	gap parameter
G_p	physical gap
G_{sec}	secant shear modulus
i	surface settlement trough width
I	moment inertia
IC	inclinometer
JSCE	Japan Society of Civil Engineers
JSST	Japanese standard for shield tunneling
Ltd	limited
K	empirical constant of proportionality or surface settlement trough width parameter, coefficient of total lateral earth pressure
K'	bulk modulus of soil skeleton
K_o	coefficient of lateral earth pressure at rest
K_w	bulk modulus of water
km	kilometer
m	meter
m	auxiliary elastic constant
ME	extensometer or magnetic extensometer
mm	millimeter
MRTA	Mass Rapid Transit Authority of Thailand
MTX	monotonic triaxial test
n	porosity
N_{60}	SPT N-value at 60% energy ratio
NATM	new Austrian tunneling method
OCR	overconsolidation ratio
OD	outer diameter
PCL	public company limited
R	radius of the tunnel
r_1, r_2	distances from the singular point and its image
R_{inter}	strength reduction factor of soil-structure interface
s	settlement
s_{max}	maximum settlement
S_u	undrained shear strength
SM-SP	poorly graded silty sand

TBM	tunnel boring machine
u	pore water pressure
u^*_{3D}	three-dimensional elastic deformation
u_x	displacement in x direction
u_y	displacement in y direction
V_s	volume of the surface settlement trough per unit length
V_L	volume loss or ground loss
x	transverse distance from the tunnel axis
z	depth from ground surface to any subsoil level
z_0	depth from ground surface to tunnel axis
α	scale factor in centrifuge model testing
δ	relative displacement caused by the ovalization of the tunnel, clearance between tunnel lining and tail skin of a TBM
Δ	thickness of tailpiece or tail skin of a TBM
ε	relative uniform radial displacement of the tunnel surface or uniform radial ground loss
ε_s	shear strain
γ_c	unit weight of concrete
γ	total unit weight
φ	friction angle
φ'	drained or effective friction angle
φ_u	undrained friction angle
κ	Cam-clay swelling index
κ^*	modified swelling index
λ	proportional parameter, Cam-clay compression index
λ^*	modified compression index
ν	Poisson's ratio
ν'	drained Poisson's ratio
ν_c	Poisson's ratio of concrete
ν_u	undrained Poisson's ratio
ρ	bulk density
ρ_w	water density

σ	total tress
σ'	effective stress
σ_0	initial tress or initial overburden
σ_h	total horizontal stress
σ'_h	effective horizontal stress
σ_v	total vertical stress
σ'_v	effective vertical stress
ω	workmanship factor
ψ	dilatancy angle

CHAPTER I

INTRODUCTION

1.1 Motivation and Background

As the problems of floods and transportation in many parts of the world have been seriously increasing for many years, some countries have taken several measures to solve these problems. One of the most acceptable solutions is a use of an available subsurface space for tunnel constructions, since these structures can be served either for subway transportation, water supply, or flood diversion.

The tunnel construction by using the cut-and cover techniques in urban areas invades the social lives of the people who are living along the construction route as well. One of the strongest impacts of these techniques on people in their vicinity is traffic congestion. In addition, these techniques usually cause the excessive ground surface movements. In order to eliminate or to reduce such problems, the tunnel boring machines (TBMs) has been invented. The most well known TBM has been used in the Southeast Asian region, especially in Thailand, is Earth Pressure Balance (EPB) shield machine. The use of EPB for soft ground tunneling is a relatively new but it is very efficient because it uses high technology developed for civil engineering works. This EPB machine enhances the availability of underground space through soft-soil tunneling, which is heavily in demand especially in such a crowded metropolis as Bangkok. The machine is possibly adjusted to be used in complicated geological conditions, for example clay, silty clay, clayey and silty sand soils below the water table where engineers previously found it difficult for tunnel construction.

The tunnel constructed using an EPB machine seems to minimize the volume of ground loss and provide a perfect appearance of the permanent structure; however, the machine operators and workers must have enough competency and knowledge relative to this work. Moreover, the prediction of ground and structural movements induced by the tunnel excavation should be accurately given in order to protect the surrounding environment and accommodate daily activities on the ground surface.

The latter could be fulfilled based on the experiences and back-analyses of the case studies from the previous tunneling projects as well as the considerations used in the analysis model.

For the past several decades, the approximate (empirical and analytical) methods have been extensively used for estimating the ground movements responding to the tunnel excavations as well as determining the internal forces of concrete lining. Nevertheless, the use of these methods seems to be difficult for the tunnel constructed in such extreme conditions as urban areas with heterogeneous soil conditions and water bearing soils presented and also with different underground obstructions for example pile foundations. To facilitate these problems, many Finite Element Method (FEM) and Finite Difference Method (FDM) programs have been developed with the window base. In the elastic or elasto-plastic analysis, the soil stiffness (E or G) and poisson's ratio (ν) play an important role in predicting the movements of the ground surface and subsurface as well as the structures in the analysis model.

Regarding the soil stiffness, it is used as a base parameter for designing a tunnel. Mair (1993) has proposed a wide range of shear modulus (G) obtained in the interval of shear strain between 0.1 and 1%. In order to simplify the way for selecting soil stiffness, the designers have linked this parameter to the shear strength with a constant number according to their work experiences on a specific area such as Prinzl and Davies (2006) used FDM with the undrained soil stiffness $E_u = 225c_u$ and $E_u = 400c_u$ for soft and stiff clays respectively to design the tunnel in Bangkok (North Contract of MRTA subways). However, to avoid the unrealistic heave in the area underneath the tunnel, the unloading elastic modulus $E_{ur} = 375c_u$ and $E_{ur} = 800c_u$ were applied to this area for soft and stiff clays respectively. However, Teparaksa (1999) and Teparaksa and Heidengren (1999) proposed the value $E_u = 240S_u$ and $E_u = 480S_u$ for soft and stiff clay, respectively, to predict the ground displacement due to EPB shield tunneling in Bangkok without distinction the loading and unloading areas. In addition, Teparaksa (2005a) used the value of drained modulus $E'(\text{kN/m}^2) = 2000.N_{60}$ (N_{60} is the SPT N-value at 60% Energy Ratio) for silty sand to design a tunnel boring in Bangkok subsoils.

1.2 Statement of the Problem

The study of ground surface and subsurface movement behaviors is remained the questions for tunnel researchers, especially for the tunnel bored in the densely populated urban area where the several obstructions are usually found along the tunneling route. Several researchers have conducted studies on tunnel construction in order to provide a better prediction related to these issues such as Peck (1969) proposed a normal contribution curve to predict the transverse settlement profile based on the field monitoring. Vereuijt and Booker (1996) proposed an analytical solution, which is an extension of a method suggested by Sagaseta (1987), for a tunnel in a homogeneous elastic half-plane to predict the ground surface and subsurface movements caused by a uniform radial ground loss. However, this analytical solution was modified by Loganathan and Poulos (1998) by redefining the equivalent ground loss parameters with respect to the gap parameter in order to predict the ground movements around the tunnel in clays.

The geological and existing conditions along the tunnel route vary depending on regions, and the empirical method of Peck (1969) is limited to such various conditions. The analytical solutions are currently proposed and based on only a few case studies for the tunnel in clays. In addition, the surface loads as well as their structures were not taken into account for the prediction.

The understanding of ground movement behaviors leads to a minimization of their displacement as well as the excessive settlements of the structures located above the tunneling route. Based on the studies of tunnel excavation and back-analyses of the case studies from the previous tunneling projects located in the same region using FE analysis program, this minimization could be achieved. Therefore, this research intends to study the behaviors of ground surface and subsurface deformations and to do a back analysis based on the FE program in order to help designers to make an accurate prediction as well as to make the most effective tunnel in Bangkok, which can last for a long time.

1.3 Research Objectives

This thesis is limited to the description of only three aspects as follows:

- 1.) The behaviors of ground surface, subsurface and structural movements in response to the EPB shield machine tunneling in Bangkok subsoils for Saensaep-Latphrao Phrakhanong Flood Diversion Tunnel project.
- 2.) The use of the Mohr Coulomb soil model to back-analyze the ground surface and subsurface displacements due to EPB tunneling based on the results of field performance in various conditions such as driving beneath the bridge foundations, service roads, and through the underground obstructions. To achieve this objective, the two-dimensional (2D) Finite Element Method (FEM) program will be carried out.
- 3.) The confirmation of the design assumptions, which are resulted from the second objective, and the new approach and appropriate parameters in design of segmental linings will be proposed.

1.4 Research Scope

The scope of this study is limited to the behaviors of ground surface and subsurface movements as well as the structural settlements of Bangkok subsoils: silty sand and silty clay from tunneling work of the Saensaep-Latphrao Phrakhanong Flood Diversion Tunnel project. Two different locations along the tunneling route where the most comprehensive monitoring system for this project was implemented are selected for this study: one is Klongtan Bridge area where the tunnel was bored in dense silty sand and the other is BTS-Sukhumvit area where the tunnel was bored in hard silty clay layer. Based on FEM program, the back analyses and simulation are carried out to obtain the appropriate design parameter of Young's modulus. The different steps of calculation were performed based on 2D-FEM program to simulate the 3D advancement of the tunnel, and the elasto-plastic failure criteria of Mohr Coulomb soil model was used in this research.

1.5 Strength of the Study

The strength of this study is the consistent agreement of FE-simulation results with field monitored data for tunnel located in dense silty sand and hard silty clay layers, where different types of surface and underground obstructions were present. These results could be achieved due to the adequate dimension of the model to be

analyzed, the generated mesh and especially the selected elastic modulus for each soil layer. Therefore, these can be applied as a practical guideline for the designers to follow in order to obtain a more accurate prediction of ground and structural movements as well as a safe, efficient, and economical tunnel construction in Bangkok.

1.6 Layout of the Thesis

The thesis is divided into eight chapters. The first chapter gives an overview of the whole study while chapter two reveals different types of tunnel boring machines and the methods of tunnel construction related to each machine are also briefly described. However, the EPB shield tunneling method used in the project of this research is explained in detail in the last section of the chapter. Chapter three provides an overview of the geological conditions of Bangkok soil, an introduction of the subsoil profile along the tunnel route of the current tunneling project and the special characteristics of the underground water. In chapter four, several causes of ground movements due to tunnel excavation are mentioned. In addition, this chapter also provides a comprehensive overview of some empirical and analytical solutions, which are well known for estimating the ground surface and subsurface settlements induced by tunnel excavation. A short introduction to different ways of finite element simulation of tunnel excavation is given as well. Chapter five introduces the selected locations for this research, highlights the different obstructions and gives a detail of specification of the EPB shield machine used in the project. Additionally, the various monitoring systems and monitoring methods are also given. Chapter six presents an overview of the PLAXIS program and the specific options of the implementation of the program for the analysis in this research. The analysis method used in this study is described in the final section of the chapter.

Chapter seven contains the results of the research and some discussions regarding to the obtained results while chapter eight is the summary of the findings and some recommendations for future works.

CHAPTER II

TBM AND TUNNELING METHOD

In order to succeed with high benefits from tunneling work in a known geological condition, it is important for tunnel engineers to gain enough knowledge about the TBM and the method of construction related to each machine. This chapter describes the different kinds of TBMs, which are commercially available, and then the criteria for selecting some soft ground TBMs are also given. A more detail about the EPB tunneling method, which is used in the current tunneling project, is described in the last section of this chapter.

2.1 History of Shield Tunneling Methods

In tunneling work, a shield is used as a temporary structure to protect the workmen during excavation through soft soil or unstable rock. Based on Sutcliffe (1996), TBMs were first developed and used with soft grounds by Marc Isambard Brunel and James Henry Greathead in England. These shields progressed by breaking the excavation into small compartments excavated by hand. The first Brunel shield, patented in 1818, excavated these compartments and advanced the shield in a spiral pattern, with lining segments following in the same spiral. The shield did not rotate, but the spiral arrangement of the head meant that the inner excavated along a spiral path at right angles to the direction of the tunnel.

Subsequently, a rectangular cross-section of tunneling shield, which was also developed by Marc Isambard Brunel, was used to excavate a tunnel beneath the River Thames between Wapping on the north bank and Rotherhithe on the south one in London. The shield consisted of 12 connected iron frames which allowed a total of 36 workers to excavate the soil at its face safely. When the workers of all the cells had excavated about 4.5 inches of soil, the shield was then pushed forward by screw jacks and successively the brick tunnel lining was assembled behind it (Figure 2.1). This

tunneling was began in 1825 and finally completed in 1841 due to some difficulties during this period (Channel4). However the tunnel was officially opened in 1843.

The initial idea of tunneling shield construction was hitting Sir Brunel up when he saw the shell of the shipworm *Teredo navalis*, a mollusk whose efficiency at boring through submerged timber he observed while working in a shipyard (WIKIPEDIA, The Free Encyclopedia).

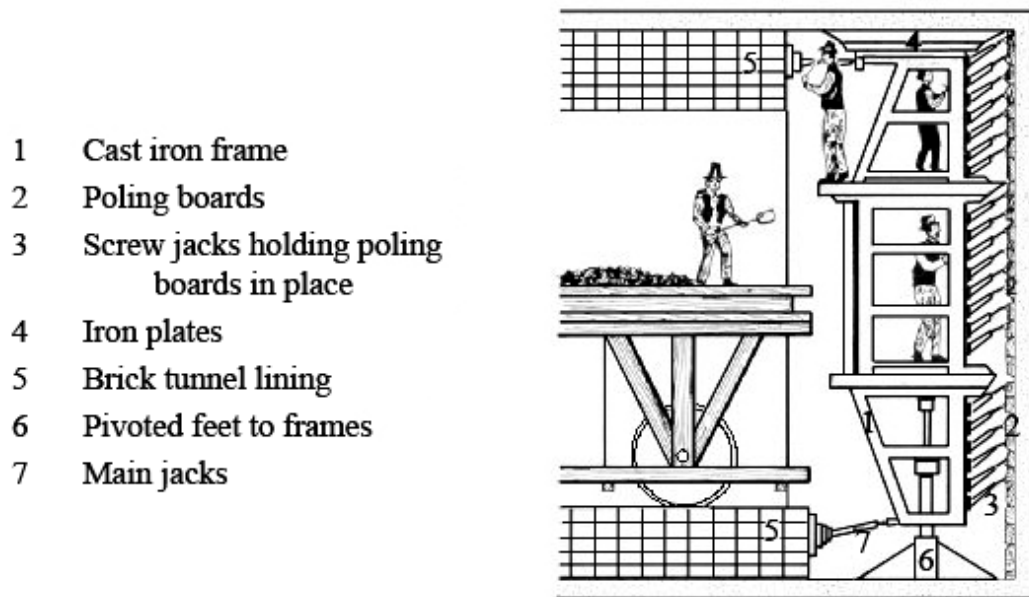


Figure 2.1 Marc Isambard Brunel's rectangular tunneling shield (Gardner, 1996)

Using a circular shield, which was in charged by James Henry Greathead, the second tunnel under the Thames was excavated in 1869. This shield offered greater protection to the miners against face collapse and it moved forward by screw jacks thrusting on the cast iron liners erected behind the shield. In addition, a lime slurry was used to grout the tail void behind the liner segments. It is the first time that the cast iron liners and lime slurry grout were used in tunnel construction. These circular shields gradually became more mechanized and exchanged features with the developing Rock TBMs (Sutcliffe, 1996).

2.2 Different Kinds of TBMs

During its service life, a TBM is heavily used day and night under the different underground environments and sometime it is subjected to very a high stress. According to Sutcliffe (1996), a TBM has five simple functions:

- To excavate the ground,
- To remove the material excavated,
- To maintain line and grade of the excavation,
- To support the excavated tunnel temporarily until permanent support can be provided,
- To handle adverse ground conditions.

Moreover, these functions must be performed:

- Safely,
- Reliably,
- Continuously for many months,
- Through any and all ground conditions,
- Quickly,
- Economically.

An overview of different kinds of TBMs, which are used for rock and/or soft ground tunneling, are given in the following sections.

2.2.1 Rock TBMs

The rock TBMs described here refer to Gripper TBMs or Open TBMs and Shielded TBMs, which are manufactured by Herrenknecht and Wirth Company. The gripper TBM (Figure 2.1) is suitable for driving in stable rock. The main elements in the construction of this open TMB are the cutter head with its associated drive housing, the support construction (the so-called gripper) and the advance mechanism. The cutter head is equipped with cutters (disks). The rotating cutter head presses the disks against the tunnel face applying high pressure. The disks perform rolling movements on the tunnel face causing the loosening of the rock. The excavated rocks, usually described as chips, are picked up by buckets (openings in the cutter head) and transported via hoppers onto the conveying system. The TBM conveyor transports the material for the complete length of the TBM to the transfer band between TBM and

backup system. From there, the excavated material is transported via conveyors either to the outside or to the loading dock of the muck cars.

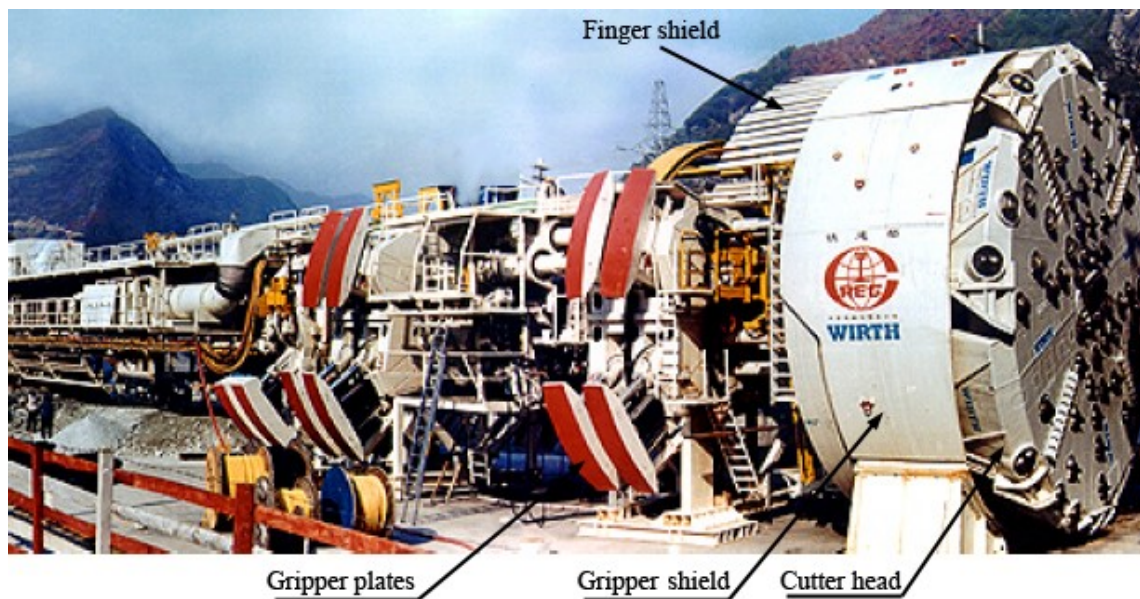


Figure 2.2 Open TBM or gripper TBM (Wirth Company)

When the boring machine is driven through unstable (or even stable) rock, the shielded TBM is necessary. The main elements in the construction of the shielded TMB, according to information issued by Wirth company on its website, consist of the shield which gives the machine its name, a construction-like steel tube in which all other components of the machine are embedded, the cutter head and its drive housing, the advance mechanism and the robot-like device for installation of the tunnel lining or the so-called erector. The tunnel lining, usually consisting of prefabricated concrete sections, is installed with the erector, protected by the rear shield mantle, the so-called tail shield. Shielded TBM, which can be used for tunneling in either stable or unstable rock is shown in Figure 2.2 (LOVAT Company).



Figure 2.3 Shielded TMB (LOVAT Company)

2.2.2 Soft Ground TBMs

Nearly all soft-ground tunneling machines are circular. Based on Monsees, (1996), these machines, including shields, have five basic components as follows:

- The *cutting edge* trims the outside perimeter of the tunnel. In a digger shield, a rotating “cheese grater” mounted on the face of a drum, the cutting edge cuts only those portions of the perimeters not excavated by the digger mechanism. With a fully mechanized tunneling machine the front edge occasionally may not cut the ground depending upon the configuration of the cutter head, specifically when gauge or perimeter cutters are used.
- The *body* of the machine is usually a steel cylinder, stiffened by generally vertical and horizontal bracing members, by the housing and attachments for the face support and propulsion jacking systems in a simple shield, and by the equipment in a tunneling machine. In a shield the bracing members also divide the face into the number of working pockets or zones that are necessary to provide safe and stable working cells for mining and mucking.

- The *tail* of the machine extends rearward from the body and provides protective cover for the workers and the out line for the erection of the tunnel support system. To assure the support system is always within the tail (or, conversely, that unsupported ground is never exposed) the tail length must be such that at least one-half of the length of the last fully erected supporting element stays within the tail shield when the shove jacks are fully extended.
- The *shove jack system* provides the forward propulsions for the machine. These jacks are located around the perimeter of the shield and are housed within the body. They usually obtain reaction for their thrust from the tunnel support system to the rear.
- The *hood* projects ahead of the body thereby providing protection for workers at the face, this portion located at the front of a classical shield. Working with this protection, the breasting or face support system is advanced stepwise to complete the excavation required for each shove of the shield. With a full-face or closed machine, there often is no hood, and face stability is provided by control of the openings in the machine face or cutting head.

(Monsees, 1996, pp. 97-121)

Since the tunnel face stabilization based on compressed air was found to be hard for human body, only two types of shields are commonly used for tunneling in water bearing soil: one is slurry shield machine and the other is EPB shield machine. The basic principle of these two machines is briefly described in the next sections, sections 2.2.3 and 2.2.4.

2.2.3 Slurry Shield Machine

Basic principle of this TBM is to maintain the tunnel's cutting face during the excavation phase by filling the working chamber, located behind the cutter head, with bentonite slurry (Wirth Company). In addition, the slurry acts as a means to transport the excavated soil, after mixing, from working chamber to the surface by pumping. The Figure 2.4 shows a schematic representation of the slurry shield machine, in which the slurry feed conduit and return pipe for suspension removal are mentioned.

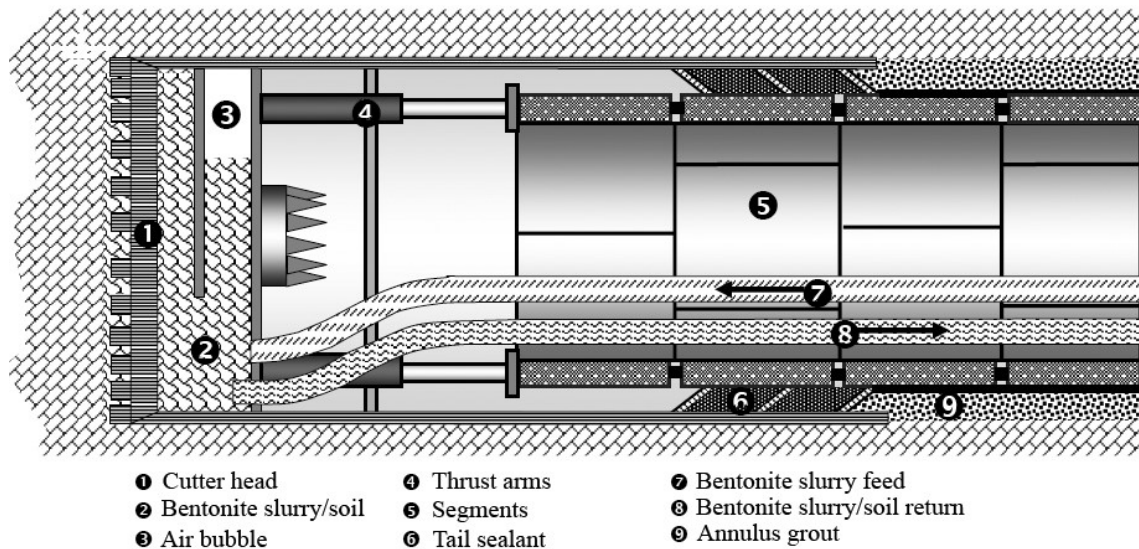


Figure 2.4 Principle of slurry shield machine (EFNARC, 2005)

2.2.4. EPB Shield Machine

In contrast to the other shields, the stability at the working face of EPB depends on a secondary support medium. In other words, the soil is loosened by the cutting wheel served to support the working face.

The shield area in which the cutting wheel rotates is designated as the extraction chamber and is separated from the shield section, which is under atmospheric pressure, by the pressure wall (Herrenknecht Company). In brief, the excavated material exits the extraction chamber by means of screw conveyor and then it is loaded in the train cars, which circulate in the tunnel, via a long reversing belt conveyor. The material is then discharged at the inlet shaft.

The EPB system is schematically shown in Figure 2.5, in which the extraction chamber, screw conveyor and erector arm are also mentioned. Since the EPB shield is selected for the current project, a relatively detailed description about the EPB tunneling method is given in section 2.4 of this chapter.

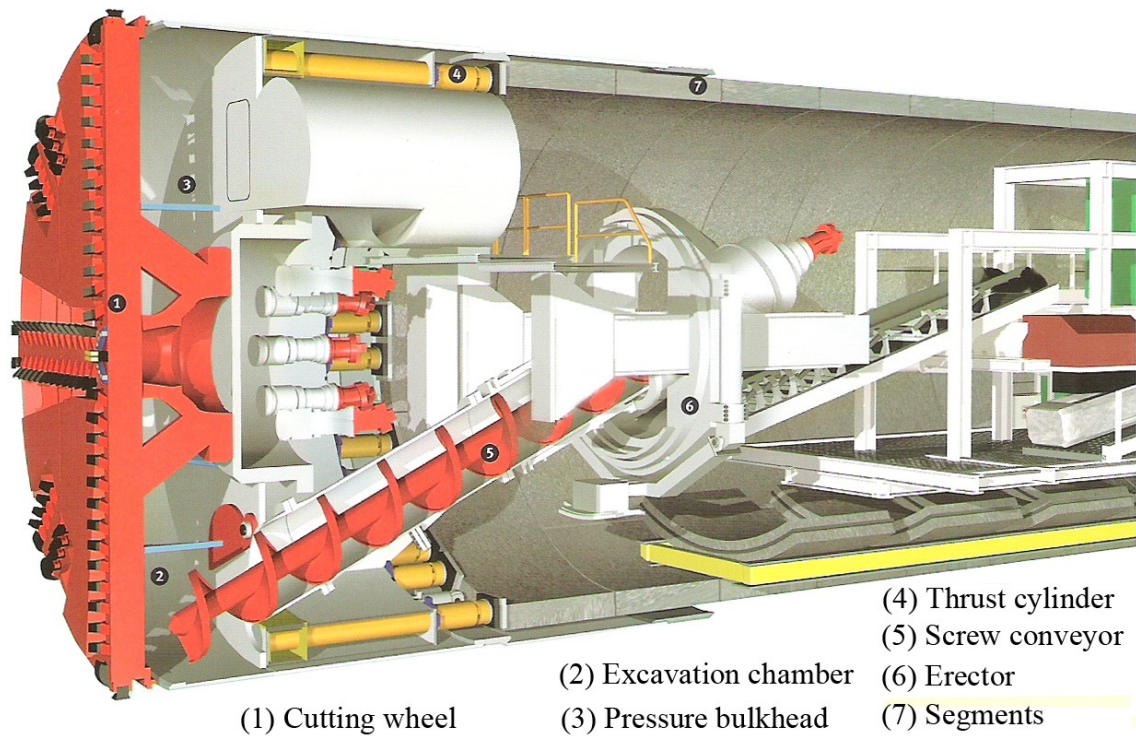


Figure 2.5 Principle of EPB shield machine (Herrenknecht Company)

2.3 Criteria for Selection of Soft Ground TBMs

In response to the development of underground space used for most urban areas, the soft ground tunneling deserves attention. However, the selection of a suitable TBM is a critical point for the success of construction. Monsees (1996) described some variables to be considered in selecting a soft-ground tunneling machine including water conditions, tunnel size, support system, excavation conditions, and the excavation environment.

Figure 2.6 shows the applicability of various soft ground machines in relation to the grain size distribution curve. Tables 2.1 and 2.2 contain a summary of the types of machines and their application to various ground conditions.

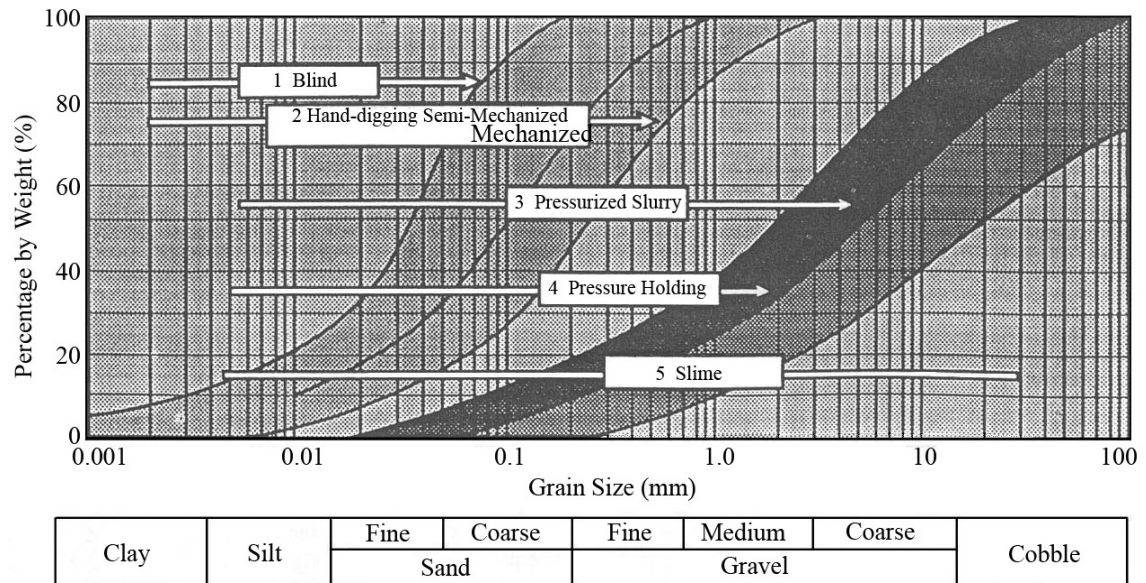


Figure 2.6 Applicability of soft ground machines versus grain size (Monsees, 1996)

An appropriate selection of TBM for a given subsoil condition leads to a high performance of tunneling work in terms of excavation speed, and problem minimization including safety. Although some tunneling machines can be used in various types of soil with different physical conditions, the selection of these machines depends also on the experience of machine operators.

Table 2.1 Conventional Machines (Monsees, 1996)

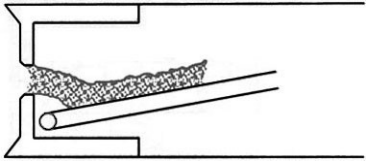
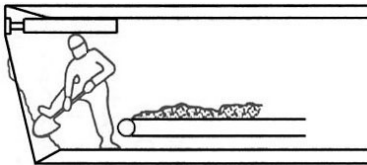
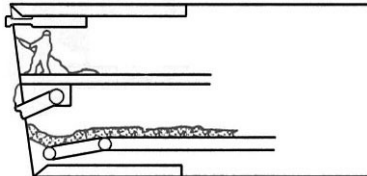
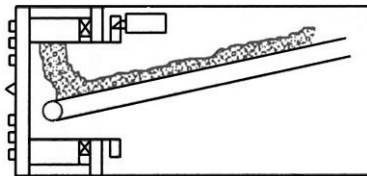
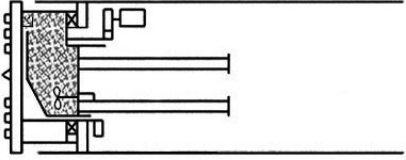
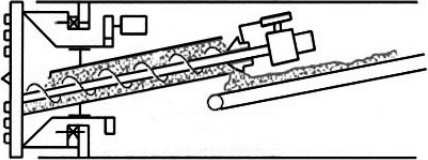
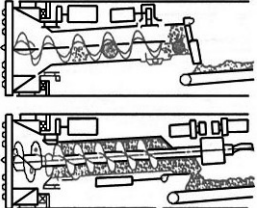
Type	Description	Notes	Sketch
Blind Shield	A closed face (or blind) simple shield used in very soft clays and silts. Muck discharge is controlled by adjusting the aperture opening and the advance rate.	Used in harbor and river crossings in very soft soils. Often results in a wave or mound of soil over the machine.	
Open face, hand-dug shield	Good for short, small tunnels in hard, non-collapsing soils. Usually equipped with face jacks to hold breasting at the face. If soft conditions require it, this machine may have movable hood and/or deck.	A direct descendent of the Brunel shield. Now largely replaced by more mechanized equipment. Sometimes used at the head of large cross-section, jacked tunnels.	
Semi-mechanized	Similar to the open face, but with a back hoe, boom cutter (roadheader) or the like.	Until very recently, the most common shield. Often equipped with “pie plate” breasting and one or more Tables. Can have trouble in soft, loose, or running ground. Compressed air may be used for face stability in poor ground.	
Mechanized	A fully mechanized machine. Excavates with a full face cutter wheel and pick or disc cutters.	Manufactured with a wide variety of cutting tools for various soils. Face openings (door, guillotine, and the like) can be adjusted to control the muck taken in versus the advance of the machine. May also be used with compressed air for face stability in poor ground.	

Table 2.2 Special Machines (Monsees, 1996)

Type	Description	Notes	Sketch
Slurry face machine	This machine uses pressurized slurry to balance the groundwater and soil pressure at the face. It has a bulkhead (closed face) to maintain the slurry pressure on the face; that slurry must be piped down and recycled from the surface. It may also be equipped with a stone crusher for occasional cobbles. This machine is good for water bearing silts and sands with the gravels.	Best for sandy soils; tends to gum up in clay soils; with coarse soils, face may collapse into the slurry. Coarse soils are defined as <ul style="list-style-type: none"> • Gravel content > 60% • Clay and silt content < 10% • Water content < 18% • Coefficient of permeability $\geq 10^{-2}$ cm/s • Cobbles greater than 8 in. 	
Earth Pressure Balance (EPB) machine	This machine has a closed chamber (bulkhead) face that uses trapped water and soil material to balance the groundwater and/or collapsing soil pressure at the face. It uses a screw discharger with a cone valve or other means to form a sand plug to control “balance” the earth pressure. It is good for clay and clayey and silty sand soils, generally below the water table	Also best for sandy soils, with acceptable conditions defined as <ul style="list-style-type: none"> • Clay and silt content > 7% • Gravel content < 70% • Cohesive soils (not less than 40% clay and silt) have N-value < 15. • Water content > 18% in sandy soils and > 25% in cohesive soils 	
EPB high-density slurry machine	A hybrid machine that injects a denser slurry (sometimes called slime) into the cutting chamber. Developed for use where soil is complex, lacks fines or water for an EPS machine, or is too coarse for a slurry machine.	Has worked in soil with 85% gravel content and cobbles and boulders up to 20 in.x10in.x7in. Has worked in sandy gravel soil with N=30 to 50 and sandy or silty soil with N=5 to 35.	

2.4 EPB Tunneling Method

The EPB shield machines are proffered machines for tunneling in clay, clayey or silty sand soils, generally below the ground water table. Moreover, in comparison with the slurry shield machines, the EPB shield makes the on site muck handling easier and eliminates the need for a sophisticated separation plant on the surface (EFNARC, 2005). The EPB shield machines are very well known in Thailand since they were used in all the previous important tunnel excavations in this country.

2.4.1 History of EPB Shield Machine: its development and implementation

Since the compressed air and slurry shield tunneling methods were found with some disadvantages and limitations, the Sato Kogyo Company Ltd. developed the first concept of EPB shield in 1963 as shown in Figure 2.7. After many experiments in the laboratory and in the field, this machine was successfully built in 1966 by Ishikawajima Harima Heavy Industries Company Ltd. The first EPB shield tunneling method was first used in 1974 on a 1900-meter collector drive in Tokyo (Suwansawat, 2002). The invention of this machine eliminated the need of slurry and compress air technique.

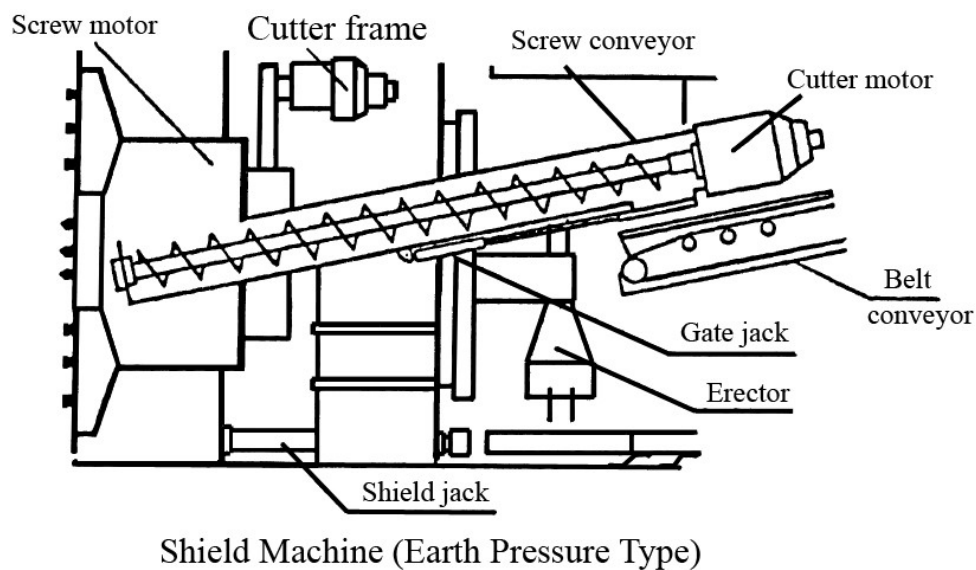


Figure 2.7 Typical EPB shield introduced by Sato Kogyo Company, 1963 (cited by Suwansawat, 2002)

Later , the EPB method had been extensively used in Japan. By 1980, around 16% of all the shield tunneling methods used for tunnel construction in this country were based on the EPB techniques (Naito, 1984 cited by Greenwood, 2003). Later on, the EPB shields were adopted and produced by the various manufacturers in order to respond to the demands of underground transportation system as well as other uses in the populated city.

Table 2.3 shows some examples of major tunneling projects where the EPB tunneling method was used. In some projects more than one EPB shield with different dimension, outer diameter (OD) and length, were used to complete the whole project. However, all the data given in the table are based on the available information provided by the related sources.

Table 2.3 Tunnels constructed with EPB tunneling method

Country, city/location	Tunnel/Project name	Length (km)	OD of tunnel (m)	OD of EPB shield (m)	Work period	Date open	Source of information
Japan, Tokyo	Tunnel excavation project of SJ51 to SJ53 (Clockwise Route)	2.0181	11.80	12.02	March 14, 2002 to February 15, 2005	-	Dobashi et al. (2006)
Thailand, Bangkok	Chaloem Ratchamongkhon Line Project of the Bangkok Mass Rapid	20	6.30	6.43	August 11, 1977 to August 4, 2002	2004	Tokuda et al. (2006)
Netherlands, Rotterdam	Botlek Rail Tunnel	3	9.45	9.775	1999 to 2002	2002	Maidl (1999)
Spain, Madrid	Line 10 of the Madrid Underground	2.15	7.20	7.38	1995 to 1996	1996	Arnaiz et al. (1998)
Canada, Sarina	St. Clair River Tunnel	1.80	9.2	9.52	March 1993 to May 1995	-	Wayss & Freytag Ingenieurbau AG
Singapore	Changi Airport line	7	5.90	6.15	1999 to -	2001	TAC (2000)
Italy, Milan	Milan Urban Link Line	3	7.5	8	-	-	Lunardi et al. (1993)

2.4.2 Tunnel Excavation

According to the information issued by Herrenknecht Company, the tunnel excavation based on EPB technique can be performed in the following procedures:

- The soil is loosened by the tools of the cutting wheel, drops through the openings in the cutting wheel into the extraction chamber (Figure 2.5) and mixes together with the plastic pulpy soil which is already there. Uncontrolled penetration of the soil from the working face into the extraction chamber is prevented by transferring the power of the tunneling jacks from the pressure wall to the pulpy soil. At the point when the pulpy soil mixture in the extraction chamber is no longer compressed by the pressure of the earth and water which lies ahead, a state of equilibrium is reached.
- The material which has been extracted is removed from the extraction chamber with a screw conveyor (Figure 2.5 and 2.7). The amount of material conveyed is regulated by the revolutions of the screw and the diameter of the opening of the upper screw valve.
- The screw conveyor transfers the extracted material to the first conveyor belt of the conveyor belt cascade (Figure 2.5). Via this belt, the extracted material reaches the so-called reversing belt. The transport cars for the extracted material in the backup system in the reversing operation are loaded via this belt.
- If the TBM is operated open (open mode), the screw for transporting the extracted material is bypassed and the extracted material is transported to the machine belts by the cutting wheel. To enable the extracted material to be offloaded to the machine belt the muck ring, located in the pressure wall, has to be retracted.

At the same time as the cutting face is rotating, screw and belt conveyor are moving the excavated soil (mud), the hydraulic jacks behind the shield are also extending in order to keep the face pressure in equilibrium as well as to advance the machine its self. For the EPB shield machine used in BMA flood diversion, Saensaep-Latphrao Phrakhanong project, each hydraulic jack has a maximum force of 1500 kPa and can extend up to 165 cm. Figures 2.8 and 2.9 show the transportation of

excavated soil by belt conveyor and train cars respectively while Figure 2.10 shows the hydraulic jacks in full extension.



Figure 2.8 Reversing belt conveyor transporting excavated soil (BMA flood diversion project, Saensaep-Latphrao Phrakhanong)



Figure 2.9 Train cars transporting excavated soil (BMA flood diversion project, Saensaep-Latphrao Phrakhanong)



Figure 2.10 Hydraulic jacks pushing on the segmental lining behind the shield (BMA flood diversion project, Saensaep-Latphrao Phrakhanong)

2.4.3 Erection of Segmental Lining

The segmental linings are commonly used with shield tunneling method, i.e. EPB method. In most purposes such as tunnel for subway transportation and sewage, the assembly of these segmental linings already provides a sufficient stability and serves as the final structure without secondary lining. For MBA flood diversion tunnel project (Saensaep-Latphrao Phrakhanong), one ring of the lining consists of five standard segments and one key segment, which is made from reinforced concrete, as shown in Figure 2.11. The installation of these segments was done within a space designated at the tail of the shield using the erector arm (Figure 2.12). A perfect look of the flood diversion tunnel after about two and half months of construction is shown in Figure 2.13.



Figure 2.11 Reinforced segmental linings of BMA flood diversion project (Saensaep-Latphrao Phrakhanong)



Figure 2.12 Erector arm installing a segmental lining at the crown of the tunnel (BMA flood diversion project, Saensaep-Latphrao Phrakhanong)

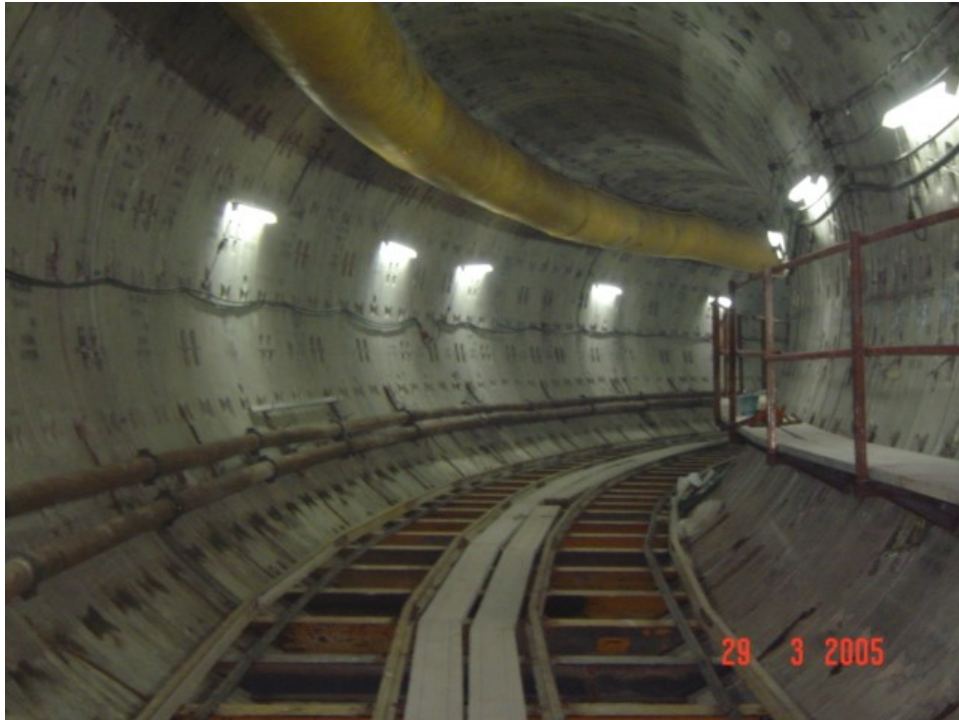


Figure 2.13 Tunnel lining after erection (BMA flood diversion project, Saensaep-Latphrao Phrakhanong)

2.4.4 Grouting of Tail Void

As the outer diameter of the tunnel lining is smaller than that of the excavation, the void always happens after the shield moves forward. This remaining void must be continuously injected with the grout material through the grout hole, which is located in the middle of each segment. For the BMA flood diversion project (Saensaep-Latphrao Phrakhanong), the injected grout is a mixture of material A and B of which a ratio is 92:8. The components of material A consist of cement, bentonite, water and stabilizer. However, material B consists of a special sodium silicate which serves as an accelerator. Figure 2.14 shows the grouting pipe attaching to a grout hole during the injection. The pipes corresponding to each material A and B are also mentioned.

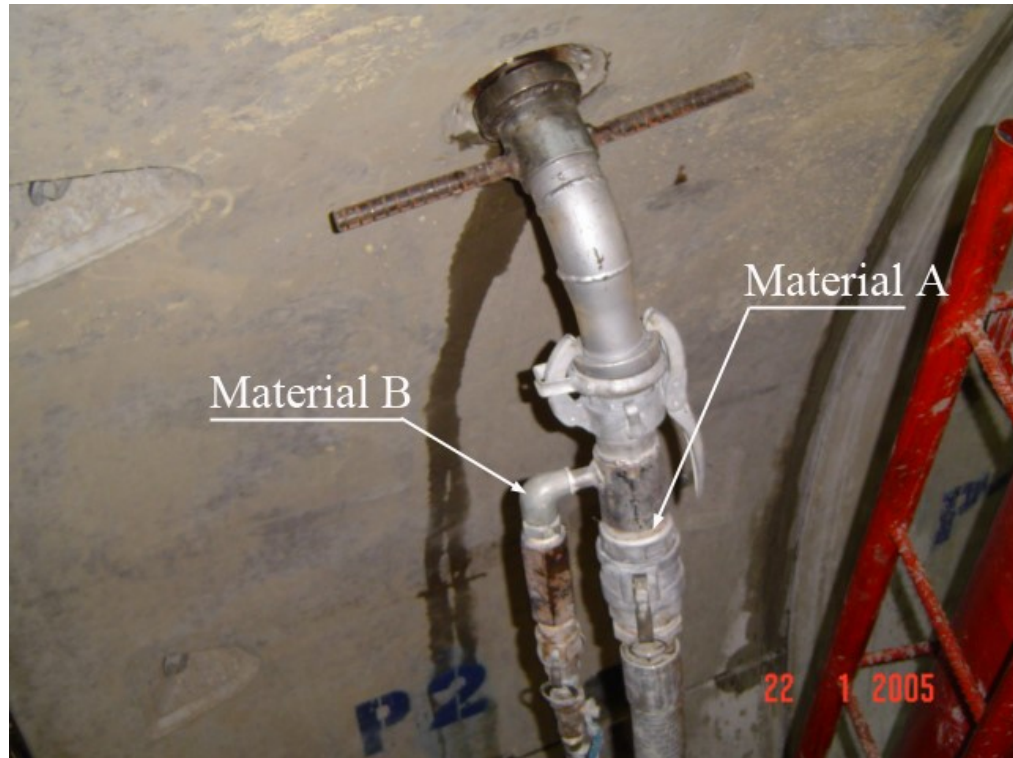


Figure 2.14 Grouting pipe attaching to grout hole (BMA flood diversion project, Saensaep-Latphrao Phrakhanong)

According to the subsoil conditions indicated in section 5.2 of Chapter V and the criteria for selecting a soft ground TBM described in section 2.3, the EPB shield machine is the most appropriate tool for this project. Moreover, the construction company already has experience with this machine during the MRTA subway project. The main components of selected EPB are also clearly mentioned in Chapter V.

CHAPTER III

GEOLOGY AND SUBSOIL CONDITIONS

A profound understanding of the geology of one area and engineering properties of its subsoils, usually lead to a better design of an underground structure and an accurate prediction of the construction effects. Therefore, the geological and geotechnical investigation is indispensable before starting an underground work within one area. This chapter describes the general geological conditions of Bangkok soil including the special characteristics of the underground water pressure as well as an introduction of the subsoil profile along the tunneling route of this study.

3.1 Geology of Bangkok Soil

The Bangkok subsoil is relatively uniform throughout the whole metropolitan area (Phienwej, 1996 and 1997; Shibuya and Tamrakar, 2003). This subsoil consists of two kinds of deposits: first, the terrestrial or quaternary deposits originated from the sedimentation at the delta of the ancient river in the Chao Phraya and second, the marine deposits occurring due to the changes in sea levels during quaternary period. Bangkok is located in the low lying Chao Phraya plain which is about 20 km north of the Gulf of Thailand (Figure 3.1). The plain becomes a slope towards Tanawrsri Mountain range on the west along Thai-Myanmar border and it is developed into Khorat Plateau on the east. The Chao Phraya River and its tributaries such as Tajeen are the major drainage system for the surrounding highlands. Therefore, the Chao Phraya basin is filled with sedimentary soil deposits, which from alternative layers of sand, gravel and clay. The marine clay of Bangkok plain, which is the uppermost clay layer, extends from 200 to 250 km in the East-West direction and 250 to 300 km in the North-South direction. The formation of this layer is known as Bangkok clay and it is believed to be approximately 4000 years ago. The deposits, which are confined within the radius of 60 to 80 km from Bangkok, had taken place during the Pleistocene and Holocene period (Shibuya and Tamrakar, 2003).

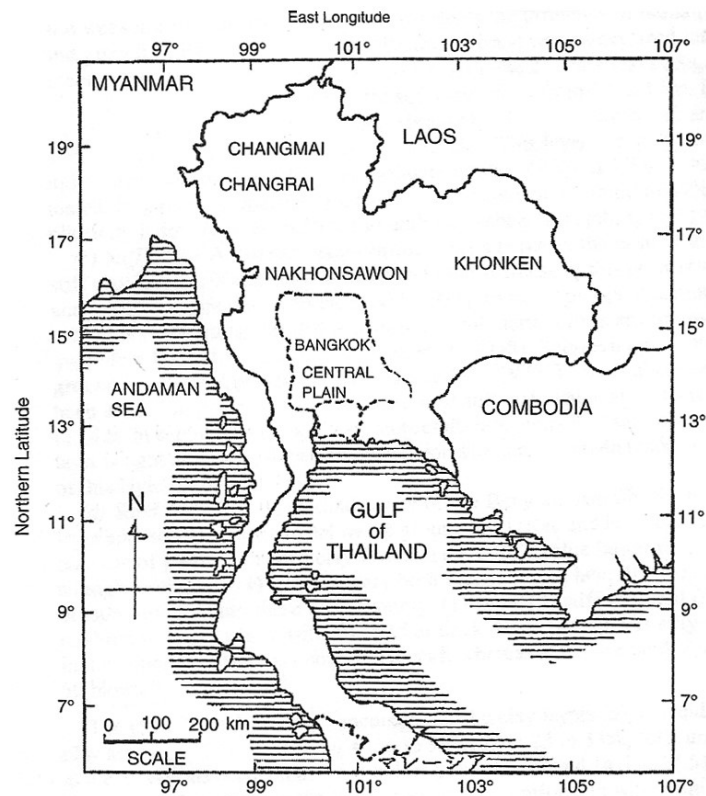


Figure 3.1 Map of Thailand (Shibuya and Tamrakar, 2003)

The general Bangkok subsoil profiles for the top 70 m thickness reported by Teparaksa (1999) based on the Mass Rapid Transit Authority of Thailand (MRTA) subway project is presented in Figure 3.2.

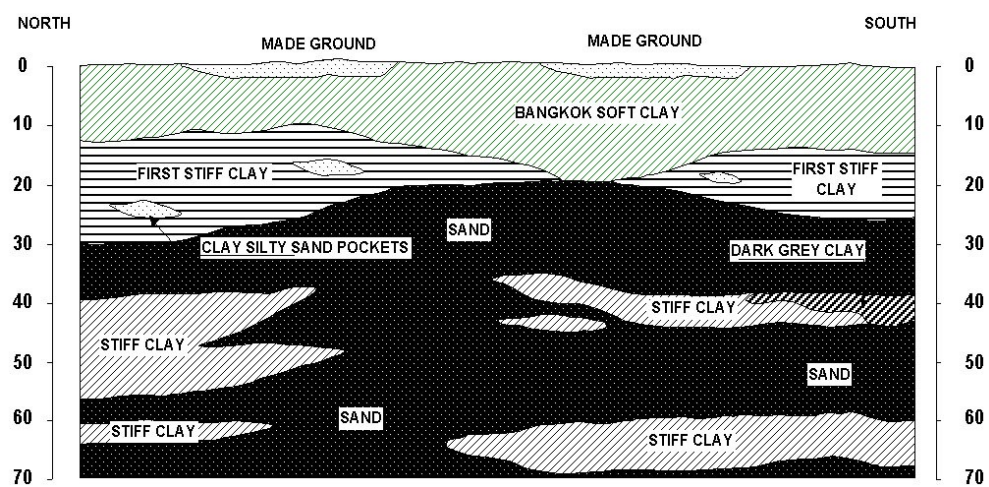


Figure 3.2 General subsoil profile (Teparaksa, 1999)

During this MRTA subway project, which is the first subway project to be built in Bangkok, the subsoil layers along the route were investigated by means of the first six self-boring pressuremeter tests ever carried out in Thailand and more than 200 boreholes were made. The subsoils consist of 13-16 m thick soft marine clay at the upper layer. This clay is sensitive, anisotropic and creep (time dependent stress-strain-strength behavior) susceptible. These characteristics have made the design and construction of deep basements, filled embankments and tunneling in soft clay difficult. The first stiff to very stiff silty clay layer is encountered below soft clay and medium clay varying from 21 to 28 m depth. This first stiff silty clay has low sensitivity and high stiffness, which is appropriate to be bearing layer for underground structures. The first dense silty sand layer located below stiff silty clay layer at 21-28 m depth contributes to variations in skin friction and mobilization of end bearing resistance of pile foundations. The similar variations are also contributed by the second dense and coarse silty sand found at about 45-55 m depth (Figure 3.2).

3.2 Underground Water of Bangkok

The piezometric profile has been known for Bangkok is hydrostatic starting from 1 to 2 m below ground level to a depth about 7 up to 10 m (Teparaksa, 1999; Teparaksa and Heidengren, 1999; Shibuya and Tamrakar, 2003). However, beneath this depth (about 10 m), due to deep well pumping from the aquifers, a successive reduction of water pressure appeared within the lower part of soft clay and the first stiff clay layers and the zero water pressure could be seen again at the depth about 23 m below ground surface as shown in Figure 3.3 (Teparaksa and Heidengren, 1999; Teparaksa, 1999; Yeow et al., 2004). The piezometer profile beyond this depth becomes a hydrostatic profile for a second time. Teparaksa and Heidengren (1999) and Teparaksa (1999) stated that “the low piezometric level contributes to the increase in effective stress, causing ground subsidence in this city. However, the benefit of this low piezometric level is easy to construct bored piles having pile tip in the first stiff clay using dry process and dry excavation for basement construction up to the silty clay level without any dewatering or pumping system”. As the stiff clay has a high stiffness, it is expected that the ground loss during the TBM boring is very low or insignificant. Therefore, The MRTA subway tunneling is designed to be seated mainly in the first silty clay layer (Kongdaeng, 1996).

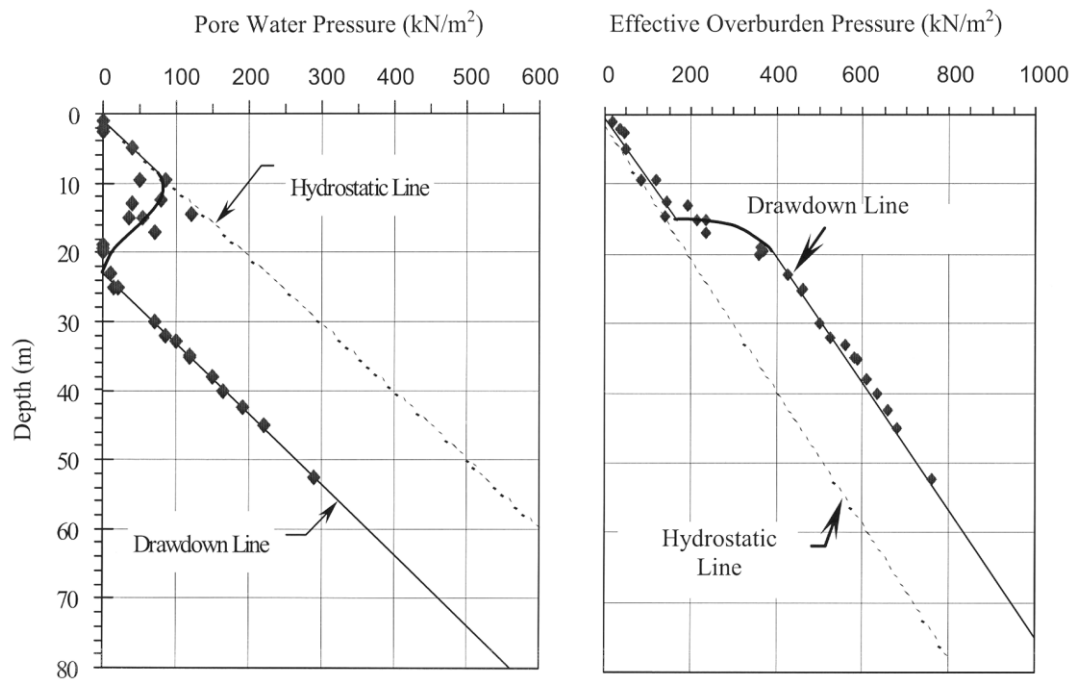


Figure 3.3 Piezometric level of Bangkok subsoils (Teparaksa, 1999)

3.3 Subsoil Conditions along the Tunneling Route of the Project

Although the various soil investigations have been previously done approximately everywhere in the Bangkok city, the additional 23 boreholes and Field Vane Shear tests were carried out along the tunneling route of the Bangkok Metropolitan Administration (BMA) Saensaeap-Latphrao Phrakhanong flood diversion tunnel project. As the quality of geotechnical works depend mainly on the certainty of soil information in the vicinity of the project, this supplementary ground investigation was done in order to elucidate the following characterizations:

- the soil boundaries between different layers, and the representative of typically geotechnical sections.
- the material and engineering properties of the different layers along the route and provide parameters for designing or using in the model of calculation.
- the ground water conditions along the working route.

The location of each borehole and the typical subsoil profile along the BMA Saensaeap-Latphrao Phrakhanong flood diversion tunnel are shown in Figure 3.4.

Figure 3.4 Boreholes and soil profile along the route of the BMA flood diversion tunnel (Saensaep-Ladphrao Phrakhanong)

The groundwater table measured 24 hours in the boreholes (surface water) was found at a depth between 0.5 and 1.1 meters from the ground surface. The geological condition and groundwater level indicated here are very similar to those mentioned in the above sections (section 3.1 and 3.2). However the BMA flood diversion tunnel is designed to be located mainly in the dense to very dense fine sand layer about 27.5 m depth below ground surface, which is found just below the stiff to very stiff clay layer since these layers had given place for the other previous tunnel projects already. Seeing that the tunnel crown is so close or gets in touch with the stiff to very stiff clay layers (Figure 3.4), the selected location of current flood diversion tunnel is expected to offer a low ground loss during and after TBM boring.

In chapter V, the more details of subsoil profiles for the analysis section will be extensively described including the research project the selected locations for Finite Element (FE) simulations and the different types of instrumentation used in the project. However, the engineering properties used in each simulation will be mentioned in numerical method and analyses (Chapter VI).

CHAPTER IV

TUNNEL INDUCED GROUND MOVEMENTS

The construction of tunnels or surface excavations in soft ground will lead to ground movements. However, the magnitude of soil movements depends mainly on the size of the opening, the distance to the excavation and the properties of the soil itself which is located around the construction site. This chapter describes the mode of soil displacements given by two model tests for the tunnel in clay and in sand as well as the different sources of ground movements generated by shield tunneling. An overview of different methods developed and used to estimate the ground surface and subsurface movements are also given in this chapter.

4.1 Causes of Soil Displacements around Tunnels in Soft Soil

4.1.1 Displacement Vectors in Soft Soils

The word soft soil may refer to one or both of cohesive and granular soils. However, the previous research studies typically classified soft soil into only one of them even there is no such one layer of soil in reality. The vectors of ground movements in response to the tunnel excavation in the two types of soils may be distinguished by two model tests (Figure 4.1), which were conducted by Mair (1979) and Potts (1976) and cited by O'Reilly and New (1982). The movements appearing in cohesive soil seem directed towards a sink located at a point somewhere below axis level of the tunnel. However, the width of the settlement is wider than that of the cohesionless soil where the movements seem to be deeper and narrower.

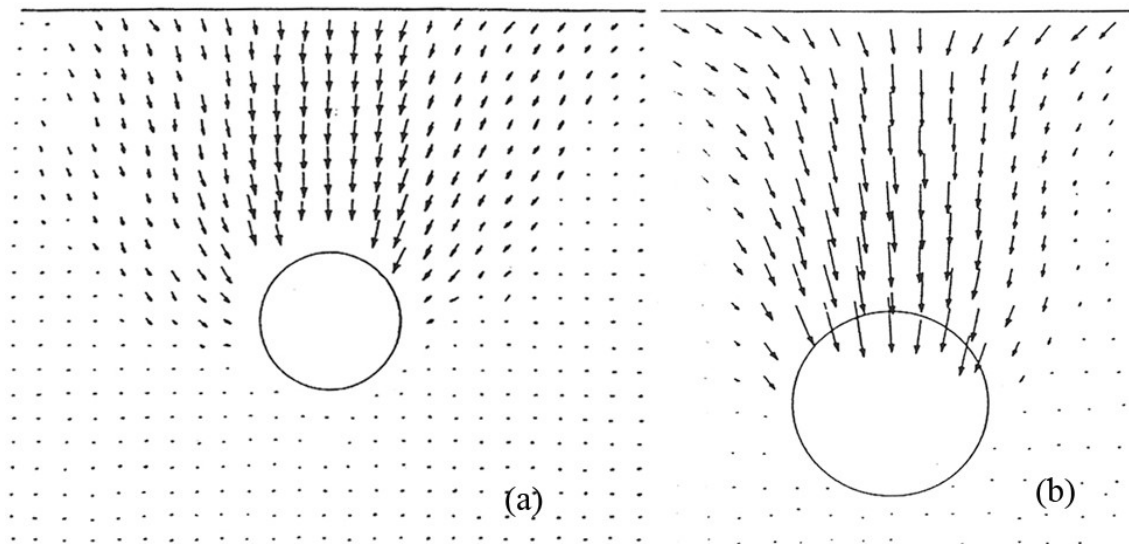


Figure 4.1 Vectors of soil displacements around model tunnel (a) in clay (Mair, 1979) and (b) in sand (Potts, 1976) (cited by O'Reilly and New, 1982)

4.1.2 Causes of Soil Displacements

The ground movements due to shield tunneling in soft soil are closely related to the ground loss, which is affected by the combination of various factors (Figure 4.2). According to Suwansawat (2002) and the real excavation process, the fundamental ground loss could be described as:

- Ground loss at the shield face (Figure 4.2a): Face loss into the tunnel develops when an open-face shield is used, or if the shield is operated at low support pressure so that the soil is allowed to move towards the face from a zone of influence ahead. In this condition, the volume balance is negative, or more volume of soil is removed than is occupied by the shield advance.
- Ground loss due to over-cutting (Figure 4.2b): In order to advance the shield it is necessary to have an over-excavation outside the tunnel perimeter at the face of the machine. This is accomplished by the presence of copy cutters, which could be extended up to 185 mm outside the perimeter of the cutting wheel according to the dimension of the shield and the machine construction techniques.
- Ground loss due to pitching (Figure 4.2c): Plowing or yawing of the machine caused by pitching can cut an ellipse of larger cross-sectional area than the area of the shield. At the same pitching angle, a shield with longer

length theoretically introduces a larger gap over its shield than a shield of shorter length.

- Ground loss due to ground disturbance (Figure 4.2d): After the cutting wheel has passed, a disturbed or remolded zone around the shield surface due to shoving of the large diameter shield can cause ground movement over the shield body.
- Ground loss due to tail void closing (Figure 4.2e): The tail void after shield passing causes an additional component of ground deformation due to closure of the soil into the gap. The void is created by the difference between the excavated periphery and the permanent outer liner surface. One usually tries to eliminate the gap by expanding the lining or by grouting around the lining as it emerges from the tail of the shield, before the soil displaces into the gap.

The magnitude of ground movements that occur from these different phases is mainly influenced by ground conditions, the construction method, and shield operation control. Operation control includes the pressure control at the face, the steering of the shield, penetration rate, and quality of workmanship. Hence, allowing movements into the face of the tunnel, introducing tail void enlargement, greater soil disturbance by poor steering practices, and slow installation of the liner due to the poor operation all lead to an increase in ground movements.

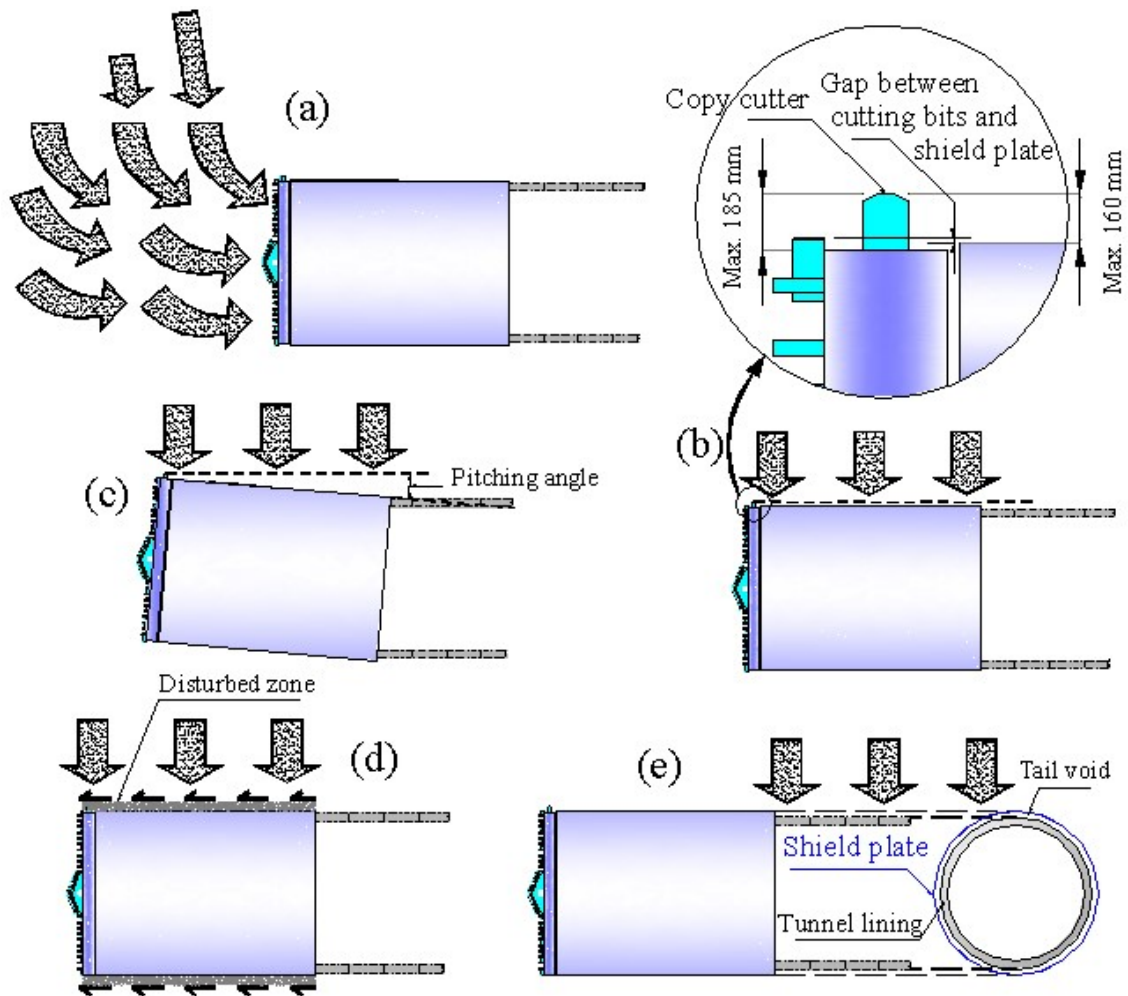


Figure 4.2 Causes of ground loss during shield tunneling

Similarly, in the Japanese Standard for Shield Tunneling (JSST), which was published by the Japan Society of Civil Engineers (JSCE, 1996), the third edition, the causes of soil displacements could be separated in five main points. Though some causes are exactly the same as what have been described previously, other causes are clearly and complementarily mentioned to be considered for identifying the sources of ground loss or ground movements. These causes are described as follows:

- 1.) Unbalanced ground and groundwater pressure at face: if the shield advancement rate and muck discharge rate are not synchronized in an EPB shield or slurry shield, the pressure inside the chamber becomes different from the ground and groundwater pressure, at the face become unbalanced, which causes ground movements. If the pressure in the chamber is smaller than the ground pressure, surface settlement occurs. In cases of contrary,

ground heave occurs. These phenomena are due to pressure release at the face and elasto-plastic deformation by an additional pressure.

- 2.) Ground disturbance during advancement: ground disturbance due to shield advancement and friction between the skin plate of the shield machine and ground may cause ground heave or settlement. Especially, extra excavation for alignment control or driving through a curved section causes ground loosening.
- 3.) Occurrence of tail void and insufficiency of backfill grouting: due to an occurrence of tail void, the ground which is supported by a skin plate, it causes deformation and ground settlement occurs. This is an elastic deformation caused by stress relief. The magnitude of ground settlement depends on the backfill grouting material, timing, grouting locations, pressure and grouted volume. Excessive pressure of backfill grouting in clayey ground may cause ground heave.
- 4.) Deformation and displacement of the primary lining: if joint bolts are not fully tightened, a segmental ring tends to be deformed. This increases ground settlement, as the nominal area of the tail void increases or the primary lining deforms due to unbalanced loads, after it is pushed out from the tail.
- 5.) Decline of groundwater table: if water flows in from the cutting face or leaks through the primary lining, the groundwater table declines, which causes ground settlement. This settlement is caused by consolidation, as the effective stress of the ground increases.

Based on the above mentioned causes (JSCE, 1996), the consequences of ground movements could be plotted in 5 different stages of occurring: i) and ii) prior to the passage of the shield machine, iii) during the passage, iv) and v) after the shield machine has passes.

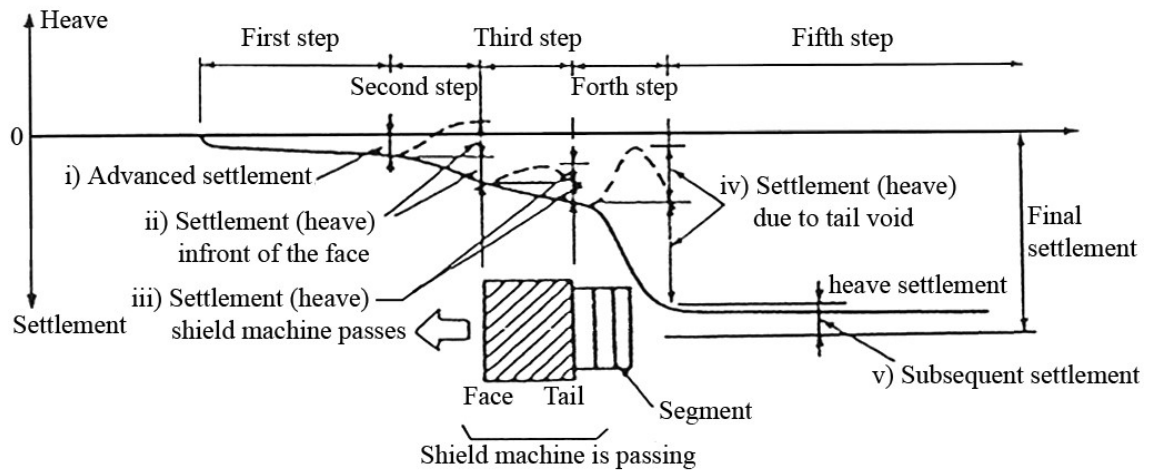


Figure 4.3 Ground movements due to shield advancement (JSCE, 1996)

The successive movements shown in Figure 4.3 could be described briefly as follows:

- i) Advanced settlement: this occurs well in advance before the shield machine passes. It is caused by the decline of groundwater table in sandy ground. In extremely soft clayey ground, it may occur as ground flows in at the face.
- ii) Settlement (or heave) in front of the face: this type of settlement or heave occurs just before the shield machine passes, which is caused by unbalanced pressures of ground and groundwater at the face.
- iii) Settlement (or heave) shield machine passes: this is caused by friction between the shield machine and ground or disturbance of the ground due to over-excavation.
- iv) Settlement (or heave) due to tail void: settlement or heave occurs immediately after the shield tail has passed. It is caused by stress relief because of tail void or by excessive backfill grouting pressure. This type of settlement is the most important settlement in shield tunneling.
- v) Subsequent settlement: this settlement occurs in soft clayey ground. Loosening or disturbance of the ground is the main cause.

(JSCE, 1996)

The magnitude and distribution of ground settlement vary depending on ground conditions, the ratio of overburden depth to shield diameter, boring condition as well as percent of ground loss and tail void.

Teparaksa (2005a) simply classified the ground surface and subsurface movements into three portions (as shown in Figure 4.4) due to EPB tunneling in Bangkok subsoils for MRTA project as:

- 1.) portion 1: settlement about 10% caused by soil flow into the shield.
- 2.) portion 2: settlement about 20% caused by soil displacement during installation of segmental lining.
- 3.) portion 3: major settlement about 70% caused by soil tail void after TBM passing.

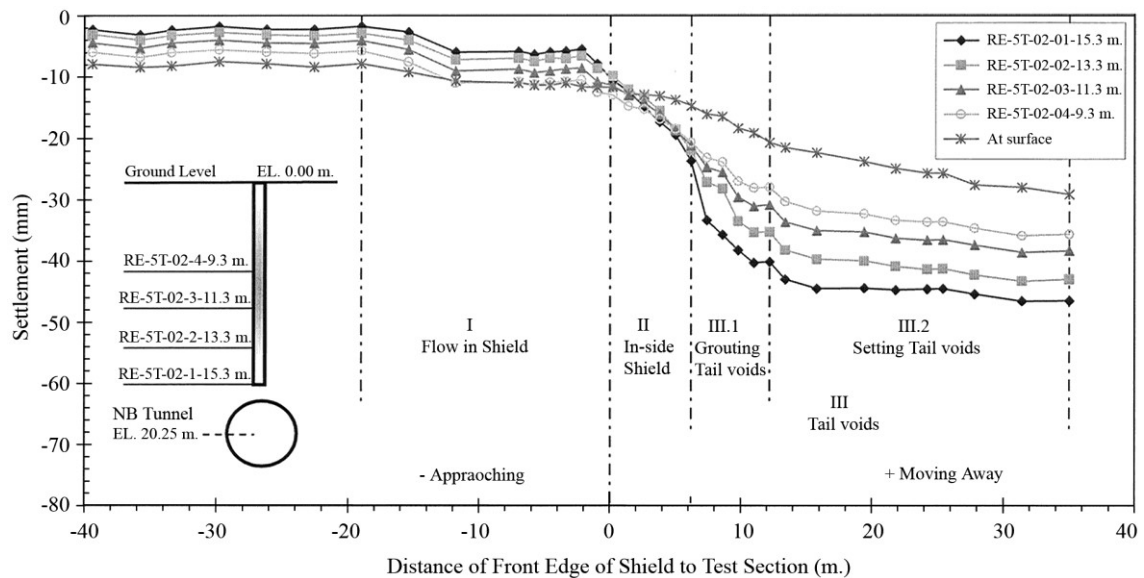


Figure 4.4: Behaviors of ground displacements caused by EPB tunneling (Teparaksa, 2005a)

Although the causes of soil displacements have been known, there is no measure to eliminate these phenomena. However, the excessive displacements could be reduced based on experiences of the shield operator and the workman shift.

4.2 Predicting Methods of Ground Displacements

The understanding of ground and structural displacement mechanisms is necessary since it helps the constructor to prepare the preventive measures in order to assure the normal function of public activities at the ground surface. Therefore, the appropriate predicting method is needed for accurately estimating the magnitude of

ground as well as structural movements before starting a tunnel construction. Until now, four kinds have been established as predicting methods, which have been used for this purpose. First, the empirical methods are proposed based on the case history of field monitored data, and normal contribution curve is used to compute the ground settlement trough. Secondly, the analytical methods (closed-form) of which the ground displacements are determined analytically. Thirdly, the Finite Element Methods (FEMs) have been extensively employed since it provides not only the ground surface movements, but also the subsurface movements. In addition, the various obstructions, i.e. buildings, structures and foundations, at ground surface and subsurface of the analysis section can be input into the model that allows designers to know in advance the tendency of those structure movements in response to the tunnel excavation. Finally, the laboratory tests, which are based on the centrifuge models to simulate the tunnel excavation and ground movements and the results obtained from the tests could be suggested for predicting the maximum surface settlements as well as the form of soil movement around the tunnel. However, the time consumed for sample preparation and the number of experiments carried out is very long. Moreover, it is difficult to simulate the real tunnel excavation and to implement the surface and subsurface structures into the model.

In general the ground surface settlement trough above and ahead of the advancing tunnel for a single tunnel in green-field site (place where there has been no previous surface or subsurface construction) is manifested as shown in Figure 4.5 (Attewell et al., 1986).

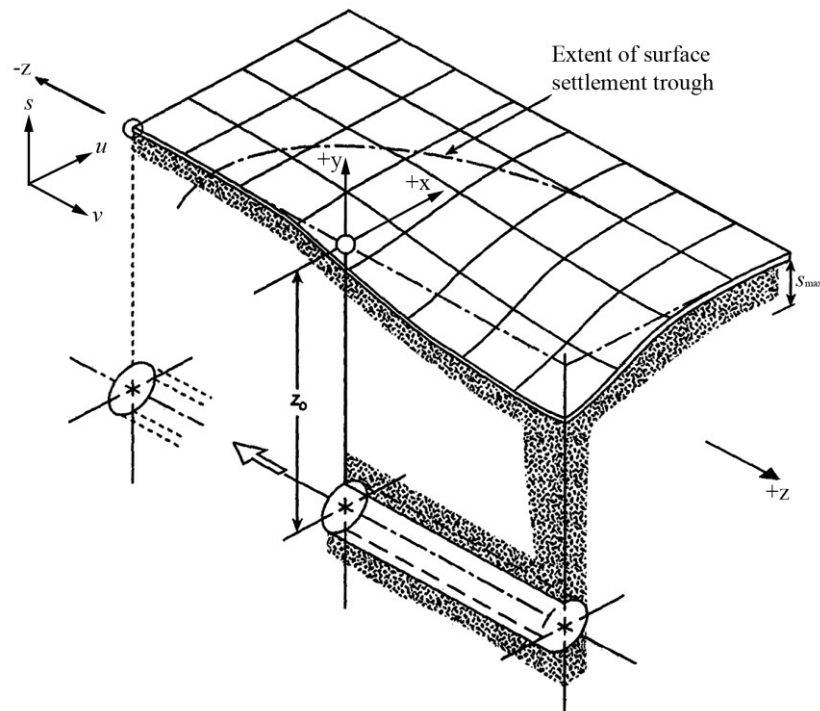


Figure 4.5 Settlement trough above an advancing tunnel (Attewell et al., 1986)

4.2.1 Empirical Methods

Several empirical methods have been developed based on the error function or normal probability curve (sometime it is called Gaussian curve) to predict the ground movements in respond to tunnel construction. However, for surface settlement, only the approach suggested by Peck (1969) and the extension developed by O'Reilly and New (1982) will be reviewed here. For subsurface settlement, the development work made by Mair et al. (1993) will be described. These approaches have been extensively used for estimating the ground surface settlements in many research studies.

Peck (1969) reported a study of ground surface settlement data, which were available from more than twenty case histories during that time, and led to a conclusion that the settlement trough induced by a single tunnel excavation could be presented by the error function or normal probability curve. Until now, this empirical approach is still widely used to predict the ground surface settlements resulting from tunnel excavation in soft ground. The vertical settlement “ s ” in the transverse direction is defined as

$$s = s_{\max} \exp\left(\frac{-x^2}{2i^2}\right) \quad (4.1)$$

where, s_{\max} is the maximum settlement measured above the tunnel axis (at $x = 0$), x is the transverse distance from the tunnel axis and i is the standard deviation of the normal distribution curve. The value of i gives a means of defining the settlement trough width and equals to x at the point of inflection of the curve. In practice, the total half-width of settlement trough is given by about $2.5i$. Figure 4.6 shows a typical transverse settlement trough above a single tunnel located at a depth of z_0 from ground surface and R is the radius of the tunnel.

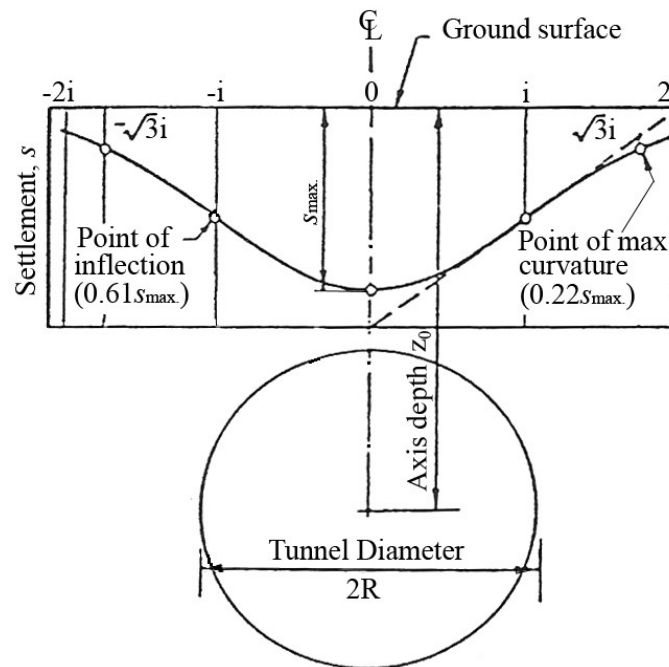


Figure 4.6 Transverse settlement trough (Peck, 1969)

The values of i had been calculated for tunnels above which reasonably reliable settlement data were available. They are illustrated in a dimensionless plot of i/R against $z_0/2R$ for different soil conditions (Figure 4.7). It can be seen that the settlement trough width parameter becomes wider for a deeper tunnel.

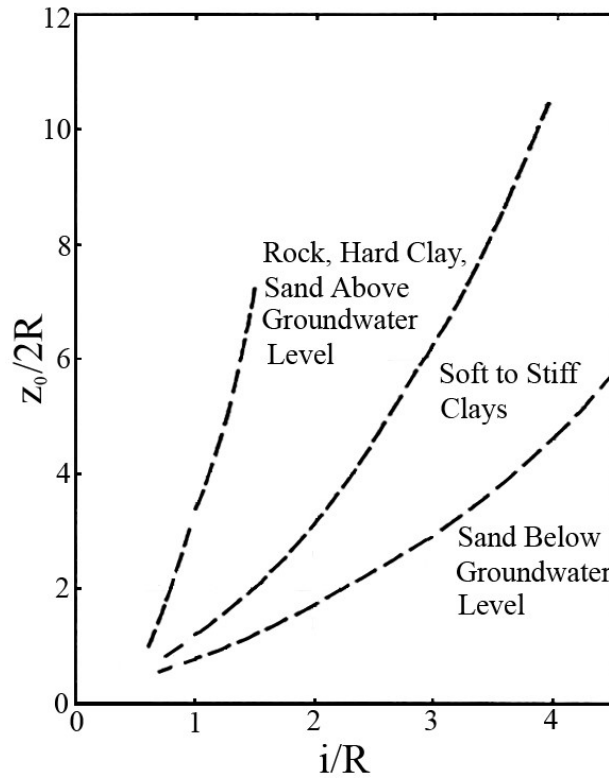


Figure 4.7 Relation between settlement trough width parameter and depth of tunnel for different soil conditions (Peck, 1969)

For practical purposes, O'Reilly and New (1982) bonded the trough width parameter i to the depth of the tunnel axis z_0 by the linear expression:

$$i = K.z_0 \quad (4.2)$$

Where K is an empirical constant of proportionality, depending on the soil type, and z_0 is the depth of tunnel axis below ground surface.

According to settlement data obtained from 19 locations of tunnel in cohesive soils and 16 locations of tunnel in granular soils, which were excavated in the United Kingdom, O'Reilly and New (1982) plotted the trough width parameter, i , versus the tunnel axis below ground level as shown in Figure 4.8. From the linear regression, two empirical relationships were established:

$$i = 0.43.z_0 + 1.1 \quad \text{for cohesive soils} \quad (4.3)$$

$$i = 0.28.z_0 - 0.1 \quad \text{for granular soils} \quad (4.4)$$

The data used to plot in Figure 4.8 cover the tunnel axis ranged from 3.4 m to 34 m and the linear relationship is better define for cohesive soils than for granular soil. As the linear regression lines pass close to the origin, the expression (4.2) is usually preferable for most purposes. In addition, the values of K vary between 0.4 for stiff clay and 0.7 for soft and silty clays. However, for granular materials above the water table K ranges between 0.2 and 0.3. As a general rule, the width of the surface settlement trough is about three times the depth of the tunnel for tunnels in clay strata (Burland et al., 2001).

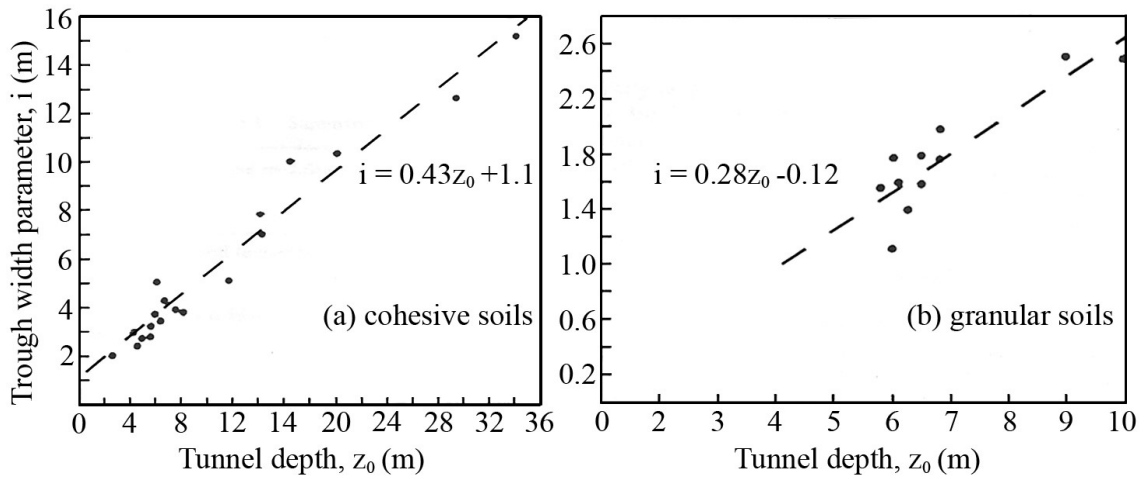


Figure 4.8 Variation of trough width parameter, i , with tunnel depth (O'Reilly and New, 1982)

Pitaksaithong (2001) used the trial error, which is based on the empirical methods of Peck (1969) and O'Reilly and New (1982) to analyze the ground surface settlement caused by a 4.18 m, outer diameter, tunneling in Bangkok subsoils (in a depth of 23.80 m under ground-surface), and he found that i varies from 8 to 12 m, while K varies in the order of 0.34 and 0.50.

The short-term settlements caused by tunnel excavation are typically characterized by the "volume loss" V_L , which is the volume of the surface settlement trough per unit length (V_s) expressed as a percentage of the notional excavated volume of the tunnel. The integration of Equation (4.1) for value of x between $-\infty$ and $+\infty$ is:

$$V_s = \sqrt{2\pi} \cdot i \cdot s_{\max} \quad (4.5)$$

Accordingly:

$$V_L = \frac{4 \cdot V_s}{\pi \cdot D^2} = \frac{3.192 \cdot i \cdot s_{\max}}{D^2} \quad (4.6)$$

Where, D is the excavated diameter of the tunnel. Combining Equations (4.1), (4.2), (4.5) and (4.6) gives the surface settlement s at any distance x from the centerline:

$$s = \left(\frac{0.313 \cdot V_L \cdot D^2}{K \cdot z_o} \right) \exp \left(\frac{-x^2}{2K^2 z_o^2} \right) \quad (4.7)$$

As mentioned previously, the value of s equals the maximum settlement s_{\max} at the vertical axis where x equals zero. Above the tunnel axis, therefore, the maximum surface settlement can be written:

$$s_{\max} = \frac{0.313 \cdot V_L \cdot D^2}{K \cdot z_o} \quad (4.8)$$

Besides the surface settlement, Mair et al. (1993) assumed that the shapes of subsurface settlement profiles developed during tunnel construction are characterized by the Gaussian distribution (Equation 4.1), in the same manner as those for surface settlement profiles, and they showed that this assumption is in reasonable agreement with monitored data. However, the substitution of the distance above the tunnel axis ($z_0 - z$) for z_0 must be done in order to determine the trough width parameter i based on Equation (4.2), where z is a depth from ground surface to the consideration subsurface level (Figure 4.9). Therefore, the Equation (4.2) can be written:

$$i = K \cdot (z_0 - z) \quad (4.9)$$

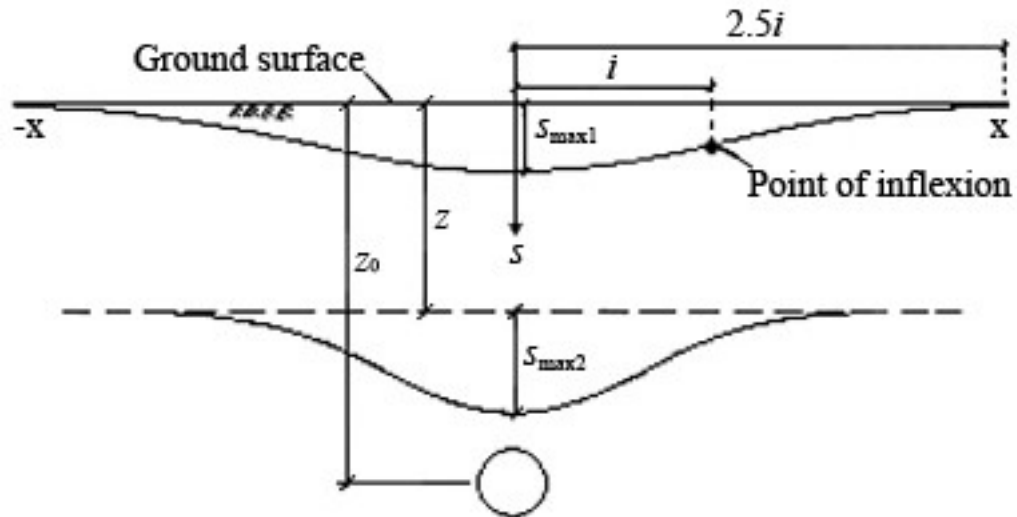


Figure 4.9 Shape of surface and subsurface settlement profiles (Mair et al., 1993)

It is important to note that, even though the value of K for surface settlements is more or less constant for a wide range of tunnel depths in the same ground, its value increases with depth for subsurface settlements and for the tunnels constructed in clays. This argument is shown in Figure 4.10, in which the trough width parameter i obtained from subsurface settlement normalized by z_0 is plotted against depth z , which is also normalized by z_0 (Mair et al., 1993).

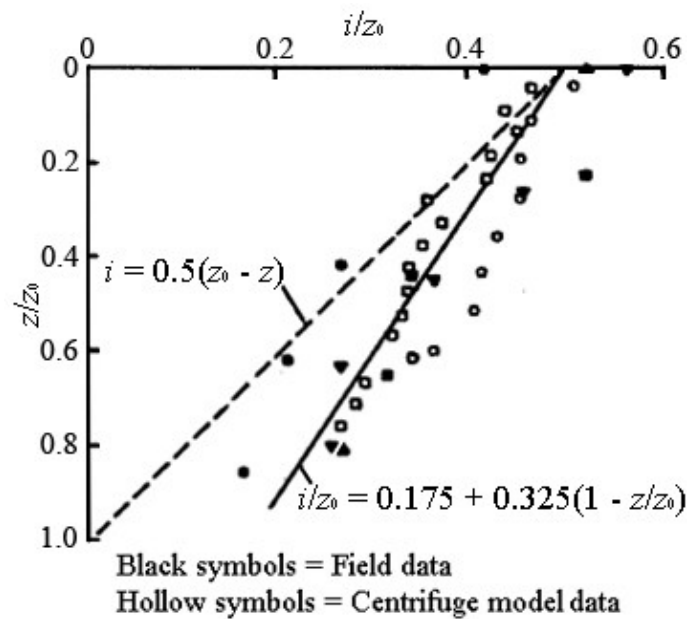


Figure 4.10 Variation of subsurface settlement trough width parameter, i , with depth for tunnel in clays (Mair et al., 1993)

It can be seen that the dash line, which represents Equation (4.9) for various depths of subsurface settlements and for $K = 0.5$, underestimates the width of subsurface settlement profile. However, the solid line, which is drawn through the data, gives a better estimation of i and is expressed by the following equation:

$$i/z_0 = 0.175 + 0.325(1 - z/z_0) \quad (4.10)$$

Combining Equation (4.9) and (4.10) gives

$$K = \frac{0.175 + 0.325(1 - z/z_0)}{1 - z/z_0} \quad (4.11)$$

The curve expressed by Equation (4.11) is plotted in Figure 4.11, together with the values of K derived from Equation (4.9) using the i values obtained from field measurements and centrifuge model data shown in Figure 4.10. One could see that if $K = 0.5$ was assumed, it would be underestimated for the large values of z/z_0 ; consequently, the magnitude of settlement would be overestimated.

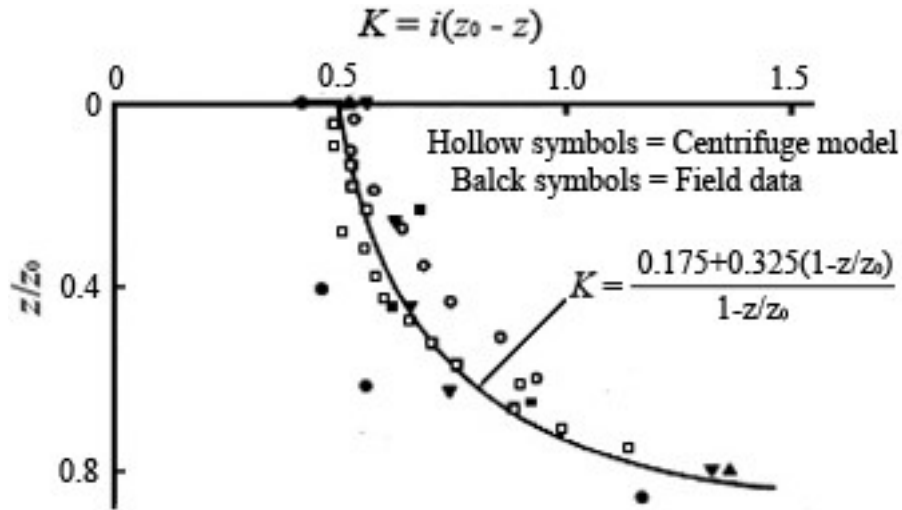


Figure 4.11 Variation of K for subsurface settlement profile with depth above tunnel in clays (Mair et al., 1993)

Combining Equation (4.8) and (4.10), gives the maximum subsurface settlement as

$$\frac{s_{\max}}{R} = \frac{1.25V_L}{0.175 + 0.325(1 - z/z_0)} \cdot \frac{R}{z_0} \quad (4.12)$$

where R is the tunnel radius. Figure 4.12 shows the maximum subsurface settlement normalized by the tunnel radius against the tunnel radius normalized by the depth of the considered subsurface level to the tunnel axis, $R/(z_0 - z)$. The field monitored data plotted in the figure were collected from the tunnel construction in London Clay for the radius 2.07 and 3.9 m. However, the tunnel depth was ranged from 20 to 41 m. The line A is plotted based on the Equation 4.8, in which K is taken as 0.5 and z_0 is substituted by $(z_0 - z)$, and the volume of ground loss is assumed to be 1.4%. In addition, the curves B and C are derived from Equation (4.12) for two different ratio of R/z_0 are also plotted in the graph except the solid line, which is drawn based on the plasticity solution given by Mair and Taylor (1993). The Figure clearly shows that the determination of s_{\max} for subsurface settlement based on Equation 4.8 for $K = 0.5$ leads to an overestimation.

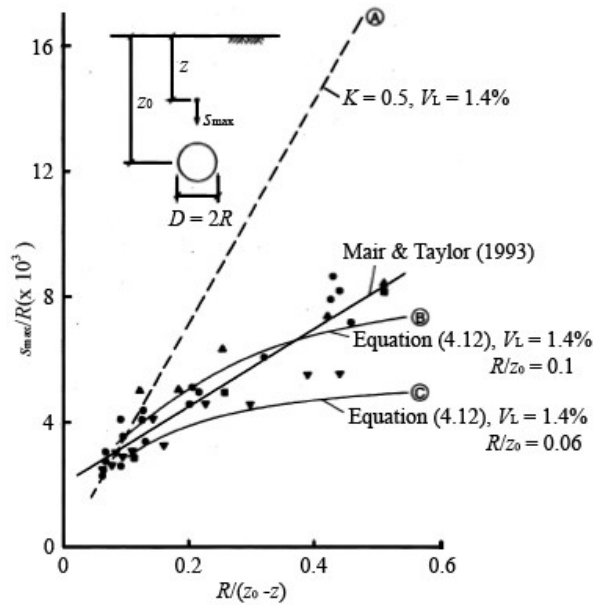


Figure 4.12 Subsurface settlements above the tunnel axis in London Clay (Mair et al., 1993)

In addition to what had been done by Mair et al. (1993), Luangpitakchumpol et al. (2005) reported based on MRTA project and water diversion project (Premprachakorn) in Bangkok subsoils that the maximum subsurface settlement s_{\max} did not only vary according to the tunnel depth, but also the tunnel radius itself as shown in Figure 4.13. This correlation; however, is applicable only to shield tunneling in the very stiff silty clay with outer diameter between 4 and 6.5 meters, and the ground loss is limited at the intervals of 1 and 3%.

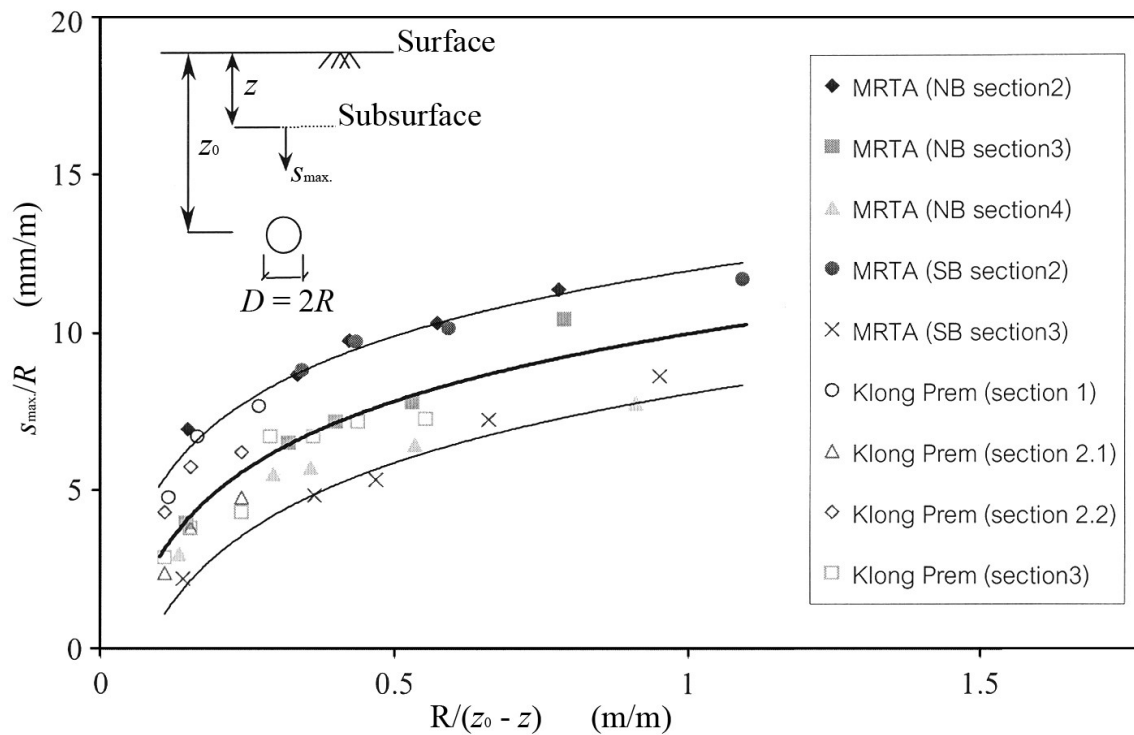


Figure 4.13 Correlation of maximum subsurface settlement (Luangpitakchumpol et al., 2005)

4.2.2 Analytical Methods

Several analytical solutions have been developed in order to predict the movements of ground induced by tunnel excavation. In general, the suggested approaches are usually modified from the basic ideas of the senior or previous researchers, and the important points in those methods vary according to the philosophy and the knowledge of the developers (researchers). In this paragraph, a series of analytical solutions, which have been developed continuously, will be briefly reviewed.

Sagaseta (1987) introduced closed form solutions for obtaining the strain field in an initially isotropic and homogenous incompressible soil (Poisson's ratio equals to 0.5) due to near surface ground loss. The strain controlled and incompressible conditions were mainly considered in the analysis problems. In addition, the virtual image technique was used at the free surface (Figure 4.14). The vertical soil displacement at any levels below ground surface could be defined as

$$s_z = -\frac{V_L}{2\pi} \left(\frac{z - z_0}{r_1^2} - \frac{z + z_0}{r_2^2} \right). \quad (4.13)$$

where V_L is the volume loss, which is expressed as the ratio of the surface settlement trough per meter run of the tunnel area. z_0 is the depth of tunnel axis from ground surface; z is a depth from ground surface to the consideration subsurface level and x is the lateral distance to the tunnel center line. Based on the simple geometry shown in Figure 4.14, the values of r_1^2 and r_2^2 could be known as $[x^2 + (z - z_0)^2]$ and $[x^2 + (z + z_0)^2]$, respectively.

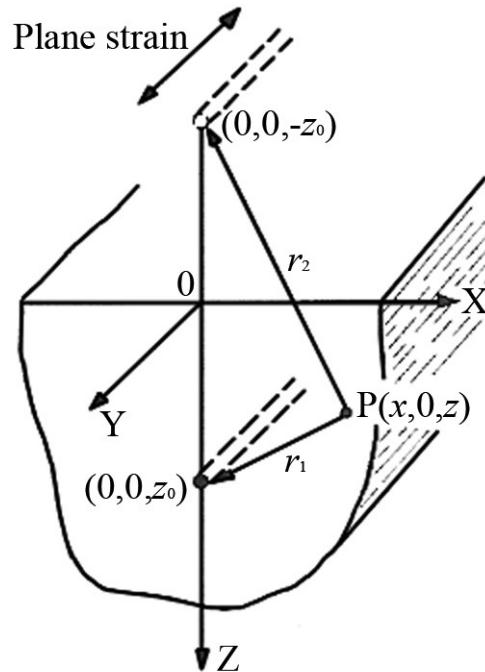


Figure 4.14 Point sink (ground loss) and virtual image technique (Sagaseta, 1987)

At ground surface, the settlement could be expressed as:

$$s = \frac{V_L}{\pi} \cdot \frac{z_0}{x^2 + z_0^2} \quad (4.14)$$

Verruijt and Booker (1996) extended the method suggested by Sagaseta (1987) for the ground loss in an incompressible soil. The solution given by Verruijt-Booker's method is not only applicable for the Poisson's ratio which equals to 0.5 (incompressible soil), but also for the arbitrary values of Poisson's ratio. Furthermore, it includes the effect of ovalization as well. The tunnel in a semi-infinite medium is considered in this approximate analytical solution, and the general ground settlement could be expressed as

$$\begin{aligned} s_z = & -\varepsilon R^2 \left(\frac{z - z_0}{r_1^2} + \frac{z + z_0}{r_2^2} \right) \\ & + \delta R^2 \left[\frac{(z - z_0)(kx^2 - (z - z_0)^2)}{r_1^4} - \frac{(z + z_0)(kx^2 - (z + z_0)^2)}{r_2^4} \right] \\ & + \frac{2\varepsilon R^2}{m} \left[\frac{(m+1)(z + z_0)}{r_2^2} - \frac{mz(x^2 - (z + z_0)^2)}{r_2^4} \right] \\ & - 2\delta R^2 z_0 \left[\frac{x^2 - (z + z_0)^2}{r_2^4} + \frac{m}{m+1} \frac{2z(z + z_0)(3x^2 - (z + z_0)^2)}{r_2^6} \right] \end{aligned} \quad (4.15)$$

where ε is a parameter indicating the relative uniform radial displacement of the tunnel surface with radius R , and δ is the relative displacement caused by the ovalization of the tunnel. For more comprehensive understanding, the parameters ε and δ are illustrated in Figure 4.15. The distances r_1 and r_2 are shown in Figure 4.14 and can be determined in the same way as those in Equation (4.13); $k = \nu(1 - \nu)$ and the auxiliary elastic constant, m , is related to Poisson's ratio by

$$m = \frac{1}{1 - 2\nu} \quad (4.16)$$

At ground surface, where $z = 0$, the first and second term in the Equation (4.15) are equal to zero. Therefore, the expression for surface settlement could be written as

$$s = 2\varepsilon R^2 \frac{m+1}{m} \frac{z_0}{x^2 + z_0^2} - 2\delta R^2 \frac{z_0(x^2 - z_0^2)}{(x^2 + z_0^2)^2} \quad (4.17)$$

Substituting the Equation (4.16) in (4.17), the surface settlement gives

$$s = 4\varepsilon R^2 (1-\nu) \frac{z_0}{x^2 + z_0^2} - 2\delta R^2 \frac{z_0(x^2 - z_0^2)}{(x^2 + z_0^2)^2} \quad (4.18)$$

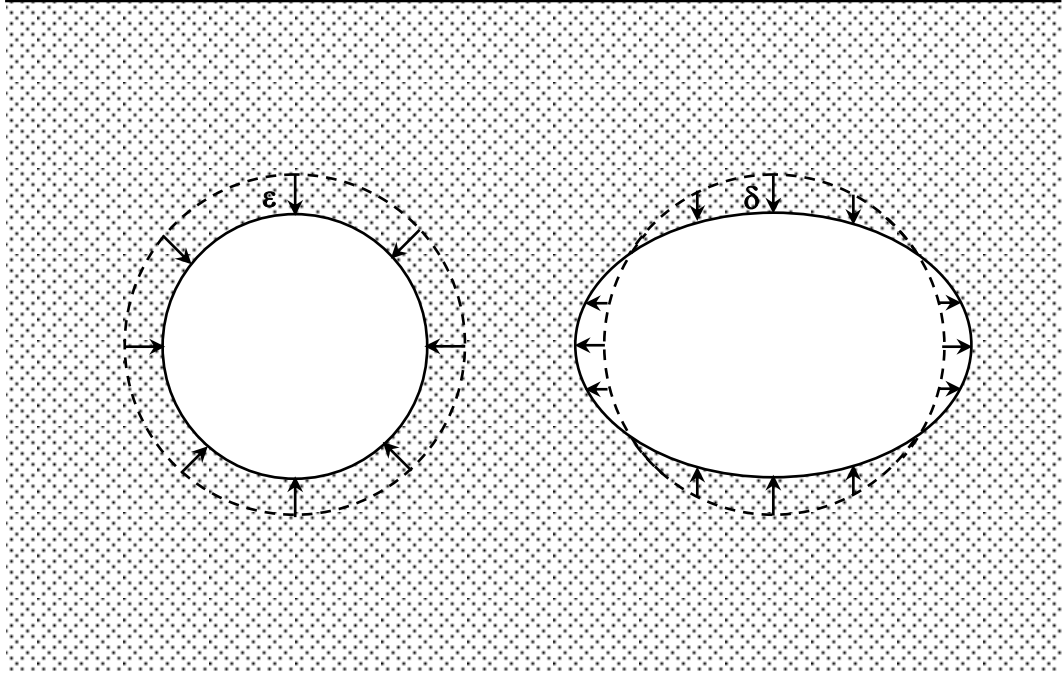


Figure 4.15 Ground loss and ovalization of a tunnel (Verruijt and Booker, 1996)

The total area (A) of settlement trough could be obtained by integrating the above equation (Equation 4.18) from $-\infty$ to $+\infty$. The result is

$$A = 4(1-\nu)\varepsilon\pi R^2 \quad (4.19)$$

So that,

$$\varepsilon = \frac{A}{4(1-\nu)\pi R^2} = \frac{V_L}{4(1-\nu)} \quad (4.20)$$

For the value of Poisson's ratio $\nu = 0.5$, the first term of Equation (4.18) could be converted to Equation (4.14) presented earlier by Sagaseta (1987).

Loganathan and Poulos (1998) redefined the traditional ground loss parameter with respect to gap parameter, G_{AP} , which was presented by Lee et al. (1992), and incorporated to the analytical solution of Verruijt and Booker (1996) to estimate the ground movements around the tunnel in clays. However, only the short-term undrained condition was considered while the ground deformations due to long-term ovalization of the tunnel lining are neglected ($\delta = 0$). Therefore, the short-term surface settlement could be expressed as

$$s = 4R^2(1-\nu) \frac{z_0}{x^2 + z_0^2} \frac{4G_{AP}R + G_{AP}^2}{R^2} \exp\left[-\frac{1.38x^2}{(z_0 + R)^2}\right] \quad (4.21)$$

where G_{AP} is the gap parameter, and the other parameters are the same as those in the previous equations. The gap parameter could be estimated by

$$G_{AP} = G_p + u_{3D}^* + \omega \quad (4.22)$$

where G_p is the physical gap ($G_p = 2\Delta + \delta$), which represents the geometric clearance between the outer skin of the shield and the lining, Δ is the thickness of tailpiece and δ is the clearance required for erection of lining. The term u_{3D}^* represents the three-dimensional (3D) elastic deformation at the tunnel face and ω takes into account the quality of workmanship. The tunnel heading and 2D plane strain representation of tunnel heading are shown in Figure 4.16. The clearance (δ) for erection of lining indicated in the figure is considered both clearances at crown and invert.

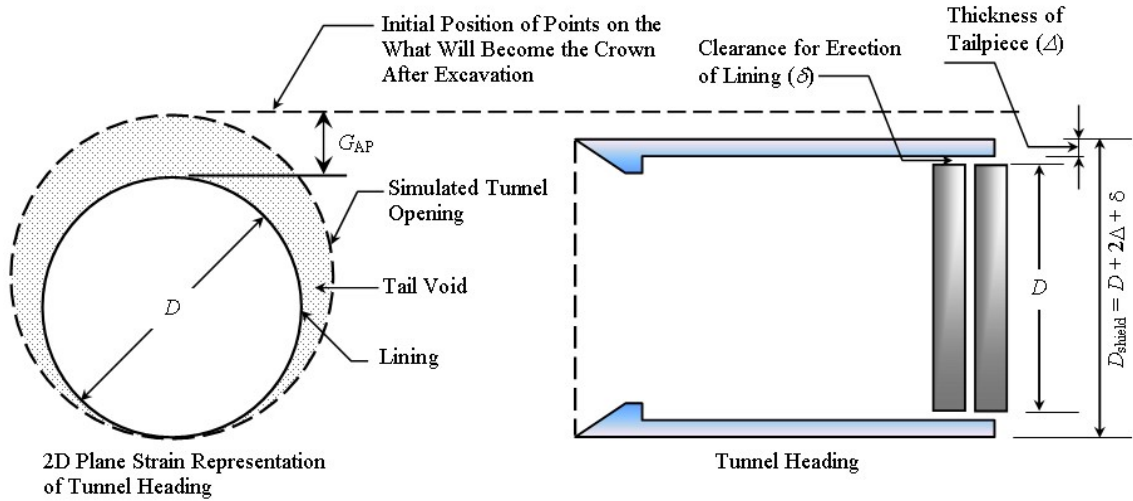


Figure 4.16 Definition G_{AP} (Lee et al., 1992)

Besides the ground surface settlement, Loganathan and Poulos also suggested the subsurface settlement profiles as

$$s_z = R^2 \left\{ -\frac{z - z_0}{x^2 + (z - z_0)^2} + (3 - 4\nu) \frac{z + z_0}{x^2 + (z + z_0)^2} - \frac{2z[x^2 - (z + z_0)^2]}{[x^2 + (z + z_0)^2]^2} \right\} \frac{4G_{AP}R + G_{AP}^2}{4R^2} \exp \left\{ -\left[\frac{1.38x^2}{(z_0 + R)^2} + \frac{0.69z^2}{z_0^2} \right] \right\} \quad (4.23)$$

It reveals that at ground surface ($z = 0$), the Equation (4.23) becomes exactly the Equation (4.20).

4.2.3 Laboratory Testing

Within these three decades, some geotechnical researchers have carried out the centrifuge tests in order to study the behaviors of ground responding to the underground opening or to find out the reasons after a collapse of a structure. The centrifugal tests or the imitations of tunnel excavation in laboratory consist of a preparation of a reduced scale model representing the tunnel diameter and its depth below ground surface. For the model tested with an acceleration of α times the Earth gravity (g), the equivalent full scale is α times the dimension in the model. In addition, the geological properties are prepared according to the desired material to be studied;

however, the principle component of tunnel liner is usually made of metal tube such as aluminum. Subsequently, the stress strain in the soil and the behaviors of ground deformations during the simulation could be examined based on the monitoring systems, which were set up in prior to the test. Although some centrifugal tests have been performed on the tunnel constructions, few case studies of these tests are briefly described here.

A series of centrifuge model tests, which could be accelerated to 75g, was performed by Atkison and Potts (1977) to simulate the tunnel excavation in an over consolidated clay and sand. The settlement data obtained from the tests were compared with one and another and with the data monitored above some actual tunnel constructions. Their research led to a suggestion of the following trough width parameter, i , for surface settlement:

- for loose sand

$$i = 0.25(z_0 + R) \quad (4.24)$$

- for dense sand and over consolidated clay

$$i = 0.25(1.5z_0 + 0.5R) \quad (4.25)$$

Loganathan et al. (2000) performed the centrifuge model testing for tunneling in clay in order to monitor the ground deformations, and then they compared the obtained data with the empirical and the analytical methods of estimation. Moreover, the behavior of a single pile and a pile group responding to the tunneling in the model was also observed. The tunnel was modeled by an aluminum tube covered by the rubber membrane and the annulus between the rubber membrane and aluminum tube (inner core of the model tunnel) filled with the silicone oil. By doing this the volume of ground loss was simulated by reducing the volume of silicone oil; thereby, decreasing the diameter of the tunnel. The detail descriptions of the centrifuge model setup were clearly mentioned in that paper. In 2003, in order to study the mechanism of the tunnel face failure of a shallow tunnel in sandy ground (the ratio of the soil cover to the tunnel diameter was fixed to 1) and the effect of the face bolting, vertical pre-reinforcement bolting and forepoling, Kamata and Mashimo (2003) conducted a set of centrifuge model tests. However, only half of cylindrical shell was created for

the model tunnel with 80 mm in diameter and the maximum centrifugal acceleration was limited to 30g. The experimental results were compared with the analytical results by the Distinct Element Method (DEM). One of their findings from the tests is that the forepoling reinforcement is less effective on face stability than the vertical pre-reinforcement bolting. Lee et al. (2006) carried a series of 100g centrifuge model tests to investigate the surface settlement troughs, excess pore water pressure generation, tunnel stability and arching effect built up during tunneling at various depths in clayey soil, which had an untrained shear strength profile of 30-40 kPa. Both single and two parallel tunnels were simulated and the experimental results were also compared with the numerical simulations.

As mentioned earlier in this section (section 4.2), the time consumed for sample preparation and the repetition of the experimentation is lengthy. Furthermore, it is costly and difficult to simulate the real behavior of tunnel excavation as well as to implement the surface and subsurface structures into the reduced scale model since the major structures are made of concrete or brickwork. Therefore, the numerical simulation is more advantageous regarding to these problems. However, these physical model tests still play an important role in providing the data for verifying and comparing the behaviors of ground movements with the existing methods, especially with the numerical analyses.

4.2.4 Numerical Analysis Methods

The prediction of ground movements in response to tunneling based on the empirical and analytical methods as well as the laboratory tests have been reviewed in the previous sections. However, those approaches were restricted to only tunneling below green field site, which are not always realistic for urban areas. The problems encountered for tunnel excavation in such locations could be cited as existing surface structures (buildings) and underground structures, which are tunnels, underground stations and pile foundations. In these situations, numerical or finite element method provides a huge advantage to input all the elements in question into one model and the ground deformations as well as the interaction between soil-structures and structures-structures could be studied. This section introduces a brief overview of the application of finite element method (FEM) to predict the ground movements caused by tunneling.

The finite element method has been used in many field of engineering practice for around forty year; however, it has begun to be widely used for analyzing geotechnical problems recently. This is probably because there are many complex issues which are specific to geotechnical engineering and which have been solved recently (Potts and Zdravković, 1999). This method consists of discretisation of a continuum into finite elements and each element has a number of nodes, which serve as connectors that fasten elements together. It is noticeable that all elements sharing a node have the same displacement components on that node.

The primary characteristics of a finite element are embodied in the element stiffness matrix. The stiffness matrix contains the geometric and material behavior information that indicates the resistance of the element to deformation when is subject to loading or external influences (Hutton, 2004).

The tunnel excavation is a 3D issue, but the 3D-FE analysis usually leads to an excessive time consuming and high capacity of storage. In practice, therefore, the 2D computation is much more preferable. Several methods have been suggested to model the tunnel excavation, and the most well known methods are briefly described in the following paragraph:

The gap method: this method was originally mentioned by Rowe et al. (1983). The expected volume loss is modeled by establishing a pre-described void into the finite element mesh, around the final tunnel perimeter. However, the invert of final tunnel lining must be in touch with the underlying soil as shown in Figure 4.16 of section 4.2.2. The tunnel excavation is simulated by removing the soil clusters inside the tunnel and around its periphery, and then the soil displacement is allowed until the gap is closed. As mentioned in section 4.2.2, the predefined gap parameter (G_{AP}) depends on the tunneling machine and lining parameters, soil type and quality of workman ship. The lower limit of gap parameter could be estimated as the difference between the outer diameter of the tunneling machine and the outer diameter of the lining.

The convergence-confinement method: this method was introduced by Panet and Guenot (1982); it is also called λ method. The parameter λ describes the proportion before the tunnel lining is constructed. At the initial condition, the pressure exerted on the tunnel boundary by the soil to be excavated is equal to σ_0 (initial soil tress), and λ is equal to 0. λ is then gradually increased to 1 to simulate the tunneling

process. During the tunnel excavation, the pressure at the lining boundary is reduced with a numbers of increment to $(1-\lambda)\sigma_0$. After lining erection, the remainder of stress reduction is still applied to create the lining stress. The stress reduction with the tunnel lining in place is, therefore, equals $(1-(1-\lambda))\sigma_0$ or $\lambda\sigma_0$, where λ continues to increase from the end of excavation step. Finally, the initial stress is then introduced into the tunnel lining. In this method, the ground loss is a predicted value. To achieve the desired ground loss, the installation of lining must be done at an appropriate calculation increment by taking into account the stiffness of the lining as well. It is noticeable that the desired ground loss given by the ground displacement normal to the tunnel perimeter should be equal to ground loss in an undrained greenfield excavation.

The progressive softening method: this method was developed for modeling of tunnel excavation using the New Austrian Tunneling Method (NATM) by Swoboda (1979). Unlike the convergence-confinement method, the tunnel excavation based on this method was simulated by reducing the stiffness soil clusters inside the future tunnel boundary.

The volume loss control method: in this method, the expected ground loss that will result on completion of excavation is prescribed prior to lining construction. This method is used to predictive analyses of tunnel excavation for which the ground loss can be determined for a given tunneling method. Moreover, it is found to be very useful for back analysis of tunnel excavation when the ground loss have been monitored (Potts and Zdravković, 2001).

The tunnel lining contraction method: If a circular tunnel is to be analyzed, a contraction of the tunnel lining (shrinkage) can be prescribed to simulate the ground loss in response to the boring process. The contraction is expressed in percentage as a ratio of the area reduction and the original outer tunnel cross section area (Brinkgreve, 2002). The application of this method is similar to the volume loss control method; however, the contraction is specified to the lining after it has been installed (activated).

Among the above mentioned methods, the simulation of tunnel excavation as well as the prediction of ground movements based on the lining contraction method is found to be much more convenient. A detail section about this last method and the overview of finite element program used for this research is described in Chapter VI.

4.3 Appropriate Methods for Analyses of the Research Project

For the fact that the analytical solutions employ more parameters, it is not always easy to estimate during the design phase. Moreover, for those analyses based on gap parameter (G_{AP}), Rowe et al. (1983) mentioned that the G_{AP} is the most critical and difficult parameter to determine. Thus, these approaches will not be considered in the analysis phases of this research. Regarding the laboratory or centrifuge test, besides time consuming, high cost, the difficulty to implement the surface and subsurface structures which are made of concrete or masonry into the model, the facility is not yet available in our laboratory. Therefore, the potential for analyses the ground surface settlements in this research will refer to the empirical approach (Peck, 1969), which has been extensively used for this purpose. Furthermore Rowe and Kack (1983) acknowledged that the empirical relationships may yield quite adequate and economical design when they are applied with appropriate judgment based on similar past experiences. At the same time, the FE analysis method will cover both ground surface and subsurface settlements as well as the structural settlements. In addition, the internal forces of the tunnel liner could be achieved as well.

CHAPTER V

PROJECT DESCRIPTION AND MONITORING SYSTEM

First this chapter gives a general description of the project, the location of the BMA flood diversion tunnel, the obstructions along the tunneling route and the specific locations for this study as well as the details of subsoil profile of the selected locations. Then an articulated EPB is introduced according to the geological conditions of the area and the tunnel alignment. Finally, the different monitoring systems are presented in order to monitor the different aspects responding to the tunnel construction. The monitoring method and data interpretation will also be given in this chapter.

5.1 General Description

As mentioned in the name of this project, the BMA flood diversion tunnel is responsible by Bangkok Metropolitan Administration (BMA). In order to protect Bangkok from flooding during the rainy season, which is one of the catastrophes to the city, by the end of 2003, this BMA gave its confidence and financial support to the joint venture of Italian-Thai Development PCL and Nishimatsu Construction Co., Ltd. for working on this construction. The present tunnel is the second shortcut flood-diversion tunnel, which has 5.55 m of outer diameter (OD) and about 5 km long. It is under construction in order to collect floodwater from the Saensaep and Ladphroa canals and divert it to the Phrakhanong pumping station. The intake shaft is located at the junction of the Saensaep and Latphroa canals while the outlet shaft and pumping station are located near the Phrakhanong canal connected directly to the Chaophraya River as shown in Figure 5.1. The slope of the tunnel is 1:10000 and the floodwater will be flowed by gravity in the tunnel under the Saensaep canal and Sukumvit 71 road before arriving the outlet shaft at the Phrakhanong pumping station, where it will

be passed through some treatment process, pumped into the Prakhanong canal and subsequently flowed into the Chaophraya River.

Along the route, the tunnel was excavated underneath the Saensaep canal which is the main canal in Bangkok metropolitan, busy roads and some underground obstructions such as pile foundations of bridges and Bangkok Mass Transit System (BTS) sky train.

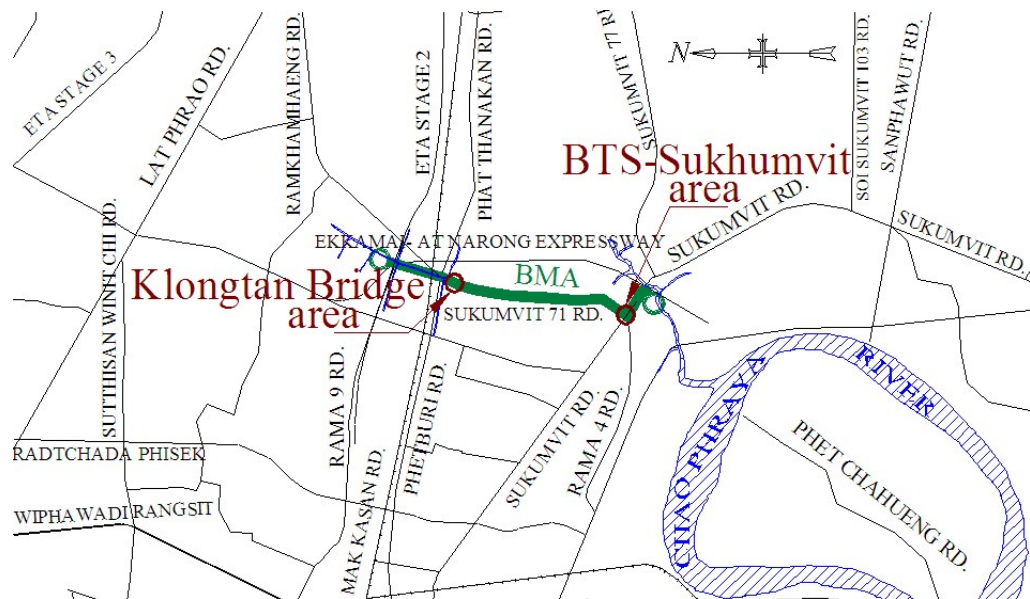


Figure 5.1 Location of BMA flood diversion tunnel (Saensaep-Latphrao Phrakhanong project)

Within the total length of the tunnel, only two locations where the most comprehensive monitoring system for this project was implemented are selected for this study: one is Klongtan Bridge area (Figures 5.2 and 5.3) where the tunnel was bored in dense silty sand and the other is BTS-Sukhumvit area (Figures 5.4 and 5.5) where the tunnel was bored in hard silty clay layer.

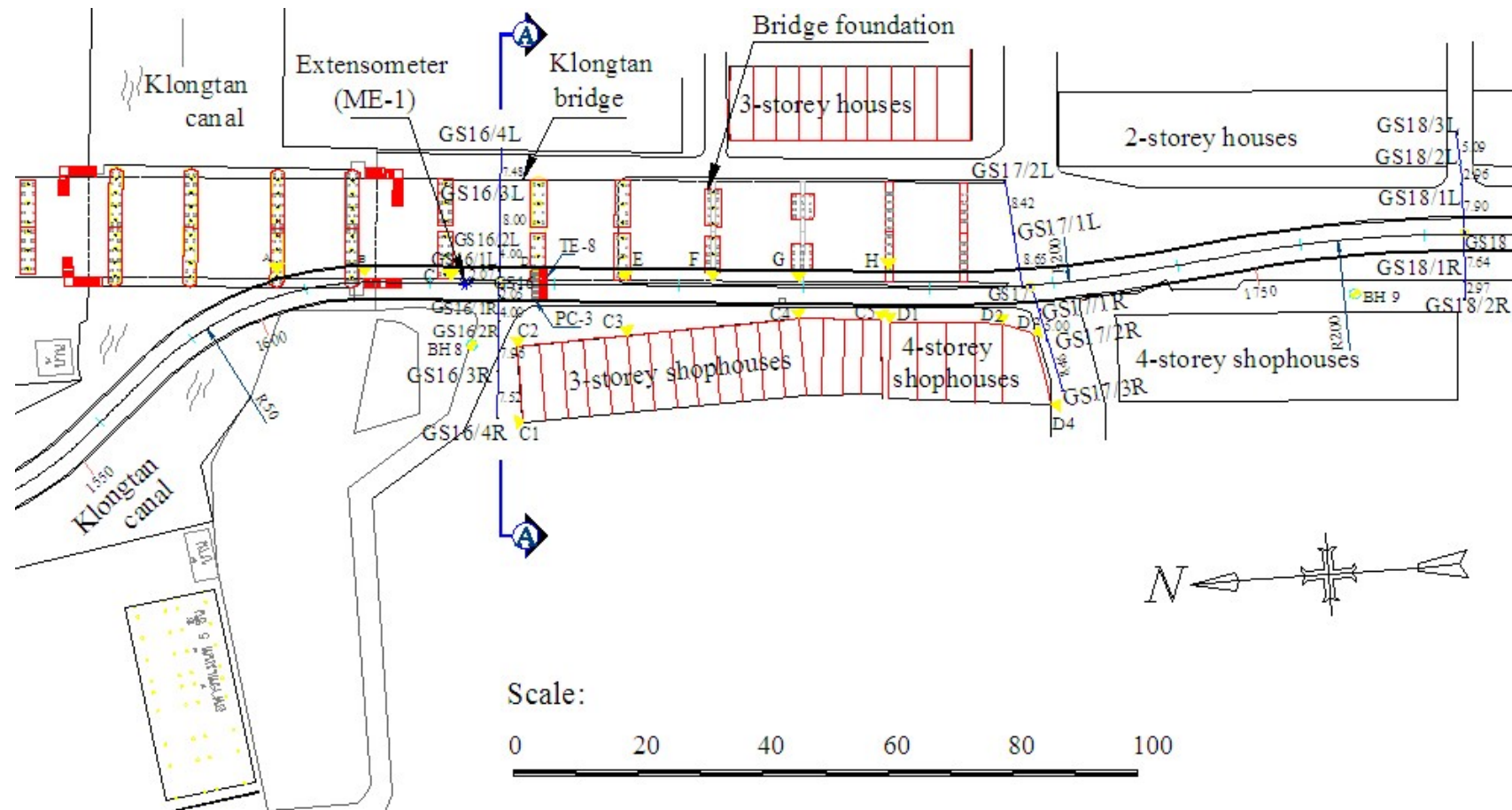


Figure 5.2 Klongtan bridge area (BMA flood diversion tunnel project)



Figure 5.3 Klongtan bridge and old shophouses

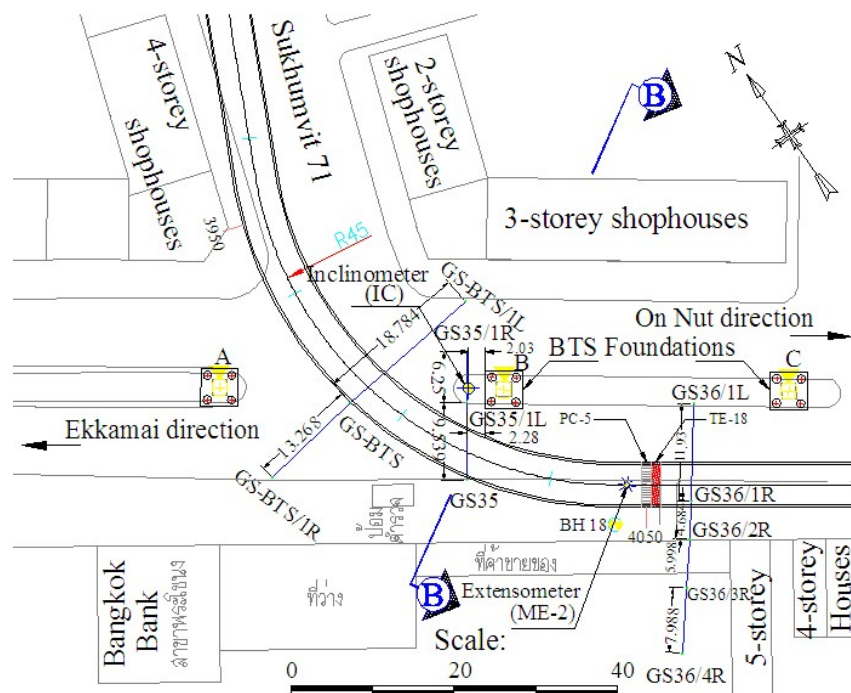


Figure 5.4 BTS-Sukumvit area (BMA flood diversion tunnel project)



Figure 5.5 BTS sky train and shophouses above the curvature alignment

5.2 Soil Profiles of Selected Analysis Sections

As mentioned in section 5.1, only Klongtan Bridge and BTS-Sukhumvit area are selected for analyses in this research. The subsoil conditions are supposed to be identical for the whole selected area, but the obstructions are varied according to the real analysis section. At Klongtan Bridge section (Figure 5.6), the tunnel was fully excavated in dense silty sand layer while at BTS-Sukhumvit section (Figure 5.7), it was bored through the hard silty clay with the crown and invert cut in the very stiff silty clay layers. Two main important structures were found at the two selected areas: an old bridge foundation at Klongtan where the tunnel was bored about 3 m. underneath the tip of the pile, and the pile foundation of BTS sky train at Sukhumvit area where the tunnel was bored 3.65 m on the right side as shown in Figures. 5.6 and 5.7, respectively.

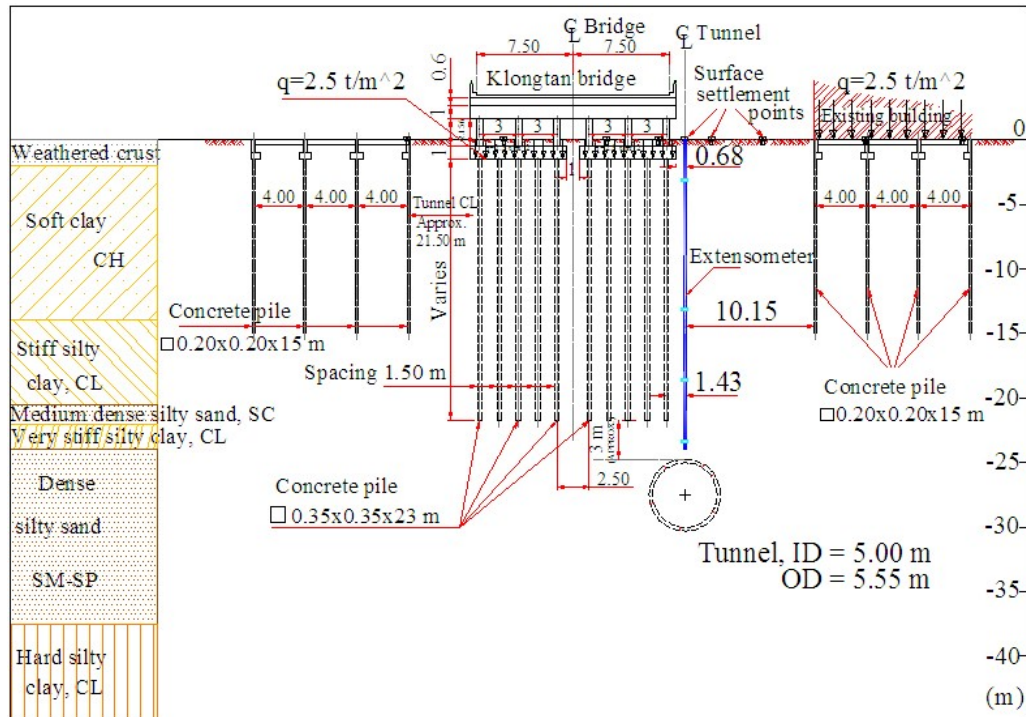


Figure 5.6 Subsoil profile at Klongtan Bridge area and cross section (section AA)

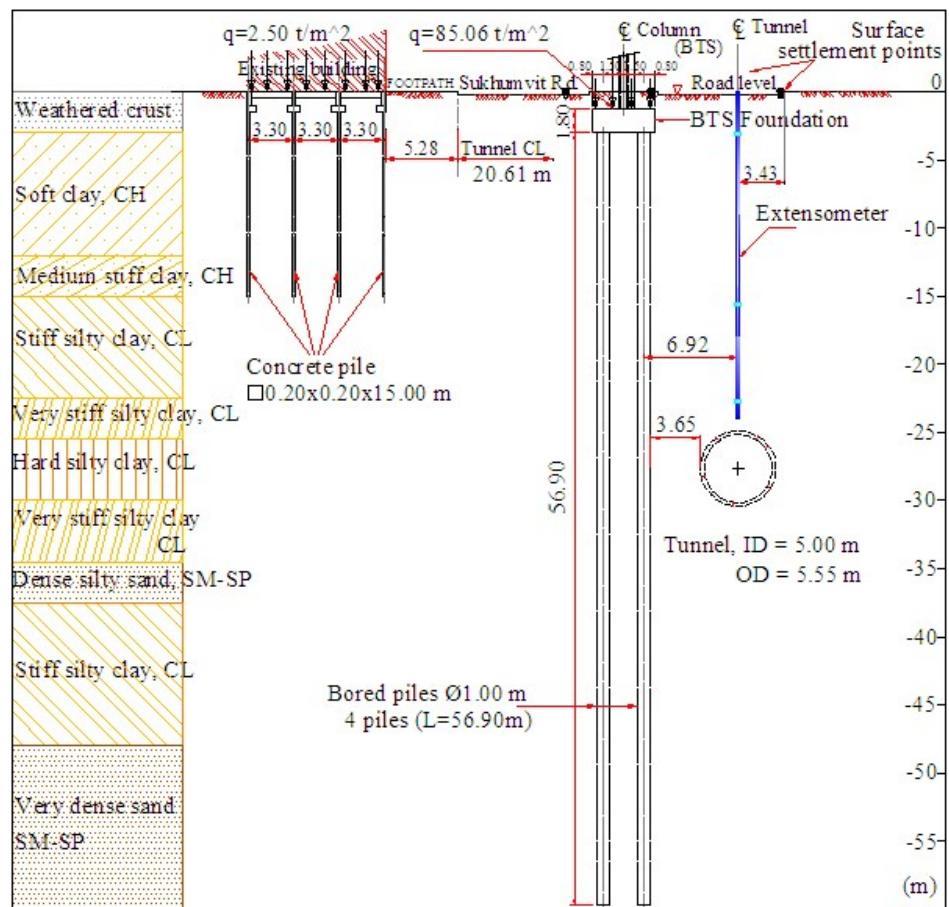


Figure 5.7 Subsoil profile at BTS-Sukumvit area and cross section (section BB)

5.3 TBM Used in the Project

Based on the geological conditions mentioned in section 5.2 and the criteria for selecting the TBM described in Chapter II, the EPB shield machine is the most appropriate tool for this project. Figure 5.2 shows that the tunnel was bored in double sharp S-curve with the radius of 50 m before reaching the straight alignment while the Figure 5.4 shows the radius of curvature alignment which is only 45 m. It is the first experience of tunneling project in Bangkok since the previous projects shown the minimum radius of the curved alignment was not less than 150 m and 93 m for the shield outer diameter of 4.18 m and 3.14 m respectively (Obayashi, 2006 and Moncrieff, 2006). Therefore, the EPB shield machine was specially designed with articulation, which made it possible to excavate in the curved alignment with such a minimum radius (40 m) as existed in the project. The eccentric force created by hydraulic jack to advance the shield against the face pressure and skin friction could cause cracks or failure of the tapered segment. Therefore, to avoid such incidents, the jack thrust was not applied as high as when the shield excavated in the straight alignment. Figure 5.8 illustrates the general feature of articulated shield (Sramoon et al., 2006).

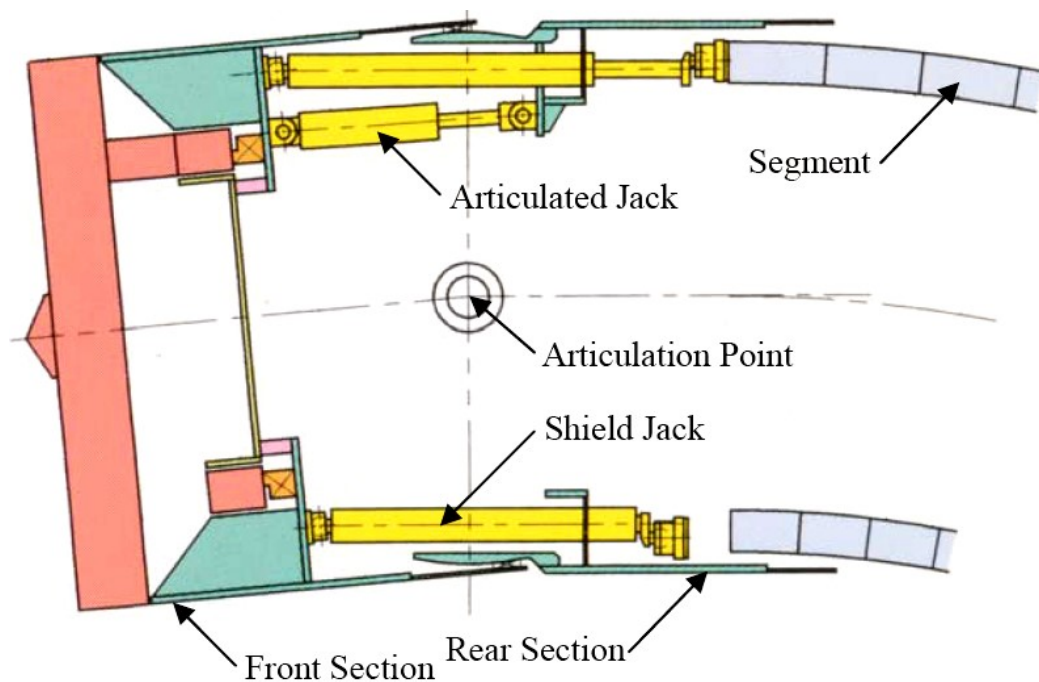


Figure 5.8 General feature of articulated shield (Sramoon et al., 2006)

The detail schematic of articulated EPB shield machine used for in this project is shown in Figure 5.9.

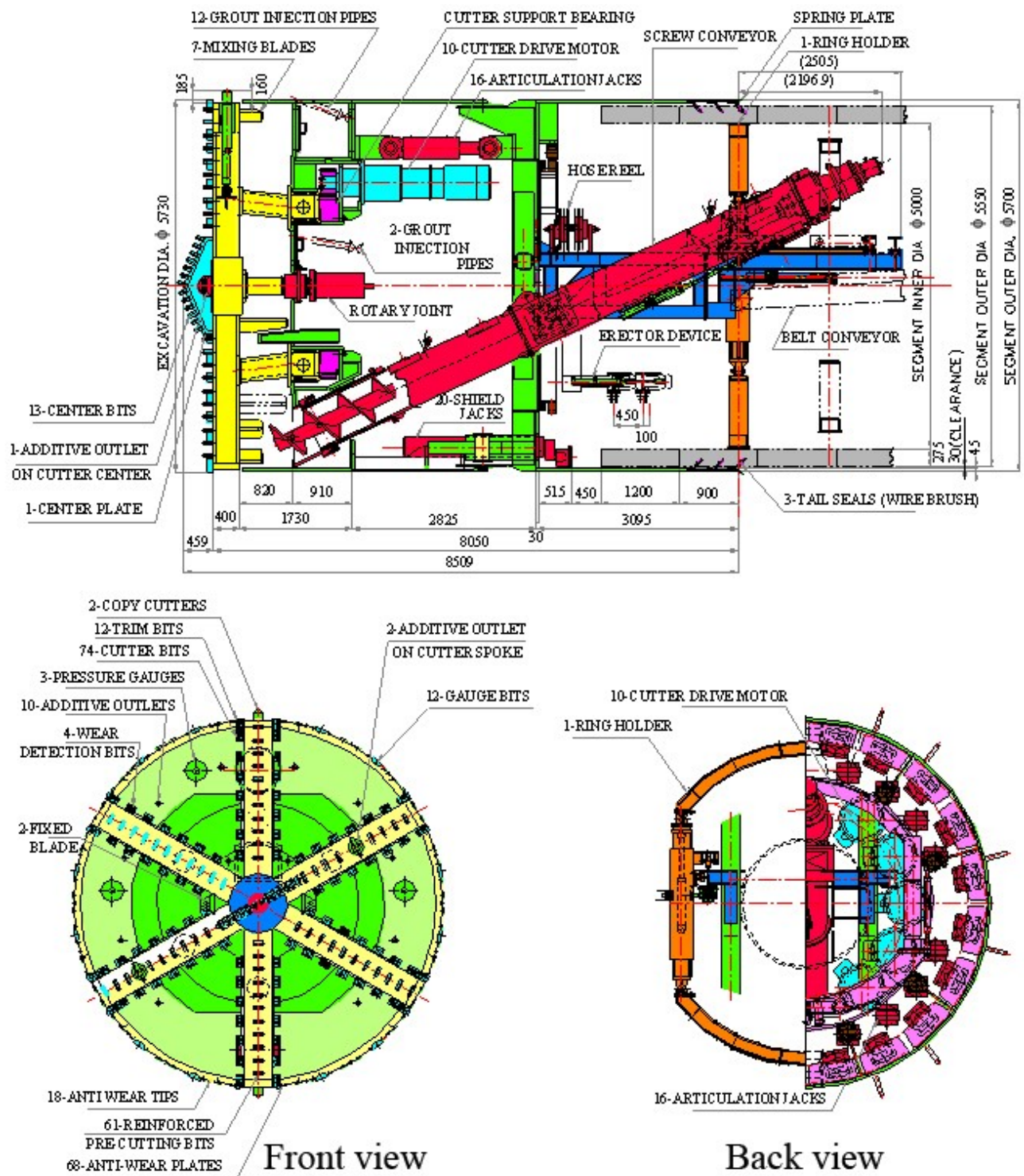


Figure 5.9 Schematic of articulated EPB shield for MBA flood diversion tunnel (Saensaep-Latphrao Phrakhanong project)

A normal EPB shield machine consists of two parts: cutting face or cutting wheel and the main part of the shield, which includes the shield body and tail together as one portion. However, the main part of EPB shield used in this project composes of two separate portions (Figure 5.9), body and tail, but they are connected by the articulation devices that allow the machine to be easily used in the curve alignment with a minimum radius of 35 m. The shield with total weight of 220 tones is advanced by 20 hydraulic jacks (shield jacks). Each hydraulic jack has a maximum jack force of 1500 kPa and a maximum speed of 10 centimeters per minute (Appendix C: picture of the actual EPB shield machine).

5.4 Tunnel Properties

The tunnel lining consists of pre-cast bolted reinforced concrete of 400 ksc of compression strength with six segments per ring in which one is called key segment (Figure 5.10). Each segment is 0.275 m thick and 1.2 m. wide for straight alignment, but this width is reduced to 0.6 m for curvature (tapered segment).

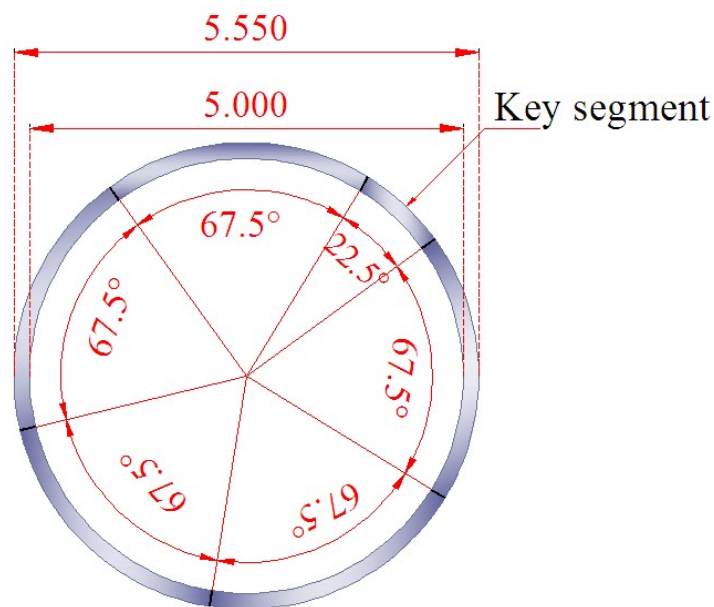


Figure 5.10 Sectional view of tunnel lining

The water sealing material named Hydrotite (RS type) is used to prevent the leakage of water at each joint (Figure 5.11).

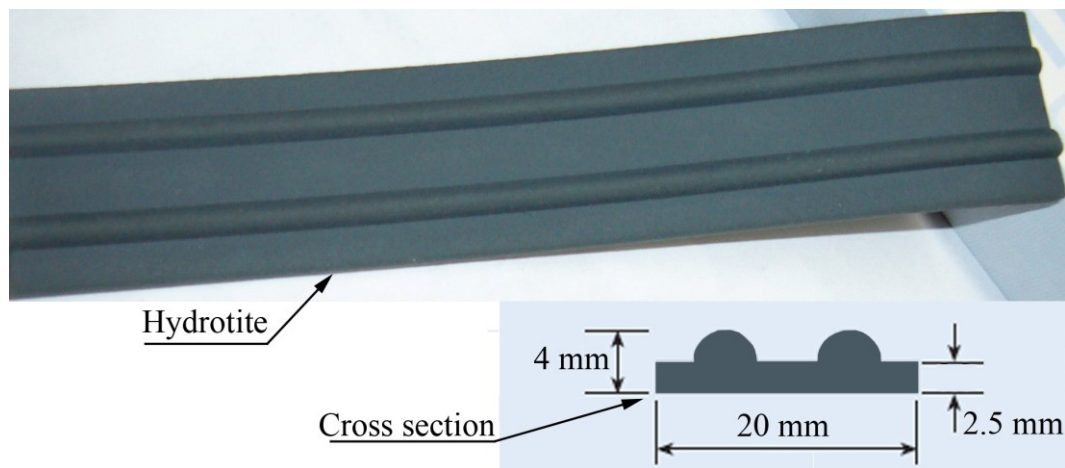


Figure 5.11 Water sealing material (Hydrotite, RS type)

5.5 Monitoring System

To keep the evaluation of the ground and structural deformations under control and for verification of the design assumptions, the defined monitoring systems were set up along the tunneling route. In this regard, Negro (1998) stated that field monitoring is necessary for the success of the tunnel construction because it makes the comparison between prediction and conformity assessment possible. In addition, the monitoring data allow the researchers to study the behaviors of ground and structural movements during construction, post construction and for long-term conditions.

The different types of instrumentation have been used in this research are listed in Table 5.1. The observation of ground surface, building and structural settlement points was done by the staffs of the construction company by means of survey equipment. However, the monitoring relative to inclinometers, extensometers, total pressure cells and convergent bolts was done by the GMT Corporation Ltd.

Table 5.1 Types of Instrumentation and Measurements

Types of Instrumentation	Measurements
Surface settlement points	Total ground surface settlements
Inclinometers	Subsurface horizontal movements in direction perpendicular to the axis of the tunnel
Extensometers	Subsurface settlements or heaves due tunnel excavation
Building and structural settlement points	Settlements of nearby buildings and structures such as bridges
Total earth pressure cells	Total pressure exerts on the tunnel lining
Convergent bolts	Deformation of tunnel geometry

Except the ground surface, building and structural settlement points in which the monitoring is simple and based on the basic knowledge of surveying, a summary of the monitoring methods and data interpretation for other instrumentation will be described in the following paragraphs. Nevertheless, only the devices and application related to tunnel excavation of this research will be mentioned.

5.5.1 Inclinometers

The inclinometers (sometimes called slope indicators) are described as devices used to monitor the deformation parallel and normal to the axis of a flexible pipe (inclinometer casing) by means of a probe passing along the pipe. The probe contains two gravity-sensing transducers (usually a force balance accelerometer) designed to measure inclination with respect to the vertical (EM1110-2-1908, 1995). The inclinometer casing can be a grooved metal (Aluminum alloy, fiberglass or steel) or plastic pipe inserted down a borehole. In order to obtain the good data of lateral deformation at different level below ground surface, the bottom of the casing must be fixed in a stable stratum and the whole casing must be placed as vertically as possible.

The main components of an inclinometer system are shown in Figure 5.12. These components consist of an inclinometer casing, a portable inclinometer probe, a control cable and a portable readout box. The casings which are suitable for most applications are manufactured from ABS (Acrylonitrile/Butadiene/Styrene) plastic,

and available in various sizes. Figure 5.12 also presents the cross section of a casing showing its four orthogonal grooves. The detail of all inclinometer components can be found in the catalog of Slope Indicator Company (2004) or on the website “www.slopeindicator.com”.

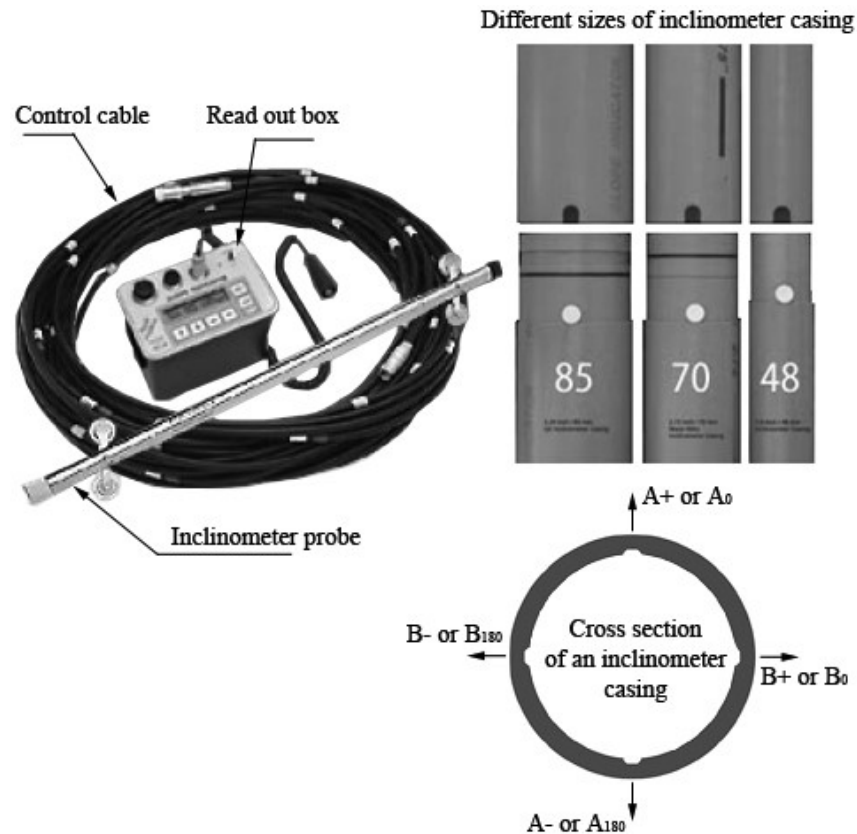


Figure 5.12 Inclinometer system (Slope Indicator Company, 2004)

After an installation of the casing and surveying of its tip location, the probe is lowered down to the bottom and an inclination reading is made. Additional readings are obtained as the probe is raised up incrementally to the top of the casing, providing data for determination of initial casing alignment (Dunnicliff, 1988). The differences between these initial readings and the successive readings, which have been taken over a period of time, give the tilt (angle of inclination) of the inclinometer casing (Figure 5.13). Therefore, the absolute horizontal deformation at any point along the casing can be determined and plotted as a function of depth. Typically, the probe is raised up at an interval of a half meter.

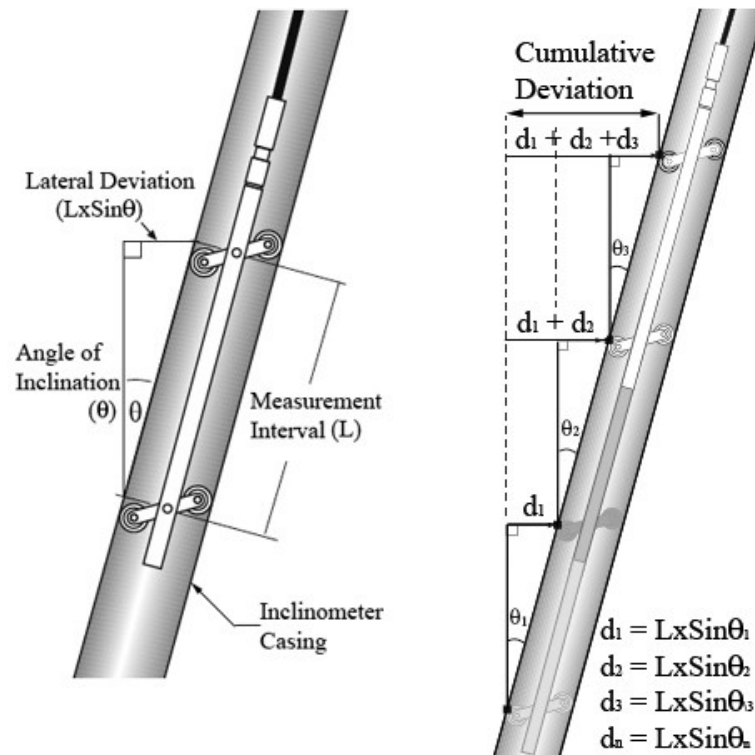


Figure 5.13 Incremental and cumulative deviation (Slope Indicator Company, 1994)

5.5.2 Extensometers

The extensometers here are referred to the magnetic extensometers, which are installed in boreholes in soil to monitor the vertical movements (settlement or heave) of points along the axis of a borehole above or at certain distances from the tunnel (Figure 5.14).

The components of magnetic extensometer consist of a probe, steel survey tape, tap reel with built-in light and a number of spider magnets (magnetic anchors) positioned along the length of an access pipe (Slope Indicator Company, 1994). Figure 5.15 illustrates the components of magnetic extensometer and their positions after an installation with the main components and other accessories.

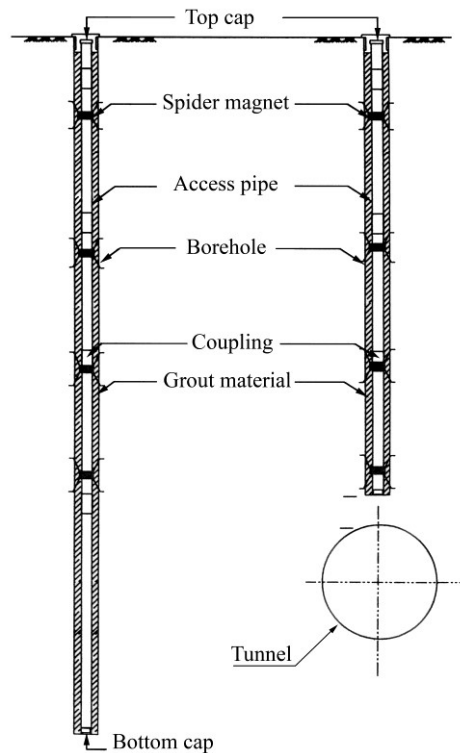


Figure 5.14 Extensometers above and at the side of the tunnel (BMA flood diversion tunnel project)

Based on the application guide of Slope Indicator Company (1994), the monitoring is done by lowering the probe to the bottom of the access pipe and raising it up to find the depth of each magnet. As soon as the probe enters a magnetic field and then a reed switch closes subsequently, the light and buzzer on the reel at the surface activate. The operator then refers to the 1 millimeter graduations on the tape and notes the depth of the magnet. If the access pipe is embedded in stable soil, the depth of each magnet is referred to a datum magnet fixed to the bottom of the pile. The settlement or heave is calculated by comparing the current depth of each magnet to its initial depth. However, if the bottom of access pipe is not embedded in stable soil, the depths of each magnet must be referenced to the top of the pipe that is precisely surveyed before starting the readings.

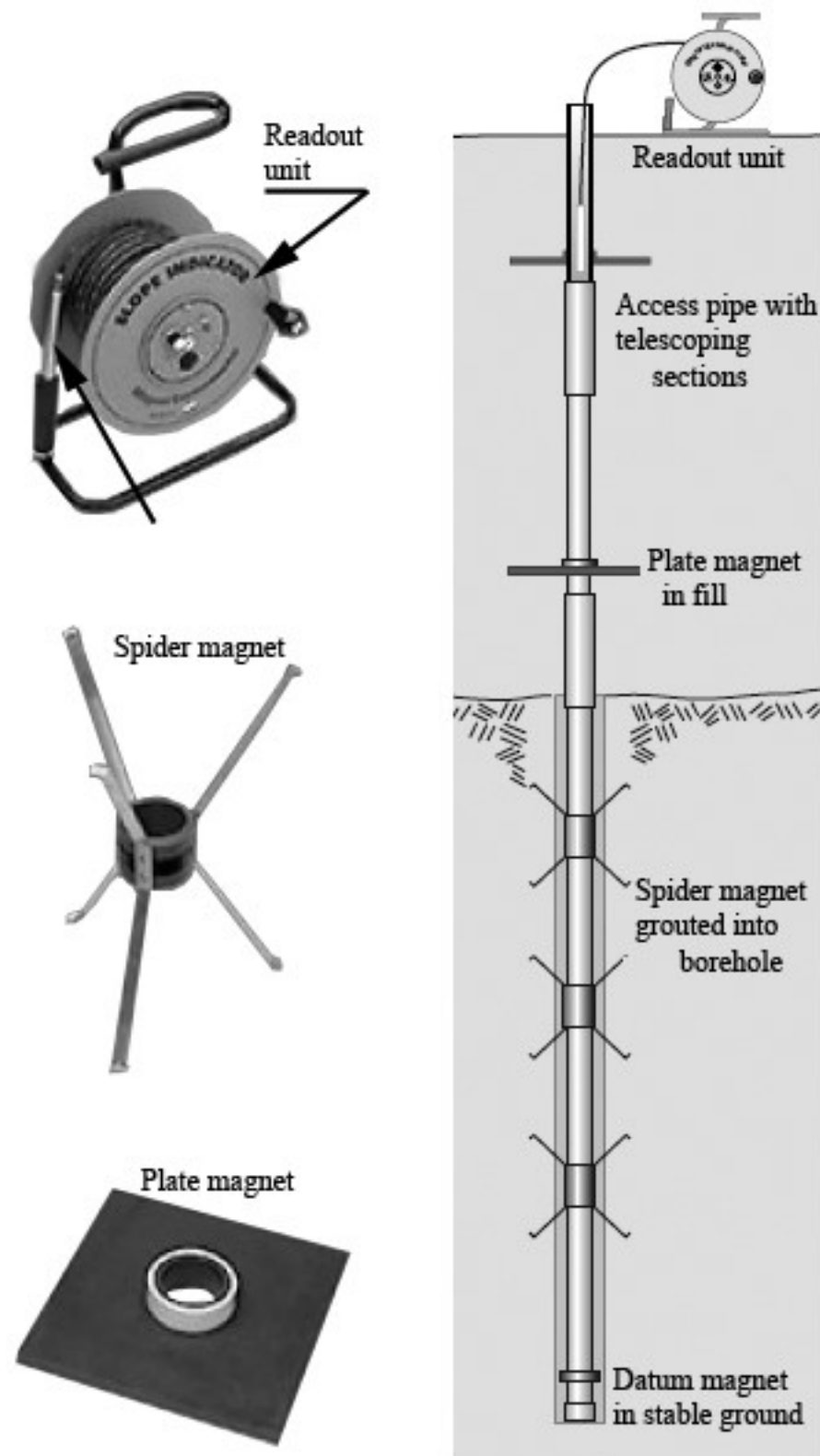


Figure 5.15 Components of magnetic extensometer and their positions after installation (Slope Indicator Company, 2004)

5.5.3 Total Earth Pressure Cells

In the tunneling work, the total earth pressure cells are used to measure the total stress exerting on the tunnel lining. In general, they are used to confirm the design assumptions, to signal a warning of soil pressures in excess of those the liner is designed to withstand, and to provide information for the improvement of future design (Dunnicliff, 1988; Slope Indicator Company, 1994).

The total pressure cell consists of two circular stainless steel plates of 229 mm in diameter and they are welded together around their periphery to form a sealed space. The cell is filled with de-aired liquid and a high pressure tube connected the cell to a pressure transducer as shown in Figure 5.16. The figure also displays the position of total earth pressure cell after embedding in the tunnel segmental lining (BMA flood diversion project, Saensaep-Latphrao Phrakhanong). The active face of the cell is placed in direct contact with the soil.

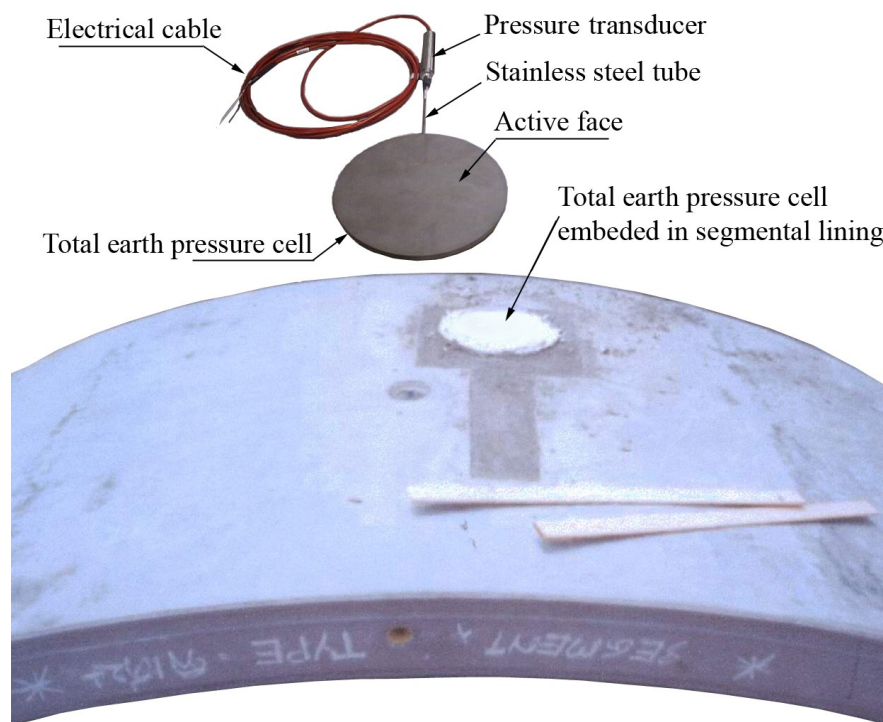


Figure 5.16 Total earth pressure cell and its position after embedding in the tunnel segmental lining (BMA flood diversion tunnel project)

Once stress is acted on the active face of the cell, it pressurizes the filled liquid which is automatically transferred to the pressure transducer. After that the pressure is converted into an electrical signal and transmitted to the readout device via cable.

5.5.4 Convergence Bolts

The convergence bolts described in this section referred to the tape extensometer system, which is used to monitor the changes in distance between reference points anchored in tunnel walls (Figure 5.17).

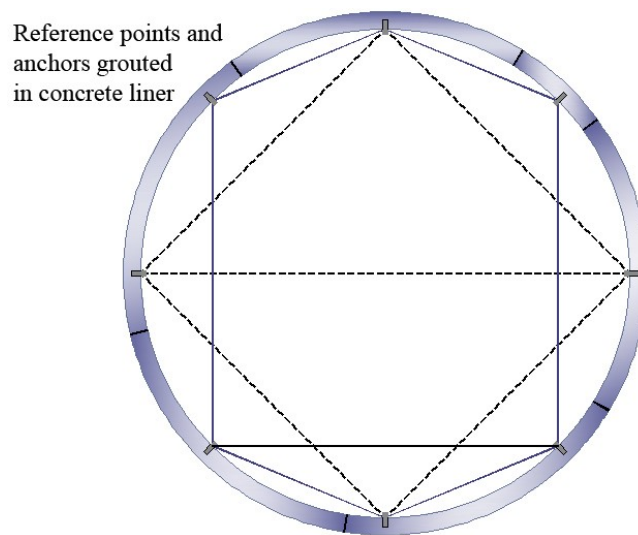


Figure 5.17 Typical installation of convergence bolts and monitoring patterns

The tape extensometer system consists of, a stainless steel tape with punched holes at regular intervals (2.5 cm), tape reel, dial gage with resolution 0.01, collar for tension adjustment for applying a constant tension to the tape, steel reference bolts and two hooks or two joints attached on the instrument body and the free end of the tape (Figure 5.18).

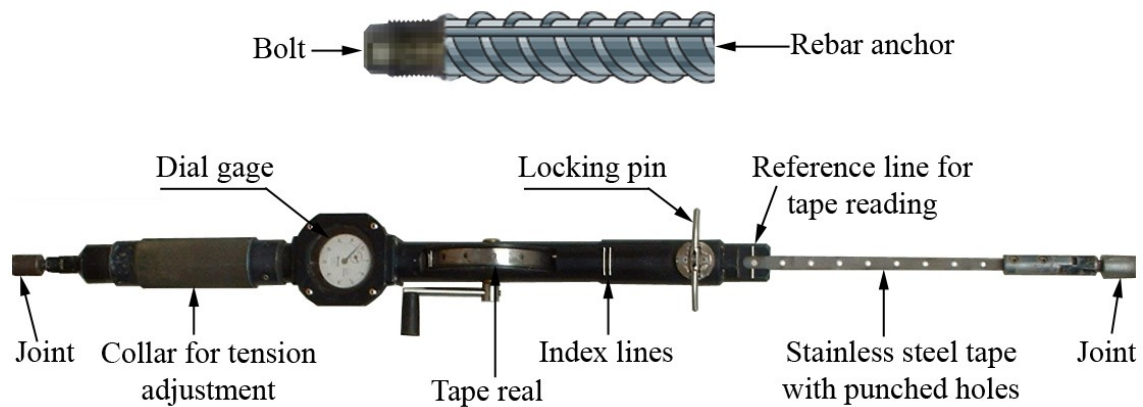


Figure 5.18 Tape extensometer (BMA flood diversion tunnel project)

To obtain a measurement, the operator stretches the tape between two reference points, connecting the free end of the tape to one point and the instrument body to the other. The operator tensions the tape by turning a knurled collar until two index marks are aligned, and then notes the reading from the tape, the internal sliding scale, and the dial gauge. The sum of these readings is the distance between the two reference points. This procedure is repeated for the remaining points at the measurement station. On comparing current readings to initial readings, the operator can calculate the change in distance between the two points (Slope Indicator Company, 2004).

5.6 Layouts of Instrumentation at the Sites of the Study

The layouts of instrumentation for the two selected areas (Klongtan Bridge and BTS elevated train) are shown in Figures 5.2 and 5.4.

At the Klongtan Bridge area (Figure 5.2), the instrumentation consists of:

- Ground surface settlement array GS16 placed below the bridge, GS17 close to the toe of the bridge and GS18 across the busy road;
- One extensometer (ME-1) placed above the tunnel centerline and close to the GS16;
- Total earth pressure cells installed at the contact between soil and a segment of ring number 1654;
- Convergence bolts attached inside the tunnel on rings numbers 1655;

- Structural settlement points fixed on the columns above the bridge foundations (Point A to H) and of the nearby old shophouse foundations (point C₁ to C₅ and D₁ to D₄).

Similarly to the Klongtan Bridge area, the instrumentation for BTS-Sukhumvit (Figure 5.4) consists of:

- Ground surface settlement array GS-BTS set at the curvilinear junction of busy roads and GS35 about 2.28 m close to the BTS pile foundation;
- One inclinometer (IC) placed about 7 m. from the tunnel centerline and about 2 m. close to the BTS pile foundation;
- One extensometer (ME-2) placed above the tunnel centerline and close to the GS36;
- Total earth pressure cells installed at the contact between soil and the segment of ring number 4050;
- Convergence bolts attached inside the tunnel on ring number 4051;
- Structural settlement points fixed on all columns of BTS pile foundations

The structural settlement points provide information regarding the stability of the structures under consideration, and the actions taken if the excessive settlements happen beyond the allowable limitation for such structures. In some circumstances, the ground surface settlements also allow researchers to evaluate the overall stabilization of the structures situated within the influenced zone. Moreover, the monitored data at the ground surface can be used to estimate the volume of surface settlement trough, which serves later as the input of the tunnel contraction for FEM analysis. Finally, the comparison of field monitored data with FEM results can be conducted and it leads to a confirmation of the various factors assumed in the FEM simulation.

CHAPTER VI

NUMERICAL METHOD AND ANALYSES

The development of numerical or FEM analysis for geotechnical engineering works has encouraged the underground constructions in complicated and difficult subsoil condition areas, i.e. metropolis zones. The principle advantages of the FEM analysis are that the interaction between soil and structure can be modeled and that both design loads and expected moments can be studied. Nowadays, there are many finite element and finite difference codes that can be used in analysis of tunnel construction in various subsoil conditions.

The finite element program called PLAXIS version 8 (Brinkgreve, 2002), licensed to Chulalongkorn University, is proposed to be used in this research. It is a finite element package specifically intended for the 2D analysis of deformation and stability for various types of geotechnical works. The word PLAXIS is an abbreviation of “pla” from the word plane strain and “axis” from axisymmetric analysis, which are generally used in geotechnical field. The plane strain model is considered when the analysis problems, i.e. tunnel or embankment, have a constant cross section for a distance in which the movements perpendicular to the section are assumed to be zero. However, the axisymmetric option is selected when the analysis problem is symmetric around the central axis and the stress state and movement can be considered identically at any distance from that axis.

This chapter provides an overview of the PLAXIS program and the specific options of the implementation of PLAXIS program for the analysis in this research. It also gives some examples of recent research studies using PLAXIS program as well as the Mohr Coulomb soil model, which is also selected for the present study. The final section provides the analysis method this study used.

6.1 Sign Conventions and Units

6.1.1 Sign Conventions

The geometry model is necessary for the subsequent input and calculation. This geometry is created in the x - y plane of the global coordinate system (Figure 6.1), where the z -direction is the out-of-plane direction with the positive direction is pointing towards users. Although PLAXIS version 8 is a 2D program, stresses are based on the 3D Cartesian coordinate system as shown in Figure 6.1. In a plane strain analysis σ_{zz} is the out-of-plane stress. In an axisymmetric analysis, x represents the radial coordinate, y the axial coordinate and z the tangential direction. In this case, σ_{xx} represents the radial stress and σ_{zz} the hoop stress.

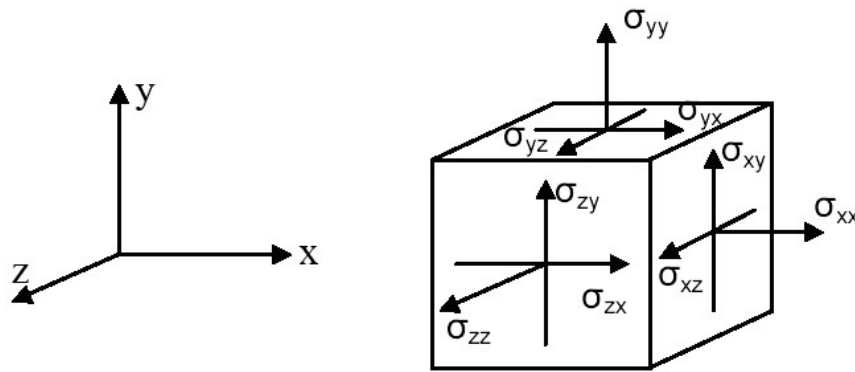


Figure 6.1 Coordinate system and sign conventions for stress components
(Brinkgreve, 2002)

Figure 6.1 shows the positive stress directions in the global coordinate system. Therefore, the compressive stresses and forces as well as pore pressures resulting from a calculation are mentioned with the negative signs while the tensile stresses and forces are mentioned with the positive one.

6.1.2 Units

In PLAXIS program, the basic units can be found in the **General settings window** of the Input program. By default, these basic units are set to m, kN and day for length, force and time, respectively. Therefore, it is necessary to select an appropriate set of basic units before starting to analyze a new problem. However, the

basic units can be changed at any time before processing to the calculation. The new units will also be automatically considered for all the input values in the input program.

In a plane strain analysis, the computed forces resulting from prescribed displacements represent forces per unit length in the out of plane direction (z -direction, Figure 6.1).

In an axisymmetric analysis, the computed forces (***Force-X***, ***Force-Y***) are those that act on the boundary of a circle subtending an angle of one radian. In order to obtain the forces corresponding to the complete problem, these forces must be multiplied by a factor of 2π . All other outputs for axisymmetric problems are given per unit width and not per radian.

6.2 Geometric Input

The problem to be analyzed in PLAXIS is represented by a geometry model, which consists of points, lines and clusters. Points and lines are entered by users based on the drawing procedures while the clusters are automatically generated by the program. Moreover, structural components or special conditions can be directly assigned to the geometry model to simulate tunnel linings, walls, plates, soil-structure interaction or loadings.

It is, therefore, recommended that the creation of a geometry model be started from drawing the full geometry contour. In addition, users may specify material layers, structural members, lines used for construction phases, loads and boundary conditions. The geometry model should not only include the initial situation, but also situations that occur in the various calculation phases. When the full geometry model has been defined and the material properties have assigned to all the geometry components, the finite element mesh can be easily generated.

6.3 Mesh Generation

When the geometry model is fully defined and material properties are assigned to all clusters and structural members, the geometry has to be divided into finite elements in order to perform finite element calculations. A composition of finite

elements is called a mesh. The basic type of element in a mesh is the 15-node triangular element or the 6-node triangular element (section 6.4).

PLAXIS allows a fully automatic generation of unstructured meshes of triangular elements. A precious time is saved by this automatic mesh generation. The options for global and local mesh refinement are available during phase. When the global refinement is selected, the mesh is automatically generated one more again and the global coarseness parameter will be increased one level for example from medium to fine. However, the local refinement is usually applied to the areas where large stress concentrations or large deformation gradients are expected. This situation often occurs when the geometry model includes edges or corners or structural members.

6.4 Elements and Accuracy of Calculation

To analyze a problem, users may select either 15-node or 6-node triangular elements (Figure 6.2) as the basic type of element to model soil layers and other volume clusters. A 6-node triangular element consists of 6 nodes and contains 3 stress points while a 15-node triangular element consists of 15 nodes and contains 12 stress points. The type of element for structures and interfaces is automatically taken to be compatible with the basic type of soil element. A mesh composed of 15-node elements usually gives a much finer distribution of nodes and thus much more accurate results than a similar mesh composed of an equal number of 6-node elements. In addition, in axisymmetric models or in the case of a bearing capacity calculation or a safety analysis by means of phi-c reduction, the 6-node elements usually yield an overprediction resulting in the failure loads or safety factors. Nevertheless, the use of 15-node elements is more time consuming than using 6-node ones.

During a finite element calculation, displacements are calculated at the nodes. On the contrary, stresses and strains are calculated at individual stress points (Gaussian integration points) rather than at the nodes.

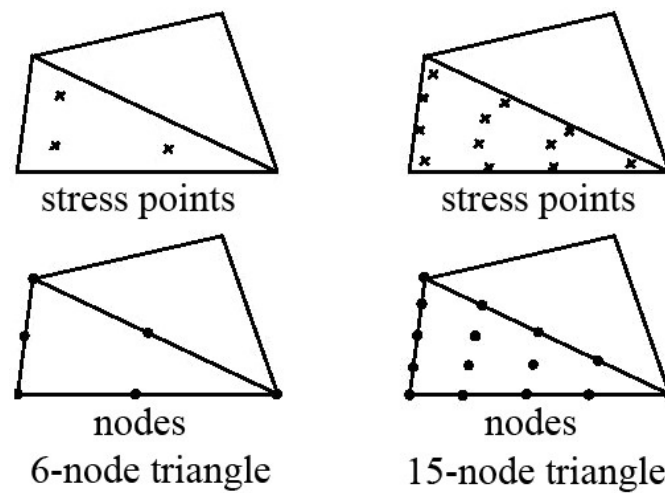


Figure 6.2 Nodes and stress points in soil elements (Brinkgreve, 2002)

6.5 Structural Elements

In PLAXIS, the structural elements could be simulated as line elements (plates or beam elements) with three degrees of freedom per node: Two degrees of freedom related to the displacement (u_x , u_y) and one rotational degree of freedom (rotation in the x - y plane: ϕ_z). Whenever the 6-node soil elements are used, the 3-node beam elements are automatically considered and each beam element contains two pairs of Gaussian stress points. On the other hand, when the 15-node soil elements are used, the 5-node beam elements are considered with four pairs of stress points as shown in Figure 6.3.

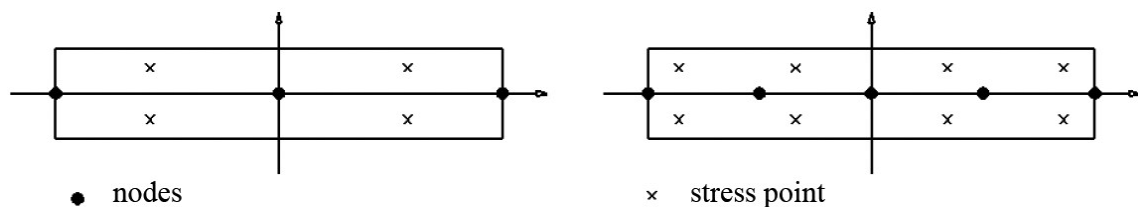


Figure 6.3 Position of nodes and stress points in a 3-node and a 5-node beam element (Brinkgreve, 2002)

The most important parameters of beam elements are the flexural rigidity (bending stiffness) EI and the axial stiffness EA . From these two parameters, an equivalent thickness, d_{eq} , of beam element can be determined based on Equation (6.1).

$$d_{eq} = \sqrt{12 \frac{EI}{EA}} \quad (6.1)$$

Attention must be paid when the beam elements are used to represent the embedded structures since they will superimpose on the soil layers. Therefore, the effective beam weight has to be considered in the analysis (Brand, 2000).

Beam elements can be activated or de-activated in calculation phases using Staged construction as loading input.

6.6 Interfaces

The interface elements are needed for calculations involving soil-structure interaction. They may be used to simulate, for example, the thin zone of intensely shearing material at the contact between a tunnel and the surrounding soil. The absence of interface between soil and structure may lead to an unrealistic stress distribution, especially for the structure involving edges or corners.

The interface properties are calculated from the surrounding soil properties in the associated data set and the strength reduction factor (R_{inter}). In the case $R_{inter} < 1$, this means that the properties of interface such as friction, cohesion and stiffness are lower than the surrounding soil properties. In contrast, the same properties for both interface and surrounding soils are executed if $R_{inter} = 1$. In the absence of detailed information, the value of R_{inter} may be assumed in an order of 2/3 for a sand-steel contact and of the order of 1/2 for clay-steel contact, whereas the interaction with rough concrete usually gives a somewhat higher value. A value of R_{inter} which is greater than 1 is not normally used.

6.7 Soil Models

The PLAXIS version 8 provides a wide range of soil models to be used for analysis a specific problem. These soil models could be cited as linear elastic, Mohr-

Coulomb, jointed rock, hardening-soil, soft-soil creep and soft soil. Moreover, this updated version offers a special option named “user-defined soil models” that allows users to implement a wide range of constitutive soil models, which are not available, into the PLAXIS program.

A brief description of the six soil models is given in the following paragraphs; however, a deeper explanation about Mohr Coulomb soil model which is chosen for this study is extended in section 6.11.1.

Linear elastic model: This model involves only two elastic parameters, i.e. Young’s modulus E and Poisson’s ratio ν . The model created is based on Hooke’s law of isotropic linear elasticity, which could not simulate the real behavior of soil. Generally, it is not considered using with soft rock but it is suitable to model the massive structural elements in soil and bedrock layers.

Mohr-Coulomb model: This elastic perfectly-plastic model is very well known and habitually used for a preliminary analysis of the problem to be studied. Basically, the model involves five parameters, in which two parameters, Young’s modulus E and Poisson’s ratio ν , control the elastic behavior, and other three, cohesion c , friction angle ϕ and angle of dilatancy ψ , control the plastic behavior. In addition, a proper K_0 -value has to be mentioned in order to calculate the initial horizontal stress which plays an important role in soil deformation problems.

Joint rock model: The model is an anisotropic elastic perfectly-plastic model, which is used to simulate the behavior of rock layers involving stratification and particular fault directions. Materials may have different properties in different directions. The intact rock is anticipated to behave fully elastically with constant stiffness properties E and ν . A reduction of elastic properties may be defined for the stratification direction.

Hardening-soil model: In the same way as Mohr-Coulomb model, the limited states of stress of hardening-soil model are also described by cohesion c , friction angle ϕ and angle of dilatancy ψ . However, soil stiffness is classified into three different kinds of stiffness: the triaxial loading stiffness, E_{50} , the triaxial unloading stiffness, E_{ur} , and the oedometer loading stiffness, E_{oed} . The hardening-soil model can be used to simulate the behavior of soft and stiff soil as well.

Soft-soil creep model: Unlike the above hardening-soil model, the soft-soil creep model also takes in to account the effect of viscosity, i.e. creep and stress

relaxation. In fact, all soils exhibit some creep and primary compression is thus followed by a certain amount of secondary compression. The model may be used to simulate the time-dependent behavior of near-normally consolidated clays, clayey silts and peat.

Soft soil model: It is a Cam-Clay type model since the basic parameters (λ^* and κ^*) of this model are linked to those (λ and κ) of the Cam-Clay via the void ratio parameter. The model can be used to simulate the behavior of primary compression of normally-consolidated clay soils. However, it does not incorporate time effects such as in secondary compression, which is available in the soft-soil creep model described previously.

6.8 Automatic Load Stepping

The PLAXIS program enables this feature to optimize the step size in order to get an efficient and robust calculation process for plastic calculations. The automatic load stepping procedures are controlled by a number of calculation control parameters. There is a convenient default setting for most control parameters, which strikes a balance between robustness, accuracy and efficiency. However, users can influence the automatic solution procedures by manually adjusting the control parameters. In this way it is possible to have a stricter control over step sizes and accuracy.

6.9 Staged Construction

This important feature enables a realistic simulation of construction and excavation processes by activating and deactivating clusters of elements, applying loads, changing water tables, etc. This procedure allows for a realistic assessment of stresses and displacements as caused, for example, by soil excavation during an underground construction project. It is also possible to change the material data set of a plate or cluster in the framework of this staged construction. However, the ratio EI/EA which determines the equivalent plate thickness (Equation 6.1) must not be changed, since this will introduce an out-of-balance force.

6.10 Upgraded Lagrangian Analysis

With this option, the finite element mesh is continuously updated during the calculation. For some situations, a conventional small strain analysis may show a significant change of geometry. In these situations it is advisable to perform an updated mesh or updated Lagrangian calculation, which is available for all types of calculations. However, one should note that an updated mesh analysis takes much more time and is less robust than a normal calculation. Hence, this option should only be used in special cases such as the construction of an embankment on soft soil.

6.11 Mohr Coulomb Model and Analysis Options

6.11.1 Mohr Coulomb Model

The Mohr-Coulomb model is a well-known soil model that can be used as a first order approximation of real soil behavior, which generally behaves a highly non-linear under load. This robust and simple non-linear model is based on soil parameters known in most practical situations, which lead to a quick and simple analysis; moreover, the procedure tends to reduce errors.

The selection of this model for analyses of the current research based on some reasonable arguments:

- As mentioned in the previous paragraph (section 6.7), the model needs only five basic soil parameters, which are very familiar with the geotechnical engineers, and can be obtained based on the simple field or laboratory tests. Unlike other advanced soil models, which need more tests and sometime complicated in terms of test procedure as well as the availability of test equipment.
- Unlike other advanced soil models, which usually take more time for computation, the model is relatively simple so it leads to a reduction of errors and quick analysis.
- The model can provide a better soil behavior than the linear elastic model, which is generally too crude to capture real behavior of soil.
- It is clearly mentioned in the material manual of PLAXIS version 8 that in unloading problems such as excavation works and tunneling, the soft-soil creep model does not provide a better prediction than the Mohr-Coulomb

model. On the other hand, the soft soil model is also certainly not recommended to use in excavation problems.

Accordingly, it is possible that this elastic-plastic model, Mohr Coulomb model, has been extensively used collaboratively with the PLAXIS program in several research studies and in practices related to the underground constructions. For example, based on the PLAXIS program, Mohr Coulomb model has been used for such recent research studies as mentioned in the last section of this chapter, section 6.12.

Figure 6.4 illustrates the real soil behavior resulting from standard drained triaxial tests and the idealized form given by the Mohr Coulomb model. The figure gives an indication of the meaning and influence of the five basic model parameters. The irreversible strain is noticeably happened when the yield point is reached as shown in Figure 6.4b and the dilatancy angle ψ is needed to model the irreversible increase in volume.

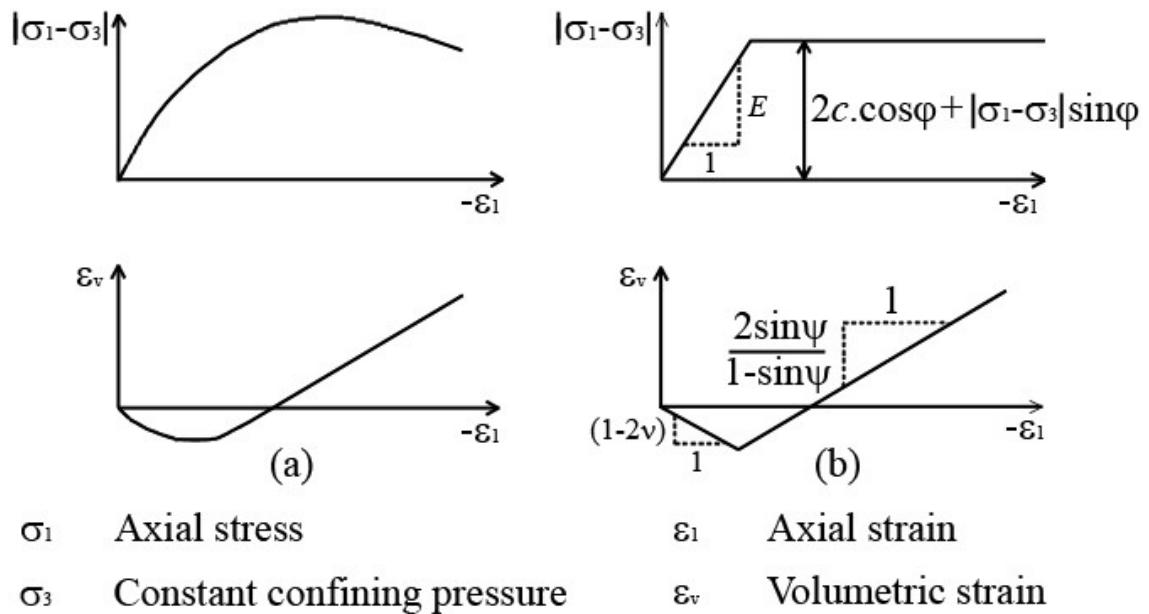


Figure 6.4 Results from standard drained triaxial tests (a) and Mohr Coulomb model (b) (Brinkgreve, 2002)

In the data set of Mohr Coulomb soil model, PLAXIS provides another option that users can enter the value of shear modulus G or the oedometer modulus E_{oed} as

alternatives to substitute the Young's modulus parameter (E). The relationship between these stiffness moduli is given by:

$$G = \frac{E}{2.(1 + \nu)} \quad (6.2)$$

$$E_{oed} = \frac{(1 - \nu).E}{(1 - 2.\nu).(1 + \nu)} \quad (6.3)$$

When formulated in terms of principal stresses, the Mohr-Coulomb failure criterion consists of six yield functions. In principal stress space these yield functions represent the surface of an irregular hexagonal pyramid as shown in Figure 6.5. This figure describes yield surface for the case of cohesionless soil such as sand. In the case of undrained cohesive soils, the convergent point of the yield surfaces will not start from the origin of the coordinate system but from a point behind that origin. The linear elastic behavior is located inside the yield surface.

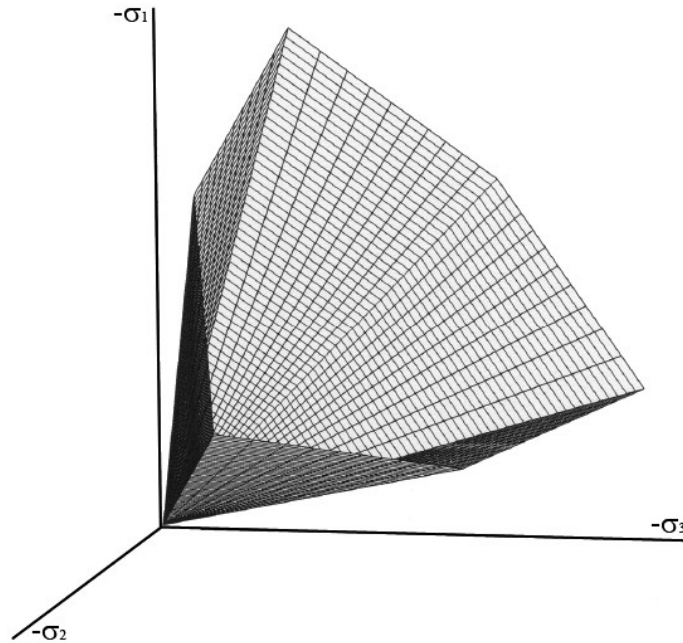


Figure 6.5 Mohr Coulomb yield surface in principal stress space for cohesionless soil
(Brinkgreve, 2002)

As the major ground displacement response to bored tunnel occurred in the short-term condition (Teparaksa 2005a and b, and Phenwej et al. 2006), the undrained analyses were appropriate for the cohesive soil layers. There are two options available in PLAXIS for users to perform the undrained analyses, and they are described in section 6.11.2 and 6.11.3.

6.11.2 Undrained Analysis with Effective Parameters

The simulation of undrained behavior by using effective model parameters is the first option provided by PLAXIS. This option is available for all material models and can be carried out by specifying the *type of material behavior* as *undrained*. In this analysis, the grain solid of the soil or soil skeleton and pore water are supposedly two separate elements, which share the same physical space.

The pore pressures between the grain solid of a soil body, usually caused by water, contribute to the total stress level. According to the basic principle of Terzaghi, total stress σ can be divided into effective stress σ' and pore pressures u . However, water is supposed not to sustain any shear stress, so the effective shear stress is equal to the total shear stress. Therefore, the effective shear modulus is equal to the total effective shear modulus accordingly.

Once this special option is selected, the program will convert the input effective parameters such as G and ν' into the undrained parameters E_u and ν_u according to Equation (6.4) to (6.7).

$$E_u = 2.G.(1+\nu_u) \quad (6.4)$$

$$\nu_u = \frac{\nu' + \mu(1 + \nu')}{1 + 2\mu(1 - 2\nu')} \quad (6.5)$$

in which

$$\mu = \frac{1}{3n} \frac{K_w}{K'} \quad (6.6)$$

where K_w is the bulk modulus of water and the bulk modulus of soil skeleton (K') can be obtained by

$$K' = \frac{E'}{3(1 - 2\nu')} \quad (6.7)$$

A fully incompressible behavior is obtained for $\nu_u = 0.5$. However, taking $\nu_u = 0.5$ leads to singularity of the stiffness matrix (Equation 6.8). In order to avoid numerical problems caused by an extremely low compressibility, by default, the PLAXIS program considers ν_u as 0.495, which makes the undrained soil body slightly compressible. Consequently, for undrained material behavior a bulk modulus of water is automatically added to the stiffness matrix. Its value is determined by Equation (6.8).

$$\frac{K_w}{n} = \frac{3(\nu_u - \nu')}{(1 - 2\nu_u)(1 + \nu')} K' = 300 \frac{0.495 - \nu'}{1 + \nu'} K' \quad (6.8)$$

where n is porosity

To ensure realistic computational results, the bulk modulus of the water must be high enough when compared with the bulk modulus of the soil skeleton, i.e. $K_w \gg n K'$. This condition is sufficiently ensured by requiring $\nu' \leq 0.35$.

The simulation of undrained material behavior on the basis of effective parameters is very convenient when such parameters are available. This enables undrained calculations to be executed with explicit distinction between effective stresses and (excess) pore pressures. For soft soil projects such as those in Bangkok, accurate data on effective parameters are not always be available. Instead, in situ tests and laboratory tests are usually performed to obtain undrained soil parameters. In these situations measured undrained Young's modulus can be easily converted into effective Young's modulus by:

$$E' = \frac{2(1 + \nu')}{3} E_u \quad (6.9)$$

Undrained shear strengths, however, cannot easily be used to determine the effective strength parameters ϕ and c . In this case, PLAXIS offers the possibility of an

undrained analysis with direct input of the undrained shear strength as described in the next section.

6.11.3 Undrained Analysis with Undrained Parameters

With this alternative, the non-porous option is selected to simulate the undrained behavior. This means that the grain solid of soil and pore water are considered as a unique body, and they directly enter undrained elastic properties $E = E_u$ and $\nu = \nu_u = 0.495$ in combination with the undrained strength properties $c = c_u$ or S_u and $\phi = \phi_u = 0^\circ$. In this case a total stress analysis is performed without distinction between effective stresses and pore pressures. Therefore, the output of effective stresses are interpreted as total stresses and all the pore water pressures of the non-porous layers are equal to zero.

As the available soil data are limited, this option is the most appropriate to be used for simulation of the tunnel excavation as well as for a study on the behaviors of ground and structural movements in response to tunneling for this research.

6.11.4 Relationship between Undrained Shear Strength and Soil Stiffness

It has been known up till now that the subsoil stiffness is not a constant value, but it depends on strain levels. Mair (1993) reported the changes of soil stiffness with different working shear strain levels for various structural systems (Figure 6.6). The typical working range of tunnels is between 0.1% and 1%.

Shibuya et al. (2001) established the relationship between shear strain and the ratio of in-situ secant shear modulus ($G_{\text{sec(in-situ)}}$) to undrained shear strength obtained from monotonic triaxial ($S_{u(\text{MTX})}$) and field vane shear tests ($S_{u(\text{FVS})}$) for Bangkok clay as shown in Figure 6.7. The average values of $G_{\text{sec(in-situ)}}/S_{u(\text{MTX})}$ in soft clay corresponding to 0.1% and 1% of shear strain were about 230 and 70 respectively while $G_{\text{sec(in-situ)}}/S_{u(\text{FVS})}$ were about 315 and 80. However, these average values in stiff clay found were about 530 and 100 for both $G_{\text{sec(in-situ)}}/S_{u(\text{MTX})}$ and $G_{\text{sec(in-situ)}}/S_{u(\text{FVS})}$.

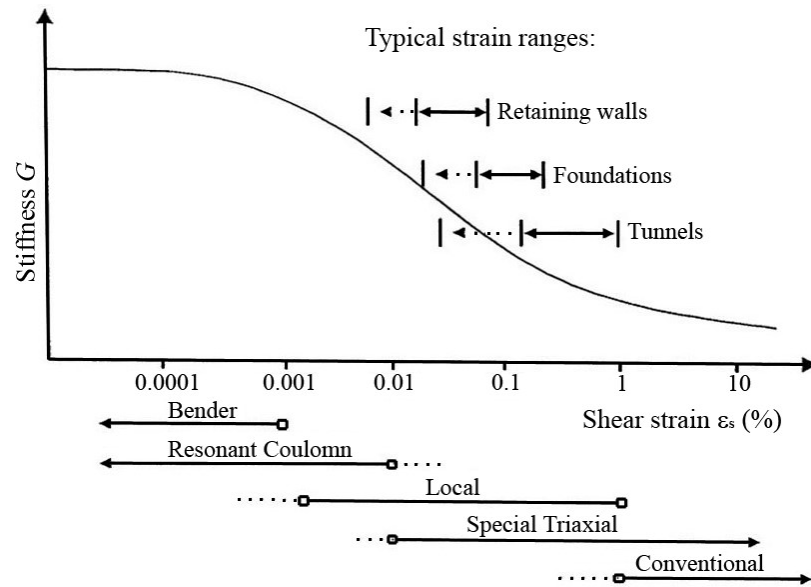


Figure 6.6 Typical shear modulus and shear strains for different geotechnical works
(Mair, 1993)

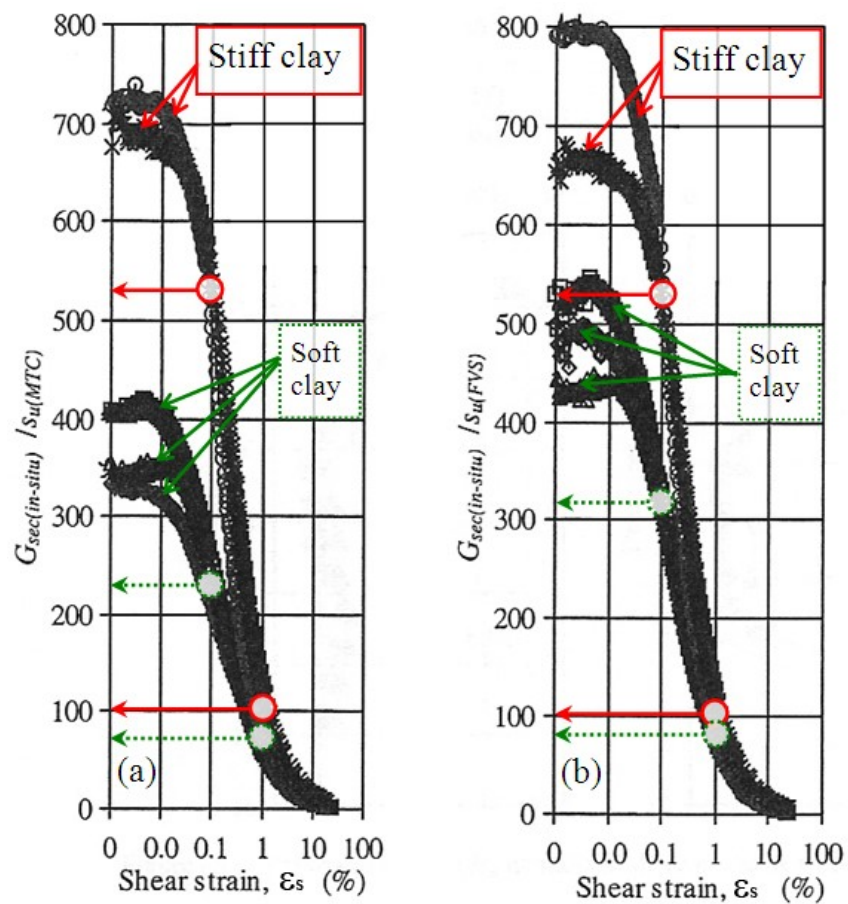


Figure 6.7 Variations of $G_{sec(in-situ)}/S_u$ with shear strains; (a) S_u from MTX, (b) S_u from field vane shear tests (Shibuya et al., 2001)

It is noticeable that the determination of $G_{\text{sec(in-situ)}}$ was based on the results of monotonic undrained triaxial compression and the in-situ seismic cone penetration tests (Shibuya and Tamrakar, 1999 and 2003; Shibuya et al., 2001). For the undrained shear condition of clay sample, the secant shear modulus (G_{sec}) is linked to the secant Young's modulus (E_{sec}) by the relation $G_{\text{sec}} = E_{\text{sec}}/3$. Consequently, the average values of E_u/S_u in soft clay corresponding to 0.1% and 1% shear strain were about 690 and 210 respectively for triaxial test; however, these values slightly increased to 945 and 240 for field vane shear tests. Moreover, these ratios (E_u/S_u) became 1590 and 300 for stiff clay layer.

Similarly, Teparaksa (2005a and b) also presented the correlation between soil stiffness in terms of shear modulus to undrained shear strength (G/S_u) and shear strain for soft and stiff Bangkok clays as shown in Figure 6.8. The curves were taken as the average of all the results given by six numbers of self boring pressuremeter tests for soft and stiff clay layers, which were performed during the design of the first MRTA blue line in Bangkok city and reported by Teparaksa and Heidengren, (1999). The values of G/S_u in soft clay corresponding to 0.1% and 1% of shear strain were about 132 and 55 respectively while the ratios of G/S_u in stiff clay were increased to about 211 and 78.

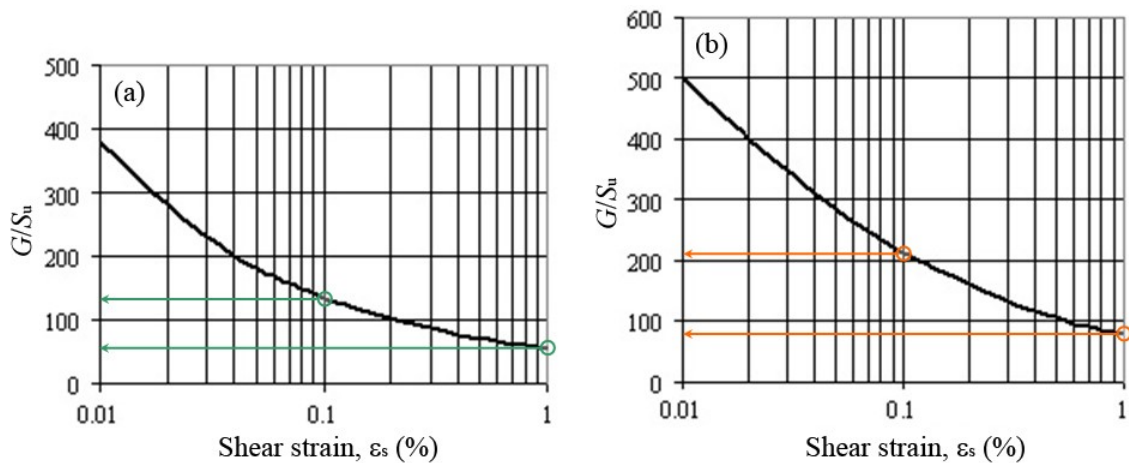


Figure 6.8 Shear modulus of Bangkok clays (a) soft clay and (b) stiff clay (Teparaksa, 2005a and b)

As the self boring pressuremeter tests were performed in undrained condition for each clay layer, the same relation between shear modulus (G) and the undrained Young's modulus (E_u) is still applicable, $G = E_u/3$. Accordingly, the values of E_u/S_u in

soft clay for shear strain of 0.1% and 1% were about 396 and 165 respectively and these ratios became 633 and 234 for stiff clay layer.

Although the ratios of E_u/S_u , which are in the ranges of shear strain between 0.1% to 1% , obtained from Figure 6.8 are smaller than those of Figure 6.7 for both soft and stiff clays, the values of these ratios are always greater for stiff clay than for soft clay.

Within the range of shear strain 0.1% and 1%, Teparaksa and Heidengren, (1999) and Teparaksa, (1999) carried out the back analysis, which was based on 2D-FEM program with Mohr-Coulomb soil model, and found that the appropriate Young's modulus ratios (E_u/S_u) for estimating the ground displacement due to EPB shield tunneling in Bangkok were 240 and 480 for soft and stiff clays, respectively. These ratios are located in the same intervals as what yielded from laboratory (monotonic undrained triaxial compression) and in-situ (seismic cone penetration) as well as from self boring pressuremeter tests described previously. In addition, Teparaksa (2005a) used the values of drained modulus E' (kN/m^2) = $2000.N_{60}$, where N_{60} was the SPT N-value at 60% energy ratio, for silty sand to design a tunnel boring in Bangkok subsoils. Therefore, for the soil stiffness, E_u/S_u and E' , 240 and 480 for soft and stiff clays respectively, and $2000.N_{60}$, are used in this study.

Table 6.1 presents the structural properties at Klongtan Bridge and BTS-Sukhumvit areas, which are used in the 2D FEM simulation. In addition, Tables 6.2 and 6.3 show the soil parameters for FEM analyses at the two studied areas.

Table 6.1 Structural properties for FEM analyses at Klongtan Bridge and BTS-Sukhumvit areas

Material	γ_c (kN/m ³)	d_{eq} (m)	E_c (kN/m ²)	ν_c (-)
Tunnel lining	23.544	0.275	29842020.00	0.16
Pile caps of shophouses	23.544	0.400	23592188.30	0.16
Concrete piles of shophouses	23.544	0.200	23592188.30	0.16
Pile caps of Klongtan bridge	23.544	1.000	23592188.30	0.16
Concrete piles of Klongtan bridge	23.544	0.350	23592188.30	0.16
Pile caps of BTS sky train	23.544	1.800	29842020.00	0.16
Concrete piles of BTS sky train	23.544	0.866	29842020.00	0.16

Table 6.2 Soil parameters for FEM analyses at Klongtan Bridge area

Depth (m)	Soil layer	γ (kN/m ³)	$S_{u(FVS)}, S_u$ (kN/m ²)	ϕ (°)	E_u, E' (kN/m ²)	ν (-)	K_o, K
0.00- 2.00	Weathered crust	17.5	30.0	-	10800	0.350	0.650
2.00- 14.00	Soft clay, CH	15.7	24.0	-	5760	0.495	0.837
14.00- 20.50	Stiff silty clay, CL	19.0	80.6	-	38688	0.495	0.620
20.50- 22.00	Medium dense silty sand, SC	20.0	-	30	33354	0.350	0.500
22.00- 24.00	Very stiff silty clay, CL	20.0	135	-	64800	0.495	0.561
24.00- 37.50	Dense silty sand, SM- SP	20.0	-	35	70632	0.350	0.426
37.50- 40.00	Hard silty clay, CL	20.5	221.0	-	106080	0.495	0.656

Table 6.3 Soil parameters for FEM analyses at BTS-Sukhumvit area

Depth (m)	Soil layer	γ_t (kN/m ³)	$S_{u(FVS)}, S_u$ (kN/m ²)	ϕ (°)	E_u, E' (kN/m ²)	$\nu(-)$	K_o, K
0.00- 3.00	Weathered crust	17.5	30.0	-	10800	0.35	0.67
3.00- 12.00	Soft clay, CH	15.7	20.5	-	4920	0.495	0.854
12.00- 15.00	Medium stiff clay, CH	17.0	46.6	-	16776	0.495	0.7
15.00- 22.50	Stiff silty clay, CL	19.0	97.2	-	46656	0.495	0.6
22.50- 25.50	Very stiff silty clay, CL	20.3	186.0	-	89280	0.495	0.572
25.50- 30.00	Hard silty clay, CL	20.5	265.5	-	127440	0.495	0.544
30.00- 34.50	Very stiff silty clay, CL	20.0	141.0	-	67680	0.495	0.63
34.50- 37.50	Dense silty sand, SM-SP	20.0	-	35	70632	0.35	0.426
37.5- 48.00	Stiff silty clay, CL	17.5	94.0	-	45120	0.495	0.66
> 48.0	Very dense sand, SM-SP	20.0	-	40	98100	0.35	0.357

In both tables, Tables 6.2 and 6.3, the coefficients of lateral earth pressure K and K_o are determined based on the procedure mentioned in section 6.11.5.

6.11.5 Determination of Coefficient of Lateral Earth Pressure

The coefficient of lateral earth pressure has been known as the effective and total coefficient. In an undisturbed ground, the ratio of the horizontal to vertical effective stress is defined as the coefficient of lateral earth pressure at rest, K_o :

$$K_o = \frac{\sigma'_h}{\sigma'_v} \quad (6.10)$$

The value of K_o can vary between about 0.2 and 6 (Coduto, 2001). Typical values are 0.35 and 0.7 for normally consolidated soils and between 0.5 and 3 for overconsolidated soils. The most accurate way to determine K_o is by measuring σ_h in-situ using methods such as the pressuremeter, dilatometer, or stepped blade, and combining it with computed value of σ_v and pore water pressure, u .

In practice, the value of K_o for a normally consolidated soil is often assumed to be related to the effective friction angle ϕ' by the empirical expression of Jaky (1944):

$$K_{oNC} = 1 - \sin\phi' \quad (6.11)$$

The most common method of assessing K_o at any degree of consolidation is given by Equation 6.12 (Mayne and Kulhawy, 1982). This formula is applicable only when the ground surface is level:

$$K_o = (1 - \sin\phi')OCR^{\sin\phi'} \quad (6.12)$$

in which OCR is the overconsolidation ratio and other parameters have been mentioned previously.

Shibuya and Tamrakar (1999) mentioned that the values of $K_{o(NC)}$ for Bangkok soft clay ranged from 0.70 to 0.75; however, the value of $K_{o(NC)}$ for stiff clay were lower than those of soft clay; i.e., over a range from 0.52 to 0.6. In both clays, the K_o was linked to OCR by the expression

$$K_o = K_{oNC} \cdot (OCR)^{0.5} \quad (6.13)$$

Interestingly, the values of K_o for a cohesionless soil are bounded by:

$$\frac{1 - \sin \varphi'}{1 + \sin \varphi'} < K_o < \frac{1 + \sin \varphi'}{1 - \sin \varphi'} \quad (6.14)$$

In the case where the undrained analysis is performed, the total coefficient of lateral earth pressure K will be needed and it can be determined by the Equation 6.15.

$$K = \frac{\sigma_h}{\sigma_v} = \frac{K_o + \frac{u}{\sigma_v}}{1 + \frac{u}{\sigma_v}} \quad (6.15)$$

where u , σ_h , σ'_h , σ_v and σ'_v are pore water pressure, total and effective horizontal and vertical stresses respectively.

For a soil deposit with the water table at the surface and bulk density ρ , the coefficient K could be determined from Equation 6.16 (Pender, 1980).

$$K = K_o - \frac{\rho_w}{\rho} \cdot (K_o - 1) \quad (6.16)$$

in which ρ_w is the water density.

6.12 PLAXIS Used in Previous Research Studies

PLAXIS, an FEM program, was initially developed to analyze the problems associated with river embankments on soft soils in Holland. This 2D finite element code started to be developed in 1987 at the Technical University of Delft as an initiative of the Dutch Department of Public Works and Water Management. After 10-year development, the Windows version was available in 1998 (Brinkgreve, 2002). Until now, many features related to geotechnical problems have been incorporated into the program that makes it broadly used in the geotechnical works. Moreover, among the six soil models available in the program, the Mohr Coulomb seems the most attractive model to use for both designers and researchers.

Some of the examples where Mohr Coulomb and PLAXIS are used as one package to analyze the geotechnical problems, specifically to study the behaviors of

ground movement responding to tunneling works are briefly given in the following paragraphs.

Teparaksa and Heidengren (1999) and Teparaksa (1999) performed a back analysis by using 2D PLAXIS with the elastic perfectly-plastic failure criteria of Mohr Coulomb model to study the interaction between soil and structures during the EPB shield tunneling and subway station box excavation in Bangkok. The aspects for the design of these structures are also mentioned. The same soil model and finite element code were also used to design the extension portion of Bangkok blue line subway (Teparaksa et al., 2006).

Vermeer et al. (2002) carried out an analysis on a circular NATM tunneling based on the program of PLAXIS 3D tunnel, and the ground surface settlement trough was well compared with empirical Gaussian curve and 2D analysis result. The Mohr Coulomb model was considered in the programs, both 2D and 3D PLAXIS. Their finding intends to suggest a fast method for 3D tunnel analysis, i.e. NATM tunnels.

Bonnier et al. (2002) used 2D and 3D PLAXIS to predict the loads on circular tunnel lining constructed by NATM method. The constitutive soil model was indicated by Mohr Coulomb soil parameters. In order to do the comparison between the internal forces obtained from both 2D and 3D analyses, the simulation of tunnel construction method based on β -value was also applied to 2D model. Although the normal forces given by 2D analysis are lower than the average value of the ones from 3D, the 2D value is still realistic and reliable. Moreover, the 2D bending moments appear to match the average ones from a 3D analysis quite well. As the time required for 2D simulation is relatively short; therefore, this approach is still retained within geotechnical research as well as in engineering practice.

Koungelis and Augarde (2004) studied three possibilities of two tunnel constructions, parallel and piggy-back geometries, based on 2D PLAXIS. Then some guidance on the possible effects between these tunnels were provided in the case where a particular soil profile was given with the basic parameters of Mohr Coulomb model.

6.13 Analysis Method of this Study

A systematic research procedure yielding a fruitful result mainly depends on a research design and the method of analysis which have been well planned in prior.

This section, therefore, depicts the necessity of the field monitored data used in this research and the procedures that the analyses are carried out. This leads to the final results in the next chapter.

6.13.1 Selection of Field Monitored Data

All analyses in this research are mainly related to the final short-term condition, which is known as the end of excessive pore water pressure dissipation. In this regard, Srisirirojanakorn (2004) pointed out an interval when the shield passed test sections for the 2000 Evanston tunnel (ET2) as between 10 and 13 days or 91 (298 ft) and 47.5 m. (156 ft.), respectively. Similarly, Phenwej et al. (2006) plotted the changing of subsurface settlement with time in which the significant settlements happened until about 20 days after the shield passed the control section. However, they revealed that in some cases, settlements in soft clay layers, almost 100 percent of short term settlements reached after three to four months.

Accordingly, the three-month data was selected. However, there was no significant difference between one-week, two-week and three-month data (Appendix B). In addition, the field monitored data used in this research was limited to the ground surface settlement arrays, subsurface settlements from borehole extensometers, building settlement points and lateral displacements from inclinometer.

6.13.2 Classification of Ground and Structural Movements

The behaviors of ground surface and subsurface movements as well as structural settlements along the direction of tunnel excavation were classified according to each position of the TBM in respect to the monitored section. These behaviors are extensively described in sections 7.1.1 and 7.2 in the next chapter, Chapter VII.

6.13.3 Empirical Method of Analysis

The monitored data of ground surface settlement arrays were plotted against the lateral distance from the tunnel centerline, and then the volume of ground surface settlement trough per unit length (V_s) was estimated. Therefore, the volume of ground

loss (V_L) expressed in percentage and the trough width parameter (i) could be determined by using Equation (4.6). Subsequently, the ground surface settlement trough could be satisfactorily reproduced based on Equation (4.1).

Moreover, the obtained volume of ground loss (V_L) was later on served as the input of the tunnel contraction for FE analysis.

6.13.4 FE Analysis

6.13.4.1 Model Configuration

For this study, it was the tunnel excavation and a 3D problem so the analysis model for this research was set to plane strain condition. In order to increase the accuracy in deformation analysis, the 15-node triangular soil element consisting of 15 nodes and 12 stress points were also considered in the analysis model. Moreover, the very fine mesh was generated for the whole model geometry and three times of mesh refinement were applied to the clusters inside the tunnel.

Since the available soil data were limited, the constitutive soil model based on elasto-plastic failure criteria of Mohr-Coulomb was the most appropriate to use in this research. In addition, the non-porous option was set to all the cohesive soil while sand and silty sand was considered as drained materials (Tables 6.2 and 6.3). With these settings, there was no ground water flowing in the clay layers and any consolidation could happen in the whole analysis. On the other hand, the tunnel lining and structural elements were simulated as line elements based on elastic properties (Table 6.1).

As the site conditions of the flood diversion tunnel are not symmetric, the full tunnel cross sections were considered in the analyses. In addition in the case where the simulation must be done for the sections, which are not far from one to another and with similar field conditions such as those along the Klongtan bridge, the analysis configurations of each bridge footing and the existing old shophouses based on 2D FEM are the same whereas only the positions of the structures to the tunnel center line are adjusted according to the real analysis sections.

6.13.4.1 Simulation of Tunnel Excavation

The different steps of calculation were performed, based on 2D-FEM program, to simulate the 3D advancement of the tunnel. The 2D-FEM simulation of tunnel construction by means of EPB shield machine could be performed in four phases:

- 1.) *Initial condition determination:* The initial conditions are described with initial in situ stress state and the initial configuration, and initial water pressures. The computation of initial conditions is done after the finite element mesh has been generated. The water pressures are easily generated based on the phreatic level while the initial stresses are calculated based on the K_0 -procedure for the sand and silty sand layers and on the coefficient of total lateral earth pressure (K) for clay and silty clay layers.
- 2.) *The deformation and stresses induced by the existing structures and surcharges:* The deformation and stress state within the soil mass in this phase is calculated immediately after the initial conditions by activating all the existing structures and surcharges at the section under an analysis. Actually this phase is also a part of initial field conditions, which already exist on the site before the tunnel construction. Therefore the displacements happening during this phase are reset to zero for the next calculation phase. One can activate the existing structures and surcharges in two phases separately without any effect on the final deformation.
- 3.) *The tunnel excavation and installation of precast concrete segmental linings:* The tunnel excavation and installation of precast concrete segmental linings are simulated by deactivating the soil clusters inside the tunnel and activating the segmental linings, which have been created in the input of the model. In addition, the changes of water pressures inside the tunnel are also calculated.
- 4.) *The simulation of ground loss after passing of EPB:* The simulation of ground loss or contraction is done after the EPB shield machine passes. This ground loss is the result of several factors which are the over-cutting, different diameter of TBM and the permanent tunnel lining, and redistribution of stress in the soil mass surrounding the tunnel (Chapter IV for more detail).

CHAPTER VII

OBSERVED AND COMPUTED GROUND AND STRUCTURAL MOVEMENTS

Literature of different kinds of TBMs, tunneling methods, the general geological conditions of Bangkok and the detail of subsoil profiles including their engineering properties at the selected locations are reviewed in the previous chapters to establish the background of this research. Moreover, the causes and the methods for predicting ground movements induced by tunnel excavation as well as the analysis method of the present study have been extensively described. This chapter explains the various results obtained from FE back-analyses and the results based on empirical method for surface settlements. The description of the behaviors of ground surface and subsurface movements in response to the advancement of EPB shield, and the interpretation of the analysis results as well as some discussions are also presented in this chapter. In addition, the internal forces of segmental lining resulted from FE analyses are also mentioned.

7.1. Ground Movements

The computed results based on FE program and the monitored data for ground surface and subsurface settlements will be compared in this section. Figures 7.1 and 7.2 show the input geometries of the different analysis sections at Klongtan Bridge and BTS-Sukhumvit areas, respectively. The global mesh for all the analysis sections is very fine; moreover, the mesh refinement is also applied to the clusters inside the tunnel. The examples of finite element mesh generated at section AA cut along GS16 and at section BB (GS35) are illustrated in Figures 7.3 and 7.4, respectively. The generated mesh along GS16 (section AA) at Klongtan Bridge area consists of 4 603 elements, 37 403 nodal points and 55 236 stress points while the mesh of section BB (GS35) is composed of 3 169 elements, 25 815 nodal points and 38 028 stress points. However, the criteria of finite element mesh depend mainly on the types of elements

selected for the input program, the dimension of model to simulate, and the input of existing structures. Some graphical input and output are shown in Appendix D.

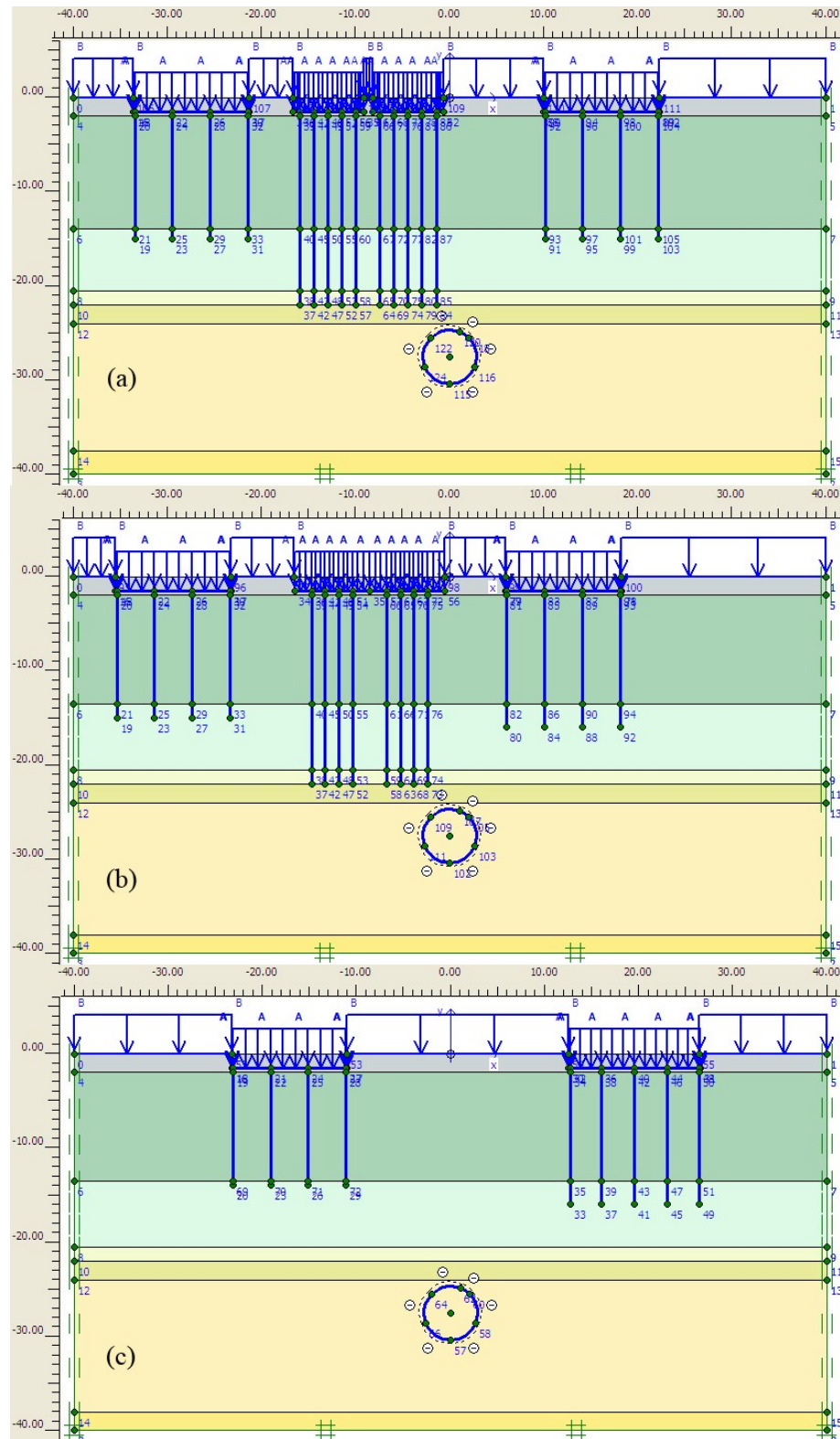


Figure 7.1 Input geometries of different analysis sections at Klongtan Bridge area; (a) GS16, (b) GS17 and (c) GS18

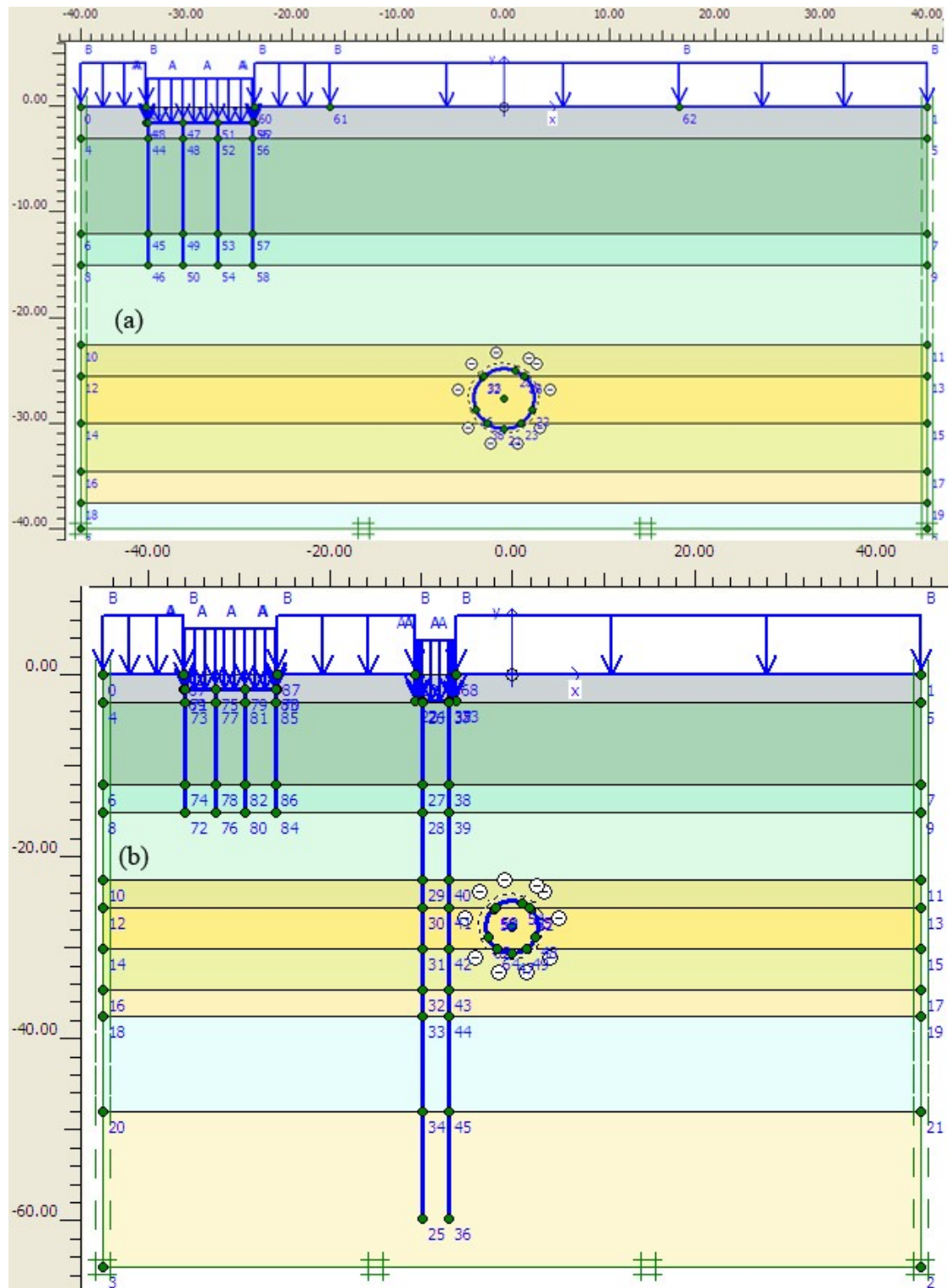


Figure 7.2 Input geometries of different analysis sections at BTS-Sukhumvit area; (a) GS-BTS and (b) GS35

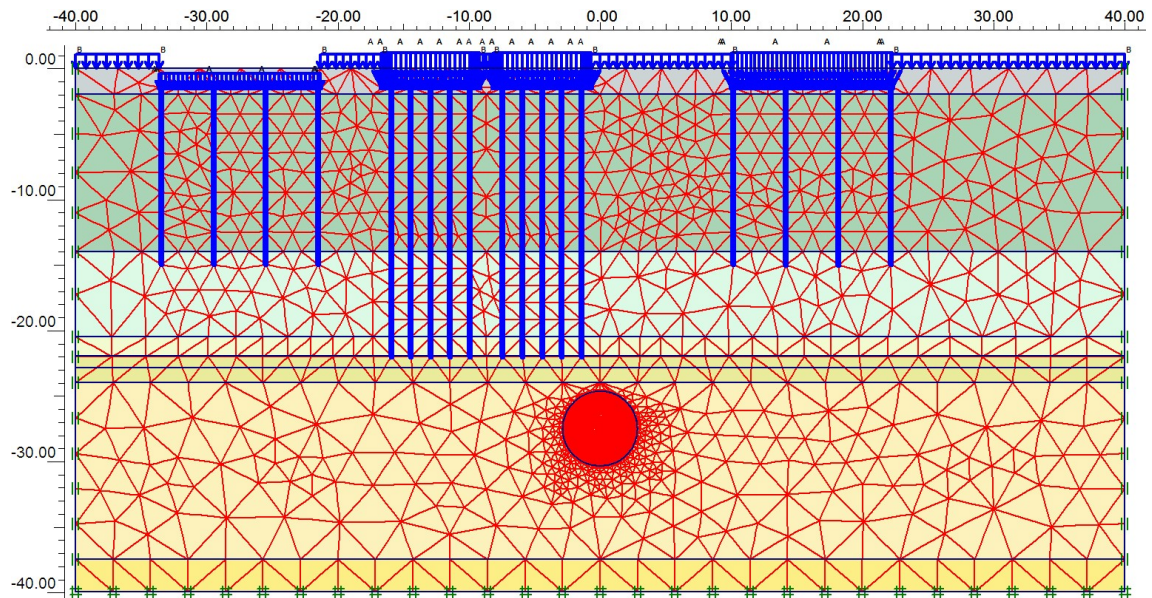


Figure 7. 3 Finite element mesh generated at section AA (Klongtan Bridge area)

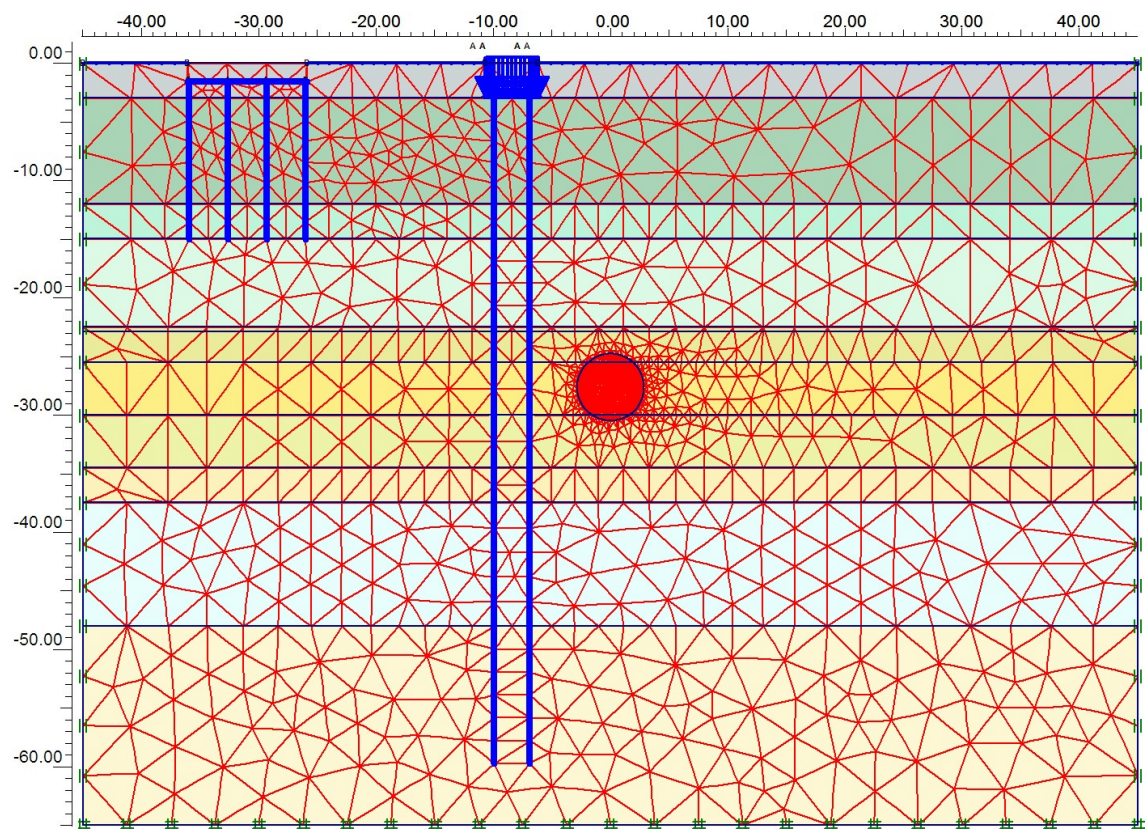


Figure 7.4 Finite element mesh generated at section BB (BTS-Sukhumvit area)

7.1.1. Behaviors of Ground Surface and Subsurface Deformation

The behaviors of the recorded ground surface and subsurface deformation at Klongtan Bridge and BTS-Sukhumvit area can be classified into 3 phases (Figures 7.5 and 7.6): deformation in front shield face, deformation within the length of shield body when the cutting face has been passed and the deformation behind the shield which consists of tail void deformation and subsequent settlement. As mentioned in section 4.1.2 of Chapter IV, the deformation in front of the shield is mainly caused by the decline of groundwater table in silty sand and the imbalance of total pressure at the TBM face. Friction between shield machine and surrounding soil or disturbance of the ground due to the over-excavation causes the deformation within the shield length. However, the deformation behind the tail of shield is due to the effects of tail void or excessive grouting pressure.

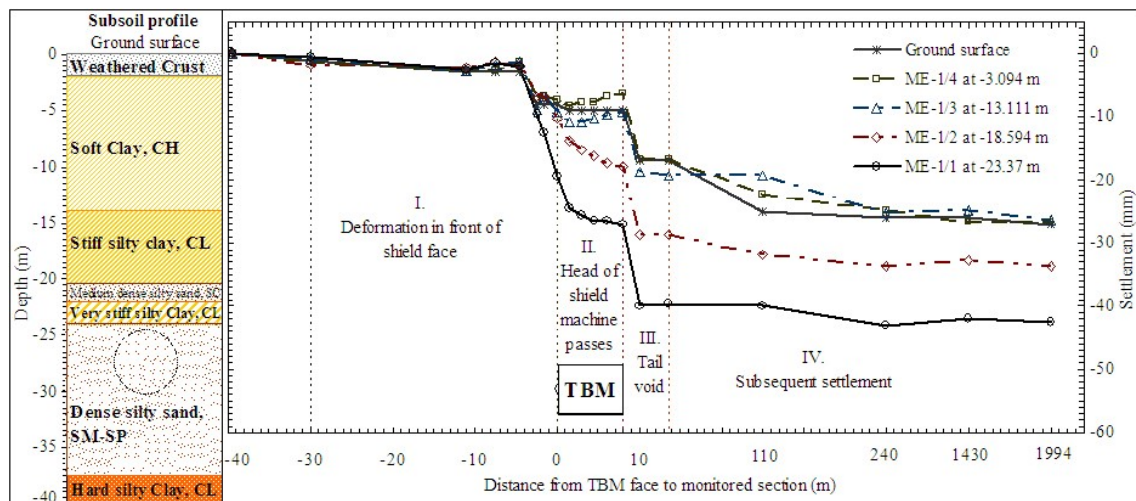


Figure 7.5 Behaviors of surface and subsurface deformation at extensometer ME-1 (Klongtan Bridge area)

The gradual settlements are found for the tunnel construction in dense silty sand at Klongtan Bridge area, and these settlements are rapidly increasing when the shield approaches close to the controlled section. The vertical movements slightly appear again for the whole shield body, and then a brutal settlement at the tail of the shield shows and remains constant during the tail void grouting. The settlements of all the layers seem constant after about one week when the TBM passes the monitored section (110 m. in Figure 7.5). The vertical deformations responding to the shield

movements of the tunnel located in hard silty clay are different from those in dense silty sand because they fluctuate within the first and second portions. Nevertheless, the settlements become more or less constant about one week after TBM passes as well (107 m. in Figure 7.6).

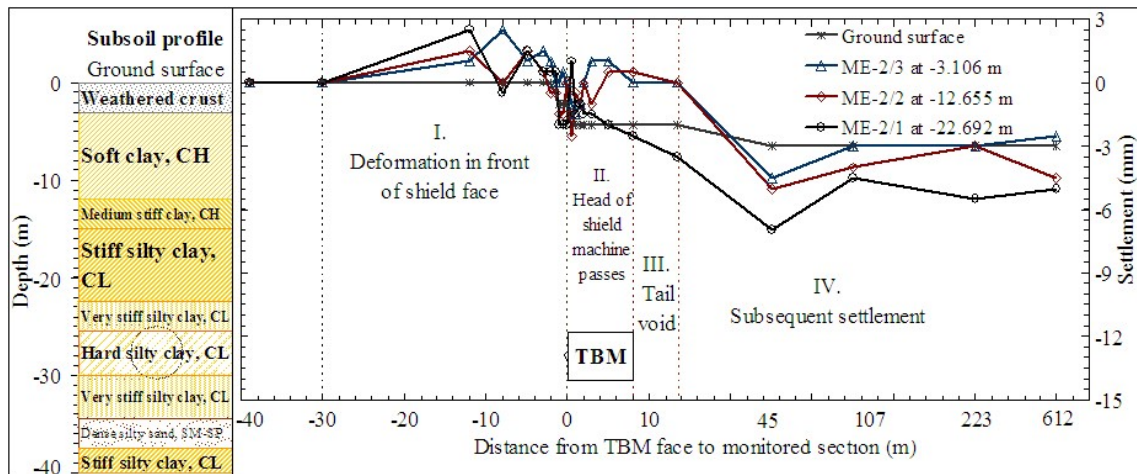


Figure 7.6 Behaviors of surface and subsurface deformation at extensometer ME-2 (BTS-Sukhumvit area)

It is noticeable when the tunnel is excavated in dense silty sand, the ground settlements corresponding to the positions of the face and tail of the TBM accelerate with average settlements about 42% and 77%, respectively, of the total settlement measured after three months. While in hard silty clay, these settlements reduce to 18% and 35 % respectively. In both cases, the average magnitude of settlement one week after the pass of the TBM reaches to 90% of the settlement after three months, which could be considered as the final short-term settlement.

7.1.2. Ground Surface Settlements

By reproducing the settlement trough based on the empirical method (Equations 4.1 and 4.6), the volume of ground loss resulting from the tunnel excavated in the dense silty sand layer at Klongtan Bridge area is 1.79% for the monitored sections GS16 and GS18 (Figure 7.7a and c). However, this ground loss is slightly increased to 1.97% for the section GS17, which is located close to the toe of the bridge. The figures show a good agreement among empirical and numerical

results and the measured data (obtained three-month after TBM passes). The values of i are $0.24z_0$, $0.26z_0$ and $0.35z_0$ for events as in Figures 7.7a, 7.7b and 7.7c respectively and where z_0 is the depth from the ground surface to the tunnel axis.

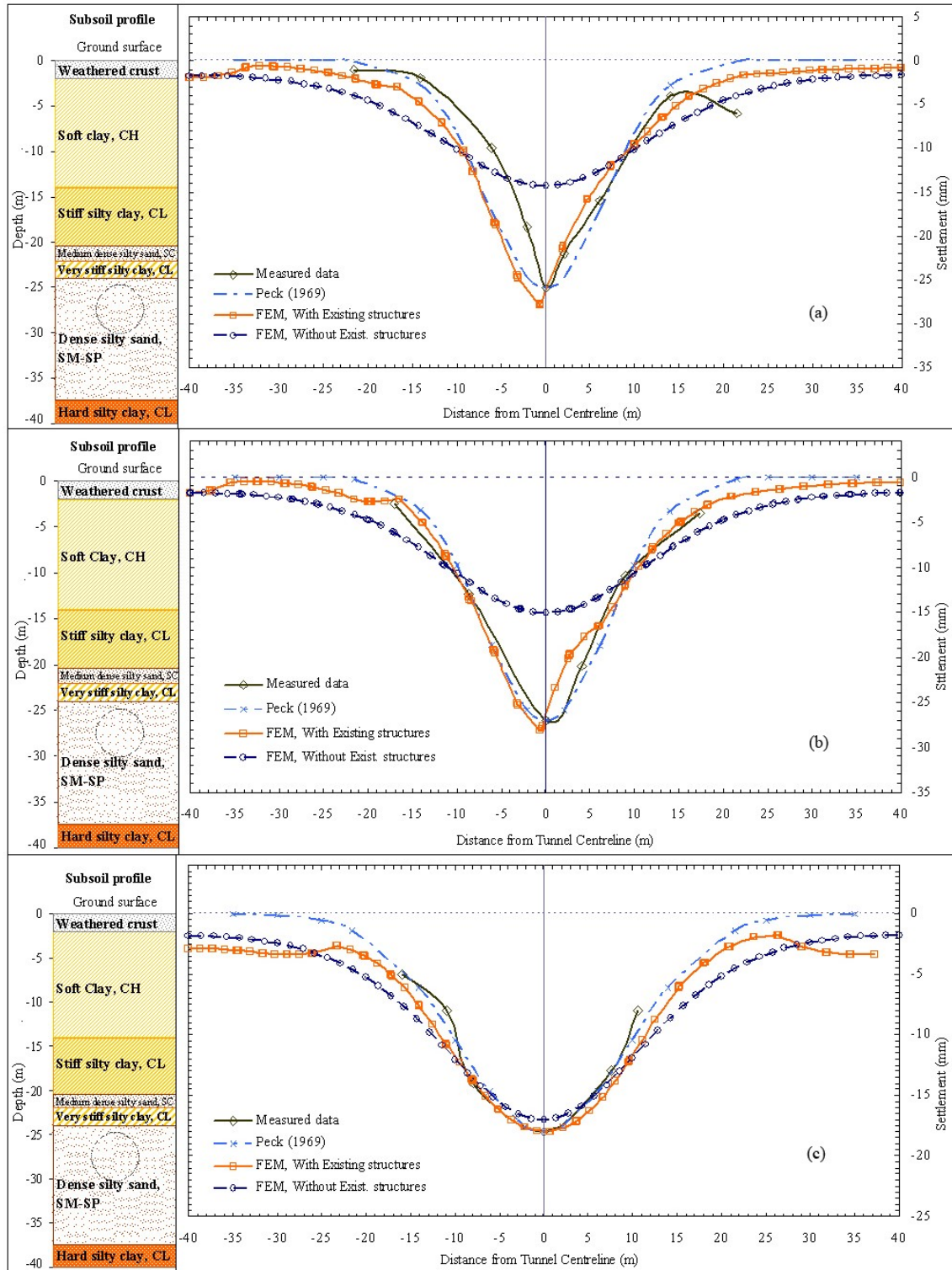


Figure 7.7 Surface settlements monitored and computed at Klontan Bridge area; (a) GS16, (b) GS17 and (c) GS18

In the same way as at Klongtan Bridge area, the surface settlement troughs at BTS-Sukhumvit area (tunnel in hard silty clay) are replicated (Figure 7.8). Based on the same empirical equations (Equations 4.1 and 4.6), the volume of ground loss of Figure 7.8a is 0.77% where the ground surface settlement points are implanted into the pavement of busy road at the curvature (GS-BTS, Figure 5.4). Consequently, the empirical prediction is in good agreement with the measured and finite element displacements. Unfortunately, the empirical result cannot agree with the measured data which are monitored along a line so close to the BTS foundation (about 2 m) while numerical result only shows an agreement in deformation shape (Figure 7.8b). Only three points are observed for this settlement array, and the middle point is implanted about 10 cm close to the curve in the middle of the road. The value of i is $0.46z_0$ for events as in Figure 7.8a.

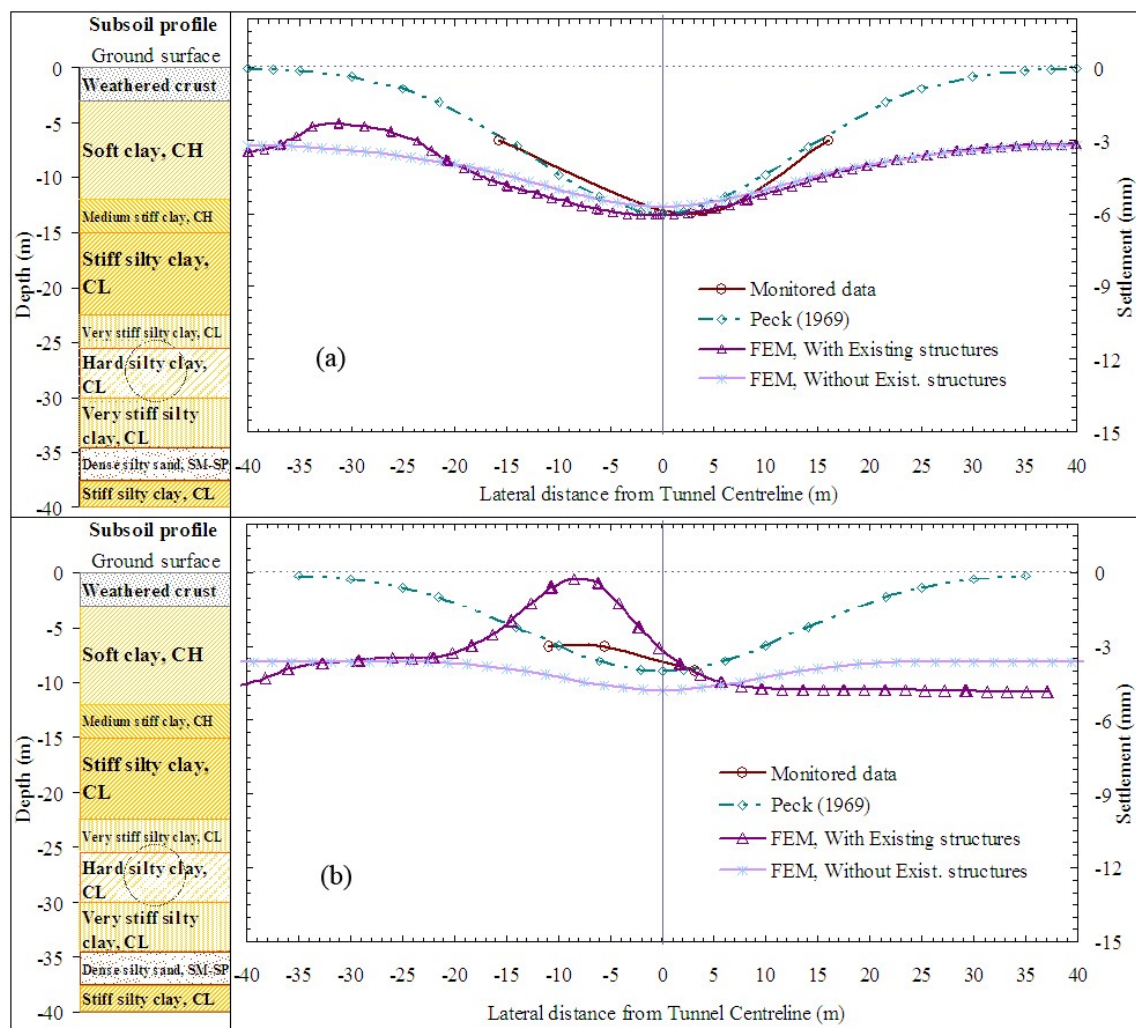


Figure 7.8 Surface settlements monitored and computed at BTS-Sukhumvit area (a) GS-BTS and (b) GS35

7.1.3. Subsurface Settlements

To monitor the subsurface settlements, two borehole extensometers are placed above the tunnel center line at Klongtan Bridge and BTS-Sukhumvit areas (Figures 5.6 and 5.7). The magnitude of subsurface settlement obtained after a three-month pass of TBM gradually increases toward the crown of the tunnel as shown in Figures 7.9 and 7.10. These two figures also show the comparison between the monitored data and the values given by the FEM. A good agreement is observed between field measured data and numerical results.

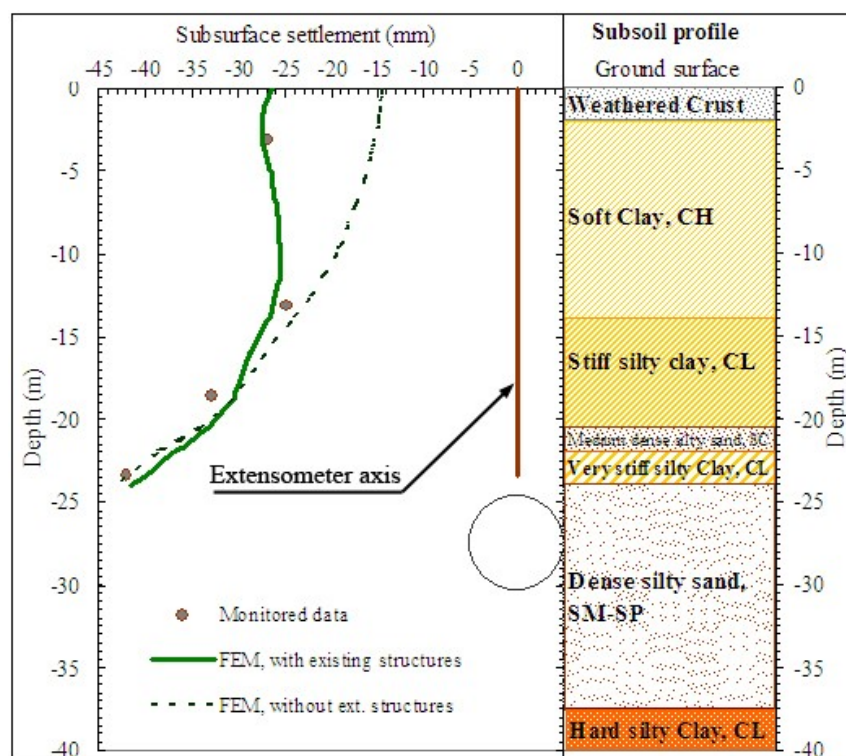


Figure 7.9 Subsurface settlements along Extensometer ME-1 at Klongtan Bridge area

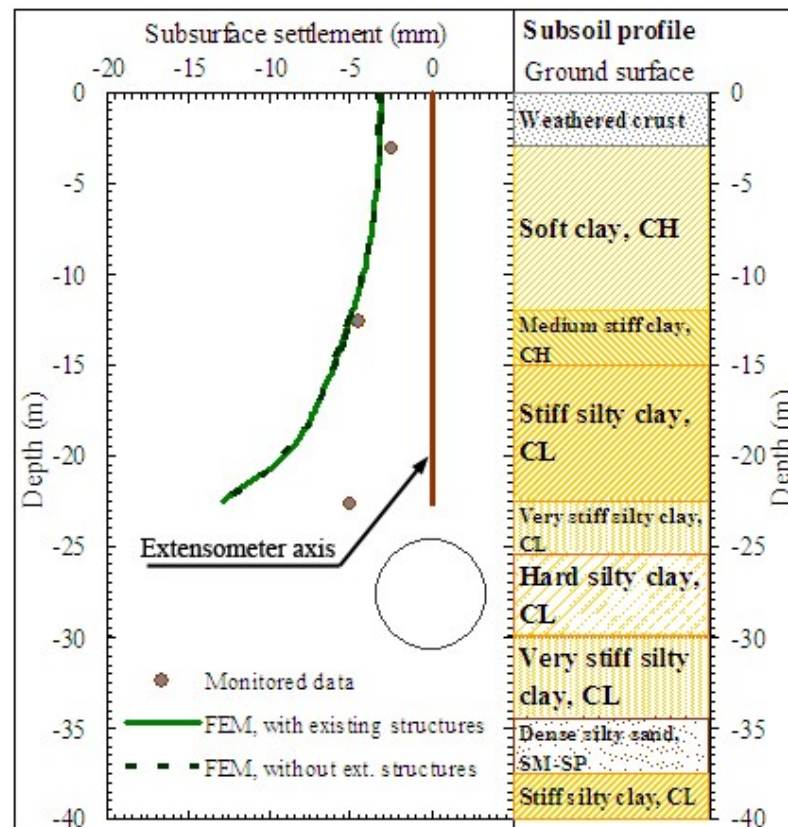


Figure 7.10 Subsurface settlements along Extensometer ME-2 at BTS-Sukhumvit area

7.1.4. Lateral Displacements

Figure 7.11 shows the lateral deformations monitored by means of an inclinometer at BTS-Sukhumvit area (Figure 5.4) responding to different positions of the TBM face. It is apparent when the TBM face is 12 m away from the monitored station, the lateral displacement is slightly moved toward the tunnel axis. This movement can possibly be caused by the low pressure applied to the TBM face. However, the movement gradually occurs outward the tunnel axis when the TBM face arrives at 8 m away from the station and reaches a maximum outward displacement when the TBM face arrives at 2 m. After reaching the maximum outward lateral displacement, the soil starts to move inward until a maximum when the TBM face is located at the monitored station, and then the inward lateral displacement reduces a few millimeters at the tunnel spring line during and after the tail void grouting. The lateral displacement remains constant after the shield face passes 12 m away from the monitored section. All the lateral movements can be closely related to the degree of

soil disturbance as well as the pressure applied to the shield face and grout pressure. The comparison between the lateral displacement and the values given by the FE analysis is also presented in the figure. However, the lateral deformations given by FE analysis are less than the final short-term deformations measured after three months; the difference can be caused by the effect of large bored pile foundation stiffness next to the instrumentation as shown in Figure 5.4 of Chapter V.

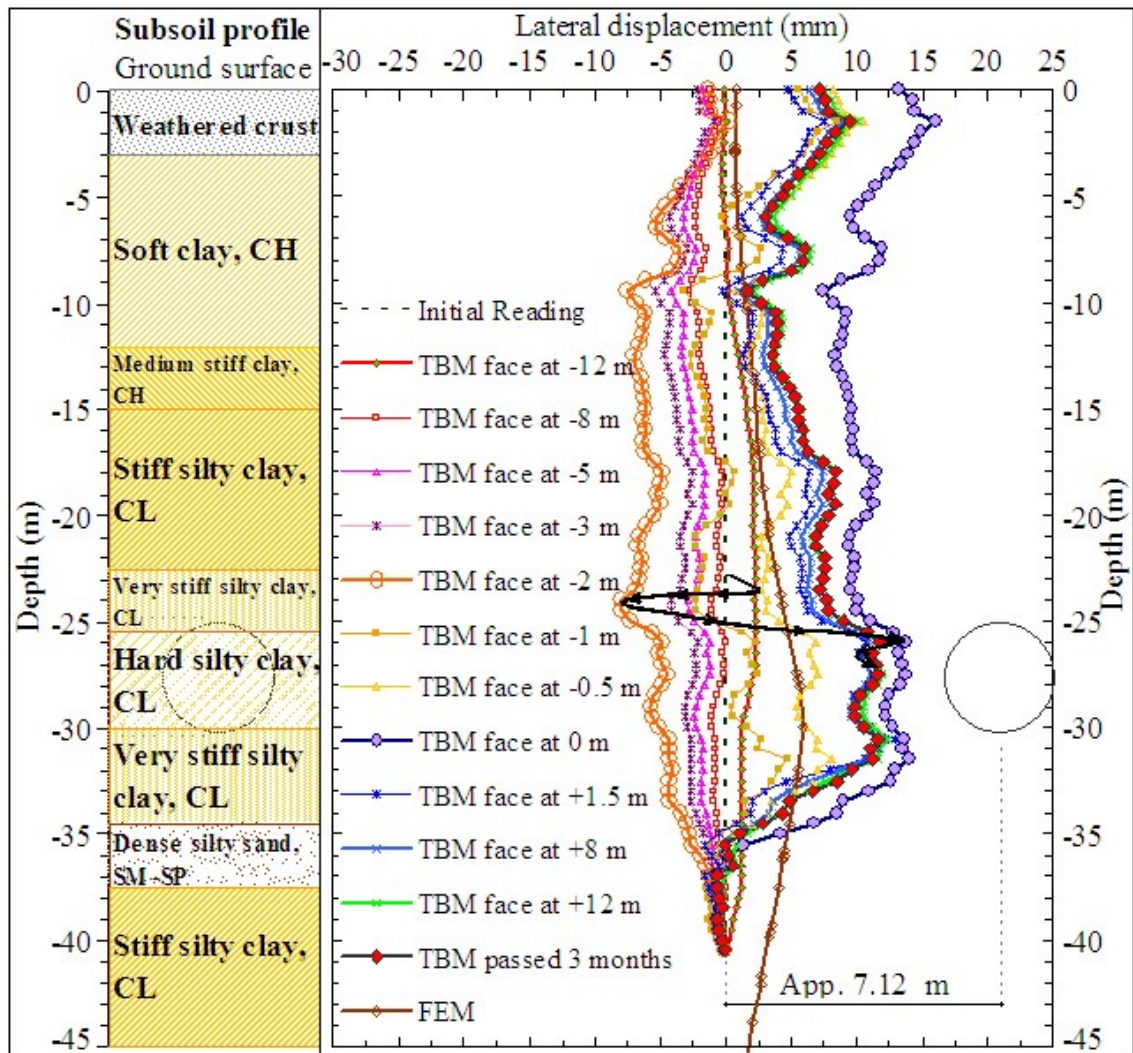


Figure 7.11 Lateral displacements caused by tunnel in hard silty clay at BTS-Sukhumvit area (Inclinometer, IC)

7.2. Structural Responses

As mentioned in section 5.2 of Chapter V, there are two important structures: old Klongtan Bridge and BTS sky train foundations at both studied areas and they are particularly monitored before, during and after the pass of EPB shield machine. However, no settlement is observed for the foundations of BTS sky train. The non-settlement of BTS sky train foundations can confirm that the tunnel excavation has no effect on the bored piles (diameter of each pile is one meter) of those foundations, which are strongly embedded in a very dense sand layer with pile tips of about 60 m below ground surface.

The settlements of the old Klongtan Bridge pile foundations where the TBM passes about 3 meters underneath are recorded. However, the foundations in the canal are not in the scope of this study. The settlement points are fixed on the columns or on the beams of the bridge at different levels from ground surface. Figure 7.12 shows the locations of monitored points except point C, which is fixed on the bridge column at the same level as point D that is not mentioned. On the contrary, point H is monitored on the bridge component, which is located at ground surface level above the pile cap embedded in the soil (Figure 7.13). Except for the portion of the shield length, where the significant settlements are also observed, the behaviors of the bridge foundation settlements (Figure 7.14) are very similar to those of the ground movements described previously. The settlements almost stop one week after the TBM passes (108 m) as well.



Figure 7.12 Location of structural settlement points monitored on Klongtan bridge



Figure 7.13 Location of point H monitored on Klongtan bridge

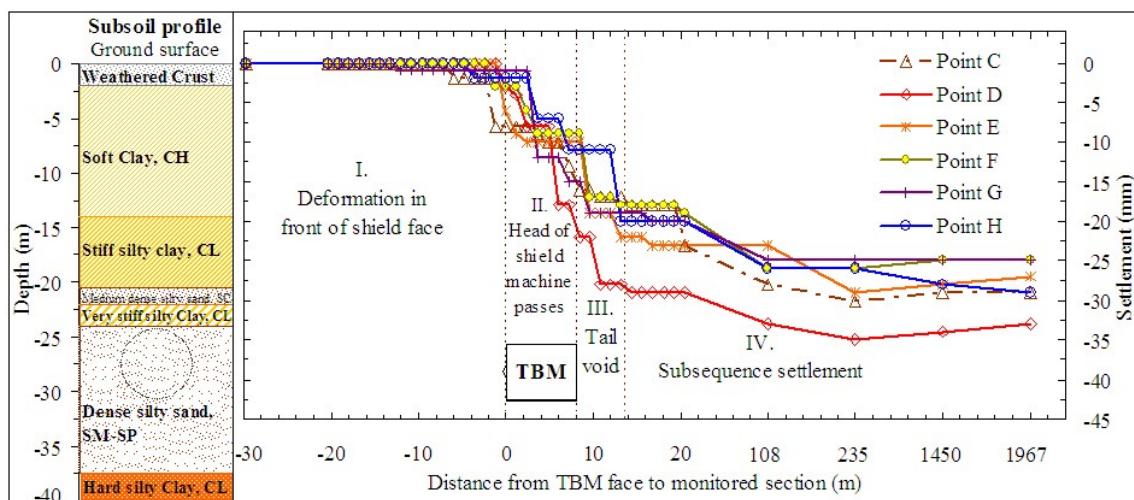


Figure 7.14 Behaviors of bridge foundation settlements caused by EPB tunneling in dense silty layer

In addition to the old bridge, some building settlement points are also placed to monitor the settlements of 3- and 4-storey old shophouses located on the right side of the bridge (Figure 5.2). The monitored points are placed on the columns of the shophouses about 1.50 m from the ground surface. However, only points C₁ and

C_2 , which are marked on the columns of the 3-storey shophouse, are shown in Figure 7.15.



Figure 7.15 Location of point C_1 and C_2 monitored on 3-storey shophouse

The behaviors of the old shophouse settlements in response to the position of the cutting face of EPB shield machine are plotted in Figures 7.16 and 7.17. Similarly to the old Klongtan Bridge, the settlements are almost dissipated after the TBM passes about one week (106 m) from the monitored sections. Since the magnitude of the settlements of old shophouses are generally smaller than that of the bridge, the bridge settlement gained more attention at this point. Therefore, the monitoring of the old shophouse settlements is not continued after the TBM moves away about two weeks from the controlling sections.

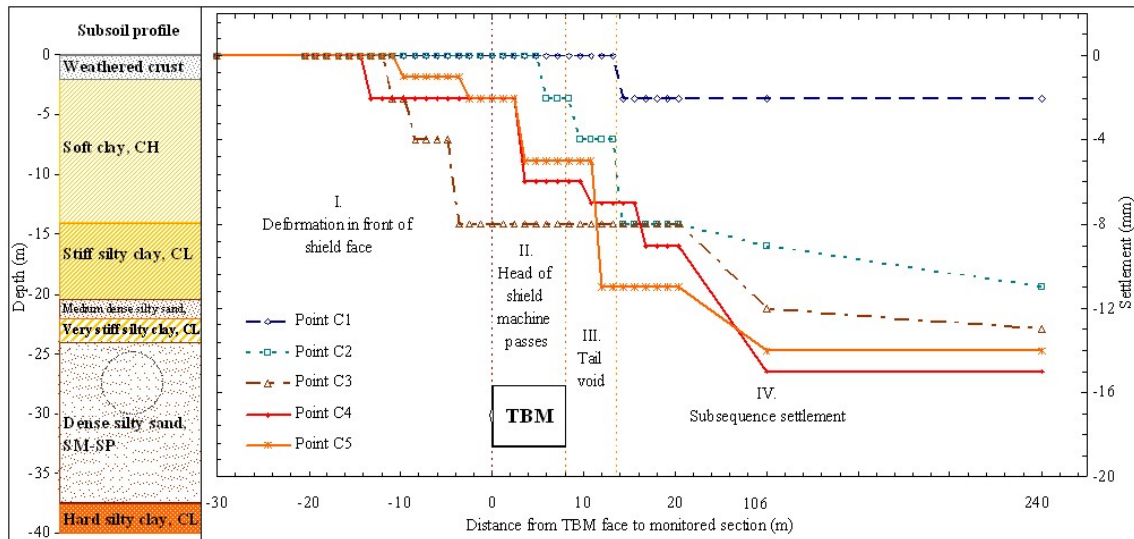


Figure 7.16 Behaviors of 3-storey old shophouse settlements in response to EPB tunneling in dense silty layer

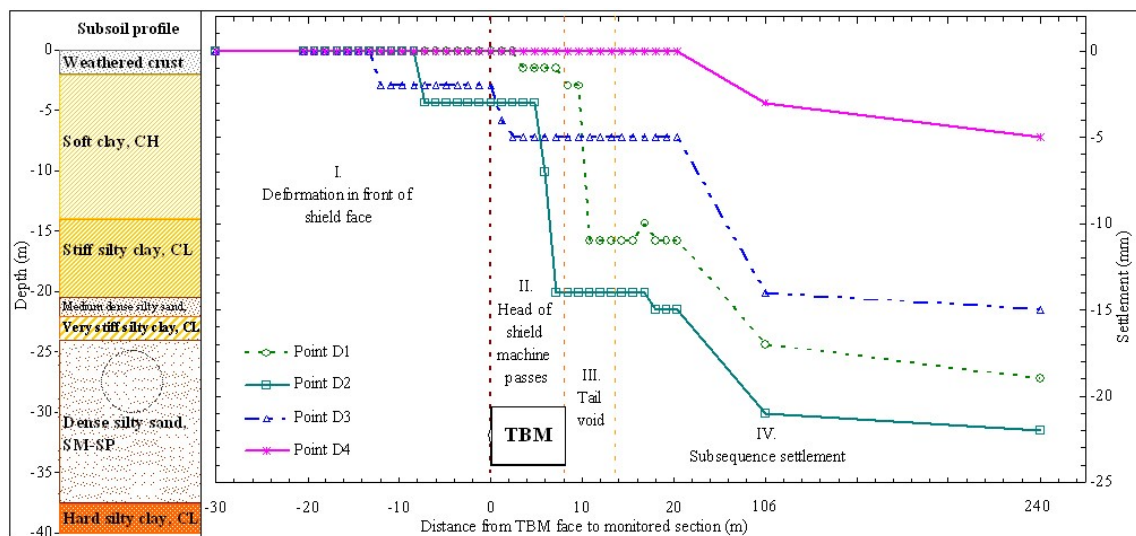


Figure 7.17 Behaviors of 4-storey old shophouse settlements in response to EPB tunneling in dense silty layer

As mentioned in Chapter VI, the analysis configurations of each bridge footing and the existing old shophouses based on 2D FEM are the same whereas only the positions of the structures to the tunnel center line are adjusted according to the real analysis sections. The magnitudes of old bridge and shophouse settlements are listed in Table 7.1. The 2D-FEM results are well comparable with the monitored data.

Table 7.1 Magnitude of structural settlements at Klongtan Bridge area

Structure	Source of data	Magnitude of settlement points					
Bridge foundation		C	D	E	F	G	H
	Monitored data	-29	-34	-28	-25	-25	-28
	2D-FEM results	-30.3	-30.8	-29.9	-25.9	-24.1	-28.2
3-storey old shophouse		C ₁	C ₂	C ₃	C ₄		
	Monitored data	-2	-11	-13	-15		
	2D-FEM results	-1.6	-9.8	-12.2	-16.7		
4-storey old shophouse		D ₁	D ₂	D ₃	D ₄		
	Monitored data	-19	-22	-15	-5		
	2D-FEM results	-17	-17.8	-17.3	-3.09		

7.3 Internal Forces of Segmental Lining

In addition to deformations given by PLAXIS after a completed analysis, various output parameters can be also investigated. However, this section focuses only on the internal forces of tunnel lining. These forces appear as a result of the water pressure, overburden pressure and loads which are transmitted from the surcharges at ground surface. For sign conventions used in PLAXIS, please refer to section 6.1.1 of Chapter VI.

Figure 7.18 shows the bending moments in tunnel lining at the final phase of simulation for the section GS16, where the tunnel is excavated in dense silty sand layer. The lining carries a positive bending moment of 151.78 kNm/m at the crown and 133.24 kNm/m at the invert, but the negative bending moment of -106.33 kNm/m and -119.62 kN/m at the left and right springline, respectively. Therefore, the extreme value of bending moment is located at crown.

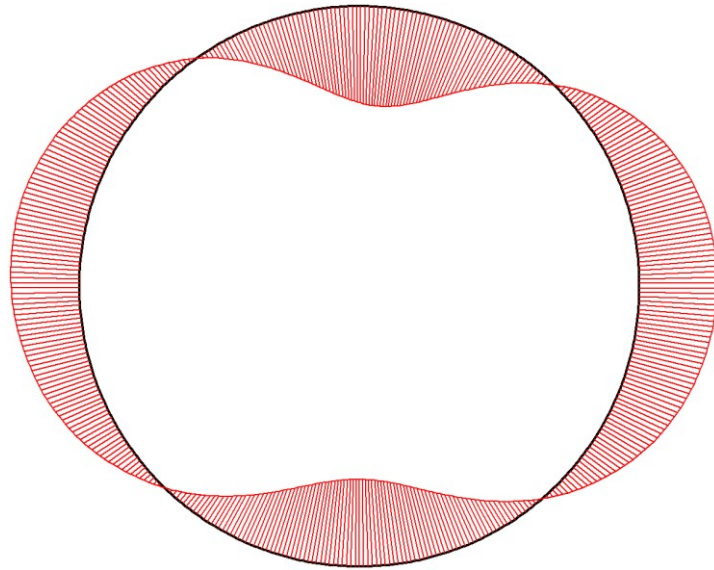


Figure 7.18 Bending moments in the tunnel lining at the final phase of simulation for section GS16, the extreme bending moment is 151.78 kNm/m

In addition, the results of axial and shear forces are presented in Figures 7.19 and 7.20. The highest compressive axial force of -510.18 kN/m is located at the springline on the right side while on the left side the axial force is only -484.83 kN/m. The maximum shear force of 115.31 kN/m is located at the right shoulder of the tunnel lining.

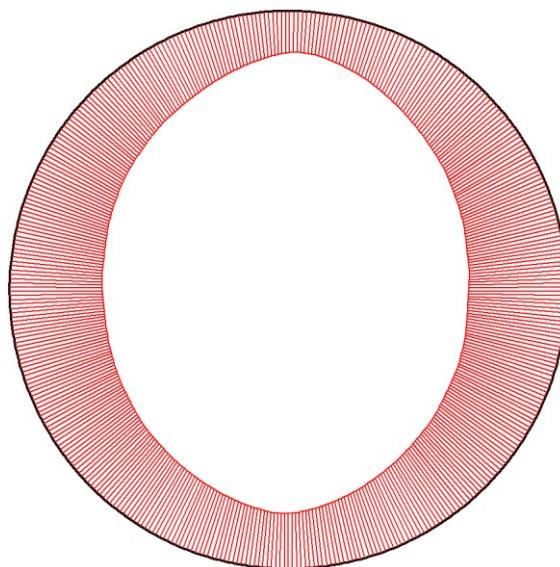


Figure 7.19 Axial forces in the tunnel lining at the final phase of simulation for section GS16, the extreme axial force is -510.18 kNm/m

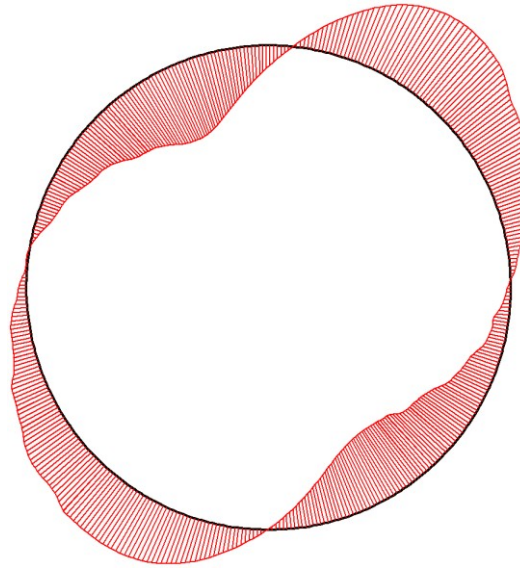


Figure 7.20 Shear forces in the tunnel lining at the final phase of simulation for section GS16, the extreme shear force is 115.31 kNm/m

Based on the same subsoil profile, Figures 7.21 to 7.26 show the axial forces, shear forces and bending moments generated in the tunnel lining at the final phase of simulation for the section GS17 and GS18. Some remarkable values of axial forces, shear forces and bending moments as well as their locations on the tunnel lining for both sections are listed below:

- The maximum compressive axial forces of -505.34 kN/m and -485.61 kN/m are located at the springline on the right and left side for sections GS17 and GS18, respectively.
- The extreme shear forces of 113.49 kN/m and 109.52 kN/m are located at the right shoulder of the tunnel lining for both sections GS17 and GS18.
- The extreme positive bending moments of 155.27 kNm/m and 150.42 kNm/m for both cases are located at the crown of the tunnel.

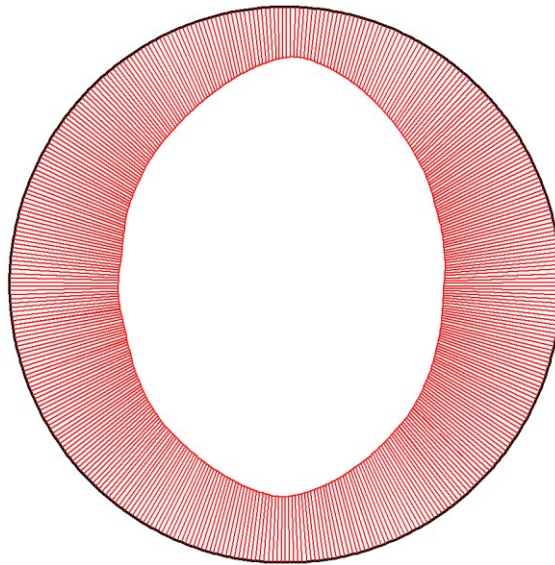


Figure 7.21 Axial forces in the tunnel lining at the final phase of simulation for section GS17, the extreme axial force is -505.34 kNm/m

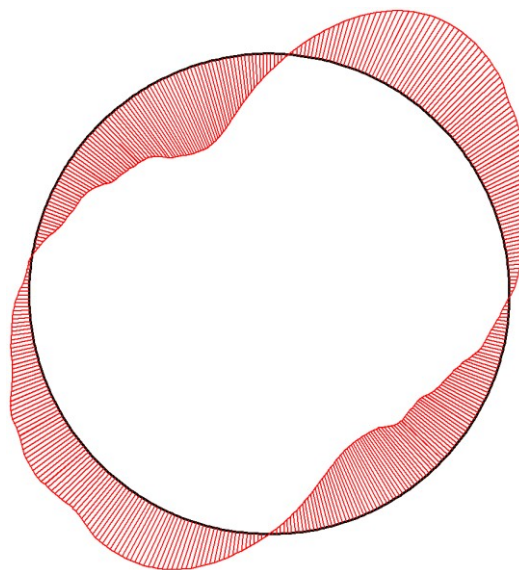


Figure 7.22 Shear forces in the tunnel lining at the final phase of simulation for section GS17, the extreme shear force is 113.49 kNm/m

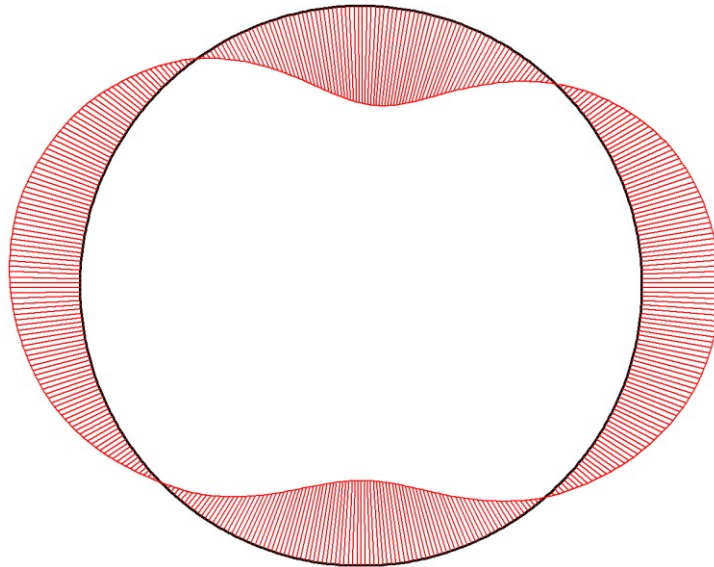


Figure 7.23 Bending moments in the tunnel lining at the final phase of simulation for section GS17, the extreme bending moment is 155.27 kNm/m

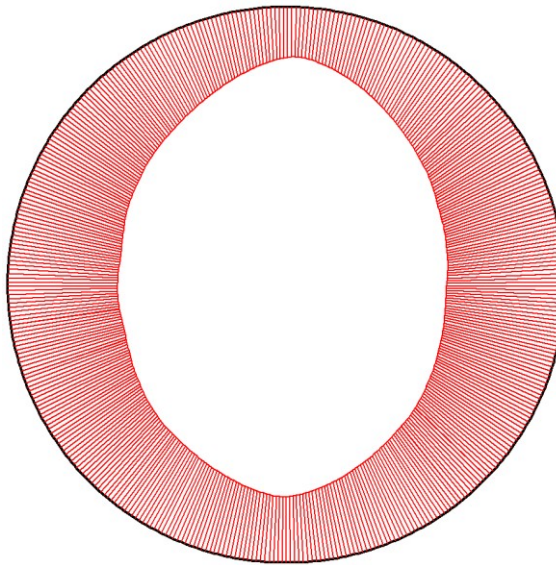


Figure 7.24 Axial forces in the tunnel lining at the final phase of simulation for section GS18, the extreme axial force is -485.61 kNm/m

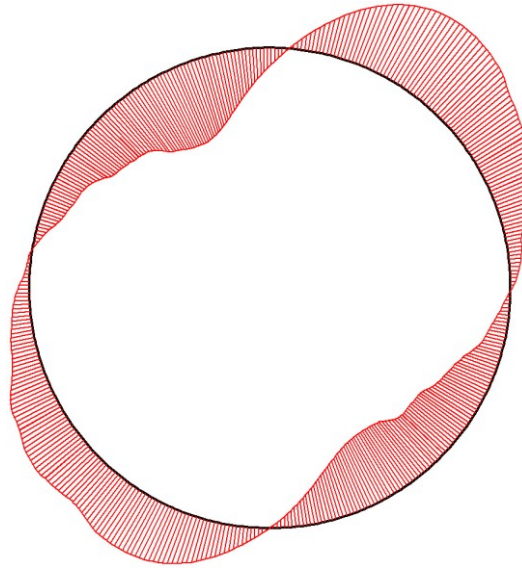


Figure 7.25 Shear forces in the tunnel lining at the final phase of simulation for section GS18, the extreme shear force is 109.52 kNm/m

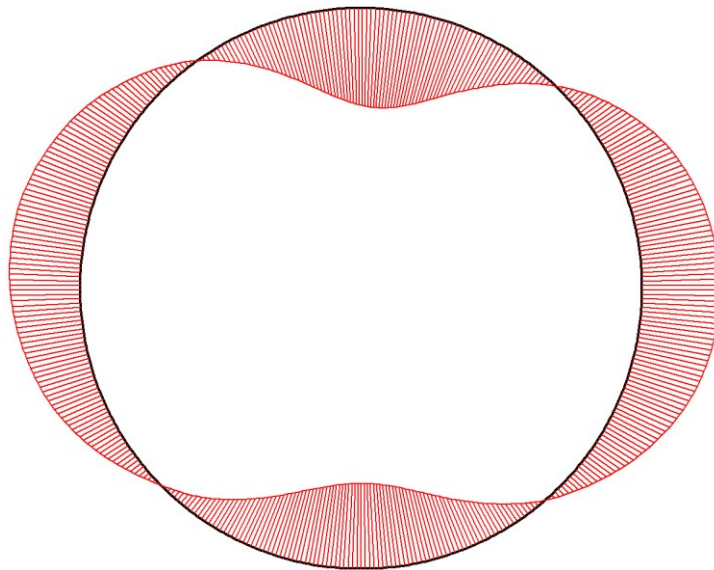


Figure 7.26 Bending moments in the tunnel lining at the final phase of simulation for section GS18, the extreme bending moment is 150.42 kNm/m

Among the three cases of tunnel in dense silty sand layer, the axial and shear forces as well as the bending moments in lining for the tunnel located under the road imprisoned by the pile foundations of two-storey residential houses and four-storey shophouses on the left and right sides (GS18, Figures 7.24 to 7.26) are lower than

those for the tunnel located below the bridge. These clearly show that the loads transmitted from both side of houses and shophouses to the tunnel lining are less than those of the bridge.

In the case where the tunnel is bored through the hard silty clay with the crown and invert cut in the very stiff silty clay layers (GS-BTS and GS35), the forces and bending moments generated in the tunnel lining are shown in Figures 7.27 to 7.32. A description of the extreme forces and bending moments for the two selected sections can be summarized as:

- The maximum compressive axial forces of -439.08 kN/m and -370.15 kN/m are located at the springline on the left and right side for sections GS-BTS and GS35, respectively.
- The extreme shear forces of 129.82 kN/m and -142.78 kN/m are located on left and right sides between the springline and the invert of the tunnel lining for both sections GS-BTS and GS35, respectively.
- The extreme positive bending moments of -132.43 kNm/m and -147.08 kNm/m at the left and right springline of the tunnel lining for both sections GS-BTS and GS35, respectively.

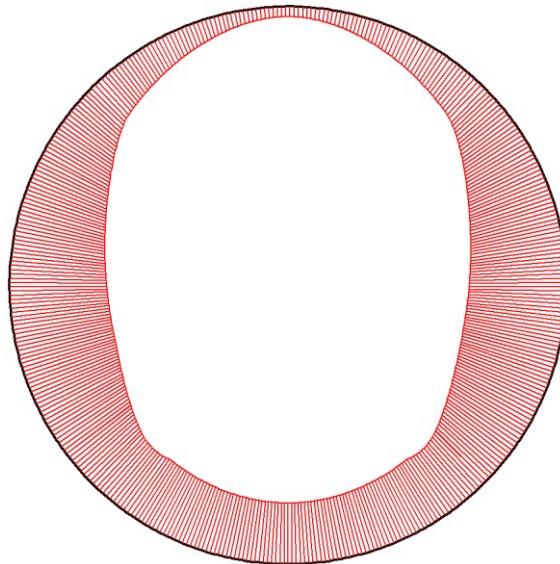


Figure 7.27 Axial forces in the tunnel lining at the final phase of simulation for section GS-BTS, the extreme axial force is -439.08 kNm/m

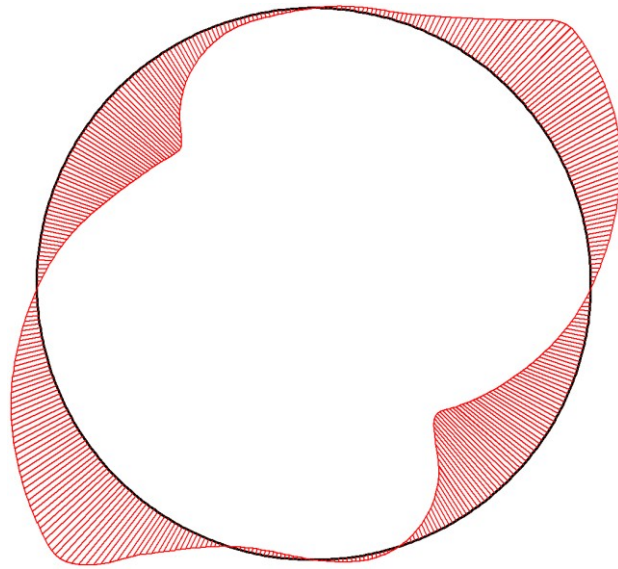


Figure 7.28 Shear forces in the tunnel lining at the final phase of simulation for section GS-BTS, the extreme shear force is 129.82 kNm/m

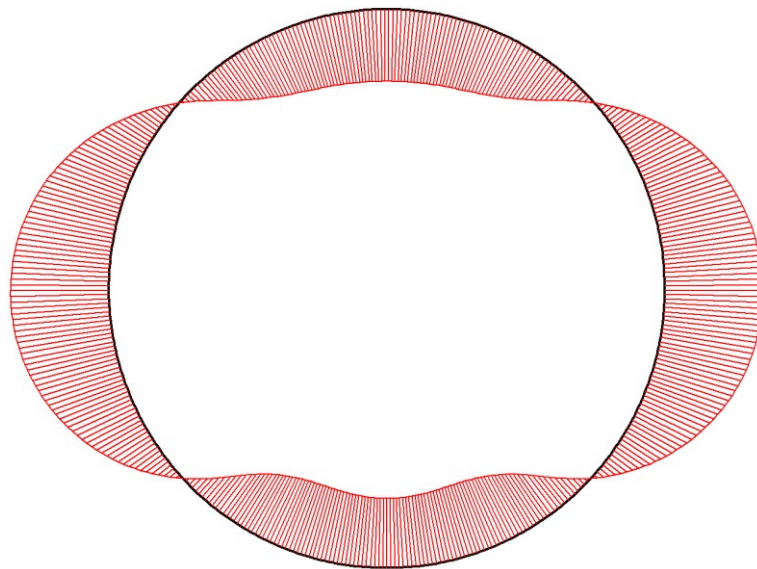


Figure 7.29 Bending moments in the tunnel lining at the final phase of simulation for the section GS-BTS, the extreme bending moment is -132.43 kNm/m

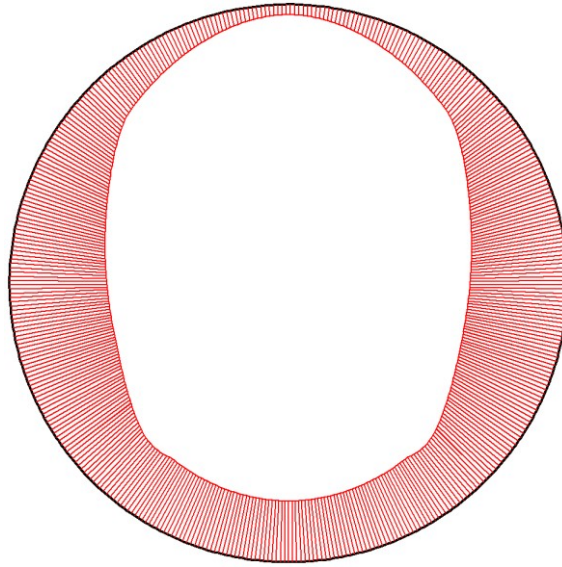


Figure 7.30 Axial forces in the tunnel lining at the final phase of simulation for section GS35, the extreme axial force is -370.15 kNm/m

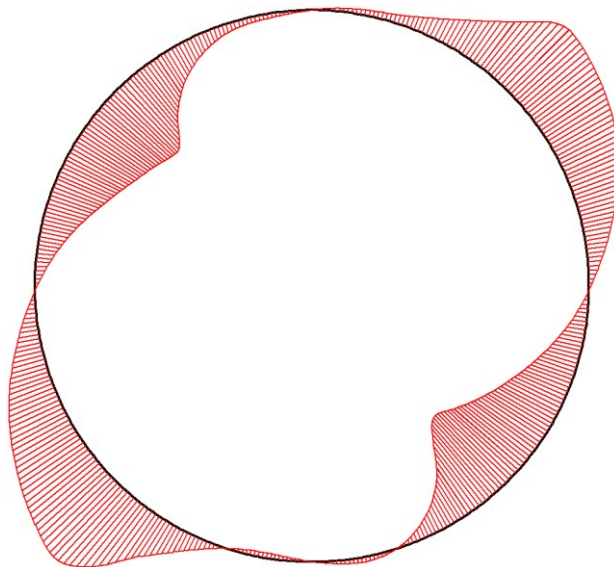


Figure 7.31 Shear forces in the tunnel lining at the final phase of simulation for section GS35, the extreme shear force is -142.78 kNm/m

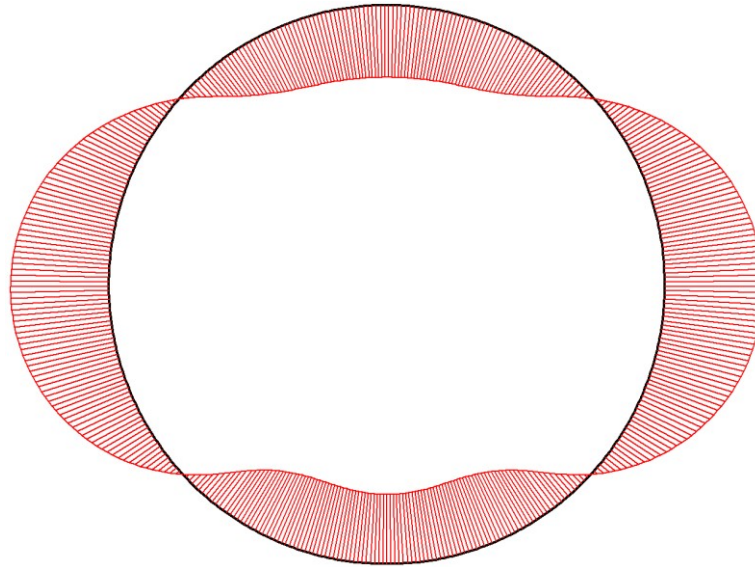


Figure 7.32 Bending moments in the tunnel lining at the final phase of simulation for section GS35, the extreme bending moment is -147.08 kNm/m

7.4. Discussion

7.4.1. Surface and Subsurface Deformation

Based on the longitudinal plots for ground surface and subsurface settlements, we observe that the significant settlement takes place at the specific positions of the shield, face and tail, especially for the subsoil layers which are in the zone of one diameter above the crown of the tunnel (ME-1/1 and ME-2/1 in Figures 7.5 and 7.6). It is probably a sensitive area. However between these two positions, some heaves are also observed for the tunnel excavated in hard silty clay layer. These also provide important information that the pressure at shield face and the grout pressure for a tunnel construction in clay layer have a remarkable effect on the surrounding soil than that for a tunnel construction in sand or silty sand layer, where the coefficient of permeability is usually high.

In addition, the magnitudes of ground surface settlement induced by tunnel in hard silty clay are 5 to 7 times smaller than settlements induced by tunnel in dense silty sand (Figures 7.7 and 7.8). It is probably because of the drawn down of groundwater level during the tunnel excavated in dense silty sand layer and the degree of disturbance of TBM in dense silty sand is higher than that in hard silty clay. For the similar reasons, the magnitude of subsurface settlements induced by tunnel in hard

silty clay is smaller than that of subsurface settlements induced by tunnel in dense silty sand (Figures 7.9 and 7.10). However, the differences of settlement magnitudes are increased up to 6 to 9 times higher for tunnel in dense silty sand than for tunnel in hard silty clay layer.

7.4.2. Effects of Existing Structures on FE Analysis

For the FE analysis, when building structures are added as a parameter, the results of the surface settlements are strongly influenced as shown in Figures 7.7 and 7.8. Therefore building structures are influential and they also are a factor to be considered in numerical analysis. When the existing structures are ignored from the analysis model, the magnitude of ground displacement will be underestimated. However, the influences of existing structures and their surcharges on subsurface settlements are reduced with depth as shown in Figure 7.9 except for Figure 7.10 where the existing three-storey shophouses are located about 30 m. from the monitored extensometer, which is implemented above the tunnel center line (Figure 5.6).

Moreover, the presence of different structures which are generally not uniform above the tunneling route leads to a non-uniform of charge repartition. Therefore, an asymmetry of ground movements across the tunnel alignment occurs (Figures 7.7 and 7.8). In addition, the forces and bending moments generated in the tunnel lining are also not symmetry as shown in Figure 7.18 to 7.32. These are the reasons that the full tunnel cross sections are necessary in each analysis.

As illustrated in Figures 7.19, 7.21, 7.24 and 7.30, the maximum of axial forces is generally located at the springline level on the side where the shortest pile foundations of the existing building are situated. The lower values of axial forces in the opposite side can be caused by the longer pile length of that side, which serves as a barrier to reduction of the lateral earth pressure.

CHAPTER VIII

CONCLUSIONS AND RECOMMENDATIONS

After the analysis yields all results of the research problems and after some possible causes related to the monitoring equipment and performances are identified, some positive conclusions and recommendations are given in the following sections.

8.1 Conclusions

The 2D-FE analyses were carried out to back-simulate and to analyze the ground surface and subsurface displacements as well as bridge structure and building settlements. The study yields the following findings:

- 1.) Behaviors of ground surface and subsurface displacements are classified into three phases as deformation in front of shield face, deformation within the length of shield body when the cutting face has passed and the deformation behind the shield which consists of tail void deformation and subsequent settlement. The average tail void settlement for the tunnel in dense silty sand and hard silty clay layers is about 77% and 35%, respectively, of the total settlement measured after three months. In both cases, the average magnitude of settlement one week after the pass of the TBM reaches to 90% of the settlement after three months, which is considered as the final short-term settlement.
- 2.) Elasto-plastic failure criteria of Mohr Coulomb soil model can be satisfactorily used for back-simulation of the ground surface and subsurface movements caused by tunnel excavation.
- 3.) When EPB shield bores the tunnel in dense silty sand underneath the Klongtan bridge pile foundation and in hard silty clay layer beside the BTS's sky train pile foundation, the 2D-FE analyses yield similar results to the analysis of the field monitored data at the ground surface and subsurface settlements whereas the lateral displacement is not well simulated.

- 4.) The results yielded from the empirical method for surface settlements are also in agreement with those from the field monitored data and FE analyses.
- 5.) The surface settlement trough width, i , found in this research is between $0.24z_0$ and $0.35z_0$ for tunnel excavated in dense silty sand layer while this trough width increases to $0.46z_0$, which is wider, for the tunnel in hard silty clay.

This study confirms that the ratios of undrained soil stiffness over the undrained shear strength (E_u/S_u) are 240 and 480 for soft and stiff clays respectively, and the value for medium stiff clay is taken as the average of these two intervals. In addition, the drained stiffness E' (kN/m^2) = $2000.N_{60}$ for medium and dense silty sand layers has also been confirmed in this research study. Therefore, the proposed undrained elastic stiffness (E_u) for tunnel design in Bangkok can be determined from the undrained shear strength (S_u) based on the ratios of 240, 360 and 480 for soft, medium and stiff clayey soil respectively. Furthermore, the drained stiffness (E') of sandy soil can be estimated from the SPT test as $2000.N_{60}$. Since the formulation of FEM program may not follow the unique concept, the suggested soil stiffness is restricted to the 2D PLAXIS program in which the Mohr Coulomb model is selected and the ground loss is simulated by tunnel contraction.

8.2 Recommendations

In order to improve the quality of geotechnical works in terms of academic research, which is the major sources for updating the knowledge of geotechnical engineers, the following recommendations are beneficial to future research:

- a.) To get a realistic longitudinal deformation, the monitor should be frequently conducted when the shield face is moving within a distance about three times its length, i.e. 25 m, before and after the controlled section.
- b.) Although the output might slightly vary from one to another, the different kind of soil models can be used and the analysis results have to be compared among them and with the real monitored data obtained from the field performance.
- c.) If the deformation of tunnel wall has to be studied, the new invented devices such as the *Tunnel Deformation Meter* presented by Hashimoto et al. (2006) should be used since this monitoring system provides a qualitative data.

However, at least one reference point must be surveyed to get the new coordinates of its current position. Therefore the polar deformation of the tunnel wall could be correctly plotted.

REFERENCES

- Arnaiz, M., Estefania, S., Fernandez Cota, A. and Oteo, C. 1998. Crossing under a river in Madrid without overburden. Proceedings of the world tunnel congress'98 on tunnels and metropolises, São Paulo, Brazil: 161-166.
- Atkinson, J. H. and Potts, D. M. 1977. Subsidence above shallow tunnels in soft ground. Journal of Geotechnical and Environmental Engineering, ASCE, Vol. 103, GT 4: 307-325.
- Attewell, P. B., Yeates, J. and Selby, A. R. 1986. Soil movements induced by tunneling and their effects on pipelines and structures. Chapman & Hall.
- Bonnier, P. G., Möller, S. C. and Vermeer, P. A. 2002. Bending moments and normal forces in tunnel linings. Proceedings of the 5th European Conference of Numerical Methods in Geotechnical Engineering (NUMGE), Presses de l'ENPC/LCPC, Paris: 515-522.
- Brand, P. 2000. CG08: Determination of soil stiffness parameters. Short courses on computational geotechnical analysis with PLAXIS, the National University of Singapore (from 13th to 16th June).
- Brinkgreve, R. B. J. 2002. PLAXIS, Finite element code for soil and rock analyses, users manual, 2D-Version 8. A. A. Balkema, Rotterdam, Netherlands.
- Burland, J. B., Standing, J. R. and Jardine, F. M. 2001. Building response to tunneling, Case studies from construction of the Jubilee Line Extension, London, Vol. 1. Projects and methods. Thomas Telford, London.
- Channel4. n.d. London: The greatest city. Retrieved March 29, 2007, from <http://www.channel4.com/history/microsites/H/history/i-m/london4.html>
- Coduto, D. P. 2001. Foundation design: Principles and practices. 2nd ed., Prentice-Hall, Inc., New Jersey

- Dobashi, H., Sakurai, Y., Konishi, Y., Ouchi, S., Matsubara, K., Kitayama, A. and Takahashi, H. 2005. Visualizing excavated soil flow in the cutter chamber of a large earth pressure balanced shield. Proceedings 31st ITA-AITES World Tunnel Congress on Underground Space Use, Analysis of the Past and Lessons for the Future, Istanbul, Turkey: 377-383.
- Dunnicliff, J. 1988. Geotechnical instrumentation for monitoring field performance. John Wiley & Sons, Inc., New York, United State of America.
- EFNARC 2005. Specification and guidelines for the use of specialist products for mechanised tunnelling (TBM) in soft ground and hard rock. April 2005. Retrieved March 16, 2007, from <http://www.efnarc.org/pdf/TBMGuidelinesApril05.pdf>
- EM1110-2-1908 1995. Engineering and design: Instrumentation of embankment dams and levees. Department of the Army, U.S. Army Corps of Engineers, Washington, DC 20314-1000.
- Gardner, B. 1996. Thames tunnel shield. Retrieved January 30, 2007, from <http://web.ukonline.co.uk/b.gardner/brunel/tunnel.html>
- Greenwood, J. D. 2003. Three-dimensional analysis of surface settlement in soft ground tunneling. Thesis (M. Eng.), Massachusetts Institute of Technology, U.S.A.
- Hashimoto, T., Koyama, Y., Yingyonggrattanukul, N., Kayukawa, K., Konda, T. and Sugimoto, M. 2006. Applications of the new deformation meter for monitoring tunnel lining deformation. Proceedings of the International Symposium on Underground Excavation and Tunnelling, Urban Tunnel Construction for Protection of Environment, Bangkok, Thailand: 221-230.
- Herrenknecht AG, Tunnelling system. n.d. Tunnelling machines and tunnel construction. Retrieved February 11, 2007, from <http://www.herrenknecht.com/>
- Hutton, D. V. 2004. Fundamentals of finite element analysis. 1st ed., McGraw-Hill Companies, Inc., New York, United State of America.

- Jaky, J. 1944. The coefficient of earth pressure at rest. Journal for society of Hungarian Architects and Engineers, Budapest, Hungary, Vol. 7: 355-358.
- JSCE 1996. Japanese standard for shield tunneling. 3rd ed., Japan Society of Civil Engineers, 1996.
- Kamata, H., & Mashimo, H. 2003. Centrifuge model test of tunnel face reinforcement by bolting. Tunnelling and Underground Space Technology, Vol. 18: 205-212.
- Kongdang, K. 1996. Performance of earth pressure balance shield in Bangkok waste water tunnel project. Thesis (M. Eng.), Asian Institute of Technology, Bangkok, Thailand.
- Koungelis, D. K. and Augarde, C. E. 2004. Interaction between multiple tunnels in soft ground. Proceedings of the 18th Australasian Conference on the Mechanics of Structures and Materials, Perth, Australia, Taylor and Francis, London: 1031-1036.
- Lee, C. J., Wu, B. R., Chen, H. T. and Chiang, K. H. 2006. Tunnel stability and arching effects during tunneling in soft clayey soil. Tunnelling and Underground Space Technology, Vol. 21, No. 2: 119-132.
- Lee, K. M., Rowe, R. K. and Lo, K. Y. 1992. Subsidence owing to tunneling. I. Estimating the gap parameter. Canadian Geotechnical Journal, Vol. 29: 929-940.
- Loganathan, N. and Poulos H. G. 1998. Analytical prediction for tunneling-induced ground movements in clays. Journal of Geotechnical and Environmental Engineering, ASCE, Vol. 124, No. 9: 829-856.
- Loganathan, N., Poulos H. G. and Stewart, D. P. 2000. Centrifuge model testing of tunneling-induced ground and pile deformations. Géotechnique, Vol. 50, No. 3: 283-294.
- LOVAT Company. n.d. Products. Retrieved March 16, 2007, from <http://www.lovat.com/>

- Luangpitakchumpol, D., Teparaksa, W. and Pitaksaithong, W. 2005. Surface and subsurface ground deformation due to EPB tunnelling in Bangkok subsoils. Proceedings of 31st ITA-AITES World Tunnel Congress on Underground Space Use, Analysis of the Past and Lessons for the Future, Istanbul, Turkey: 889-894.
- Lunardi, P., Pizzarotti, E. M. and Rivoltini, M. 1993. Prefabricated linings for metropolitan underground railway tunnels constructed using mechanised shields. Proceedings of the International Congress on Options for Tunneling 1993, Amsterdam, Netherlands: 453-462.
- Maidl, U. 1999. Design features of the botlek rail tunnel in the Betuweroute. Tunnelling and Underground Space Technology, Vol. 14, No. 2: 135-140.
- Mair, R. J. 1993. Developments in geotechnical engineering research: Application to tunnels and deep excavations. The unwinn Memorial Lecture 1992, Proceedings of the Institution of Civil Engineers and Civil Engineering: 27-41.
- Mair, R. J., Taylor, R. N. and Bracegirdle, A. 1993. Subsurface settlement profile above tunnels in clay. Géotechnique, Vol. 43, No. 2: 315-320.
- Mayne, P. W. and Kulhawy, F. H. 1982. K_0 -OCR relationships in soil. Journal of Geotechnical Engineering Division, ASCE, Vol. 108, GT6: 851-872.
- Moncrieff, R. L. 2006. 31 km of water transmission tunnel in Bangkok. Proceedings of the International Symposium on Underground Excavation and Tunnelling, Urban Tunnel Construction for Protection of Environment, Bangkok, Thailand: 141-150.
- Monsees, J. E. 1996. Soft ground tunneling. In Bickel, J. O., Kuesel, T. S. and King, E. H. (Eds.), Tunnel Engineering Handbook. 2nd ed., Chapman & Hall, New York: 97-121.
- Negro, A. Jr 1998. General report: Design criteria for tunnels in metropolises. Proceedings of the world tunnel congress 98 on tunnels and metropolises, São Paulo, Brazil: 201-214.

- Obayashi, H. 2006. Tunnel excavation with shield machine for Bangkok ground condition. Proceedings of the International Symposium on Underground Excavation and Tunnelling, Urban Tunnel Construction for Protection of Environment, Bangkok, Thailand: 207-212.
- O'Reilly, M. P. and New, B. M. 1982. Settlement above tunnels in the United Kingdom – their magnitude and prediction. Tunnelling'82, London: 173-181.
- Panet, M. and Guenot A. 1982. Analysis of convergence behind the face of a tunnel. Tunnelling'82, London: 197-204.
- Peck, R. B. 1969. Deep excavations and tunneling in soft ground. Proceedings of the 7th International Conference on Soil Mechanics and Foundation Engineering, State of the Art, Mexico City: 225-290.
- Pender, M. J. 1980. Elastic solution for a deep circular tunnel. Géotechnique, Vol. 30, No. 2: 216-222.
- Phienweij, N. 1996. Geotechnical experiences from previous tunnel project in Bangkok soils. Proceedings of the International Symposium on Geotechnical Aspects of Underground Construction in Soft Ground, London, U.K: 311-316.
- Phienweij, N. 1997. Ground movements in shield tunneling in Bangkok soils. Proceedings of the 14th International Conference on Soil Mechanics and Foundation Engineering, Hamburg, Germany: 1469-1472.
- Phienweij, N., Sirivachiraporn, A., Timpong, S., Tavaratum, S. and Suwansawat, S. 2006. Characteristics of ground movements from shield tunnelling of the first Bangkok subway line. Proceedings of the International Symposium on Underground Excavation and Tunnelling, Urban Tunnel Construction for Protection of Environment, Bangkok, Thailand: 319-330.
- Pitaksaithong, W. 2001. Effect of tunneling on soil displacements around nearby construction facilities. Thesis (M. Eng.), Chulalongkorn University, Bangkok, Thailand.

- Potts, D. M. and Zdravković, L. 1999. Finite element analysis in geotechnical engineering, theory, Vol. 1. Thomas Telford, London.
- Potts, D. M. and Zdravković, L. 2001. Finite element analysis in geotechnical engineering, Application, Vol. 2. Thomas Telford, London.
- Prinzl, F. and Davies J. A. 2006. Some aspects of design of tunnel linings in anisotropic ground conditions. Proceedings of the International Symposium on Underground Excavation and Tunnelling, Urban Tunnel Construction for Protection of Environment, Bangkok, Thailand: 231-238.
- Rowe, R. K. and Kack, G. J. 1983. A theoretical of the settlements induced by tunnelling: four case histories. Canadian Geotechnical Journal, Vol. 20: 299-314.
- Rowe, R. K., Lo, K. Y. and Kack, G. J. 1983. A method of estimating surface settlement above tunnel constructed in soft ground. Canadian Geotechnical Journal, Vol. 20: 11-22.
- Sagaseta, C. 1987. Analysis of undrained soil deformation due to ground loss. Géotechnique, Vol. 37, No. 3: 301-320.
- Shibuya, S. and Tamrakar, S. B. 1999. In-situ and laboratory investigations into engineering properties of Bangkok clay. Proceedings of the International Symposium on Characterization of Soft Marine Clays, Yokosuka, Japan: 107-132.
- Shibuya, S. and Tamrakar, S. B. 2003. Engineering properties of Bangkok clay. Proceedings of International Symposium on Characterisation and Engineering properties of Natural Soils, Singapore: 645-692.
- Shibuya, S., Tamrakar, S. B. and Theramast, N. 2001. Geotechnical site characterization on engineering properties of Bangkok clay. Journal of the Southeast Asian Geotechnical Society, Vol. 32, No. 3: 139-151.
- Slope Indicator Company 1994. Applications guide. 2nd ed., Seattle, USA.

- Slope Indicator Company 2004. Slope Indicator 2004 Catalog. Retrieved December 24, 2004, from <http://www.slopeindicator.com>
- Sramoon, A., Passara, M., Boonyaporn, P., Butpunya, N., Jantakoo P. and Manopim C. 2006. Articulated shield tunnelling performance at S-curved tunnel construction. Proceedings of the International Symposium on Underground Excavation and Tunnelling, Urban Tunnel Construction for Protection of Environment, Bangkok, Thailand: 201-206.
- Srisirirojanakorn, T. 2004. Pore pressure response and ground displacements in Chicago clay during tunneling and over long term. Thesis (Ph.D.), Graduate College of the University of Illinois at Urbana-Champaign, USA.
- Sutcliffe, H. 1996. Tunnel boring machines. In Bickel, J. O., Kuesel, T. S. and King, E. H. (Eds.), Tunnel Engineering Handbook. 2nd ed., Chapman & Hall, New York. pp. 203-219.
- Suwansawat, S. 2002. Earth pressure balance (EPB) shield tunneling in Bangkok: Ground response and prediction of surface settlements using artificial neural networks. Thesis (Ph.D.), Massachusetts Institute of Technology, USA.
- Swoboda, G. 1979. Finite element analysis of the new Austrian tunneling method (NATM). Proceedings of the 3rd International Conference on Numerical Methods Geomechanics, Aachen, Germany: 581-586.
- TAC 2000. LOVAT sells 2 additional metro TBMs to Singapore. Retrieved April 1, 2007, from http://pages.interlog.com/~tac/News_old/lovat.htm
- Teparaksa, W. 1999. Principal and application of instrumentation for the first MRTA subway project in Bangkok. Proceedings of the 5th International Conference on Field Measurement in Geomechanics, Singapore: 411-416.
- Teparaksa, W. 2005a. Prediction of ground deformation response for double tunnel Bangkok MRT subway. Proceedings 31st ITA-AITES World Tunnel Congress on Underground Space Use, Analysis of the Past and Lessons for the Future, Istanbul, Turkey: 991-996.

- Teparaksa, W. 2005b. FEM analysis of EPB tunnelling bored underneath through underground obstruction. Proceedings 31st ITA-AITES World Tunnel Congress on Underground Space Use, Analysis of the Past and Lessons for the Future, Istanbul, Turkey: 883-888.
- Teparaksa, W. and Heidengren, C. R. 1999. Geotechnical aspects of the design and construction of the MRTA initial system project - The Bangkok Subway. Journal of the Society of Professional Engineers, Thailand, No. 24 (November 1998 - November 1999): 21-34.
- Teparaksa, W., Photayanuvat, C., Boonsong C. and Boonard, J. 2006. Design of subway tunnel under the Chao Phraya River for Bangkok south blue line extension. Proceedings of the International Symposium on Underground Excavation and Tunnelling, Urban Tunnel Construction for Protection of Environment, Bangkok, Thailand: 181-189.
- Tokuda, T., Kinoshita, K. and Miki, K. 2006. Construction of MRT Chaloem Ratchamongkhon line underground structures north and Japanese shield tunnel technology. Proceedings of the International Symposium on Underground Excavation and Tunnelling, Urban Tunnel Construction for Protection of Environment, Bangkok, Thailand: 47-56.
- Vereuijt, A. and Booker, J. R. 1996. Surface settlements due to deformation of a tunnel in an elastic half plane. Géotechnique, Vol. 46, No. 4: 753-756.
- Vermeer, P. A., Bonnier, P. G. and Moler, S. C. 2002. On a smart use of 3D-FEM in tunnelling. Proceedings of the 8th International Symposium on Numerical Models in Geomechanics, Rom, Italy: 361-366.
- Wayss & Freytag Ingenieurbau AG. n.d. St. Clair River tunnel, Sarina, Canada. Retrieved April 2, 2007, from http://www.wf-ingbau.de/de/brochure/download/st_clair_canada_eng.pdf
- WIKIPEDIA, The Free Encyclopedia. n.d. Tunnelling shield. Retrieved February 10, 2007, from http://en.wikipedia.org/wiki/Tunnelling_shield

Wirth Company. n.d. Tunnling. Retrieved February 15, 2007, from <http://www.wirth-asia.com/index.php?id=5&L=0>

Yeow, H. C., Gaba, A. R. and Pillai, A. K. 2004. Concurrent tunnelling and station excavation at Bangkok MRTA North. Proceedings of the 15th Southeast Asian Geotechnical Society Conference, Bangkok, Thailand: 753-758.

APPENDICES

Appendix A

Summary of Soil Testing Results

Table A.1 Summary of test results from borehole No.8

Summary of test results, borehole No.8																
Project: BMA flood diversion tunnel (Saensaep Latphrao-Phrakhanong project)										Ground Water Level: - 0.5 m						
Sample	Depth (m)			γ_t	Natural	Atterberg Limit (%)			S_u	SPT	Sieve Analysis, % Finer					Classi-
No.	From	To	Avg.	kN/m ³	w _n (%)	LL	PL	PI	kN/m ²	(blows/ft)	3/8"	4	10	40	200	fication
ST-01	3.00	3.50	3.25	15.30	74.00				17.66							CH
ST-02	4.50	5.00	4.75	14.72	95.50				10.79							CH
ST-03	6.00	6.50	6.25	15.01	89.40	101.70	35.30	66.40	14.72							CH
ST-04	7.50	8.00	7.75	14.62	102.00				10.79							CH
ST-05	9.00	9.50	9.25	14.42	104.40				13.73							CH
ST-06	10.50	11.00	10.75	15.01	88.50				14.72							CH
ST-07	12.00	12.50	12.25	15.70	72.70				15.70							CH
ST-08	13.50	14.00	13.75	15.01	77.30				42.18							CH
ST-09	15.00	15.50	15.25	18.54	35.40				48.07							CL
SS-10	16.50	16.95	16.73	20.99	31.90	94.90	32.30	62.60	63.77	10						CL
ST-11	17.50	18.00	17.75													CL
SS-12	18.00	18.45	18.23		30.60					12						CL
SS-13	19.50	19.95	19.73		22.10					17						CL
SS-14	21.00	21.45	21.23							19		100	99	95	39	SC/CL
SS-15	22.50	22.95	22.73	20.31	21.70				212.88	25						CL
SS-16	24.00	24.45	24.23	20.80						36	100	98	91	61	18	SM-SP
SS-17	25.50	25.95	25.73							28	100	98	84	43	10	SM-SP
SS-18	27.00	27.45	27.23							43						SM-SP
SS-19	28.50	28.95	28.73							38	100	99	93	63	9	SM-SP
SS-20	30.00	30.45	30.23							36						SM-SP
SS-21	31.50	31.95	31.73							25		100	98	64	9	SM-SP
SS-22	33.00	33.45	33.23							50	100	98	96	39	11	SM-SP
SS-23	34.50	34.95	34.73							33						SM-SP
SS-24	36.00	36.45	36.23							33		100	99	24	12	SM-SP
SS-25	37.50	37.95	37.73		23.80	52.80	27.60	25.20		29						CL
ST-26	39.00	39.50	39.25													CL
SS-27	39.55	40.00	39.78	20.70	19.30				196.20	42						CL

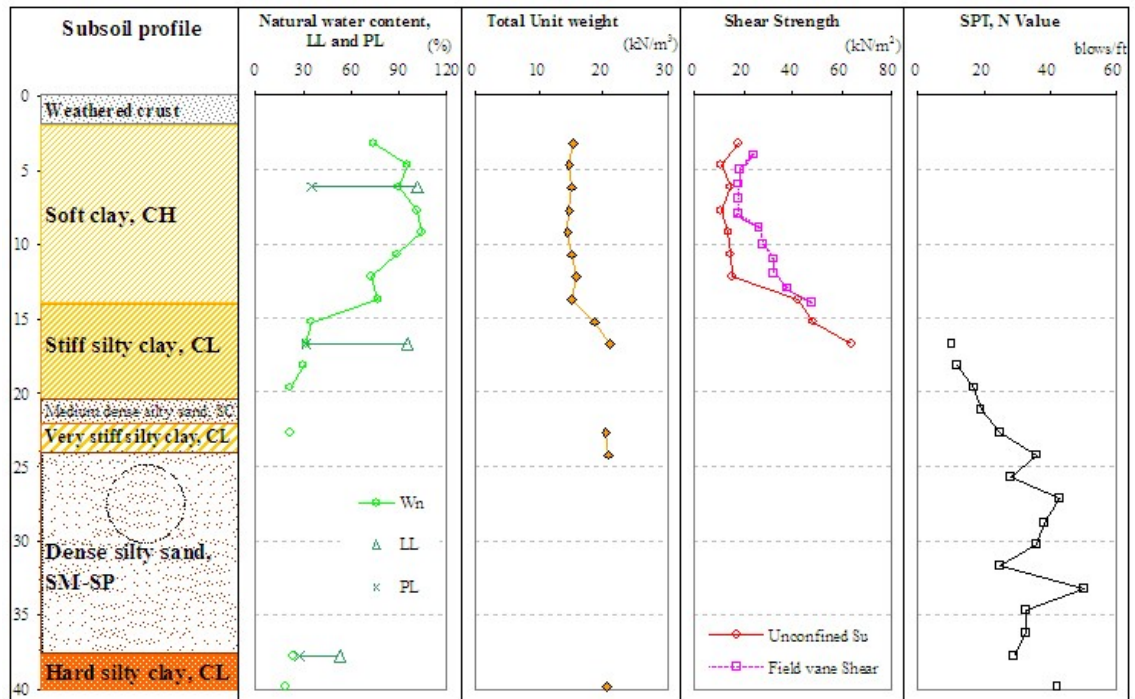


Figure A.1 Typical soil profile of borehole No.8

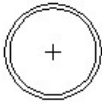
Borehole No. 8				0.00
Weathered crust	$\gamma_t = 17.5 \text{ kN/m}^3$	$S_u = 30 \text{ kN/m}^2$	$\phi = 0$	-2.00 m
Soft clay, CH	$\gamma_t = 15.7 \text{ kN/m}^3$	$S_{u(FVS)} = 24.0 \text{ kN/m}^2$	$\phi = 0$	-14.00 m
Stiff silty clay, CL	$\gamma_t = 19.0 \text{ kN/m}^3$	$S_u = 80.6 \text{ kN/m}^2$	$\phi = 0$	-20.50 m
Medium dense silty sand, SC	$\gamma_t = 20 \text{ kN/m}^3$	$S_u = 0$	$\phi = 30$	N = 17 blows/ft
Very stiff silty clay, CL	$\gamma_t = 20.0 \text{ kN/m}^3$	$S_u = 135 \text{ kN/m}^2$	$\phi = 0$	-24.00 m
Dense silty sand, SM-SP	$\gamma_t = 20 \text{ kN/m}^3$			-24.743
	$S_u = 0$			-27.518
	$\phi = 35$			-30.293
	N = 36 blows/ft			
			Tunnel, ID = 5.000 m	
			OD = 5.550 m	-37.50 m
Hard silty clay, CL	$\gamma_t = 20.5 \text{ kN/m}^3$	$S_u = 221.0 \text{ kN/m}^2$	$\phi = 0$	-40.00 m

Figure A.2 Engineering properties of borehole No.8 for FE analysis

Table A.2 Summary of test results from borehole No.9

Summary of test results, borehole No.9																
Project: BMA flood diversion tunnel (Saensaep Latphrao-Phrakhanong project)											Ground Water Level: -0.8 m					
Sample	Depth (m)			γ_t	Natural	Atterberg Limit (%)			S_u	SPT	Sieve Analysis, % Finer					Classi-
No.	From	To	Avg.	kN/m ³	w_n (%)	LL	PL	PI	kN/m ²	(blows/ft)	3/8"	4	10	40	200	fication
ST-01	3.00	3.50	3.25	15.60	70.70				41.20							CH
ST-02	4.50	5.00	4.75	16.19	68.80				28.45							CH
ST-03	6.00	6.50	6.25	15.21	85.00	88.30	35.90	52.40	19.62							CH
ST-04	7.50	8.00	7.75	14.81	93.90				22.56							CH
ST-05	9.00	9.50	9.25	14.52	102.40				23.54							CH
ST-06	10.50	11.00	10.75	15.50	79.10				26.49							CH
ST-07	12.00	12.50	12.25	15.40	84.60				9.81							CH
ST-08	13.50	14.00	13.75	18.25	39.20				60.82							CL
SS-09	15.00	15.45	15.23	19.23	27.40	66.70	23.70	43.00		9						CL
SS-10	16.50	16.95	16.73	18.54	32.50				92.21	12						CL
ST-11	17.50	18.00	17.75	18.34	41.30				104.97							CL
SS-12	18.00	18.45	18.23	17.56	36.90					16						CL
SS-13	19.50	19.95	19.73	18.44	33.30				67.69	11						CL
SS-14	21.00	21.45	21.23		23.40					14			100	96	39	SC
SS-15	22.50	22.95	22.73	20.40	17.80				93.20	20		100	94	75	58	CL
SS-16	24.00	24.45	24.23							23	100	96	87	52	15	SM
SS-17	25.50	25.95	25.73							32		100	98	81	13	SM
SS-18	27.00	27.45	27.23							32						(SM)
SS-19	28.50	28.95	28.73							38			100	94	78	CL
SS-20	30.00	30.45	30.23							33	100	99	88	48	8	SM-SP
SS-21	31.50	31.95	31.73							56		100	98	72	11	SM-SP
SS-22	33.00	33.45	33.23							51						SM-SP
SS-23	34.50	34.95	34.73							40		100	98	24	14	SM
SS-24	36.00	36.45	36.23							29						SM-SP
SS-25	37.50	37.95	37.73							28	100	99	79	22	9	SM-SP
SS-26	39.55	40.00	39.78	20.80	19.00	57.30	27.20	30.10		33						CL

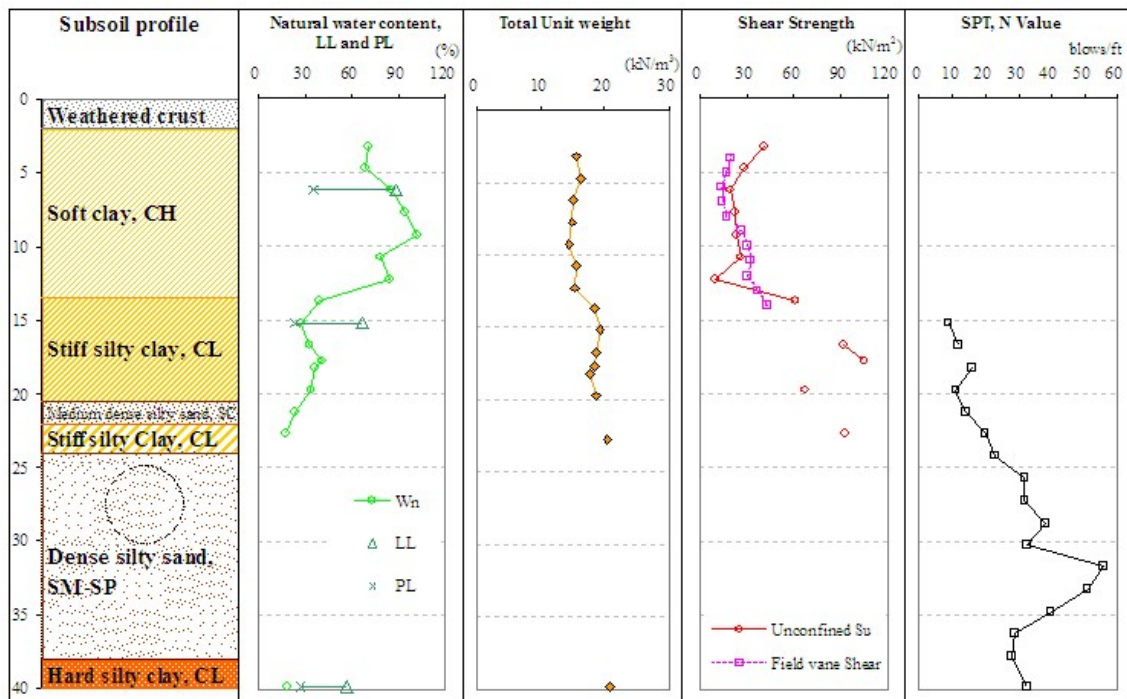


Figure A.3 Typical soil profile of borehole No.9

Borehole No. 9					0.00
Weathered crust	$\gamma_t = 17.5 \text{ kN/m}^3$	$S_u = 30 \text{ kN/m}^2$	$\phi = 0$		▼ -2.00 m
Soft clay, CH	$\gamma_t = 15.7 \text{ kN/m}^3$	$S_{u(FV)} = 24.0 \text{ kN/m}^2$	$\phi = 0$		▼ -13.50 m
Stiff silty clay, CL	$\gamma_t = 19.0 \text{ kN/m}^3$	$S_u = 80.6 \text{ kN/m}^2$	$\phi = 0$		▼ -20.50 m
Medium dense silty sand, SC	$\gamma_t = 20 \text{ kN/m}^3$	$S_u = 0$	$\phi = 30$	$N = 17 \text{ blows/ft}$	▼ -22.00 m
Very stiff silty clay, CL	$\gamma_t = 20.0 \text{ kN/m}^3$	$S_u = 135 \text{ kN/m}^2$	$\phi = 0$		▼ -24.00 m
Dense silty sand, SM-SP	$\gamma_t = 20 \text{ kN/m}^3$	$S_u = 0$	$\phi = 35$	$N = 36 \text{ blows/ft}$	▼ -24.777
					▼ -27.552
					▼ -30.327
				Tunnel, ID = 5.000 m OD = 5.550 m	▼ -38.00 m
Hard silty clay, CL	$\gamma_t = 20.5 \text{ kN/m}^3$	$S_u = 221.0 \text{ kN/m}^2$	$\phi = 0$		▼ -40.00 m

Figure A.4 Engineering properties of borehole No.9 for FE analysis

Table A.3 Summary of test results from borehole No.18

Summary of test results, borehole No.18																
Project: BMA flood diversion tunnel (Saensaep Latphrao-Phrakhanong project)											Ground Water Level: -1.10 m					
Sample	Depth (m)			γ_t	Natural	Atterberg Limit (%)			S_u	SPT	Sieve Analysis, % Finer					Classi-
No.	From	To	Avg.	kN/m ³	w_u (%)	LL	PL	PI	kN/m ²	(blows/ft)	3/8"	4	10	40	200	fication
ST-01	3.00	3.50	3.25	14.72	95.10				13.73							CH
ST-02	4.50	5.00	4.75													CH
ST-03	6.00	6.50	6.25	16.58	62.00	65.30	25.90	39.40	11.77							CH
ST-04	7.50	8.00	7.75	16.28	69.80				13.73							CH
ST-05	9.00	9.50	9.25	14.72	90.30				12.75							CH
ST-06	10.50	11.00	10.75	15.11	86.30				15.70							CH
ST-07	12.00	12.50	12.25	15.60	72.90				41.20							CH
ST-08	13.50	14.00	13.75	17.76	40.20				51.99							CH
ST-09	15.00	15.50	15.25	19.33	30.40	62.80	22.70	40.10	51.01							CH
ST-10	16.00	16.50	16.25	19.23	31.80				80.44							CL
SS-11	16.50	16.95	16.73	17.85	34.00				115.76	19						CL
SS-12	18.00	18.45	18.23	17.76	41.30					13						CL
SS-13	19.50	19.95	19.73	19.13	25.30					15						CL
SS-14	21.00	21.45	21.23	19.52	21.40					22						CL
SS-15	22.50	22.95	22.73	20.31	22.70				191.30	28						CL
SS-16	24.00	24.45	24.23	20.31	23.40					27						CL
SS-17	25.50	25.95	25.73	21.19	14.50				243.29	29						CL
SS-18	27.00	27.45	27.23	20.01	20.50					48						CL
ST-19	28.00	28.50	28.25													CL
SS-20	28.50	28.95	28.73	20.11	19.50					38						CL
SS-21	30.00	30.45	30.23	20.21	21.90	45.70	17.20	28.50	119.68	22						CL
SS-22	31.50	31.95	31.73		20.50					18						CL
SS-23	33.00	33.45	33.23	20.01	23.10					24						CL
SS-24	34.50	34.95	34.73							41			100	85	11	SM-SP
SS-25	36.00	36.45	36.23							32			100	43	17	SM
SS-26	37.50	37.95	37.73		30.30	52.60	27.30	25.30		8						CL
SS-27	39.55	40.00	39.78		36.20					7						CL

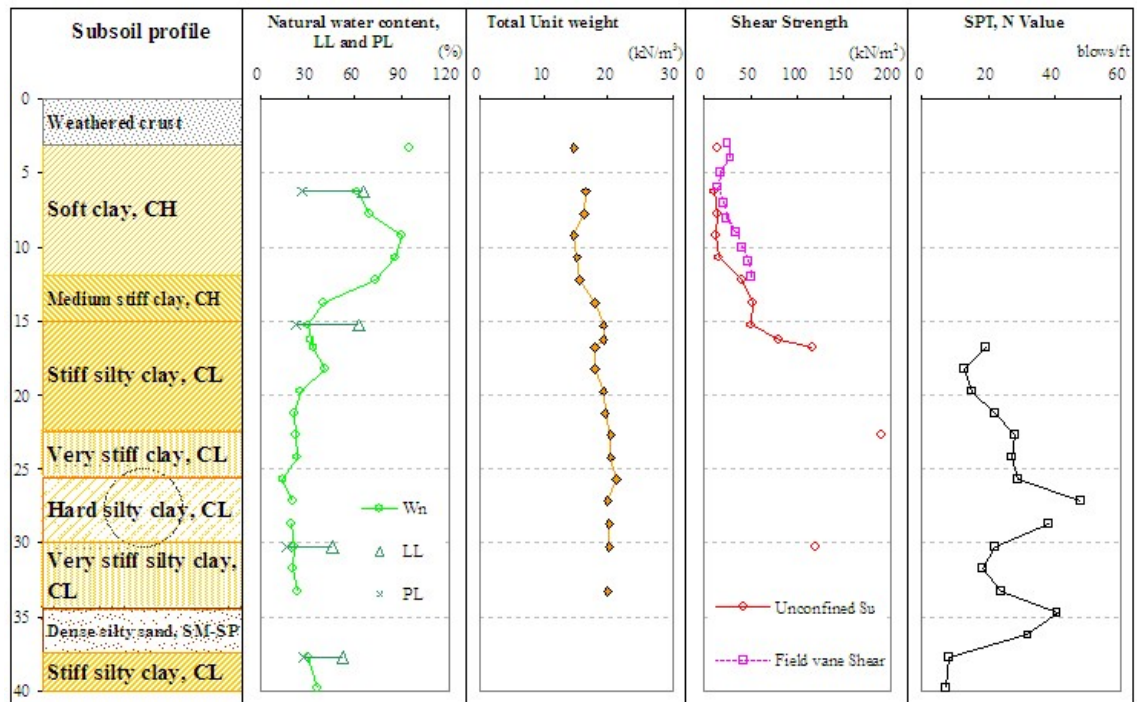


Figure A.5 Typical soil profile of borehole No.18

Borehole No. 18				0.00
Weathered crust	$\gamma_t = 17.5 \text{ kN/m}^3$	$S_u = 30 \text{ kN/m}^2$	$\phi = 0$	-3.00
Soft clay, CH	$\gamma_t = 15.7 \text{ kN/m}^3$	$S_{u(FV)} = 20.5 \text{ kN/m}^2$	$\phi = 0$	-12.00 m
Medium stiff clay, CH	$\gamma_t = 17.0 \text{ kN/m}^3$	$S_u = 46.6 \text{ kN/m}^2$	$\phi = 0$	-15.00 m
Stiff silty clay, CL	$\gamma_t = 19.0 \text{ kN/m}^3$	$S_u = 97.20 \text{ kN/m}^2$	$\phi = 0$	-22.50 m
Very stiff silty clay, CL	$\gamma_t = 20.30 \text{ kN/m}^3$	$S_u = 186.0 \text{ kN/m}^2$	$\phi = 0$	-25.50 m
Hard silty clay, CL	$\gamma_t = 20.50 \text{ kN/m}^3$	$S_u = 265.5 \text{ kN/m}^2$	$\phi = 0$	-30.00 m
Very stiff silty clay, CL	$\gamma_t = 20.00 \text{ kN/m}^3$	$S_u = 141.0 \text{ kN/m}^2$	$\phi = 0$	-34.50 m
Dense silty sand, SM-SP	$\gamma_t = 20 \text{ kN/m}^3$	$N = 36 \text{ blows/ft}$	$S_u = 0$	-37.50 m
Stiff silty clay, CL	$\gamma_t = 20.5 \text{ kN/m}^3$	$S_u = 94.0 \text{ kN/m}^2$	$\phi = 0$	

Figure A.6 Engineering properties of borehole No.18 for FE analysis

Appendix B

Monitored Data

Table B.1 Data of ground surface settlement, array number GS16

GROUND SURFACE SETTLEMENT ARRAY No. GS16															
Activity date		09/07/05	10/07/05	11/07/05	11/07/05	11/07/05	11/07/05	11/07/05	11/07/05	12/07/05	12/07/05	18/07/05	25/07/05	11/10/05	11/01/06
Activity	<i>Initial</i>	EX P1607	EX P1638	EX P1642	EX P1644	EX P1645	EX P1646	EX P1647	EX P1648	EX P1650	EX P1654	EX P1735	EX P1845	EX P2833	EX P3273
Tunnel face sta. (m)	<i>reading</i>	-30	-10	-5	0	+1	+2	+3.5	+5	+8	+13	1 week	2 weeks	3 months	6 months
Point No.	Vertical movements (mm)														
GS16/4L	<i>0.000</i>	0	0	0	0	0	0	0	0	0	0	-1	-1	-1	-1
GS16/3L	<i>0.000</i>	0	0	0	-1	-1	-2	2	2	4	1	-3	-2	-2	-3
GS16/2L	<i>0.000</i>	0	0	0	-3	-3	-3	-3	-3	-3	-4	-10	-10	-10	-11
GS16/1L	<i>0.000</i>	0	0	0	-1	-1	-2	-2	-2	-3	-10	-19	-19	-19	-20
GS16R	<i>0.000</i>	-1	-3	-3	-8	-8	-9	-9	-9	-9	-17	-25	-26	-26	-27
GS16/1R	<i>0.000</i>	0	-1	-1	-6	-6	-6	-5	-5	-6	-13	-22	-22	-22	-23
GS16/2R	<i>0.000</i>	0	0	0	-3	-3	-3	-3	-3	-3	-8	-16	-16	-16	-16
GS16/3R	<i>0.000</i>	0	0	0	-2	-2	-2	-2	-2	-3	-2	-4	-4	-4	-4
GS16/4R	<i>0.000</i>	0	0	0	0	0	0	0	0	0	-5	-6	-6	-6	-6

Table B.2 Data of ground surface settlement, array number GS17

GROUND SURFACE SETTLEMENT ARRAY No. GS17															
Activity date		15/07/05	16/07/05	16/07/05	17/07/05	17/07/05	17/07/05	17/07/05	17/07/05	17/07/05	17/07/05	24/07/05	31/07/05	17/10/05	17/01/06
Activity	<i>Initial</i>	EX P1690	EX P1706	EX P1711	EX P1713	EX P1714	EX P1715	EX P1716	EX P1717	EX P1719	EX P1724	EX P1829	EX P1939	EX P2833	EX P3380
Tunnel face sta. (m)	<i>reading</i>	-30	-10	-5	-2	-1	0	+1	+2	+5	+10	1 week	2 weeks	3 months	6 months
Point No.	Vertical movements (mm)														
GS17/2L	0	0	0	0	0	0	0	0	0	0	-1	-2	-2	-3	-3
GS17/1L	0	0	0	0	0	-2	-2	-2	-4	-6	-7	-11	-11	-13	-13
GS17	0	0	-2	-2	-2	-6	-9	-9	-11	-14	-14	-25	-25	-27	-27
GS17/1R	0	0	-2	-2	-2	-4	-4	-4	-8	-9	-10	-20	-20	-21	-21
GS17/2R	0	0	0	0	0	-4	-4	-4	-4	-4	-4	-11	-11	-11	-11
GS17/3R	0	0	0	0	0	-2	-2	-2	-2	-2	-2	-4	-4	-4	-4

Table B.3 Data of ground surface settlement, array number GS18

GROUND SURFACE SETTLEMENT ARRAY No. GS18															
Activity date		18/07/05	19/07/05	20/07/05	20/07/05	20/07/05	20/07/05	20/07/05	20/07/05	20/07/05	21/07/05	27/07/05	03/08/05	20/10/05	20/01/06
Activity	<i>Initial</i>	EX P1747	EX P1763	EX P1768	EX P1770	EX P1771	EX P1772	EX P1773	EX P1774	EX P1776	EX P1781	EX P1878	EX P1969	EX P2833	EX P3425
Tunnel face sta. (m)	<i>reading</i>	-30	-10	-5	0	+1	+2	+4	+5	+8	+13	1 week	2 weeks	3 months	6 months
Point No.	Vertical movements (mm)														
GS18/3L	0	0	0	0	0	0	-2	-2	-2	-2	-1	-5	-5	-5	-5
GS18/2L	0	0	0	0	-1	-1	-1	-1	-1	-1	-2	-8	-8	-8	-8
GS18/1L	0	0	0	-1	-2	-2	-3	-3	-3	-5	-6	-14	-14	-14	-14
GS18	0	0	0	-2	-4	-4	-5	-5	-5	-6	-8	-18	-18	-18	-18
GS18/1R	0	0	0	-1	-2	-3	-4	-4	-4	-6	-6	-13	-13	-13	-13
GS18/2R	0	0	0	0	0	-1	-2	-2	-2	-3	-4	-8	-8	-8	-8

Table B.4 Data of ground surface settlement, array number GS-BTS

GROUND SURFACE SETTLEMENT ARRAY No. GS-BTS														
Activity date	03/03/06	03/03/06	06/03/06	07/03/06	07/03/06	07/03/06	07/03/06	07/03/06	07/03/06	08/03/06	09/03/06	16/03/06	23/03/06	-
Activity	EX P3930	EX P3930	EX P3970	EX P3980	EX P3986	EX P3988	EX P3990	EX P3992	EX P3994	EX P4000	EX P4010	EX P4121	EX P4212	-
Tunnel face sta. (m)	<i>Initial</i>	-30	-10	-5	-2	-1	0	+1	+2	+5	+10	1 week	2 weeks	3 months
Point No.	Vertical movements (mm)													
GS-BTS/1L	0.000	0	0	0	-1	-1	-1	-1	-1	-3	-3	-3	-3	-3
GS-BTS	0.000	0	-1	-1	-3	-3	-3	-3	-4	-5	-5	-5	-6	-6
GS-BTS/1R	0.000	0	-1	-1	-1	-1	-1	-1	-1	-2	-3	-3	-3	-3

Table B.5 Data of ground surface settlement, array number G35

GROUND SURFACE SETTLEMENT ARRAY No. GS-35														
Activity date	05/03/06	05/03/06	07/03/06	08/03/06	08/03/06	08/03/06	08/03/06	08/03/06	08/03/06	09/03/06	09/03/06	16/03/06	23/03/06	-
Activity	EX P3954	EX P3954	EX P3994	EX P4004	EX P4010	EX P4012	EX P4014	EX P4016	EX P4018	EX P4024	EX P4034	EX P4128	EX P4220	-
Tunnel face sta. (m)	<i>Initial</i>	-30	-10	-5	-2	-1	0	+1	+2	+5	+10	1 week	2 weeks	3 months
Point No.	Vertical movements (mm)													
GS35/1R	0.000	0	0	0	0	0	0	0	0	-1	-1	-3	-3	-3
GS35/1L	0.000	0	0	0	0	0	0	0	0	0	0	-3	-3	-3
GS35	0.000	0	0	0	0	0	0	0	0	-1	-1	-4	-4	-4

Table B.6 Data of extensometer number ME-1 (Klongtan Bridge area)

Extensometer No. ME-1																				
Tunnel face (m)		Initial	-30.0	-11.00	-7.50	-4.50	-2.40	-1.50	0.00	+1.50	+3.00	+4.50	+6.00	+8.00	+10.00	+13.50	1 week	2 weeks	3 months	6 months
Surface settlement (mm)		0.00	-1.00	-3.00	-3.00	-3.00	-8.00	-8.00	-8.00	-9.00	-9.00	-9.00	-9.00	-9.00	-17.00	-17.00	-25.00	-26.00	-26.00	-27.00
Spider magnet No.	Depth (m)	Cumulative vertical movements (mm)																		
ME-1/4	-3.094	0.00	-1.25	-2.75	-2.75	-1.25	-7.25	-6.75	-7.25	-8.25	-7.75	-7.75	-6.75	-6.25	-16.75	-16.75	-22.25	-24.75	-26.75	-26.75
ME-1/3	-13.111	0.00	-0.75	-2.75	-1.75	-1.25	-8.75	-6.75	-9.25	-10.75	-10.75	-10.25	-9.75	-9.25	-18.75	-19.25	-19.25	-25.25	-24.75	-26.25
ME-1/2	-18.594	0.00	-1.75	-2.25	-1.25	-1.75	-6.75	-6.75	-10.25	-13.75	-15.25	-16.25	-17.25	-17.75	-28.75	-28.75	-31.75	-33.75	-32.75	-33.75
ME-1/1	-23.37	0.00	-0.50	-2.50	-1.50	-2.00	-9.50	-12.5	-19.5	-24.5	-25.50	-26.50	-26.50	-27.00	-40.00	-39.50	-40.00	-43.00	-42.00	-42.50

Table B.7 Data of extensometer number ME-2 (BTS-Sukumvit area)

Extensometer No. ME-2																						
Tunnel face (m)		Initial	-30.0	-12.0	-8.00	-5.00	-3.00	-2.00	-1.50	-1.00	-0.50	0.00	+0.50	+1.00	+1.50	+2.00	+3.00	+5.00	+8.00	+13.50	0.5 week	1 week
Surface sett. (mm)		0.00	0.00	0.00	0.00	0.00	0.00	0.00	-0.50	-1.00	-1.00	-1.00	-1.50	-2.00	-2.00	-2.00	-2.00	-2.00	-2.00	-2.00	-3	-3
Spider magnet No.	Depth (m)	Cumulative vertical movements (mm)																				
ME-1/3	-3.106	0.00	0.00	1.00	2.50	1.00	1.50	1.00	0.00	0.00	0.50	0.00	-1.00	-1.50	-1.00	0.00	1.00	1.00	0.00	0.00	-4.5	-3
ME-1/2	-12.655	0.00	0.00	1.50	0.00	1.50	0.50	-0.50	-0.50	-1.50	-1.50	0.00	-2.50	-0.50	-1.00	0.00	-1.00	0.50	0.50	0.00	-5	-4
ME-1/1	-22.692	0.00	0.00	2.50	-0.50	1.50	0.50	0.50	0.50	-2.00	-2.00	-2.00	1.00	-1.50	-1.00	-1.50	-1.50	-2.00	-2.50	-3.50	-7	-4.5

Table B.8 Lateral movements obtained from IC (BTS-Sukumvit area)

Depth (m)	Position of TBM's face (m)											
	Initial	-12	-8	-5	-3	-2	-1.5	-1	-0.5	0	+0.5	+1
	Lateral movements (mm)											
0.00	0.00	-0.16	-1.20	-1.67	-2.13	-1.30	-0.94	5.51	8.20	13.25	8.65	11.55
-0.50	0.00	-0.12	-1.07	-1.58	-2.00	-1.17	-0.81	6.15	8.58	14.34	9.38	12.28
-1.00	0.00	-0.06	-1.05	-1.52	-1.93	-1.15	-0.79	6.56	8.80	14.45	9.55	12.45
-1.50	0.00	-0.01	-0.50	-0.72	-0.98	0.40	0.86	8.50	10.50	16.10	11.20	14.10
-2.00	0.00	-0.14	-0.88	-1.20	-1.57	-0.53	-0.08	7.12	9.27	14.97	10.02	12.92
-2.50	0.00	-0.19	-1.08	-1.45	-1.82	-0.88	-0.48	6.52	8.72	14.47	9.52	12.42
-3.00	0.00	-0.27	-1.27	-1.68	-2.10	-1.27	-0.86	5.83	8.13	13.84	8.93	11.83
-3.50	0.00	-0.31	-1.45	-1.92	-2.33	-1.65	-1.24	5.20	7.60	13.35	8.40	11.35
-4.00	0.00	-0.34	-1.68	-2.35	-2.87	-2.53	-2.18	3.87	6.52	12.37	7.32	10.27
-4.50	0.00	-0.32	-1.97	-2.68	-3.35	-3.42	-3.11	2.58	5.48	11.44	6.33	9.23
-5.00	0.00	-0.24	-2.03	-2.80	-3.57	-3.83	-3.63	1.82	4.92	10.97	5.82	8.72
-5.50	0.00	-0.19	-2.18	-3.10	-3.97	-4.58	-4.43	0.57	3.97	10.17	4.92	7.82
-6.00	0.00	-0.12	-2.27	-3.28	-4.25	-5.17	-5.01	-0.32	3.23	9.54	4.23	7.13
-6.50	0.00	0.01	-2.23	-3.25	-4.22	-5.28	-5.18	-0.13	3.42	9.72	4.37	7.27
-7.00	0.00	0.11	-1.93	-2.80	-3.72	-4.58	-4.43	1.22	4.52	10.67	5.37	8.27
-7.50	0.00	0.19	-1.50	-2.27	-3.04	-3.55	-3.29	2.70	5.80	11.90	6.60	9.50
-8.00	0.00	0.11	-1.63	-2.40	-3.22	-3.68	-3.43	2.42	5.62	11.72	6.42	9.32
-8.50	0.00	0.08	-1.87	-2.73	-3.65	-4.22	-4.06	1.13	4.63	10.94	5.53	8.43
-9.00	0.00	0.04	-2.45	-3.57	-4.64	-6.15	-5.89	-1.75	2.25	8.80	3.30	6.20
-9.50	0.00	0.16	-2.78	-4.15	-5.37	-7.48	-7.33	-3.33	0.82	7.42	1.87	4.77
-10.00	0.00	0.29	-2.50	-3.82	-4.99	-6.95	-6.74	-2.20	1.70	8.20	2.70	5.60
-10.50	0.00	0.43	-2.12	-3.33	-4.35	-6.12	-5.86	-1.07	2.73	9.19	3.73	6.58
-11.00	0.00	0.56	-2.03	-3.30	-4.32	-6.18	-5.93	-1.23	2.67	9.17	3.67	6.52
-11.50	0.00	0.69	-2.00	-3.32	-4.39	-6.35	-6.14	-1.60	2.45	9.00	3.45	6.30
-12.00	0.00	0.81	-1.98	-3.35	-4.52	-6.68	-6.53	-2.18	2.02	8.67	3.07	5.92
-12.50	0.00	0.93	-1.97	-3.38	-4.65	-7.02	-6.86	-2.67	1.63	8.34	2.68	5.53
-13.00	0.00	1.06	-1.83	-3.25	-4.47	-6.88	-6.78	-2.68	1.72	8.47	2.77	5.62
-13.50	0.00	1.19	-1.60	-2.97	-4.14	-6.50	-6.34	-2.10	2.25	9.00	3.30	6.15
-14.00	0.00	1.34	-1.45	-2.85	-3.99	-6.35	-6.19	-1.90	2.50	9.25	3.55	6.40
-14.50	0.00	1.48	-1.32	-2.71	-3.90	-6.27	-6.16	-1.62	2.73	9.44	3.78	7.13
-15.00	0.00	1.59	-1.20	-2.55	-3.74	-6.15	-5.99	-1.50	2.90	9.60	3.95	7.30
-15.50	0.00	1.69	-1.20	-2.60	-3.74	-6.35	-6.14	-1.60	2.80	9.50	3.85	7.10
-16.00	0.00	1.78	-1.07	-2.41	-3.55	-6.12	-5.91	-1.37	3.08	9.79	4.13	7.38
-16.50	0.00	1.93	-1.02	-2.46	-3.60	-6.37	-6.16	-1.72	2.83	9.59	3.93	7.48
-17.00	0.00	2.01	-0.93	-2.33	-3.52	-6.28	-6.13	-1.33	3.12	9.77	4.17	7.72
-17.50	0.00	2.08	-0.62	-1.91	-3.00	-5.52	-5.36	-0.02	4.23	10.79	5.23	8.78
-18.00	0.00	2.11	-0.32	-1.56	-2.55	-4.87	-4.71	0.73	4.98	11.49	5.93	9.48
-18.50	0.00	2.13	-0.35	-1.65	-2.64	-5.00	-4.89	0.45	4.75	11.25	5.75	9.30
-19.00	0.00	2.15	-0.44	-1.78	-2.87	-5.38	-5.33	-0.08	4.27	10.82	5.32	8.87
-19.50	0.00	2.17	-0.27	-1.56	-2.55	-4.97	-4.86	0.33	4.73	11.34	5.83	9.33
-20.00	0.00	2.10	-0.44	-1.78	-2.87	-5.43	-5.38	-0.38	4.17	10.76	5.22	8.77

Note:

Outward lateral movement is mentioned with negative sign (-)

Table B.9 Lateral movements obtained from IC (cont.)

Depth (m)	Position of TBM's face (m)											
	Initial	-12	-8	-5	-3	-2	-1.5	-1	-0.5	0	+0.5	+1
	Lateral movements (mm)											
-20.50	0.00	2.03	-0.62	-2.11	-3.25	-6.07	-6.06	-1.42	3.38	10.03	4.48	8.03
-21.00	0.00	2.11	-0.74	-2.28	-3.47	-6.63	-6.68	-2.23	2.72	9.47	3.82	7.37
-21.50	0.00	2.21	-0.69	-2.23	-3.47	-6.78	-6.83	-2.23	2.67	9.42	3.77	6.82
-22.00	0.00	2.28	-0.47	-1.96	-3.15	-6.42	-6.46	-1.57	3.28	9.93	4.38	7.43
-22.50	0.00	2.28	-0.47	-2.01	-3.20	-6.52	-6.56	-1.72	3.13	9.83	4.68	7.33
-23.00	0.00	2.26	-0.59	-2.13	-3.37	-6.63	-6.73	-1.88	2.97	9.67	4.52	7.17
-23.50	0.00	2.21	-0.74	-2.28	-3.52	-6.83	-6.93	-2.13	2.72	9.47	4.32	6.92
-24.00	0.00	2.16	-1.14	-2.83	-4.22	-7.93	-8.08	-2.18	3.12	10.12	4.82	6.87
-24.50	0.00	2.21	-1.09	-2.78	-4.17	-7.98	-8.08	-2.28	3.02	10.07	4.72	6.77
-25.00	0.00	2.28	-0.77	-2.32	-3.60	-7.27	-7.31	-1.07	4.08	11.08	5.73	7.98
-25.50	0.00	2.28	-0.31	-1.60	-2.59	-5.60	-5.64	1.30	6.05	12.90	7.65	9.90
-26.00	0.00	2.28	-0.09	-1.23	-2.12	-4.78	-4.78	2.27	6.97	13.77	8.57	11.17
-26.50	0.00	2.28	-0.26	-1.45	-2.39	-5.15	-5.14	1.60	6.40	13.25	8.05	10.65
-27.00	0.00	2.28	-0.17	-1.27	-2.20	-4.82	-4.76	2.03	6.73	13.53	8.38	10.98
-27.50	0.00	2.10	-0.16	-1.25	-2.19	-4.45	-4.34	2.35	7.00	13.80	8.70	11.30
-28.00	0.00	1.95	-0.40	-1.55	-2.49	-4.80	-4.69	1.70	6.50	13.35	8.20	10.80
-28.50	0.00	1.75	-0.75	-2.00	-2.89	-5.50	-5.34	0.70	5.60	12.45	7.30	9.85
-29.00	0.00	1.58	-0.97	-2.22	-3.10	-5.72	-5.56	0.43	5.33	12.18	7.03	9.58
-29.50	0.00	1.42	-1.10	-2.35	-3.19	-5.65	-5.54	0.65	5.45	12.25	7.10	10.60
-30.00	0.00	1.25	-1.07	-2.22	-3.05	-5.12	-5.01	1.58	6.13	12.78	7.73	11.23
-30.50	0.00	1.25	-0.85	-1.80	-2.69	-4.30	-4.19	2.60	7.00	13.60	8.55	11.85
-31.00	0.00	1.25	-0.83	-1.78	-2.62	-4.28	-4.18	2.37	6.87	13.52	8.47	11.47
-31.50	0.00	1.25	-0.87	-1.82	-2.60	-4.27	-4.16	4.78	8.03	14.08	9.33	12.03
-32.00	0.00	1.25	-0.83	-1.73	-2.57	-4.08	-3.98	4.07	7.07	12.97	8.32	10.97
-32.50	0.00	1.25	-0.88	-1.83	-2.67	-4.28	-4.18	3.52	6.62	12.57	7.87	8.02
-33.00	0.00	1.25	-0.92	-1.87	-2.65	-4.27	-4.16	2.88	5.28	10.88	6.33	6.48
-33.50	0.00	1.25	-0.95	-1.85	-2.64	-4.25	-4.04	1.55	3.60	9.05	4.55	4.70
-34.00	0.00	1.25	-0.72	-1.47	-2.20	-3.42	-3.21	1.68	3.28	8.48	4.08	4.23
-34.50	0.00	1.25	-0.63	-1.28	-1.97	-3.03	-2.83	0.87	2.02	6.82	2.72	2.87
-35.00	0.00	1.25	-0.55	-1.15	-1.74	-2.80	-2.59	-0.45	0.55	4.15	1.10	1.25
-35.50	0.00	1.25	-0.55	-1.10	-1.64	-2.60	-2.39	-1.40	-0.60	1.40	-0.10	0.05
-36.00	0.00	1.25	-0.37	-0.77	-1.30	-1.92	-1.71	-0.77	-0.27	0.08	0.18	0.33
-36.50	0.00	1.25	-0.25	-0.60	-1.14	-1.45	-1.24	-0.35	0.15	0.45	0.55	0.70
-37.00	0.00	1.25	-0.17	-0.52	-1.00	-1.17	-1.01	-1.62	-1.12	-0.72	-0.72	-0.57
-37.50	0.00	1.25	-0.10	-0.45	-0.94	-1.05	-0.94	-1.50	-1.00	-0.65	-0.65	-0.50
-38.00	0.00	1.05	-0.05	-0.35	-0.84	-0.85	-0.80	-1.30	-0.80	-0.50	-0.50	-0.40
-38.50	0.00	0.85	-0.05	-0.30	-0.59	-0.65	-0.65	-1.10	-0.60	-0.40	-0.30	-0.30
-39.00	0.00	0.62	-0.28	-0.43	-0.68	-0.83	-0.78	-1.33	-0.83	-0.63	-0.58	-0.58
-39.50	0.00	0.43	-0.22	-0.32	-0.52	-0.62	-0.62	-1.12	-0.62	-0.52	-0.47	-0.47
-40.00	0.00	0.22	-0.08	-0.13	-0.23	-0.28	-0.33	-0.28	-0.28	-0.28	-0.23	-0.23
-40.50	0.00	0.00	0.00	0.00	0.00	0.00	0.00	0.00	0.00	0.00	0.00	0.00

Note:

Outward lateral movement is mentioned with negative sign (-)

Table B.10 Lateral movements obtained from IC (cont.)

Depth (m)	Position of TBM's face (m)										
	Initial	+1.5	+2	+3	+5	+8	+12	0.5 week	1 week	2 weeks	3 months
	Lateral movements (mm)										
0.00	0.00	4.70	10.76	6.75	6.05	6.45	7.45	5.55	8.33	8.35	7.15
-0.50	0.00	5.28	10.89	7.38	6.53	6.98	8.13	6.03	8.82	8.73	7.58
-1.00	0.00	5.70	10.91	7.75	6.85	7.30	8.40	6.30	9.03	8.95	7.85
-1.50	0.00	7.55	12.46	9.50	8.60	9.05	10.10	8.05	10.99	10.65	9.55
-2.00	0.00	6.47	11.48	8.37	7.42	7.87	8.92	6.82	9.85	9.47	8.32
-2.50	0.00	6.07	11.08	7.92	6.92	7.37	8.42	6.27	9.40	8.92	7.72
-3.00	0.00	5.58	10.64	7.38	6.38	6.83	7.83	5.73	8.72	8.33	7.13
-3.50	0.00	5.15	10.26	6.90	5.85	6.35	7.30	5.25	8.23	7.80	6.60
-4.00	0.00	4.12	9.37	5.92	4.82	5.32	6.27	4.22	7.27	6.77	5.57
-4.50	0.00	3.18	8.49	5.03	3.88	4.43	5.38	3.38	6.43	5.88	4.73
-5.00	0.00	2.72	8.07	4.62	3.42	4.02	4.97	2.97	6.02	5.47	4.32
-5.50	0.00	1.87	7.32	3.82	2.57	3.22	4.22	2.22	5.27	4.72	3.62
-6.00	0.00	1.28	6.74	3.23	1.93	2.63	3.63	1.68	4.73	4.13	3.08
-6.50	0.00	1.62	6.82	3.57	2.27	2.97	4.07	2.02	5.02	4.42	3.42
-7.00	0.00	2.87	7.57	4.82	3.52	4.22	5.27	3.27	6.12	5.57	4.67
-7.50	0.00	4.30	8.65	6.20	4.90	5.60	6.60	4.65	7.40	6.85	6.05
-8.00	0.00	4.22	8.52	6.07	4.82	5.47	6.42	4.52	7.22	6.72	5.92
-8.50	0.00	3.38	7.94	5.23	4.18	4.58	5.53	3.63	6.48	5.93	5.03
-9.00	0.00	1.05	6.00	2.95	2.35	2.30	3.30	1.40	4.35	3.85	2.85
-9.50	0.00	-0.28	4.67	1.67	1.17	1.02	2.02	0.17	3.12	2.62	1.67
-10.00	0.00	0.80	5.30	2.75	1.95	2.05	3.05	1.20	4.10	3.45	2.65
-10.50	0.00	1.98	6.24	3.93	2.98	3.23	4.23	2.38	5.23	4.53	3.83
-11.00	0.00	2.07	6.22	4.07	3.12	3.32	4.32	2.52	5.32	4.62	3.97
-11.50	0.00	1.95	6.05	4.00	3.10	3.25	4.25	2.50	5.25	4.55	3.95
-12.00	0.00	1.62	5.72	3.72	2.87	2.97	3.97	2.27	4.97	4.27	3.72
-12.50	0.00	1.38	5.39	3.53	2.68	2.73	3.73	2.08	4.73	4.03	3.53
-13.00	0.00	1.57	5.47	3.72	2.87	2.92	3.92	2.27	4.92	4.22	3.72
-13.50	0.00	2.25	5.95	4.40	3.50	3.60	4.60	2.95	5.55	4.85	4.40
-14.00	0.00	2.65	6.15	4.80	3.85	4.00	5.00	3.35	5.90	5.20	4.80
-14.50	0.00	3.08	6.29	5.23	4.13	4.38	5.38	3.73	6.23	5.48	5.18
-15.00	0.00	3.35	6.40	5.50	4.35	4.65	5.65	4.00	6.45	5.70	5.45
-15.50	0.00	3.40	6.25	5.45	4.35	4.65	5.60	4.05	6.40	5.65	5.45
-16.00	0.00	3.88	6.54	5.93	4.78	5.08	6.03	4.48	6.83	6.03	5.88
-16.50	0.00	3.78	6.34	5.83	4.73	4.98	5.93	4.43	6.73	5.93	5.83
-17.00	0.00	4.22	6.42	6.27	4.97	5.37	6.32	4.82	7.07	6.22	6.22
-17.50	0.00	5.53	7.29	7.58	5.98	6.63	7.58	6.13	8.28	7.33	7.48
-18.00	0.00	6.38	7.94	8.43	6.78	7.43	8.38	6.98	9.08	8.13	8.33
-18.50	0.00	6.30	7.81	8.30	6.75	7.30	8.20	6.85	8.90	8.00	8.20
-19.00	0.00	5.97	7.42	7.92	6.47	6.92	7.77	6.47	8.52	7.62	7.82
-19.50	0.00	6.53	7.89	8.48	7.03	7.43	8.33	6.98	9.03	8.13	8.33
-20.00	0.00	6.07	7.42	7.97	6.67	6.92	7.77	6.47	8.52	7.67	7.87

Note:

Outward lateral movement is mentioned with negative sign (-)

Table B.11 Lateral movements obtained from IC (cont.)

Depth (m)	Position of TBM's face (m)										
	Initial	+1.5	+2	+3	+5	+8	+12	0.5 week	1 week	2 weeks	3 months
	Lateral movements (mm)										
-20.50	0.00	5.38	6.78	7.33	6.13	6.28	7.13	5.88	7.93	7.08	7.33
-21.00	0.00	4.87	6.22	6.82	5.67	5.77	6.67	5.42	7.47	6.57	6.87
-21.50	0.00	5.02	6.12	6.97	5.72	5.87	6.77	5.52	7.52	6.57	6.97
-22.00	0.00	5.68	6.53	7.63	6.28	6.53	7.43	6.18	8.13	7.18	7.63
-22.50	0.00	5.73	6.43	7.63	6.28	6.48	7.53	6.13	8.13	7.08	7.53
-23.00	0.00	5.72	6.27	7.57	6.22	6.37	7.42	5.97	8.02	6.97	7.42
-23.50	0.00	5.62	6.07	7.42	6.07	6.22	7.22	5.82	7.82	6.77	7.22
-24.00	0.00	6.07	6.92	7.92	6.97	6.67	7.77	6.22	8.42	7.37	7.72
-24.50	0.00	6.12	6.82	7.97	7.02	6.72	7.77	6.27	8.42	7.37	7.77
-25.00	0.00	7.33	7.73	9.13	8.03	7.88	8.88	7.43	9.48	8.43	8.93
-25.50	0.00	9.50	9.40	11.20	9.75	9.90	10.80	9.40	11.35	10.25	10.80
-26.00	0.00	10.62	10.22	12.22	10.62	10.87	11.77	10.37	12.27	11.07	11.72
-26.50	0.00	10.20	9.80	11.65	10.25	10.30	11.20	9.75	11.65	10.55	11.15
-27.00	0.00	10.63	10.08	12.03	10.58	10.68	11.53	10.03	11.98	10.78	11.43
-27.50	0.00	11.10	10.40	12.45	10.95	11.00	11.90	10.30	12.30	10.75	11.60
-28.00	0.00	10.70	10.05	12.35	10.65	10.65	11.60	9.90	12.00	10.30	11.15
-28.50	0.00	9.90	9.25	11.50	9.90	9.80	10.70	9.00	11.10	9.45	10.25
-29.00	0.00	9.83	8.98	11.33	9.68	9.58	10.48	8.73	10.88	9.13	9.93
-29.50	0.00	10.05	9.05	11.45	9.80	9.70	10.55	8.80	10.95	9.20	9.95
-30.00	0.00	10.88	9.53	12.18	10.33	10.43	11.13	9.48	11.53	9.73	10.53
-30.50	0.00	12.95	10.30	14.05	11.15	12.00	12.50	10.25	12.80	10.50	11.55
-31.00	0.00	11.52	10.32	12.77	10.82	11.02	11.67	10.27	12.07	10.32	11.12
-31.50	0.00	10.68	10.28	12.08	11.48	10.83	11.53	10.23	11.78	10.73	11.13
-32.00	0.00	7.92	9.12	9.52	10.47	8.72	9.57	9.07	9.87	9.62	9.62
-32.50	0.00	4.62	8.82	6.52	7.57	6.47	7.57	8.77	8.07	8.62	8.42
-33.00	0.00	2.98	6.83	4.83	6.08	4.88	6.38	6.78	6.38	6.88	6.63
-33.50	0.00	2.05	4.85	3.75	4.20	3.65	4.95	4.80	4.85	5.00	4.90
-34.00	0.00	1.88	4.13	3.48	3.78	3.33	4.08	4.08	4.23	4.43	4.33
-34.50	0.00	0.82	2.52	2.27	2.27	2.12	2.87	2.47	2.87	2.87	2.82
-35.00	0.00	-0.60	0.75	0.65	0.70	0.60	1.60	0.70	1.25	1.20	1.15
-35.50	0.00	-1.55	-0.55	-0.55	-0.45	-0.55	0.85	-0.45	0.15	-0.05	-0.05
-36.00	0.00	-1.07	-0.42	-0.37	-0.12	-0.27	0.58	-0.17	0.13	0.18	0.18
-36.50	0.00	-0.50	0.05	0.10	0.30	0.20	0.95	0.30	0.55	0.60	0.60
-37.00	0.00	-1.62	-1.17	-1.12	-0.92	-1.07	-0.12	-0.97	-0.67	-0.82	-0.72
-37.50	0.00	-1.35	-1.05	-0.95	-0.80	-0.90	-0.30	-0.85	-0.65	-0.70	-0.65
-38.00	0.00	-1.05	-0.85	-0.70	-0.65	-0.65	-0.15	-0.60	-0.45	-0.55	-0.50
-38.50	0.00	-0.75	-0.65	-0.50	-0.50	-0.45	0.00	-0.40	-0.30	-0.40	-0.35
-39.00	0.00	-0.83	-0.83	-0.63	-0.73	-0.63	-0.58	-0.63	-0.63	-0.63	-0.63
-39.50	0.00	-0.62	-0.62	-0.52	-0.57	-0.52	-0.47	-0.52	-0.52	-0.52	-0.52
-40.00	0.00	-0.28	-0.28	-0.28	-0.28	-0.28	-0.23	-0.28	-0.28	-0.28	-0.28
-40.50	0.00	0.00	0.00	0.00	0.00	0.00	0.00	0.00	0.00	0.00	0.00

Note:

Outward lateral movement is mentioned with negative sign (-)

Table B.12 Data of Klongtan bridge's settlement

	<i>Settlement points on the Klongtan Bridge's columns</i>											
TBM's face st. (m)	Point C		Point D		Point E		Point F		Point G		Point H	
	Activity date	Sett. (mm)	Activity date	Sett. (mm)	Activity date	Sett. (mm)	Activity date	Sett. (mm)	Activity date	Sett. (mm)	Activity date	Sett. (mm)
-30.00	08/07/05	0	09/07/05	0	10/07/05	0	11/07/05	0	13/07/05	0	13/07/05	0
-20.40	09/07/05	0	10/07/05	0	11/07/05	0	12/07/05	0	14/07/05	0	14/07/05	0
-19.20	09/07/05	0	10/07/05	0	11/07/05	0	12/07/05	0	14/07/05	0	14/07/05	0
-18.00	09/07/05	0	10/07/05	0	11/07/05	0	12/07/05	0	14/07/05	0	15/07/05	0
-16.80	09/07/05	0	10/07/05	0	11/07/05	0	13/07/05	0	14/07/05	0	15/07/05	0
-15.60	09/07/05	0	10/07/05	0	11/07/05	0	13/07/05	0	14/07/05	0	15/07/05	0
-14.40	09/07/05	0	10/07/05	0	11/07/05	0	13/07/05	0	14/07/05	0	15/07/05	0
-13.20	10/07/05	0	10/07/05	0	11/07/05	0	13/07/05	0	14/07/05	0	15/07/05	0
-12.00	10/07/05	0	11/07/05	0	12/07/05	0	13/07/05	0	14/07/05	-1	15/07/05	0
-10.80	10/07/05	0	11/07/05	0	12/07/05	0	13/07/05	0	14/07/05	-1	15/07/05	0
-9.60	10/07/05	0	11/07/05	0	12/07/05	0	13/07/05	0	14/07/05	-1	15/07/05	0
-8.40	10/07/05	0	11/07/05	0	12/07/05	0	14/07/05	0	14/07/05	-1	15/07/05	0
-7.20	10/07/05	0	11/07/05	0	12/07/05	0	14/07/05	0	14/07/05	-1	15/07/05	0
-6.00	10/07/05	-2	11/07/05	0	12/07/05	0	14/07/05	0	14/07/05	-1	15/07/05	0
-4.80	10/07/05	-2	11/07/05	0	12/07/05	0	14/07/05	0	14/07/05	-1	15/07/05	0
-3.60	10/07/05	-2	11/07/05	0	12/07/05	0	14/07/05	0	15/07/05	-1	15/07/05	-2
-2.40	10/07/05	-2	11/07/05	0	12/07/05	0	14/07/05	0	15/07/05	-1	15/07/05	-2
-1.20	10/07/05	-8	11/07/05	0	12/07/05	0	14/07/05	-3	15/07/05	-1	15/07/05	-2
0.00	10/07/05	-8	11/07/05	-3	13/07/05	-6	14/07/05	-3	15/07/05	-1	15/07/05	-2
1.20	10/07/05	-8	12/07/05	-4	13/07/05	-9	14/07/05	-3	15/07/05	-1	15/07/05	-2
2.40	11/07/05	-8	12/07/05	-8	13/07/05	-10	14/07/05	-6	15/07/05	-1	16/07/05	-2
3.60	11/07/05	-9	12/07/05	-8	13/07/05	-10	14/07/05	-9	15/07/05	-12	16/07/05	-7
4.80	11/07/05	-10	12/07/05	-8	13/07/05	-10	14/07/05	-9	15/07/05	-12	16/07/05	-7
6.00	11/07/05	-10	12/07/05	-18	13/07/05	-10	14/07/05	-9	15/07/05	-12	16/07/05	-7
7.20	11/07/05	-13	12/07/05	-18	14/07/05	-10	14/07/05	-9	15/07/05	-15	16/07/05	-11
8.40	11/07/05	-16	12/07/05	-22	14/07/05	-10	14/07/05	-9	15/07/05	-15	16/07/05	-11
9.60	11/07/05	-16	12/07/05	-22	14/07/05	-19	14/07/05	-17	15/07/05	-19	16/07/05	-11
10.80	11/07/05	-17	13/07/05	-28	14/07/05	-19	14/07/05	-17	15/07/05	-19	16/07/05	-11
12.00	11/07/05	-17	13/07/05	-28	14/07/05	-19	15/07/05	-17	15/07/05	-19	16/07/05	-11
13.20	11/07/05	-17	13/07/05	-28	14/07/05	-22	15/07/05	-18	15/07/05	-19	16/07/05	-20
14.40	11/07/05	-18	13/07/05	-29	14/07/05	-22	15/07/05	-18	15/07/05	-19	16/07/05	-20
15.60	11/07/05	-18	13/07/05	-29	14/07/05	-22	15/07/05	-18	15/07/05	-19	16/07/05	-20
16.80	11/07/05	-18	13/07/05	-29	14/07/05	-23	15/07/05	-18	16/07/05	-20	16/07/05	-20
18.00	11/07/05	-18	13/07/05	-29	14/07/05	-23	15/07/05	-18	16/07/05	-20	16/07/05	-20
19.20	11/07/05	-18	14/07/05	-29	14/07/05	-23	15/07/05	-18	16/07/05	-20	16/07/05	-20
20.40	11/07/05	-23	14/07/05	-29	14/07/05	-23	15/07/05	-19	16/07/05	-20	17/07/05	-20
1 week	17/07/05	-28	18/07/05	-33	20/07/05	-23	21/07/05	-26	22/07/05	-25	22/07/05	-26
2 weeks	24/07/05	-30	25/07/05	-35	27/07/05	-29	28/07/05	-26	29/07/05	-25	29/07/05	-26
3 months	07/10/05	-29	11/10/05	-34	13/10/05	-28	14/10/05	-25	15/10/05	-25	15/10/05	-28
6 months	07/01/06	-29	11/01/06	-33	13/01/06	-27	14/01/06	-25	15/01/06	-25	15/01/06	-29

Table B.13 Data of 3-storey chophouses' settlement

<i>Settlement points above the foundations of 3-storey shophouses located on the right side of Klongtan Bridge</i>										
TBM's face st. (m)	Point C ₁		Point C ₂		Point C ₃		Point C ₄		Point C ₅	
	Activity Date	Sett. (mm)	Activity Date	Sett. (mm)	Activity Date	Sett. (mm)	Activity Date	Sett. (mm)	Activity Date	Sett. (mm)
-30.00	09/07/05	0	09/07/05	0	10/07/05	0	13/07/05	0	14/07/05	0
-20.40	10/07/05	0	10/07/05	0	11/07/05	0	14/07/05	0	14/07/05	0
-19.20	10/07/05	0	10/07/05	0	11/07/05	0	14/07/05	0	14/07/05	0
-18.00	10/07/05	0	10/07/05	0	11/07/05	0	14/07/05	0	14/07/05	0
-16.80	10/07/05	0	10/07/05	0	11/07/05	0	14/07/05	0	15/07/05	0
-15.60	10/07/05	0	10/07/05	0	11/07/05	0	14/07/05	0	15/07/05	0
-14.40	10/07/05	0	10/07/05	0	11/07/05	0	14/07/05	0	15/07/05	0
-13.20	10/07/05	0	10/07/05	0	12/07/05	0	14/07/05	-2	15/07/05	0
-12.00	10/07/05	0	10/07/05	0	12/07/05	0	14/07/05	-2	15/07/05	0
-10.80	10/07/05	0	10/07/05	0	12/07/05	-2	14/07/05	-2	15/07/05	0
-9.60	10/07/05	0	10/07/05	0	12/07/05	-2	14/07/05	-2	15/07/05	-1
-8.40	11/07/05	0	11/07/05	0	12/07/05	-4	14/07/05	-2	15/07/05	-1
-7.20	11/07/05	0	11/07/05	0	12/07/05	-4	14/07/05	-2	15/07/05	-1
-6.00	11/07/05	0	11/07/05	0	12/07/05	-4	14/07/05	-2	15/07/05	-1
-4.80	11/07/05	0	11/07/05	0	12/07/05	-4	14/07/05	-2	15/07/05	-1
-3.60	11/07/05	0	11/07/05	0	13/07/05	-8	15/07/05	-2	15/07/05	-1
-2.40	11/07/05	0	11/07/05	0	13/07/05	-8	15/07/05	-2	15/07/05	-2
-1.20	11/07/05	0	11/07/05	0	13/07/05	-8	15/07/05	-2	15/07/05	-2
0.00	11/07/05	0	11/07/05	0	13/07/05	-8	15/07/05	-2	15/07/05	-2
1.20	11/07/05	0	11/07/05	0	13/07/05	-8	15/07/05	-2	15/07/05	-2
2.40	11/07/05	0	11/07/05	0	13/07/05	-8	15/07/05	-2	15/07/05	-2
3.60	11/07/05	0	11/07/05	0	13/07/05	-8	15/07/05	-6	16/07/05	-5
4.80	12/07/05	0	12/07/05	0	14/07/05	-8	15/07/05	-6	16/07/05	-5
6.00	12/07/05	0	12/07/05	-2	14/07/05	-8	15/07/05	-6	16/07/05	-5
7.20	12/07/05	0	12/07/05	-2	14/07/05	-8	15/07/05	-6	16/07/05	-5
8.40	12/07/05	0	12/07/05	-2	14/07/05	-8	15/07/05	-6	16/07/05	-5
9.60	12/07/05	0	12/07/05	-4	14/07/05	-8	15/07/05	-6	16/07/05	-5
10.80	12/07/05	0	12/07/05	-4	14/07/05	-8	15/07/05	-7	16/07/05	-5
12.00	12/07/05	0	12/07/05	-4	14/07/05	-8	15/07/05	-7	16/07/05	-11
13.20	12/07/05	0	12/07/05	-4	14/07/05	-8	15/07/05	-7	16/07/05	-11
14.40	13/07/05	-2	13/07/05	-8	14/07/05	-8	15/07/05	-7	16/07/05	-11
15.60	13/07/05	-2	13/07/05	-8	14/07/05	-8	15/07/05	-7	16/07/05	-11
16.80	13/07/05	-2	13/07/05	-8	14/07/05	-8	16/07/05	-9	16/07/05	-11
18.00	13/07/05	-2	13/07/05	-8	14/07/05	-8	16/07/05	-9	16/07/05	-11
19.20	13/07/05	-2	13/07/05	-8	14/07/05	-8	16/07/05	-9	16/07/05	-11
20.40	13/07/05	-2	13/07/05	-8	14/07/05	-8	16/07/05	-9	16/07/05	-11
1 week	18/07/05	-2	18/07/05	-9	20/07/05	-12	22/07/05	-15	22/07/05	-14
2 weeks	25/07/05	-2	25/07/05	-11	27/07/05	-13	29/07/05	-15	29/07/05	-14
3 months	11/10/05	-	11/10/05	-	13/10/05	-	15/10/05	-	15/10/05	-
6 months	11/01/06	-	11/01/06	-	13/01/06	-	15/01/06	-	15/01/06	-

Table B.14 Data of 4-storey chophouses' settlement

<i>Settlement points above the foundations of 4-storey shophouses located on the right side of Klongtan Bridge</i>								
TBM's face st. (m)	Point D ₁		Point D ₂		Point D ₃		Point D ₄	
	Activity Date	Settlement (mm)	Activity Date	Settlement (mm)	Activity Date	Settlement (mm)	Activity Date	Settlement (mm)
-30.00	14/07/05	0	15/07/05	0	15/07/05	0	15/07/05	0
-20.40	14/07/05	0	15/07/05	0	16/07/05	0	16/07/05	0
-19.20	14/07/05	0	15/07/05	0	16/07/05	0	16/07/05	0
-18.00	15/07/05	0	15/07/05	0	16/07/05	0	16/07/05	0
-16.80	15/07/05	0	15/07/05	0	16/07/05	0	16/07/05	0
-15.60	15/07/05	0	16/07/05	0	16/07/05	0	16/07/05	0
-14.40	15/07/05	0	16/07/05	0	16/07/05	0	16/07/05	0
-13.20	15/07/05	0	16/07/05	0	16/07/05	0	16/07/05	0
-12.00	15/07/05	0	16/07/05	0	16/07/05	-2	16/07/05	0
-10.80	15/07/05	0	16/07/05	0	16/07/05	-2	16/07/05	0
-9.60	15/07/05	0	16/07/05	0	16/07/05	-2	16/07/05	0
-8.40	15/07/05	0	16/07/05	0	16/07/05	-2	16/07/05	0
-7.20	15/07/05	0	16/07/05	-3	16/07/05	-2	16/07/05	0
-6.00	15/07/05	0	16/07/05	-3	16/07/05	-2	16/07/05	0
-4.80	15/07/05	0	16/07/05	-3	16/07/05	-2	16/07/05	0
-3.60	15/07/05	0	16/07/05	-3	16/07/05	-2	16/07/05	0
-2.40	15/07/05	0	16/07/05	-3	17/07/05	-2	17/07/05	0
-1.20	15/07/05	0	16/07/05	-3	17/07/05	-2	17/07/05	0
0.00	15/07/05	0	16/07/05	-3	17/07/05	-2	17/07/05	0
1.20	15/07/05	0	16/07/05	-3	17/07/05	-4	17/07/05	0
2.40	16/07/05	0	17/07/05	-3	17/07/05	-5	17/07/05	0
3.60	16/07/05	-1	17/07/05	-3	17/07/05	-5	17/07/05	0
4.80	16/07/05	-1	17/07/05	-3	17/07/05	-5	17/07/05	0
6.00	16/07/05	-1	17/07/05	-7	17/07/05	-5	17/07/05	0
7.20	16/07/05	-1	17/07/05	-14	17/07/05	-5	17/07/05	0
8.40	16/07/05	-2	17/07/05	-14	17/07/05	-5	17/07/05	0
9.60	16/07/05	-2	17/07/05	-14	17/07/05	-5	17/07/05	0
10.80	16/07/05	-11	17/07/05	-14	17/07/05	-5	17/07/05	0
12.00	16/07/05	-11	17/07/05	-14	17/07/05	-5	17/07/05	0
13.20	16/07/05	-11	17/07/05	-14	17/07/05	-5	17/07/05	0
14.40	16/07/05	-11	17/07/05	-14	17/07/05	-5	17/07/05	0
15.60	16/07/05	-11	17/07/05	-14	18/07/05	-5	18/07/05	0
16.80	16/07/05	-10	17/07/05	-14	18/07/05	-5	18/07/05	0
18.00	16/07/05	-11	17/07/05	-15	18/07/05	-5	18/07/05	0
19.20	16/07/05	-11	17/07/05	-15	18/07/05	-5	18/07/05	0
20.40	16/07/05	-11	18/07/05	-15	18/07/05	-5	18/07/05	0
1 week	22/07/05	-17	23/07/05	-21	23/07/05	-14	23/07/05	-3
2 weeks	29/07/05	-19	30/07/05	-22	30/07/05	-15	30/07/05	-5
3 months	15/10/05	-	16/10/05	-	16/10/05	-	16/10/05	-
6 months	15/01/06	-	16/01/06	-	16/01/06	-	16/01/06	-

Appendix C

EPB Shield Machine

The real pictures of EPB shield machine used in the BMA flood diversion tunnel and the backup unit are shown in Figure B.1 to B.4.



Figure C.1 Articulated EPB shield for MBA flood diversion tunnel (Saensaeplathphrao Phrakhanong project)

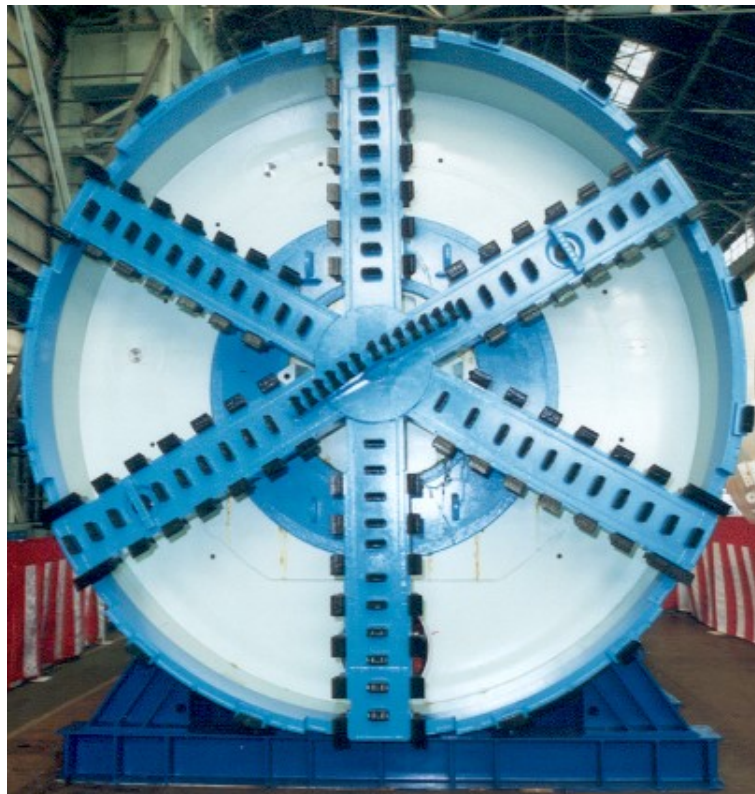


Figure C.2 Front view of EPB



Figure C.3 Back view of EPB



Figure C.4 Backup unit of EPB

Appendix D

Model Geometries for FE Analyses and Output Graphics

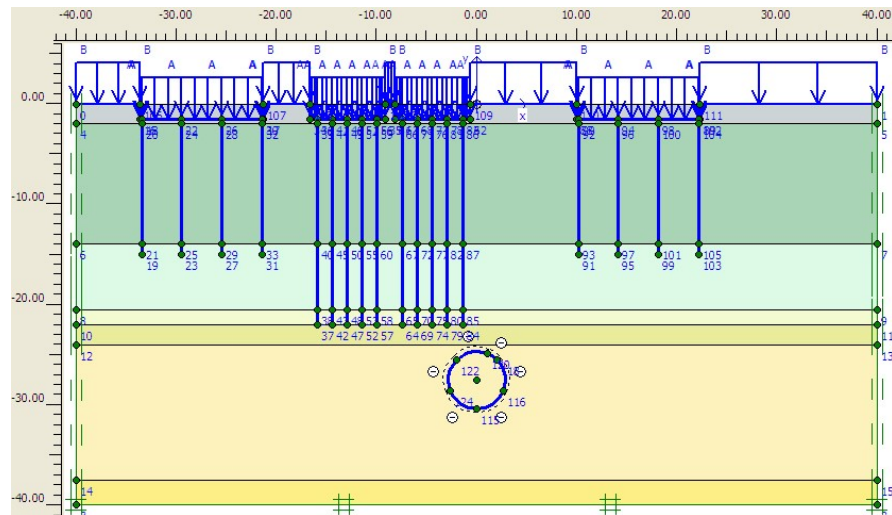


Figure D.1 Input geometry of section GS16

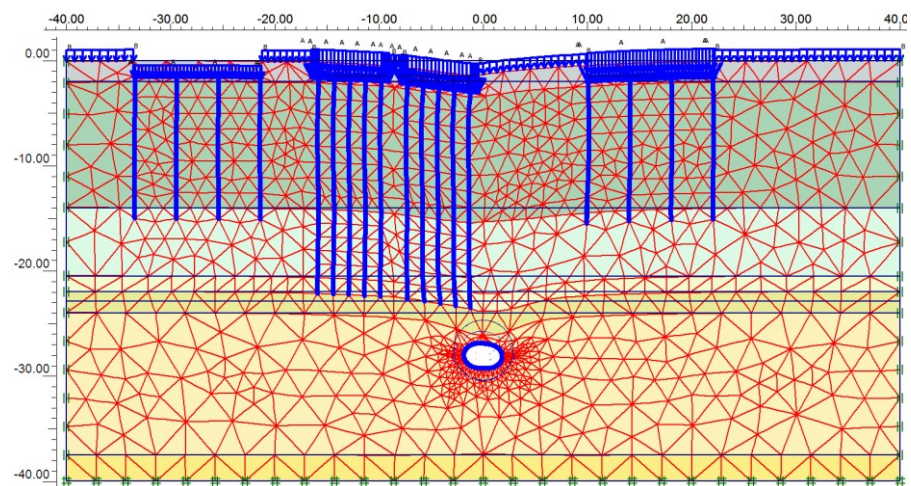


Figure D.2 Deformation mesh generated at section GS16

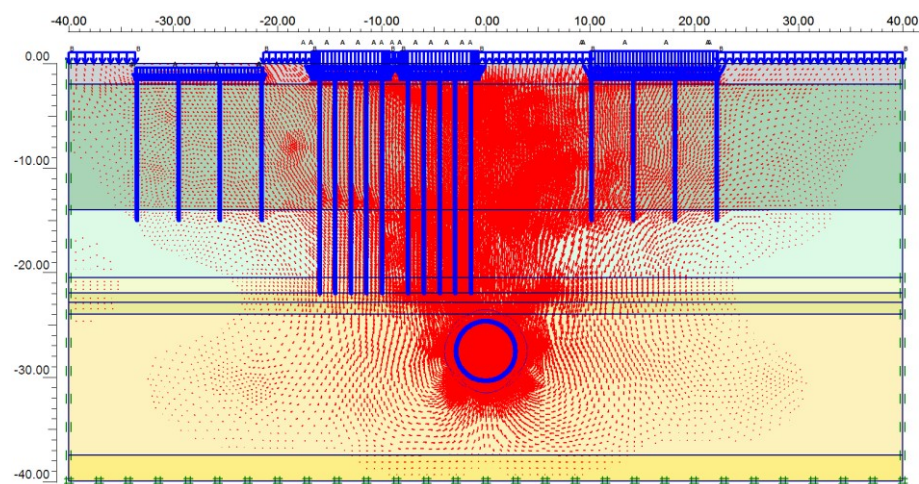


Figure D.3 Total displacement arrows at section GS16

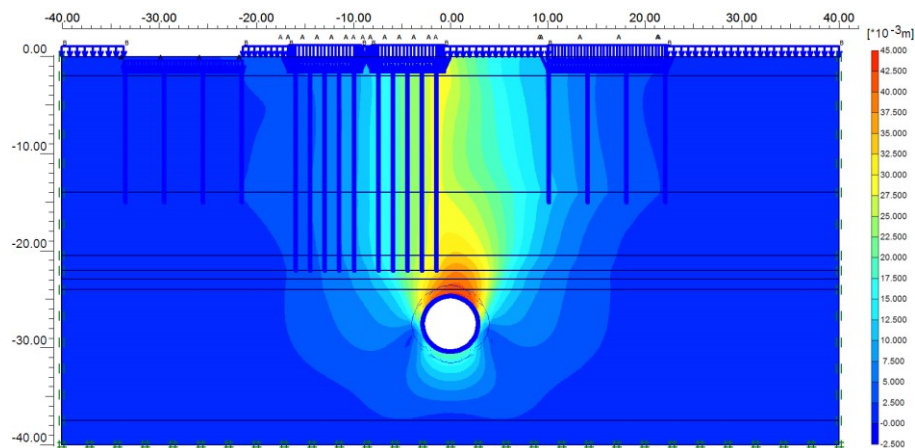


Figure D.4 Total displacement shadings at section GS16

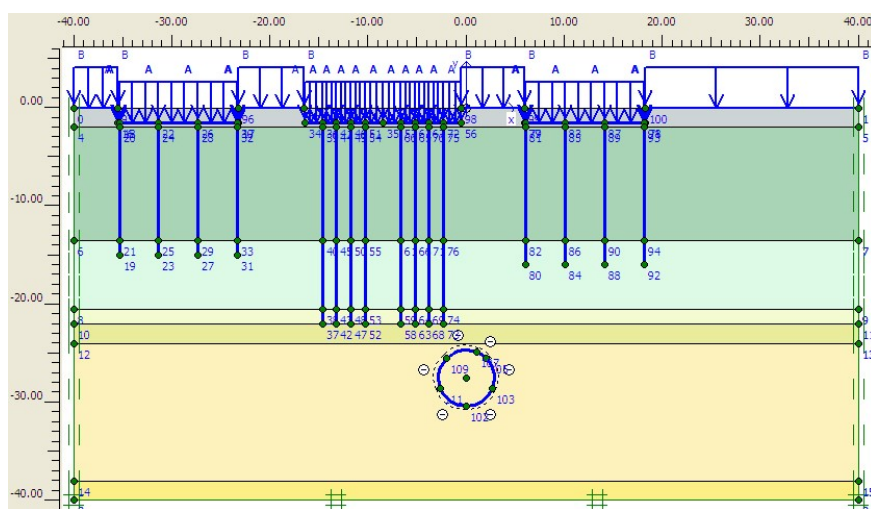


Figure D.5 Input geometry of section GS17

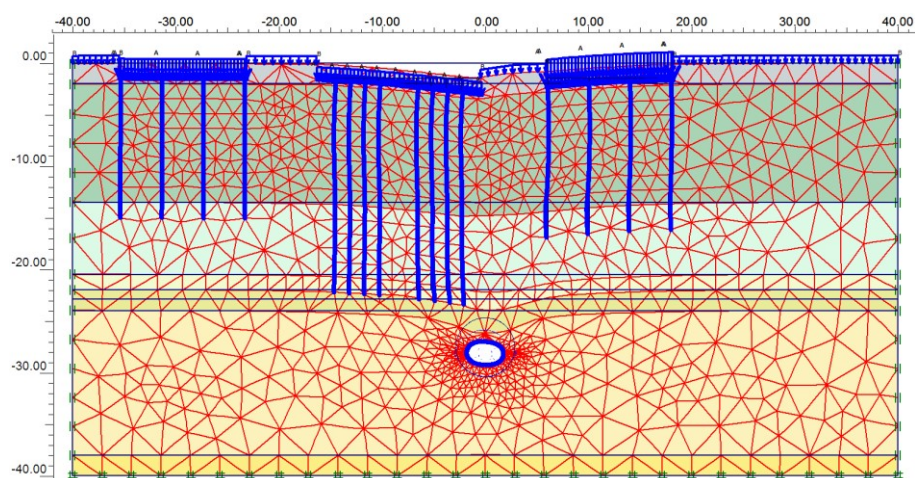


Figure D.6 Deformation mesh generated at section GS17

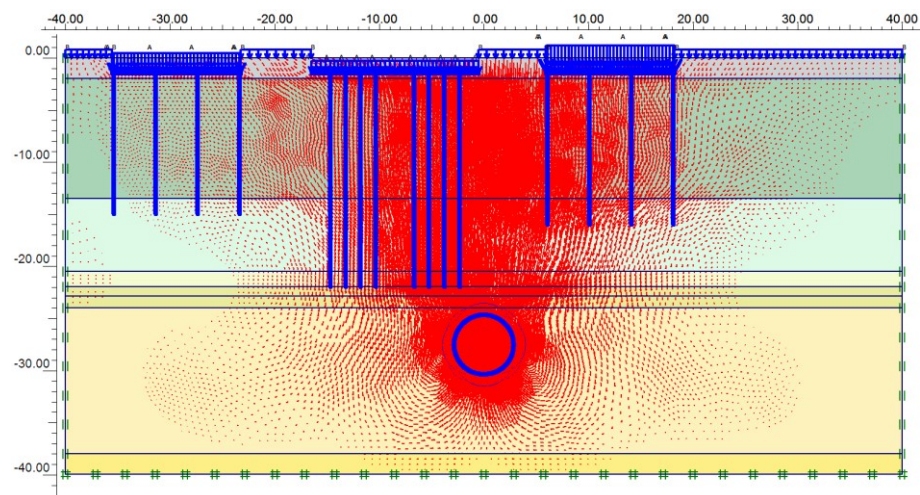


Figure D.7 Total displacement arrows at section GS17

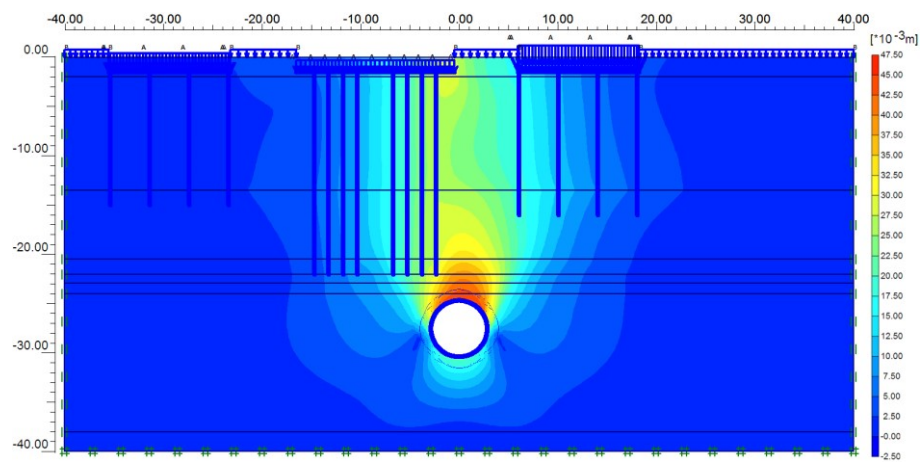


Figure D.8 Total displacement shadings at section GS17

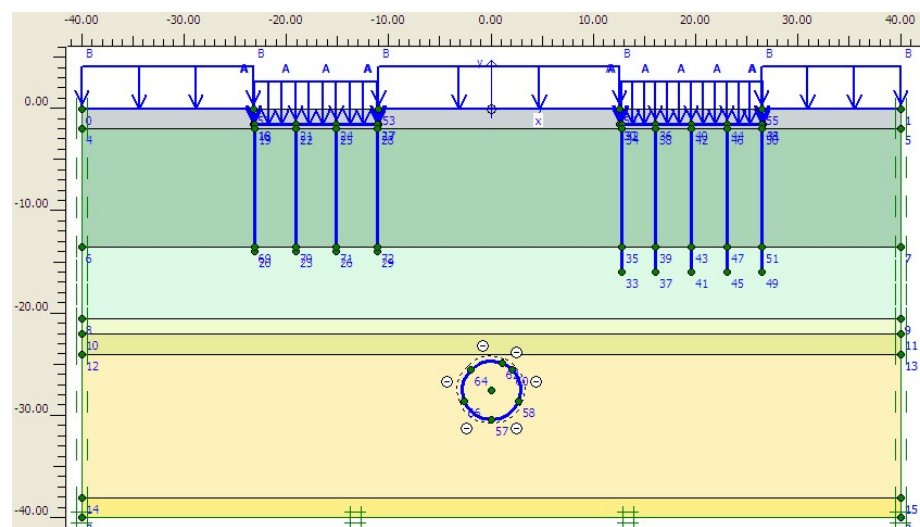


Figure D.9 Input geometry of section GS18

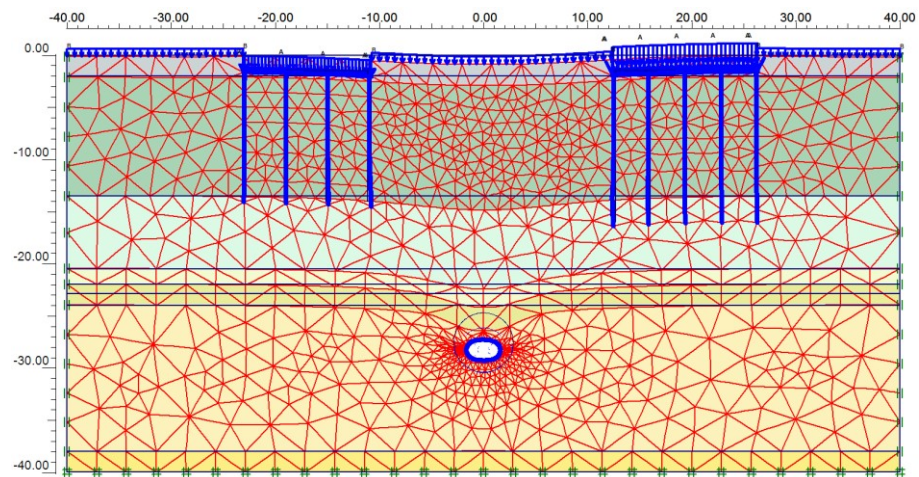


Figure D.10 Deformation mesh generated at section GS18

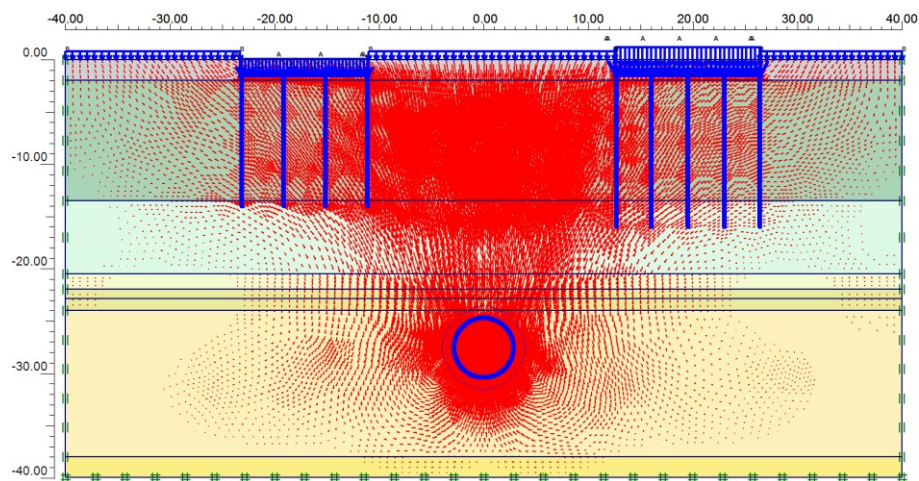


Figure D.11 Total displacement arrows at section GS18

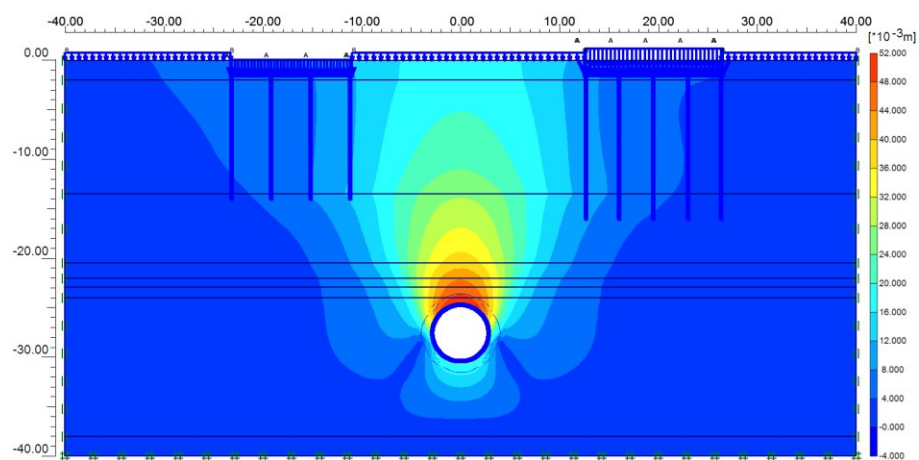


Figure D.12 Total displacement shadings at section GS18

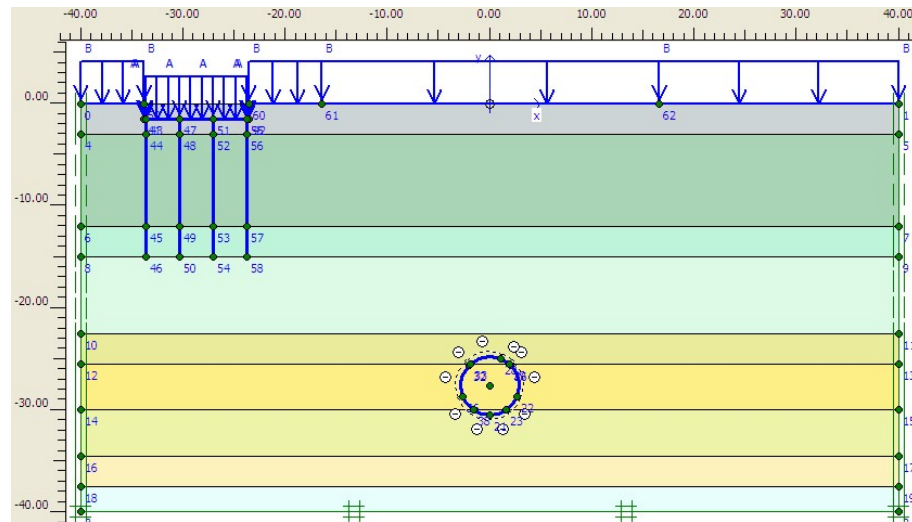


Figure D.13 Input geometry of section GS-BTS

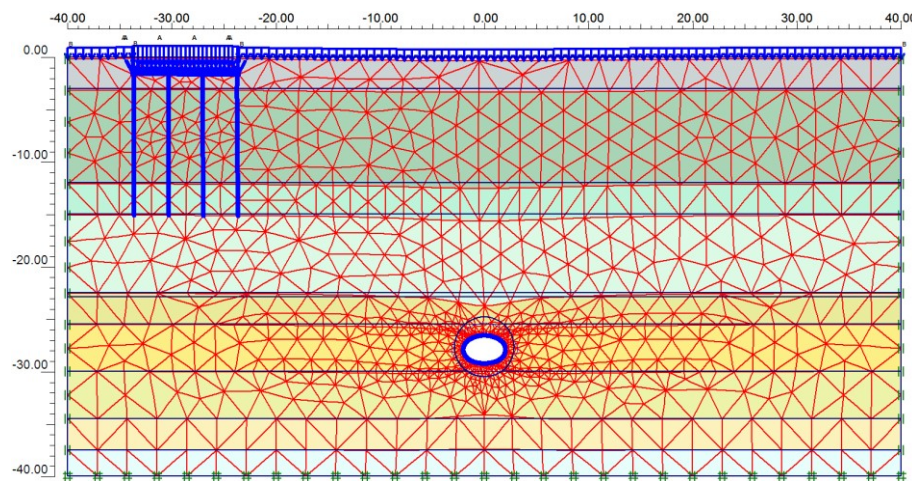


Figure D.14 Deformation mesh generated at section GS-BTS

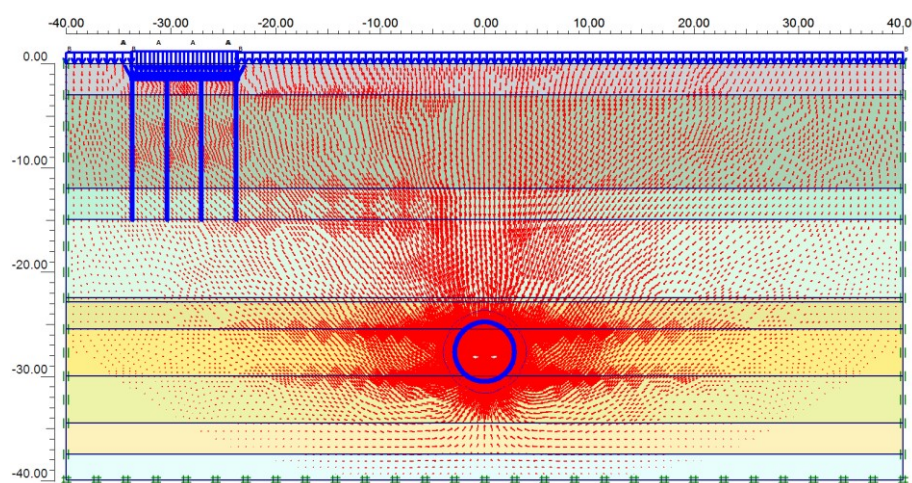


Figure D.15 Total displacement arrows at section GS-BTS

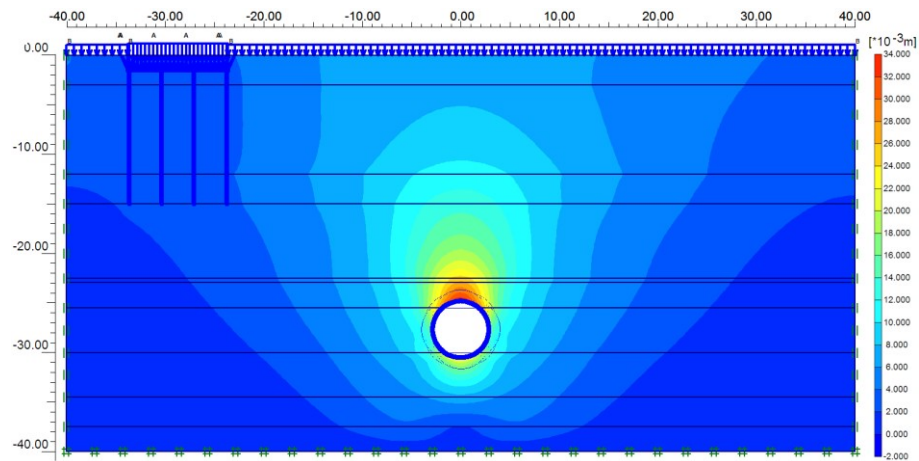


Figure D.16 Total displacement shadings at section GS-BTS

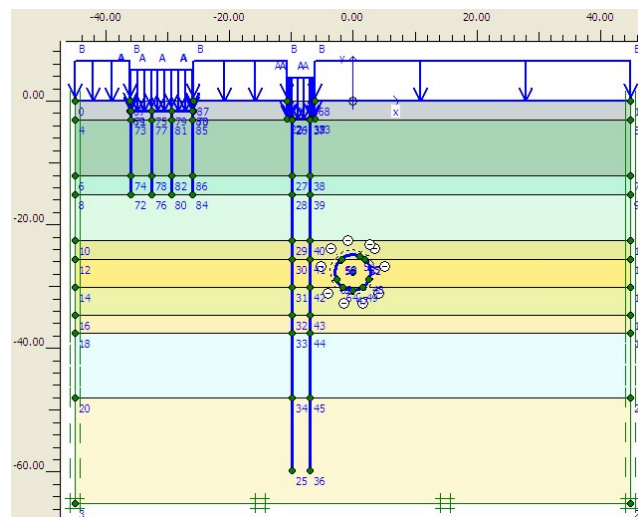


Figure D.17 Input geometry of section GS35

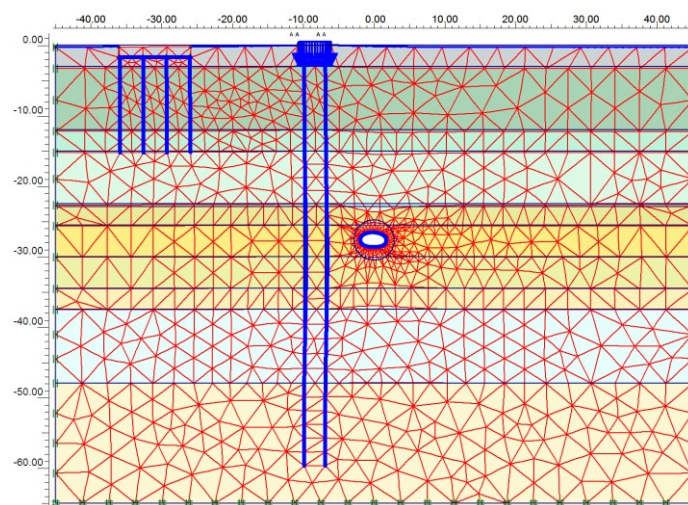


Figure D. 18 Deformation mesh generated at section GS35

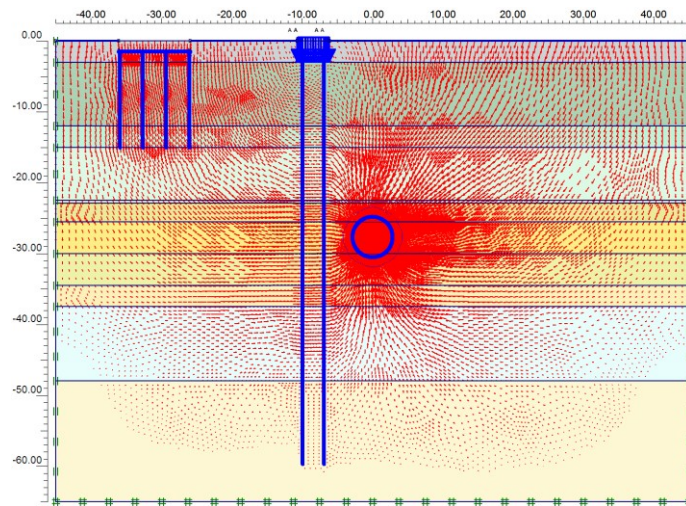


Figure D.19 Total displacement arrows at section GS35

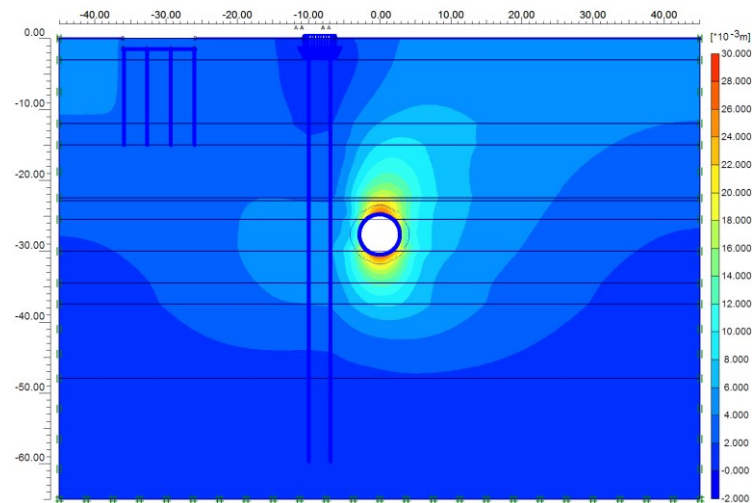


Figure D.20 Total displacement shadings at section GS35

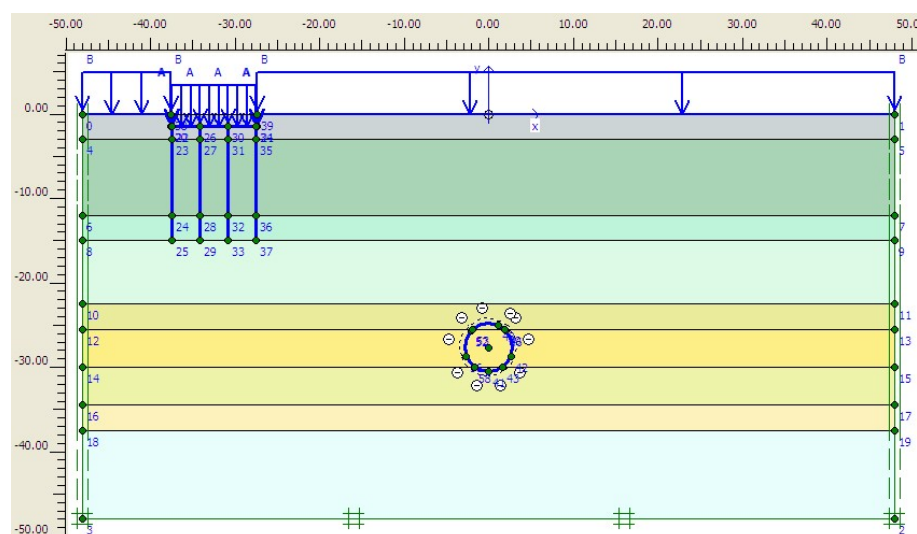


Figure D.21 Input geometry of section ME-2

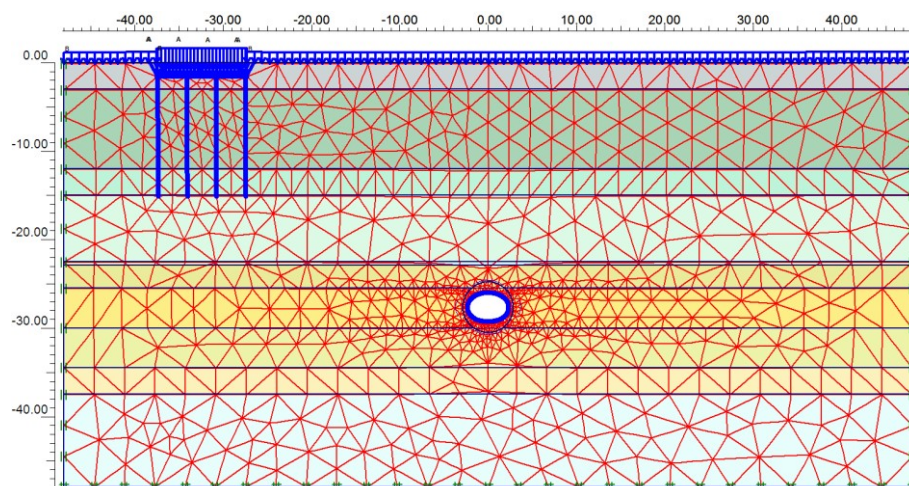


Figure D.22 Deformation mesh generated at section ME-2

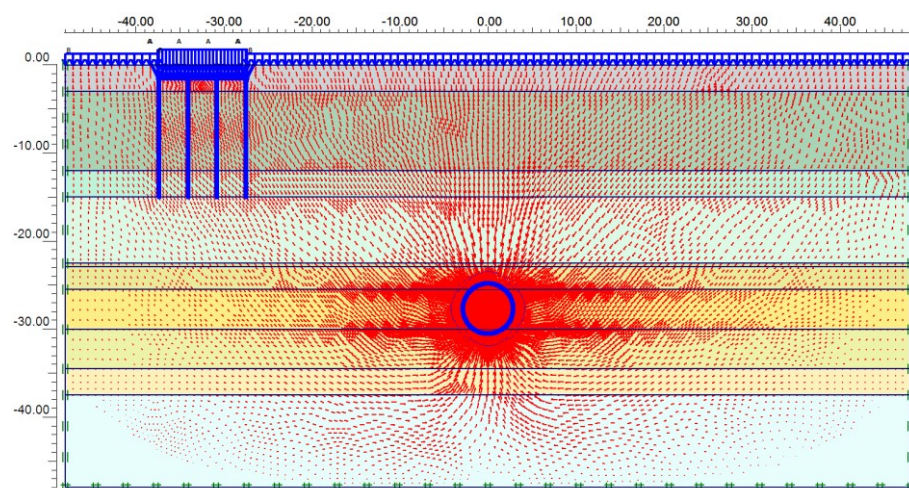


Figure D.23 Total displacement arrows at section ME-2

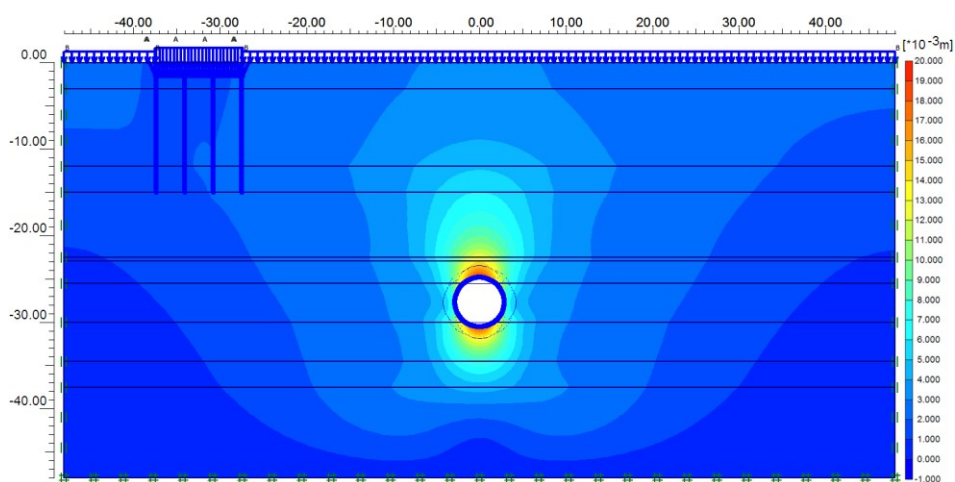


Figure D.24 Total displacement shadings at section ME-2

VITA

Soktay LIM was born on November 11, 1974 in Kompomg Speu province, Cambodia. After one year studying in preparative class, he passed the entrant examination at the Institute of Technology of Cambodia (ITC) as the first generation under the support from AUPELF-UREF, a French speaking agency for research and university.

In summer 1996, he was sponsored by the AUPELF-UREF for linguistic practicum and French culture at the Michel de Montaigne University, France. Subsequently, he was awarded a scholarship to finish his fifth year of engineering study in Belgium at Gembloux Agricultural University (Faculté Universitaire des Sciences Agronomiques de Gembloux, FUSAGx). His research within this one year was focus on the stability of the earthen dam, where the necessary data was given from a project in Algeria.

Soktay was selected as a young lecturer in the Department of Rural Engineering at ITC in 1999 after getting his bachelor degree in that year. After one year of hard working in the department, he was grained another scholarship to continue his Postgraduate Diploma (in French: Diplôme d'Etudes Approfondies, DEA) at Catholic University of Louvain (Université catholique de Louvain), Belgium. During this time his work was mainly concentrated on hydrology of micro-watersheds in brabant wallonia region of that country. After one year and one month of his intensive work, he got a Postgraduate Diploma in agronomic sciences and biological engineering (DEA en sciences agronomiques et ingénierie biologique). However, his diploma was issued on January 18, 2002, about three months after his oral defense.

After continuing his lecture about two years at ITC and in order to create a good relationship within the engineering network in the region, he was delighted to accept a scholarship from AUN/Seed-Net (ASEAN University Network/Southeast Asia Engineering Education Development Network), which was supported by JICA (Japan International Cooperation Agency), to carry on his Ph.D. research in Geotechnical Engineering at Chulalongkorn University. Throughout this three and half-year period, he also had occasion of six months to pursue his work and to perform some tests in the geotechnical laboratory at Kobe University, Japan, where he was warmly welcome by Professor Satoru SHIBUYA as his co-advisor.